Dissipation of Magnetohydrodynamic Waves in the Upper Solar Atmosphere

Thesis

UNRESTRICTED

Dissipation of Magnetohydrodynamic Waves in the Upper Solar Atmosphere

Gordon Bremner Laing

B.Sc. (Glasgow)

The Open University

Thesis submitted for the degree of Doctor of Philosophy,
in the Department of Applied Mathematics of The Open University.

10th May 1996

Date of submission: 15 May 1996
Date of award: 4 December 1996

ProQuest LLC.
789 East Eisenhower Parkway
P.O. Box 1346
Ann Arbor, MI 48106 – 1346

Abstract

The upper solar atmosphere, the *corona*, is an example of a hot (10^6 K), tenuous, structured plasma. This thesis concentrates on two main aspects regarding our understanding of the corona, namely the existence of oscillatory phenomena and their possible connection with explaining the high observed coronal temperatures. The oscillatory phenomena are interpreted in terms of magnetohydrodynamic (mhd) waves and the thesis investigates how the energy of such waves might be converted into heat by the dissipation mechanisms of ion viscosity, electron thermal conduction and radiation in an optically thin atmosphere. An overview of coronal features and the observational evidence for waves are given and coronal heating theories together with dissipative mechanisms are discussed. Detailed calculations of the energy carried by waves in structured media are given showing that the waves can carry sufficient energy to meet the coronal heating requirements provided that the waves are associated with large root-mean-square-velocity amplitudes. The lengths over which ducted waves lose their energy in a weakly dissipative environment for both warm and cold plasmas are calculated. The results show that fast waves with periods 2 - 10 s are likely to dissipate in regions of low magnetic field strength ($\lesssim$ 15 G), and slow waves that are likely to dissipate have periods in the range 15 - 225 s. Dissipation lengths and rates for waves propagating in slender structures are calculated by two methods. One method considers an isothermal environment; the other considers large Péclet number, and it is found that slow, symmetric waves are likely to dissipate with periods in the range 2 - 80 s and 2 - 38 s, respectively. The final chapter compares the models with each other and with the models in the literature. Period ranges of dissipating and non-dissipating waves are compared with observed waves and it is proposed that waves of 2 - 10 s might contribute to coronal heating, whilst those waves that might survive dissipation have periods of a few and many tens of seconds.

To Mum and Dad

To describe the *phenomena* of nature, to explain their causes, to trace the relations and dependencies of those causes, and to enquire into the whole constitution of the universe, is the business of natural philosophy. A strong curiosity has prompted men in all times to study nature; every useful art has some connection with this science; and the unexhausted beauty and variety of things makes it ever agreeable, new and surprizing.

in *An Account of Sir Isaac Newton's Philosophical Discoveries, In Four Books*,
Colin MacLaurin, A.M., London, MDCCXLVIII.

Contents

Acknowledgements

I should like to express my sincere thanks to Dr P.M. Edwin for her unfailing help, encouragement and supervision during the past three and a half years. I am grateful to The Open University for financial support through the award of a Regionally Based Research Studentship. I have the pleasure of thanking the School of Mathematical and Computational Sciences of University of St Andrews, especially Professor E.R. Priest, for affording me the facilities of the school, and thus allowing the pursuit of my postgraduate studies within the *Solar Theory Group*. I am grateful to Professor B. Roberts for his help and advice throughout my research and I should also like to thank the members of the Solar Theory group, past and present, for all their helpful discussions regarding the nature of solar magnetic fields. In particular, I should like thank my long-time office-mate Mr P. Ferguson for our many engrossing mathematical and non-mathematical discussions and I am especially grateful to Dr P.M. Heggie for her unfailing assistance regarding computing matters. Further, I am grateful to Miss C.E. Martin for proof-reading this thesis.

I should also like to express my thanks to a number of people outside of the Solar Theory Group. Firstly, I thank Dr R.P. Edwin for ferrying many books, reports etc. between myself and my supervisor. I thank the members of Kinburn Bowling Club, St Andrews, for making my summer evenings pleasurable and the members of the University of St Andrews Celtic Society and the St Andrews Branch of the Royal Scottish Country Dance Society for making my winter evenings colourful. To my beloved Raith Rovers FC, I thank them for contributing to my enjoyment of Saturday afternoons and also that their best period (i.e. two First Division championships, Premier Division football, the winning of the League Cup and the heady heights of competing in the UEFA Cup) in their 113 year history should coincide with my return to Fife. For stimulating my interest in mathematics I thank my former (but not *old!*) school teachers Mr Perry, Mr Kilpatrick and Mr Dunachie and I also thank Mr MacInnes for many illuminating discussions concerning mathematical and physical concepts. I express my thanks to my Great Auntie Rosie for all our cheery conversations and supplying me with cups of coffee, tea and loads of biscuits during my many visits to her on Sunday/Monday evenings. For keeping me mobile between St Andrews - Kirkcaldy - Glasgow, I should like to thank my Grandad for all our battles (which usually consisted of the phrase: 'Oot the road Gordon! Ah've been workin' wi' tools a' ma life!') with the *Turbo Charged Ferrari* (VSC 671V) and its successor (OSP 524Y) in the annual pursuit of a MOT certificate. I thank also my Gran for keeping me supplied with her home made cakes and I further thank my Gran and Grandad for always being pleased to see me. I say 'thanks' to my Aunt Roberta (*whyter@red.sps.mot.com*) and her husband Colin (*Colin_COPLAND@bourns.com*) for keeping me sane with their all too infrequent e-mail messages. I thank also my Uncle Sid and his wife Jacqui (not to mention Sammantha and Douglas) for their much welcome hospitality whenever I've turned up unexpectedly at their doorstep. Finally, I cannot thank enough two very special people, namely my Mum and Dad, for all their love and support throughout my education and for always being there when I've needed them most.

Publications

The contents of Section 2.4 and Chapter 3 have been published in *Solar Physics* (Laing and Edwin, 1994 and Laing and Edwin, 1995a, b). In addition to the publications in *Solar Physics* poster presentations of this work have been given by Dr P.M. Edwin at the conferences on 'Solar Coronal Structures' IAU Colloquium 144, Tatranská Lomnica, Slovakia, 1993 (published as Edwin and Laing, 1994) and 'Current Trends in Solar and Astrophysical Magnetohydrodynamics' Boulder, Colorado, USA, 1994.

List of Figures

List of Tables

Chapter 1

Introduction

Mankind has always regarded the Sun as an object of beauty, fascination and worthwhile study. The Ancients worshipped the Sun as a god and early scientific questions centred on: What was it made of? How big was it? How far from the Earth was it? These questions have since been answered satisfactorily. We now know that the Sun is a slightly oblate sphere (radius, $R_{\odot}, 6.96 \times 10^8$ km) of hot plasma, consisting mainly of hydrogen ($\sim$ 90%) and helium ($\sim$ 10%), held together by gravity. The Sun is divided into two main areas, the solar *interior* where nuclear energy is converted into radiation and then convected into the solar *atmosphere*. However, it was not until the mid-nineteenth century, following a rapid increase in the knowledge of solar phenomena, that the true physical nature of the Sun and the features of the various regions of its atmosphere, the *photosphere*, *chromosphere* and *corona*, became clear. Magnetic fields were first detected on the Sun by Hale in 1908 but their origin is still unknown although *dynamo theory* (e.g. see Gilman, 1986) is attempting an explanation. The problem of explaining the extremely hot (10^6 K) corona, first realized by Edlén in 1940, still remains. It is not clear whether the upper atmospheric heating is due to *waves*, or due to the other major contender, topological-magnetic-field-change-related processes. In 1942 British Army radar operators, completely by accident, detected radio emission from the Sun. Nowadays information concerning the oscillatory nature of the Sun's outer atmosphere mainly comes from radio-wave data. In the Sun, waves are of interest because firstly, they are able to transport energy from one location to another, and therefore have the ability to modify the solar atmospheric structure. Secondly, waves can effect the strengths, widths and shapes of spectral lines which are emitted by the Sun, and are a useful probe for gaining information about the solar atmosphere. Rocket and satellite observations during the last thirty years from missions such as *Skylab*, the *Solar Maximum Mission*, and *NIXT* (Normal Incidence X-ray Telescope) have provided an ever-improving view of the Sun and have revealed much about the structuring of the solar atmosphere. Such observations have revealed that coronal structures are capable of supporting waves. Currently there are many instruments, both ground-based, and in space, with which the rich and diverse

phenomena that our nearest star has to offer may be observed.

1.1 A Description of the Solar Atmosphere

The solar atmosphere is traditionally classified into three regions, the thin surface layer of the photosphere, and the highly non-uniform regions of the chromosphere and corona which are only ever seen at the time of a solar eclipse. However, it must be borne in mind that, although such a classification is convenient for descriptive purposes, such a division is in fact only roughly appropriate. It must be stressed that the solar atmosphere is a very dynamic atmosphere, and is highly structured, as well as stratified by gravity.

The photosphere is often loosely referred to as the Sun's surface but unlike the Earth's crust, it is *not* solid. Visible light is radiated from this thin (550 km) layer and the Sun is viewed as a disc in the day time sky (provided that there are no clouds overhead!). From detailed measurements of solar magnetic fields via the Zeeman splitting of spectral lines, Stenflo (1989) states that over 90% of the magnetic field of this region is confined to sunspots (2 - 4 kG) and intense magnetic flux tubes (1.5 kG). Typically the photosphere has a density of 10^{-4} kg m^{-3} and a temperature of 6 000 K which falls to about 4 200 K at the top of the photosphere (the *temperature minimum*).

The region immediately above the temperature minimum is the highly inhomogeneous region called the chromosphere within which the temperature rapidly increases with increasing altitude. The magnetic field from the intense magnetic flux tubes, located in the photosphere, expands into a near-horizontal canopy filling the whole of the chromosphere. A striking feature of the chromosphere is that of numerous fine jet-like structures known as spicules (e.g. Beckers, 1972). Essentially spicules are narrow tubes of plasma with diameters of 500 - 12 000 km which radially extend outwards to a height of 9 000 km with velocities of about 30 km s^{-1}. They are guided by the chromospheric magnetic field and cover about 1% of the solar disc. Viewed at the limb, spicules are seen every few hundred kilometres and give the impression of a 'burning prairie'.

The corona is the Sun's hot (10^6 K), tenuous outer atmosphere which in open-field regions expands outwards in the form of the solar wind, well beyond the Earth's orbit. The corona is dominated by intense magnetic forces, which penetrate into it from the lower, denser regions of the solar atmosphere. Coronal gas accumulates around magnetized regions to produce the intriguing shapes and structures observed during a solar eclipse, with a coronagraph, or viewed in X-rays (wavelength $< 10 \times 10^{-10}$ m), EUV ($15 - 80 \times 10^{-10}$ m) or H_α (656.3×10^{-10} m).

A large part of the energy emission from the corona is concentrated along well-defined curved paths, called *loops*, but the precise mechanisms by which loops, and other coronal structures, are heated, are still uncertain. Typically the corona has a magnetic field strength of 10 - 100 G although fields of 1 800 G have been reported (White, Kundu and Gopalswamy, 1992).

When the Sun is fairly inactive, the corona is viewed as a faint, uniform halo during an eclipse (Shklovskii, 1965). However, a great deal of structuring with large streamers extending

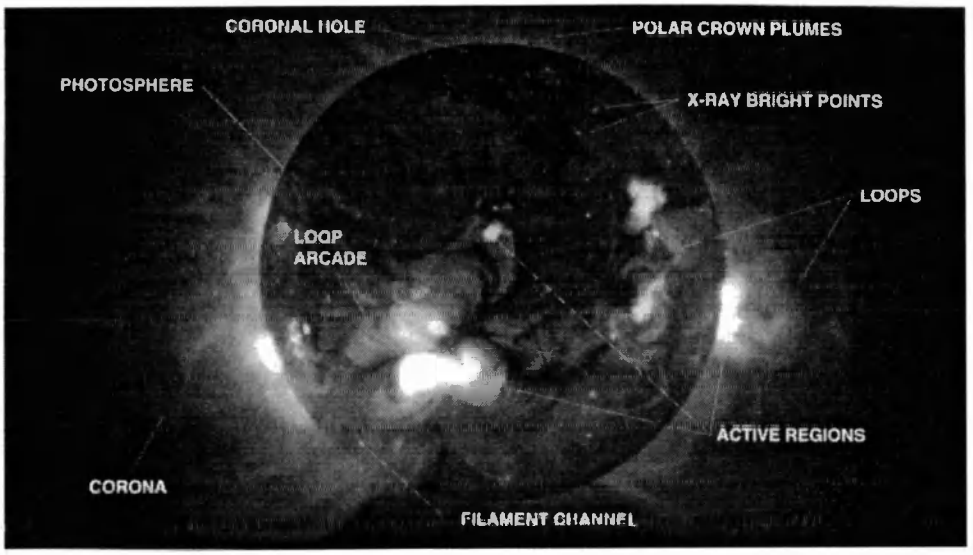

Figure 1.1: X-ray image of the Sun obtained from the Soft X-ray Telescope on board the orbiting Yohkoh satellite on 8 May 1992 (Lockheed Missile and Space Co.).

radially outwards to distances of 10 $R_\odot$, and the inhomogeneous nature of the corona can be seen at solar maximum (e.g. see the papers of Panel 1: Solar Eclipse Results in Rušin, Heinzel and Vial, 1994).

The gases of the photosphere and chromosphere are too cool to emit X-rays but when viewed in the X-ray range of the electromagnetic spectrum, the corona is seen to be highly structured and inhomogeneous. A great deal of progress in understanding the structure of the corona has come from X-ray imagery. In addition to the large-scale structures of the corona there are also small ($6 - 9 \times 10^3$ km) point-like features, called *X-ray bright points*, of relatively bright soft X-ray emission. They occur throughout quiet regions and coronal holes and are not associated with active regions.

The *Skylab* mission highlighted the need to explain the importance of the confinement of the coronal plasma between magnetic field lines and the mechanisms for energy transfer in order to keep the plasma hot. Recent soft X-ray images (see Figures 1.1 and 1.2) of the solar corona taken with the Soft X-ray Telescope (SXT) on board the *Yohkoh* spacecraft (launched in 1991) have shown, besides a much more detailed X-ray view of the Sun, that the corona has a much higher time variability than appeared from previous space experiments. The corona is *never* static and transient phenomena occur on a variety of length scales (Hiei, 1994):

1. transient brightenings of small size (less than several tens of arcsecs[1]) occur in X-ray bright points in active regions;

2. flare loops, jets and bright points associated with prominence disappearances of medium size

[1] 1 arcsec ≡ 726 km.

(0.1 to 0.5 $R_\odot$);

3. large-scale restructuring of the solar corona on a size larger than 0.5 $R_\odot$ occurs in coronal-mass-ejection events.

Prior to the *Skylab* mission in 1973, a decade of rocket experiments had shown that the corona is essentially composed of magnetic loops. Vaiana, Krieger and Timothy (1973) and references therein identified the following coronal structures: active regions, active-region interconnections (arches), coronal holes, large-scale, quiet coronal structures, coronal structures forming cavities, bright points and the identification of solar flares.

The solar-flare phenomenon is a manifestation of an explosive process of stored energy (10^{22} - 10^{25} J) in the lower corona. The coronal plasma may be heated up to temperatures of 5×10^7 K and the acceleration of charged particles gives rise to coronal emissions in radio through to gamma ray wavelengths (see Priest, 1981).

With the exception of solar flares, active regions are the most noticeable features of the X-ray corona. Viewed at the limb of the Sun, they appear as complex tubular arches or loops of enhanced density and temperature (see Figures 1.1 and 1.2 (B)). In addition, the many connecting loops within individual active regions, may extend from the active region itself to its peripheral area. Neighbouring active regions may be linked by large-scale arch structures (see Figure 1.2 (G)). Typical temperatures associated with active regions are $2 - 3 \times 10^6$ K and electron densities of $0.4 - 1.8 \times 10^{10}$ cm^{-3} (see Table 1.4).

X-ray images of the solar corona show clearly defined areas of reduced coronal emission, known as *coronal holes*, which are regions of open magnetic field, low densities and low temperatures. It is well known, e.g. see Parker (1991), that the expansion of the coronal plasma in the region of coronal holes is the source for the high-speed streams (400 - 600 km s^{-1}) in the solar wind. Typically, at their base, coronal holes have magnetic field strengths of 10 G, temperatures of 1.5×10^6 K, and electron densities of 2.7×10^9 cm^{-3} (Krieger, Timothy and Roelof, 1973; Vaiana, Krieger and Timothy, 1973).

The quiet corona represents between 60% and 80% of the observed corona and can be regarded as regions which are free from coronal holes or active regions. In a quiet region there may be many loops, called 'quiet loops', often observed as an arcade and possessing a lower temperature and density than loops in active regions.

In their comprehensive account of plasma loops in the solar corona, Bray *et al.* (1991) have reviewed extensively the observed properties of loop structures in the upper solar atmosphere. Two distinct sub-classes of coronal loops have been identified, namely *flare* and *non-flare* loops.

Observations show that non-flare coronal loops, depending upon their temperature, can be divided into two distinct categories. Loops with temperatures in excess of 10^6 K are usually referred to as *hot* loops, while those formed at lower temperatures are termed *cool* loops. The morphological and physical properties of the two types, listed in Tables 1.1 to 1.4, differ greatly.

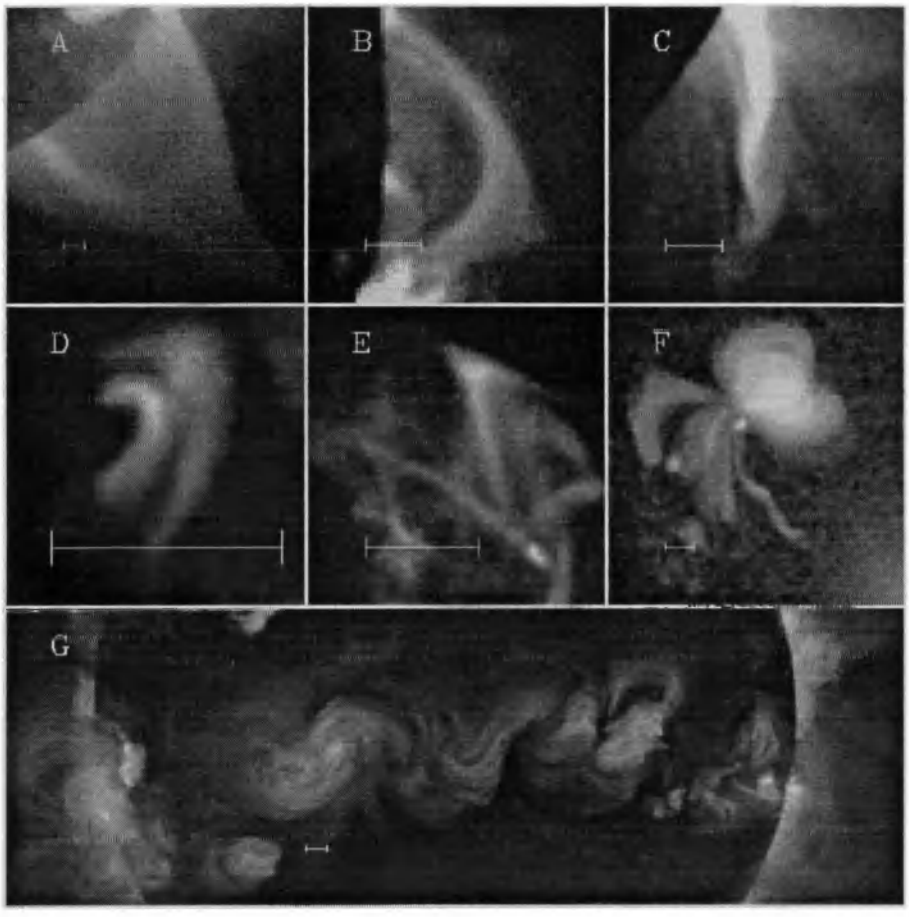

Figure 1.2: Menagerie of coronal loops obtained from the Soft X-ray Telescope on board the Yohkoh satellite from 3 October 1991 to 25 January 1992 (from Acton *et al.*, 1992).

Quantity	Value (km)	Observed wavelength
Height	40 000 - 53 000	H_α
Length	130 000	H_α
	22 000 - 109 000	EUV
Separation of footpoints	71 000 - 109 000	H_α
Diameter	1 600	H_α
	< 2000 - 22 000	EUV

Table 1.1: Morphological properties of cool loops (from Bray *et al.*, 1991).

It is seen that over the temperature range characterizing cool loops (20 000 - 10^6 K), both the heights and lengths are comparable. However, there appears to be a small increase in loop diameter with increase in temperature. Bray *et al.* (1991) note that the gas pressure is restricted to a small range (0.1 - 1.0 dyne cm^{-2}), perhaps reflecting the fact that the stability of a loop depends upon pressure equilibrium being maintained with the surrounding coronal plasma and that temperature is not a factor. Typical lifetimes of cool loops, along with those for hot ones, are given in Table 1.5.

Viewed overall, the data listed in Tables 1.1 and 1.2 indicate that, with the exception of temperature, all cool loops appear to have similar properties and can be thought of as being manifestations of the same physical structure.

Hiei (1994) indicates that the SXT images of the solar corona show several kinds of loops of different sizes with a homogeneous background corona. The homogeneity of the background corona may well be due to any fine structure being smaller than the spatial resolution of the SXT telescope (3 arcsecs) (Yoshida *et al.*, 1995). Observations of hot ($> 10^6$ K) loops lead to the following classification:

1. flare loops;
2. loops in active regions,
   (a) occurring in the core of active regions (type a),
   (b) surrounding the core of active regions (type b),
   (c) loops connecting between active regions and their periphery (type c);
3. loops connecting two active regions (type d);
4. loops in a quiet region (type e).

Quantity	Value	Observed wavelength
Temperature (electron)	2.1×10^4 K	H_α
	7×10^3 - 2.5×10^4 K	Visible
	6.0×10^4 - 10^6 K	EUV
Density (electron)	5.6×10^{10} cm^{-3}	H_α
	3.0×10^9 - 6.0×10^{12} cm^{-3}	Visible
	4.0×10^8 - 3.0×10^{11} cm^{-3}	EUV
Gas pressure	0.36 dyne cm^{-2}	H_α
	0.14 - 0.58 dyne cm^{-2}	Visible
	0.1 - 1.0 dyne cm^{-2}	EUV
Gas density	1.3×10^{-13} g cm^{-3}	H_α
Magnetic field strength	4 - 45 G	Visible

Table 1.2: Physical conditions in cool loops (from Bray *et al.*, 1991).

Quantity	Value (km)	Observed wavelength	Type of loop
Height	110 000 - 130 000	EUV	d
	45 000	21 cm	-
Length	18 000 -29 000	EUV	-
	7 000 - 44 000	X-ray	a
	10 000 - 100 000	X-ray	b
	5 000 - 500 000	X-ray	c
	70 000 - 100 000	6, 20 cm	-
Separation of footpoints	250 000 - 100 000	X-ray	e
Diameter	3 000 - 500 000	530.3 nm	-
	3 000 - 18 000	EUV	-
	5 000 - 11 000	X-ray	a
	5 000 - 20 000	X-ray	b
	10 000 - 30 000	X-ray	c
	15 000	3.7 - 20 cm	-

Table 1.3: Morphological properties of hot loops (from Bray *et al.*, 1991).

In Figure 1.2 a large helmet structure extending radially outwards from the Sun is seen in Panel (A). In Panel (B) an arcade of loops is viewed end-on. A dynamic eruption is shown in (C) and in (D) there is a flaring loop. Two cusped loops are seen in Panel (E) and there is a tightly beamed X-ray jet in (F). Panel (G) shows loops connecting active regions.

Hot loops (usually observed in X-rays and EUV) are typically thicker, longer, higher and longer-lived than cool loops (usually observed in H_α). It is difficult to compare electron densities in the two types of loop, since both cover a wide range and there is considerable overlap. The values of gas pressure seem to be very much the same for cool and hot loops, covering the same range. This seems to suggest that, just like cool loops, hot loops are in pressure equilibrium with their surroundings. Bray *et al.* (1991) comment that there are not enough measurements of the total magnetic field to give a meaningful comparison between hot and cool loops. Overall, all hot loops

Quantity	Value	Observed wavelength	Type of loop
Temperature (electron)	1.0×10^6 - 2.6×10^6 K	Visible	-
	$2.0\ 10^6$ - 2.2×10^6 K	EUV	-
	2.0×10^6 - 3.2×10^6 K	X-ray	-
	1.7×10^6 - 3.0×10^6 K	20 cm	-
Density (electron)	1.5×10^8 - 2.0×10^9 cm^{-3}	530.3, 737.4 nm	-
	1.8×10^9 - 2.0×10^{10} cm^{-3}	EUV	-
	8.0×10^8 - 6.0×10^9 cm^{-3}	X-ray	-
	5.0×10^8 - 2.5×10^9 cm^{-3}	20 cm	-
Gas pressure	0.5 dyne cm^{-2}	Visible	a
	0.7 - 16.6 dyne cm^{-2}	EUV	-
	2.4 dyne cm^{-2}	X-ray	b
	2.0 dyne cm^{-2}	20 cm	-
Magnetic field strength	130 - 200 G	20 cm	-

Table 1.4: Physical conditions in hot loops (from Bray *et al.*, 1991).

appear to have similar properties regardless of the wavelength range in which they are observed.

The loops observed in the corona represent regions where the coronal gas has been *trapped* by magnetic field lines. Leblanc (1970), Foukal (1975) and Cheng (1980) estimate that the surrounding medium may be 1/3, 1/4 and 2/3 as dense, respectively, as the loops. Stewart (1976) and Pick, Trottet and MacQueen (1979) state that measurements indicate that coronal loop structures are about 8 to 10 times more dense than the background corona. In other words, loops may be regarded as *dense ducts.*

Another important set of structures observed in the corona, as yet unmentioned, is that of *prominences.* Possessing temperatures of a hundred times lower and densities of a hundred or a thousand times greater than background coronal values, prominences can be classified into two basic types (Priest, 1982): quiescent prominences which are extremely stable in structure and may persist for many months in the corona; and active prominences, with lifetimes of minutes or hours, which are located in active regions and are associated with flares. Priest (1982) has summarized the observed properties that exist in prominences and has also given consideration as to their formation.

So, overall, the coronal magnetic field plays a major role in shaping the morphology of the outer layers of the solar atmosphere. As each generation of X-ray instrumentation has improved, it has become clear that the solar magnetic field has a highly inhomogeneous structure which has, probably, yet to be resolved to its full extent.

1.2 Observed Wave Phenomena in the Solar Atmosphere

It has already been mentioned that wave motions in the solar atmosphere have an effect on spectral lines and that a great deal of information concerning oscillatory motions in the corona comes from radio wave data.

Type of loop	Lifetime	Observed wavelength
Cool, loop system	3 - 6 hr	H_α
Cool, single loop	$\lesssim$ 15 mins	H_α
Hot, small loop	hr	530.3 nm
Hot, large loop	days	530.3 nm
Hot loop	$\gtrsim$ 6 hr	EUV
d	$>$ 31 hr	EUV
a	$>$ 10 hr	X-ray
d	hours - days	X-ray
Hot loop	hours - days	microwave

Table 1.5: Lifetimes of coronal loops (from Bray *et al.*, 1991).

Velocity fluctuations, associated with density and temperature fluctuations, can produce complicated and puzzling effects on spectral lines. Essentially a spectral line represents an integral over several hundred kilometres of depth of the solar atmosphere, and an average over an area typically greater than 250 000 square kilometres. At each point in this region, the line profile function is shifted by an amount determined by the local line-of-sight velocity, and has a depth determined by the opacity which depends upon temperature and density. The effects that a velocity field, such as a wave or a pulsation, can have on an observed spectrum are: a simple Doppler shift; broadening of the line, i.e. an increase in the frequency range of the line; change in line strength, i.e. change in the integrated area under the line profile; and asymmetry of the shape of the line.

The corona is also observed to contain ubiquitous non-thermal motions which are interpreted as waves but are unresolved both in space and time. Line-broadening measurements of optically thin emission lines provide a means of estimating the amplitudes, v_{rms}, of these unresolved, small-scale motions. There are values of v_{rms} of 3 - 10 km s^{-1} given by Athay and White (1979), medium-sized values in the range 10 - 30 km s^{-1} (e.g. Feldman and Behring, 1974; Leibenberg, Bessey and Watson, 1975; Doschek, Feldman and Bohlin, 1976; Doschek and Feldman, 1977; Feldman and Doschek, 1977; Cheng, Doschek and Feldman, 1979; Hassler *et al.*, 1990) and values like these, and substantially larger ones of $\gtrsim$ 60 km s^{-1}, given by Kjeldseth Moe and Nicolas (1977), Acton *et al.* (1981) and Saba and Strong (1991).

Wave motions have been detected in all levels of the solar atmosphere. In the photosphere, oscillations in sunspots were first detected by Beckers and Tallant (1969). Sunspot penumbrae are also know to exhibit oscillations, typically with periods of 3 - 5 minutes (Lites, 1988). Coherent wave-fronts, typically with velocities of 20 - 35 km s^{-1}, have been observed propagating outwards from sunspot umbrae into their penumbrae (Giovanelli, 1972; Zirin and Stein, 1972).

The chromosphere is known to exhibit oscillations with periods of many tens of seconds and of several minutes. Endler and Deubner (1983) detected wave periods in the range 40 - 140 s. Athay and White (1979) and White and Athay (1979) detected periods in the ranges 200 - 300 s and

170 - 500 s, respectively, which were thought to be associated with acoustic waves. Kneer and von Uexküll (1985) have reported waves with periods of 50 s and also periods of between 80 and 200 s.

Fast coronal oscillations, typically with periods of less than 10 s have been reported in the extensive literature cited by, for example, Edwin (1984), Aschwanden (1987) and Tsubaki (1988). Pasachoff and Ladd (1987) reported coronal oscillations with periods in the range 0.5 - 4 s and Fu *et al.* (1990) report oscillations over a similar range, namely 0.4 - 3 s. Li, Messerotti and Zlobec (1987) have detected pulsations of approximately 7 s and Mangeney and Pick (1989) give oscillations in the range 1 - 6 s, as do Zhao, Mangeney and Pick (1991). Pasachoff (1991) has further reported periods in the range 0.5 - 3 s. More recent work by Aschwanden and co-workers has seen the following wave periods detected: 1.6 and 1.7 s by Aschwanden *et al.* (1993, 1994); and 2.3 s by Aschwanden, Benz and Montello (1994). Usually, magnetic field strengths are not quoted along with the observed wave periods but Zlobec *et al.* (1992) have detected oscillations with a period of 12 s in a 67 G field and Wright and Nelson (1987) report periods of 180, 240 and 300 s in fields of 26 and 45 G.

Koutchmy, Žugžda and Locăns (1983) have detected wave periods in excess of 43 s. Antonucci, Gabriel and Patchett (1984) have reported oscillations with periods of 70, 117 and 141 s. There is also ample evidence for periods of 300 s such as reported by Leibenberg and Hoffmann (1974) and Tsubaki (1977).

Much longer periods have also been detected. Švestka (1994) has detected oscillations with periods of about 20 minutes and Harrison (1987) has detected oscillations of about 24 minutes.

Prominence structures are also known to exhibit wave motion with periods in the range of about 5 minutes to about 90 minutes.

Clearly, then, there is ample evidence for oscillatory motion in the upper solar atmosphere ranging from the sub-second periods, such as those detected by Takakura *et al.* (1983), to periods of many minutes such as those reported by Harrison (1987).

As well as possessing wave motions on a local scale, as listed above, the Sun also possesses oscillations on a global scale, namely a 5 - minute oscillation of trapped, standing, small-amplitude acoustic waves. Thus, on a global scale, the Sun is akin to a vibrating drum. Detailed investigation of these standing acoustic waves has led to the area of Solar Physics known as *Helioseismology.*

1.3 Waves and Dissipation in the Solar Corona

The previous section has listed the wide range of oscillatory phenomena detected in the various layers of the solar atmosphere. One of the tasks of Solar Physics is to explain the observed wave motions from a theoretical point of view. Of course, it is of no surprise that the Sun is able to sustain oscillations of many kinds. Since the Sun is a compressible plasma, it is able to support sound waves. The presence of a magnetic field leads to magnetic *pressure* and *tension* forces (to be considered later) which further help to sustain wave disturbances. The effect of a gravitational field, lower in the solar atmosphere, would also appear to sustain wave motion. Thus, simply from

a theoretical point of view alone, wave propagation is worthy of consideration.

One of the most puzzling aspects of solar physics is the existence of the hot (10^6 K) corona. As yet no well-accepted, convincing argument has been presented. Ever since Biermann (1946) pointed out that the turbulent kinetic motions of granulation must generate powerful sound waves, waves have been thought of having some contributory role in heating the solar atmosphere. They have the attraction that if they originate at low heights in the photosphere, then, in principle, they can heat the lower atmosphere as well as the corona. If we consider waves to be guided, or ducted, along the dense coronal loop structures, described in Section 1.1, then the idea of waves being ducted from their origins low in the photosphere and convective regions, to the corona, is appealing. However, what is less clear, is that once the waves reach the upper solar atmosphere, then how do they surrender their energies to maintain the hot corona? In reality, the solar atmosphere is probably far from an ideal situation (in which wave motions suffer no decay in amplitude or decrease in energy). It is only natural, then, to consider magnetic-type waves which might be damped due to dissipation and so heat the corona. Moreover, any mechanical heating process requires that the convection zone does work and that, as a result, the solar atmosphere must move. As it will be shown in the remainder of this chapter, most but not all of the motions, or disturbances, in the solar atmosphere obey hyperbolic equations which yield wave, or wave-like, solutions. Thus it is reasonable to think of motions as waves.

However, if wave dissipation is to explain the hot corona, or if an alternative view is taken - the fact that wave motions are detected at all may indicate that any damping on the waves is ineffective - then there still remains the unanswered question of *how* the waves dissipate. What precisely are the dissipative mechanisms, if any, operating on wave motion in the solar atmosphere? Here the task is to investigate some dissipative mechanisms upon ducted waves in the corona and to suggest likely wave candidates that might play a role in contributing towards explaining the hot corona, and those which might exist by surviving the dissipative mechanisms under consideration.

1.4 Coronal Heating

Cargill (1995) gives a résumé of the observational evidence for coronal heating. In fact there are two coronal-heating puzzles, namely the one of heating active regions (coronal loops) to temperatures of 2 - 3 $\times$ 10^6 K and secondly the heating of coronal holes to 1.5 $\times$ 10^6 K. The coronal-heating problem is not merely confined to our nearest star; it is apparent from the results of the satellite mission, Einstein, and other missions, that many stars similarly possess hot coronae (Phillips, 1992; Haisch and Schmitt, 1996).

Hollweg (1990) stresses that the coronal-heating problem has been inappropriately emphasized in the past and the energy requirements for the corona should not be treated separately from those of the chromosphere and the high-speed solar wind. So, questions concerning the heating of the solar chromosphere, and the high-speed solar wind, must also be addressed. Indeed, Hollweg

Feature of atmosphere	Required energy flux density (erg cm^{-2} s^{-1})
Quiet corona	3×10^5
Coronal hole with high-speed wind	8×10^5
Chromosphere	few $\times$ 10^6
Spicules	few $\times$ 10^6
Active region loops	10^7

Table 1.6: Required energy flux densities for the coronal heating problem (after Hollweg, 1990).

comments further that any theory of the heating of the solar atmosphere must account for the required energy flux densities given in Table 1.6.

In the coronal-heating literature it is believed that the energy source for heating the coronal gas is the kinetic energy of plasma motions in the photosphere caused by sub-surface convection. The coronal magnetic field is distorted by the continual movements of the magnetic foot points which anchor the field in the photosphere. As a result of Ampère's Law, currents are generated and consequently magnetic energy is stored in the corona which, in principle, can be dissipated by, for example, the Fourier heat law.

Browning (1991) suggests that wave theories and those involving topological changes in the magnetic field form two classes of heating mechanism. The relation between the time scale of the photospheric velocity field, t_v, and the Alfvén transit time across a coronal structure, t_A, determines which theory is applicable. If a and l represent the radius and the length, respectively, of a coronal loop then t_v and t_A are given by

$$t_v = \frac{a}{v_p}, \; t_A = \frac{l}{v_A},$$

where v_p is the photospheric speed, and v_A is the Alfvén speed. The two classes of heating mechanism are:

1. AC (Alternating Current) heating theories: if $t_v < t_A$, then the movements of footpoints launch mhd waves into the atmosphere;

2. DC (Direct Current) heating theories: if $t_v > t_A$, then the coronal magnetic field is always approximately in field-free equilibrium. The positions of the foot points constrain the magnetic field and DC currents are generated which may dissipate and release heat.

Unfortunately, the motions of the photospheric flux tubes are beyond current observable resolutions and so are unknown. Therefore, it is unclear whether the Alfvénic time scale is greater than, or less than, the driving time scale of the photospheric motions and so probably both classes must remain viable candidates for coronal heating. The literature concerned with coronal heating contains mainly theoretical arguments. The observations for heating are usually cited in support of one coronal heating mechanism or another. It is quite clear that until there are improved diagnostics

for observations of heating mechanisms then the coronal-heating problem will remain unanswered. However, it is hoped that the CDS (Coronal Diagnostic Spectrometer) and SUMER (Solar Ultraviolet Measurements of Emitted Radiation) instruments onboard the SOHO (SOlar and Heliospheric Observatory) spacecraft (launched in December 1995) will firmly establish the existence of mhd waves in the corona by detecting fluctuations in density and temperature and will also allow the current wave-heating mechanisms to be critically tested.

Historically, wave theories have long played a role in trying to explain the coronal-heating problem ever since Biermann (1946) and Schwarzschild (1948) independently suggested that sound waves, which are generated from turbulent motions in the convection zone, would form shock-wave fronts as they propagate upwards and so heat the chromosphere and corona. Osterbrock (1961) developed the ideas of Biermann and Schwarzschild further and presented the first qualitative study on the heating of the solar chromosphere and corona by mhd waves. The ideas of Biermann, Schwarzschild and Schwarzschild were generally accepted until the 1970's when it became apparent that the upper chromosphere and corona, and the solar wind, did not obtain their energies from sound waves or their shocks. Basri and Linsky (1979) and Vaiana *et al.* (1981) demonstrated that chromospheric emission in typical stars is connected with a magnetic-heating mechanism rather than a result of acoustic processes. Deubner and Fleck (1990) are also critical of acoustic heating. However, sound waves and waves of a similar nature like the slow magnetoacoustic waves, have been advocated as a possible source of energy by several authors over the years (e.g. Leibenberg, Bessey and Watson, 1975; Ulmschneider and Bohn, 1981; Cram and Damé, 1983; Kneer and von Uexküll, 1985; Anderson and Athay, 1989; and Schrijver, 1992).

However, most workers agree that the magnetic field plays a vital role and that the likely heating phenomena in the chromosphere and corona (and indeed in stellar chromospheres and coronae) cannot be explained by a single process but rather are due to the action of a variety of mechanisms.

As Hollweg (1990) points out, 'the principal difficulty with wave theories is getting enough energy into the corona'. Dismissing the problems of how waves reach the corona in the first instance, or whether the waves shock, the energy being carried by these waves, and therefore available to be dissipated (for waves travelling in a spatially infinite atmosphere) is summarized as

$$E_{\rm fd} = \rho v_{rms}^2 v_{\rm g}, \tag{1.1}$$

(see Athay and White, 1978; and Hollweg, 1983, 1991). In Equation (1.1) ρ is the density of the medium, v_{rms} is the root-mean-square of the waves' velocity (phase speed) and $v_{\rm g}$ represents the group speed of the waves. Now the values of ρ in the corona (interpreted as a particle density, N, for an electrically neutral, fully-ionized, hydrogen plasma) can range from about 10^8 cm^{-3} to about 5×10^{12} cm^{-3} (see Section 1.1) and the group speed, $v_{\rm g}$, will depend on whether the waves are mainly acoustic or magnetic ones. In turn, the speeds of these component waves will depend on the coronal temperatures, T, and magnetic field strengths, B, which, as was indicated in the previous

chapter, may range, respectively, from 2×10^4 to $\sim 3 \times 10^6$ K and from a few gauss to as much as 1800 G. Thus applying the standard formulae for Alfvénic and acoustic speeds in the corona, namely $v_A = B_0/(\mu\rho_0)^{1/2}$ and $c_0 = (\gamma p_0/\rho_0)^{1/2}$ respectively, there is a range of speeds from about 5×10^5 cm s^{-1} to 10^9 cm s^{-1}. Note that μ represents the permeability of free space and p is the gas pressure.

The remaining parameter to be estimated in Equation (1.1) is v_{rms} and in many ways the determination of this parameter is at the crux of the above argument concerning the magnitude of $E_{\rm fd}$. A range of values for v_{rms} has been given in Section 1.2. As a result, from Equation (1.1), it would appear that values of $E_{\rm fd}$ can range from as low as 4 to as large as 1.5×10^{11} erg cm^{-2} s^{-1}. These are extrema, determined by the simple model of waves propagating in an unrestricted, homogeneous corona. So, superficially at least, in comparing with Table 1.6, it seems as though there could be waves in the corona supplying the energy requirements of the 'coronal-heating problem'.

However, many authors interpret observations of acoustic-type waves, not with the non-thermal line broadenings listed in Section 1.2, but with Doppler shifts which have velocity amplitudes of 3 - 7 km s^{-1} (Bruner, 1978; Athay and White, 1978; White and Athay, 1979). It is then evident from Equation (1.1) that the slow waves are unable to supply an adequate energy flux for even the smallest of the energy requirements. However, as Porter, Klimchuk and Sturrock (1994a) point out, Doppler shift measurements may greatly underestimate the values of v_{rms} since the measurements do not account for unresolved small-scale motions. Moreover, it must be emphasized that Athay and White (1978) indicate that their values may have been underestimated by at least a factor of 10 because the observational instrument suffered a decrease in sensitivity.

Many authors are also swift to reject heating by fast waves. Assuming the plasma pressure to be small compared with the magnetic pressure (i.e. assuming the low-beta approximation), the fast mode dispersion relation is approximately $\omega^2 \simeq k^2 v_A^2$ where ω is the angular frequency.. Splitting the wave number, k, into horizontal (h) and vertical (v) components Hollweg (1978) writes

$$k_{\rm v}^2 = \frac{\omega^2}{v_A^2} - k_{\rm h}^2. \tag{1.2}$$

He makes the point that ω and $k_{\rm h}$ are not free parameters but are determined by the structure for the known motions in the photosphere and corona. He further argues that, in the corona, v_A is large, and k_h is expected to be large if the horizontal spatial scale is associated with the distance between magnetic flux tubes. Hollweg conjectures that for reasonable vlaues of ω, $k_v^2 < 0$ and so fast mode waves in the corona should be evanescent. However, Hollweg himself states 'the complex structure of the solar atmosphere could alter this conclusion'. Thus, the simple argument suggesting the total internal reflection of waves is invalid in a structured atmosphere, and one must be wary of the negative results of wave-heating relating to studies carried out on unstructured atmospheres (e.g. Schwartz and Leroy, 1982).

Although Alfvén waves also have sufficient energy to heat the corona (see the earlier discussion concerning Equation (1.1)), there still remain the questions of how they are generated by

photospheric motions and how subsequently they can propagate into the corona. Thus there remains the more difficult question of how they surrender their energy before propagating into the solar wind or back down to the photosphere. Narain and Ulmschneider (1990, 1995) indicate that Alfvén-wave-dissipation mechanisms such as resonant absorption, phase-mixing, turbulent heating and nonlinear interactions are the more promising ways by which Alfvén waves may dissipate their energy.

The rough arguments outlined above do not take into account the fact that the corona is not a homogeneous medium but is highly structured, partitioned into subregions by, for example, coronal loops. So, surface (and body) waves would appear to be excellent candidates for coronal heating since they are supported by the inhomogeneities that characterize the solar corona. One can pose the question, 'Can the energy being carried by the ducted waves be converted into heat energy?', that is, are there effective mechanisms, at the appropriate frequencies, to dissipate the waves? Before addressing this question in Chapters 3 and 4, the effects, if any, that a structured medium has on the energy flux density of magnetohydrodynamic waves, are examined. However, this task is left until Section 2.3.

Habbal, Leer and Holzer (1979) put forward the idea that coronal loops are heated by the collisionless damping of fast-mode waves. By representing coronal loops by dipole fields and using ray-tracing techniques they show that waves propagating outwards from the coronal base are refracted into regions of low Alfvén speed (i.e. high density). Further, they suggest that collisional damping of such waves is important in the formation and heating of the loops. Zweibel (1980) considers damping of fast modes by collisionless wave-particle interactions, electron thermal conduction and viscosity. Zweibel calculates the period ranges for which each of the dissipative mechanisms is important. It is found that the fastest growing instability occurs perpendicular to the field lines and it is concluded that the instability is important for producing the observed fine structure in coronal loops. Flå *et al.* (1984) argue that Alfvén and slow waves, in the corona, are limited to transporting energy along the background magnetic field but fast modes can propagate in any direction relative to the background field (see Equations (1.32) and (1.36) and Figure 1.3). They suggest that fast-mode waves transport energy from magnetically closed regions to coronal holes by refraction and deposit most of their energy in the region of supersonic flow of high-speed solar wind streams.

A very popular and widely investigated heating mechanism for mhd surface waves is that of *resonant absorption*. Ionson (1978) begins his analysis from a set of strictly non-dissipative, ideal mhd equations and subsequently obtains a non-zero value for the damping rate. Lee (1980) recognised that there can be no true dissipation in the system, and has suggested along with Rae and Roberts (1981) and Lee and Roberts (1986) that the wave decay rate of the surface Alfvén wave should be interpreted as a mode-conversion rate because the decaying surface wave is associated with the smooth interface at the boundary of the loop and is not a normal mode of the system. As a result the decay rate should not be viewed as a dissipation rate. However Lee and Roberts and Hollweg (1987) interpret the mode conversion rate as a plasma heating rate in cases where

dissipative mechanisms are present – as they will be in any real-world situation.

Using an incompressible mhd approximation Steinolfson *et al.* (1986) studied analytically and numerically the viscous damping of Alfvén surface waves. They showed that the waves experience very small damping below the chromosphere-corona transition layer. Waves with a high frequency were found to decay in the lower corona while waves with a low frequency decayed further out in the corona. Further, Steinolfson *et al.* showed that damping by viscosity was about two orders of magnitude faster than by resistivity. Steinolfson and Davila (1993) investigate numerically for a compressible, low-β, resistive plasma the resonant absorption of Alfvén waves for the heating of active region coronal loops. They conclude that resonant absorption is an efficient heating process. Davila (1987) compares the results of the heating rate of the resonant absorption of Alfvén waves in the solar corona with observations and concludes that resonant absorption is an efficient heating mechanism. Grossmann and Smith (1988) have studied the effect of resonant absorption of Alfvén waves in a 'twisted' cylindrical coronal loop. They use an incident power spectrum in the form of 300 s oscillations and they found that the energy was principally deposited towards the outside of the loop. Their overall conclusion is that the resonant absorption of Alfvén waves is a very efficient heating mechanism. Poedts, Goossens and Kerner (1990) model coronal loops as straight cylindrical columns with the background quantities varying only in the radial direction. Their investigation found that most of the energy supplied by the external driver (the photosphere) was dissipated. Advances in the analytical study of resonant absorption, providing a clearer physical insight into the mechanism, have come from Sakurai, Goossens and Hollweg (1991), Goossens (1994) and Goossens, Ruderman and Hollweg (1995). It is also found that the time scale of the dissipation is much smaller than the typical life-time of coronal loops. From all these investigations concerning resonant absorption it certainly appears that resonant absorption is a viable coronal heating process.

Returning to the idea of phase-mixing, many authors claim that the process enhances the damping of Alfvén waves and is a viable mechanism for coronal heating. Basically the difference between phase-mixing and resonant absorption is that the former is concerned with Alfvén waves with velocity fluctuations perpendicular to the gradient of the inhomogeneity, but the latter requires displacements parallel to the inhomogeneity gradient. Nocera, Leroy and Priest (1984) develop further the work of Heyvaerts and Priest (1983) and conclude that the propagation of phase-mixed waves is actually more complicated than the simple treatment presented in the original paper by Heyvaerts and Priest. However, Nocera, Leroy and Priest do find that the statement by Heyvaerts and Priest regarding enhanced damping is still valid and that phase-mixing does give rise to very effective dissipation. Browning and Priest (1984) find that the velocity gradients may also be subject to Kelvin-Helmholtz instability which further enhances the damping of the Alfvén waves by viscosity or ohmic dissipation, thus providing a viable heating mechanism. Browning (1991) cautions that, in reality, phase-mixing cannot take place in isolation from other processes such as resonant absorption and turbulence. (Priest, 1992 has summarized coronal heating by mhd turbulence.)

Although wave-heating theories seem to be attractive and be able to provide the necessary

heating they still have their fierce critics, notably Parker (1987, 1990, 1992) who emphasises that the X-ray corona is not conducive to wave phenomena and the dissipation of any such waves plays only a small part. The many ideas involving non-wave theories are summarized in Narain and Ulmschneider (1990, 1995), Hollweg (1990), Browning (1991) and Zirker (1993).

1.5 Basic Equations of Magnetohydrodynamics

In describing the solar atmosphere (Section 1.1), the term *plasma* has been mentioned but no indication of its meaning has, as yet, been given. By the term *plasma*, one means the 'fourth' state of matter (the other states being solid, liquid and gas) in which the heating of a gas leads to ionization of the gas's molecules, or atoms, into its constituent neutral particles, ions and electrons (Sturrock, 1994). The term *magnetohydrodynamical* is understood to mean the study of fluid conductors in the presence of a magnetic field (Priest, 1982).

In adopting a *magnetohydrodynamic* (mhd) model to describe a plasma such as the solar atmosphere, several simplifying assumptions are made. First the plasma is regarded as a single fluid which, at each point in space, $\mathbf{r}(x, y, z)$, and at each time, t, has well-defined density, $\bar{\rho}$, pressure, $\bar{p}$, and velocity, $\bar{\mathbf{v}}$. Along with these hydrodynamical quantities is the magnetic induction field $\bar{\mathbf{B}}(\mathbf{r}, t)$. Secondly, a continuum description can be applied if the frequency, which is characteristic for the process under consideration, is appreciably smaller than the collision frequency of the separate particles. Put alternatively, the continuum description is valid if the mean free path of the particles is much smaller than a typical characteristic length scale of the object under study.

The idea of a continuum description of a plasma is well-known and is commonly used (see for example Ferraro and Plumpton, 1961; Roberts, 1967; Cowling, 1976; Parker, 1979; Priest, 1982; Sturrock, 1994). The equations of mhd (Priest, 1982) are the following (in SI units):

The equation of mass conservation is written

$$\frac{\partial \bar{\rho}}{\partial t} + \nabla \cdot (\bar{\rho}\bar{\mathbf{v}}) = 0. \tag{1.3}$$

The equation of motion is given by

$$\bar{\rho}\left(\frac{\partial \bar{\mathbf{v}}}{\partial t} + \bar{\mathbf{v}} \cdot \nabla \bar{\mathbf{v}}\right) = -\nabla \bar{p} + \bar{\mathbf{j}} \times \bar{\mathbf{B}} + \mathbf{F}_v, \tag{1.4}$$

where $\bar{\mathbf{j}} \times \bar{\mathbf{B}}$ is the Lorentz force and $\mathbf{F}_v$ represents the effects of viscosity.

The current density, $\bar{\mathbf{j}}$, is calculated from Ampère's Law:

$$\bar{\mathbf{j}} = \frac{1}{\mu} \nabla \times \bar{\mathbf{B}}, \tag{1.5}$$

where μ is the permeability of free space ($4\pi \times 10^{-7}$ H m^{-1}).

One of Maxwell's Equations, namely,

$$\nabla \cdot \bar{\mathbf{B}} = 0, \tag{1.6}$$

requires that the magnetic induction field is solenoidal (i.e. there are no magnetic monopoles).

The electric field, $\bar{\mathbf{E}}$, may be calculated by using Ohm's Law in the form:

$$\bar{\mathbf{E}} = \bar{\mathbf{j}}/\sigma - \bar{\mathbf{v}} \times \bar{\mathbf{B}}, \tag{1.7}$$

where σ is the (constant) electrical conductivity, measured in mho m^{-1}. For a fully ionized collision-dominated plasma, Priest (1982) gives the electrical conductivity as

$$\sigma = 1.53 \times 10^{-2} \frac{T^{3/2}}{\ln \Lambda_{cl}}, \tag{1.8}$$

where T is the temperature (in K) and $\ln \Lambda_{cl}$ is the Coulomb logarithm. Typically in the solar corona $\ln \Lambda_{cl} \approx 22$ for 10^6 K temperatures (Priest, 1982), and thus it is seen from Equation (1.8) that, in the corona, σ may range from 6.95×10^5 to 3.61×10^6 mho m^{-1} for temperatures ranging from $1 \times 10^6 - 3 \times 10^6$ K.

Using $\bar{\mathbf{j}}$ and $\bar{\mathbf{E}}$ (Equations (1.5) and (1.7)), one can write the Maxwell Equation

$$\frac{\partial \bar{\mathbf{B}}}{\partial t} = -\nabla \times \bar{\mathbf{E}}, \tag{1.9}$$

as the *mhd induction* equation:

$$\frac{\partial \bar{\mathbf{B}}}{\partial t} = \nabla \times (\bar{\mathbf{v}} \times \bar{\mathbf{B}}) + \bar{\eta} \nabla^2 \bar{\mathbf{B}}, \tag{1.10}$$

where $\bar{\eta} = 1/(\mu\sigma)$ is the magnetic diffusivity measured in $m^2\ s^{-1}$. From Equation (1.8) it is seen that $\bar{\eta}$ may typically range from 0.22 to 1.14 $m^2\ s^{-1}$ in the corona.

Many authors have considered different forms for the energy equation, see, for example, Braginskii (1965), Field (1965), Cowling (1976), Priest (1982) and Sturrock (1994). The energy equation given by Priest (1982) is

$$\frac{\partial \bar{p}}{\partial t} + \bar{\mathbf{v}} \cdot \nabla \bar{p} - \gamma \frac{\bar{p}}{\bar{\rho}} \left(\frac{\partial \bar{\rho}}{\partial t} + \bar{\mathbf{v}} \cdot \nabla \bar{\rho} \right) = -(\gamma - 1) L, \tag{1.11}$$

where $\gamma = 5/3$ is the ratio of specific heats and L is the energy loss function, which may be written as the rate of energy loss minus the rate of energy gain. Equation (1.11) will be discussed in detail in Chapter 2 but it is noted here that when there are no dissipative mechanisms present, $L = 0$.

For simplicity, the plasma is assumed to obey the ideal gas law

$$\bar{p} = \frac{\tilde{R}}{\tilde{\mu}} \bar{\rho} \bar{T}, \tag{1.12}$$

where $\bar{T}$ is the temperature, $\tilde{R}$ is the gas constant ($8.30 \times 10^3\ m^2\ s^{-2} K^{-1}$) and $\tilde{\mu} = m/m_p$ is the mean atomic weight in terms of the mean particle mass, m, and the proton mass, m_p (1.67×10^{-27} kg).

By replacing $\bar{\rho} = \tilde{\mu}\, m_p \bar{N} = m\bar{N}$ and $\tilde{R} = k_B/m_p$, where k_B is the Boltzmann constant (1.38×10^{-23} J K^{-1}) in Equation (1.12), then for a fully-ionized hydrogen plasma, in terms of the

total number of particles (electrons plus protons), $\bar{N} = \bar{N}_{el} + \bar{N}_p$, per unit volume, the ideal gas law becomes

$$\bar{p} = \bar{N} k_B \bar{T}. \tag{1.13}$$

The *ideal* mhd equations, in which the dissipative effects in Equations (1.4), (1.7), (1.10) and (1.11) are neglected, will be employed for the remainder of this chapter. In brief, the ideal equations of mhd are Equations (1.3), (1.6) and (1.12) together with:
the ideal momentum equation,

$$\bar{\rho}\left(\frac{\partial \bar{\mathbf{v}}}{\partial t} + \bar{\mathbf{v}} \cdot \nabla \bar{\mathbf{v}}\right) = -\nabla\left(\bar{p} + \frac{\bar{B}^2}{2\mu}\right) + \frac{1}{\mu}\left(\bar{\mathbf{B}} \cdot \nabla\right)\bar{\mathbf{B}}, \tag{1.14}$$

which may be derived using Equation (1.4) with $\mathbf{F}_v = \mathbf{0}$ together with (1.5) and a vector identity;
the adiabatic energy equation,

$$\frac{\partial \bar{p}}{\partial t} + \bar{\mathbf{v}} \cdot \nabla \bar{p} - \gamma \frac{\bar{p}}{\bar{\rho}}\left(\frac{\partial \bar{\rho}}{\partial t} + \bar{\mathbf{v}} \cdot \nabla \bar{\rho}\right) = 0; \tag{1.15}$$

and the ideal mhd induction equation,

$$\frac{\partial \bar{\mathbf{B}}}{\partial t} = \nabla \times \left(\bar{\mathbf{v}} \times \bar{\mathbf{B}}\right). \tag{1.16}$$

In writing the Lorentz $(\bar{\mathbf{j}} \times \bar{\mathbf{B}})$ force as

$$\bar{\mathbf{j}} \times \bar{\mathbf{B}} = -\nabla\left(\frac{\bar{B}^2}{2\mu}\right) + \frac{1}{\mu}(\bar{\mathbf{B}} \cdot \nabla)\bar{\mathbf{B}}, \tag{1.17}$$

in the right-hand side of Equation (1.4), it is seen that it has two important contributions:

1. The first contribution is the term $-\nabla(\bar{B}^2/(2\mu))$ which is analogous to the gas pressure gradient $-\nabla\bar{p}$. Hence, the presence of a magnetic field in a plasma gives rise to a magnetic pressure force, in addition to the natural fluid pressure, p, of the plasma. An important parameter relating compressible and magnetic effects is the plasma beta, β, which is defined as the ratio:

$$\beta = \frac{\text{gas pressure}}{\text{magnetic pressure}} = \frac{\bar{p}}{\bar{B}^2/2\mu}. \tag{1.18}$$

The plasma beta provides a convenient guide as to whether magnetic effects are weak ($\beta \gg 1$), as is the case in the solar interior, or strong ($\beta \ll 1$), as in the corona.

2. The second contribution, namely $(\bar{\mathbf{B}} \cdot \nabla)\bar{\mathbf{B}}/\mu$, corresponds to a tension force which acts in a direction parallel to the magnetic field. Thus a magnetic field-line is like an elastic wire under tension, and if it is disturbed at some point, it behaves like an elastic wire and springs back, vibrating with a wave-like motion. So, waves can be associated with a magnetic field, both through the magnetic tension force and through the magnetic pressure force.

Thus, from just a theoretical view of the plasma of the solar atmosphere, waves are worthy of consideration, since it is clear that magnetic pressure and tension forces can help sustain any wave motion.

1.6 Wave Propagation in an Unstructured Atmosphere

In order to describe mhd wave motion in the solar atmosphere, we must ultimately take into account the observed magnetic structuring. Eventually we shall consider simple models of the solar atmosphere for magnetic field configurations such as those shown in Figures 1.2 A, B, C and D, for example. However, in order to get a flavour for the physics we are trying to understand, we shall first give consideration to waves propagating in an atmosphere which is both uniform and unstructured.

Consider, then, a uniform magnetic field embedded in a uniform gas which has the (constant) equilibrium state:

$$\mathbf{B} = B_0\hat{\mathbf{z}},\ p = p_0,\ \rho = \rho_0,\ \mathbf{v} = \mathbf{0}. \tag{1.19}$$

The background magnetic field is assumed to be directed in only the z-direction. Further, only waves propagating in the direction of the background magnetic field will be assumed here. Since we shall be concerned with motions in the upper solar atmosphere, gravitational effects will be ignored.

A Cartesian coordinate system (x, y, z) orientated with the z-axis aligned along the background equilibrium magnetic field is assumed.

In order to investigate wave motions, the equilibrium state (1.19) is perturbed and the behaviour of the perturbations is considered. If ρ, p, $\mathbf{b}$ and $\mathbf{v}$ are small perturbations in density, pressure, magnetic induction and velocity fields respectively, about corresponding equilibrium values, so that

$$\bar{\rho} = \rho_0 + \rho,\ \bar{p} = p + p_0,\ \bar{\mathbf{B}} = B_0\hat{\mathbf{z}} + \mathbf{b} \text{ and } \bar{\mathbf{v}} = \mathbf{v}, \tag{1.20}$$

then substituting in Equations (1.3), (1.6), (1.14), (1.15) and (1.16) and then linearizing by neglecting the products and squares of the perturbed quantities, we arrive at the linearized equations of ideal mhd:

$$\frac{\partial \rho}{\partial t} + \rho_0\Delta = 0, \tag{1.21}$$

where, following Lighthill (1960), we have written

$$\Delta = \nabla\cdot\mathbf{v} = \frac{\partial v_x}{\partial x} + \frac{\partial v_y}{\partial y} + \frac{\partial v_z}{\partial z},$$

and in which

$$\nabla = \left(\frac{\partial}{\partial x}, \frac{\partial}{\partial y}, \frac{\partial}{\partial z}\right),$$

and the velocity, $\mathbf{v} = (v_x, v_y, v_z)$, and

$$\rho_0\frac{\partial \mathbf{v}}{\partial t} = -\nabla\left(p + \frac{B_0 b_z}{\mu}\right) + \frac{B_0}{\mu}\frac{\partial \mathbf{b}}{\partial z}, \tag{1.22}$$

$$\nabla \cdot \mathbf{b} = 0, \tag{1.23}$$

$$\frac{\partial \mathbf{b}}{\partial t} = -\Delta B_0 \hat{\mathbf{z}} + B_0 \frac{\partial \mathbf{v}}{\partial z}, \tag{1.24}$$

$$\frac{\partial p}{\partial t} = c_0^2 \frac{\partial \rho}{\partial t}, \tag{1.25}$$

where

$$c_0^2 = \gamma \frac{p_0}{\rho_0}$$

and

$$p = \frac{\tilde{R}}{\tilde{\mu}} \rho T_0 + \frac{\tilde{R}}{\tilde{\mu}} \rho_0 T. \tag{1.26}$$

In Equation (1.26), T_0 denotes the background temperature and it is seen from Equation (1.12) that T_0 is related to the background pressure and density by

$$p_0 = \frac{\tilde{R}}{\tilde{\mu}} \rho_0 T_0.$$

Then, after some manipulation, Equations (1.21) to (1.25) may be written as the *magnetoacoustic wave equation* (Lighthill, 1960):

$$\frac{\partial^4 \Delta}{\partial t^4} - (c_0^2 + v_A^2) \frac{\partial^2 \nabla^2 \Delta}{\partial t^2} + c_0^2 v_A^2 \frac{\partial^2 \nabla^2 \Delta}{\partial z^2} = 0, \tag{1.27}$$

where v_A is the Alfvén speed given by

$$v_A = \frac{B_0}{(\mu \rho_0)^{1/2}}, \tag{1.28}$$

and c_0 is the sound speed given by

$$c_0 = \left(\gamma \frac{p_0}{\rho_0} \right)^{1/2}. \tag{1.29}$$

Following Roberts (1988) it is seen that one solution of Equation (1.27) is $\Delta = 0$, i.e. $\nabla \cdot \mathbf{v} = 0$. This is *not* a trivial solution but corresponds to the *Alfvén wave*. Close examination of Equations (1.21) to (1.25) reveals that $\rho = p = v_z = b_z = 0$. Thus an Alfvén wave is incompressible, there is no perturbation in density, gas or magnetic ($B_0 b_z / \mu$) pressure, and there is no wave motion in the direction of the background magnetic field. Moreover, it is seen that the perturbations in the magnetic field and flow are perpendicular to the background magnetic field, and from Equations (1.22) and (1.24), it is clear that the Alfvén wave satisfies the one-dimensional wave equation

$$\frac{\partial^2 \Psi}{\partial t^2} = v_A^2 \frac{\partial^2 \Psi}{\partial z^2}, \tag{1.30}$$

for Ψ any one of v_x, v_y, b_x or b_y.

In very simple terms the Alfvén wave is like a wave propagating on an elastic string. It involves no compressions of the plasma, and since the *perturbed* total (gas plus magnetic) pressure is zero, the wave is driven entirely by tension forces.

Considering, more generally for the moment, waves propagating with wave number vector $\mathbf{k} = (k_x, k_y, k_z)$ (and not just confined to the direction of the background magnetic field) then introducing the Fourier representation for wave motions by writing

$$\Psi = \Psi_0 e^{i(\omega t - \mathbf{k}\cdot\mathbf{r})} \tag{1.31}$$

for angular frequency, ω, and constant wave amplitude, Ψ_0, into Equation (1.30), gives the dispersion relation for Alfvén waves:

$$\omega^2 = k_z^2 v_A^2 = k^2 cos^2(\theta) v_A^2, \tag{1.32}$$

where θ is the angle between the wave number vector, $\mathbf{k}$, and the background magnetic field $B_0\hat{\mathbf{z}}$. The highly anisotropic nature of the Alfvén wave is seen in Equation (1.32) and it is noted that the Alfvén wave is unable to propagate across magnetic field lines ($\theta = \pi/2$) (see also Figure 1.3.) Note that when the wave number vector is entirely in the direction of the background magnetic field Equation (1.32) simply becomes

$$\omega^2 = k^2 v_A^2. \tag{1.33}$$

Consider now the case $\Delta \neq 0$ of Equation (1.27). Introducing the Fourier representation

$$\Delta = \Delta_0 e^{i(\omega t - \mathbf{k}\cdot\mathbf{r})}, \tag{1.34}$$

where Δ_0 is a constant amplitude, into Equation (1.27) (and noting that $\partial^2/\partial t^2 \rightarrow -\omega^2, \nabla^2 \rightarrow -k^2$) yields the dispersion relation for magnetoacoustic waves (Roberts, 1988):

$$\omega^4 - (c_0^2 + v_A^2)\omega^2 k^2 + c_0^2 v_A^2 k^2 k_z^2 = 0. \tag{1.35}$$

Equation (1.35) is a quadratic in ω^2 and it can be solved for fixed k but varying θ, where θ is again the angle between the wave number vector, $\mathbf{k}$, and the background magnetic field, to obtain

$$\frac{\omega^2}{k^2} = \frac{1}{2}(c_0^2 + v_A^2) \stackrel{+}{-} \left[(c_0^2 + v_A^2)^2 - 4c_0^2 v_A^2 \cos^2(\theta)\right]^{1/2}. \tag{1.36}$$

The two solutions of Equation (1.36) are referred to as the *fast magnetoacoustic wave* and the *slow magnetoacoustic wave*. It is noted that both these waves are compressive. From Figure 1.3 it is seen that the fast wave is only mildly anisotropic. It propagates at all angles θ and has its greatest phase speed when propagating across the magnetic field. It is also apparent that the slow wave is highly anisotropic and, like the Alfvén wave, it, too, is unable to propagate across the background magnetic field. The low-β extreme of Equation (1.36) for the fast magnetoacoustic wave gives

$$\omega^2 \simeq k^2 v_A^2, \tag{1.37}$$

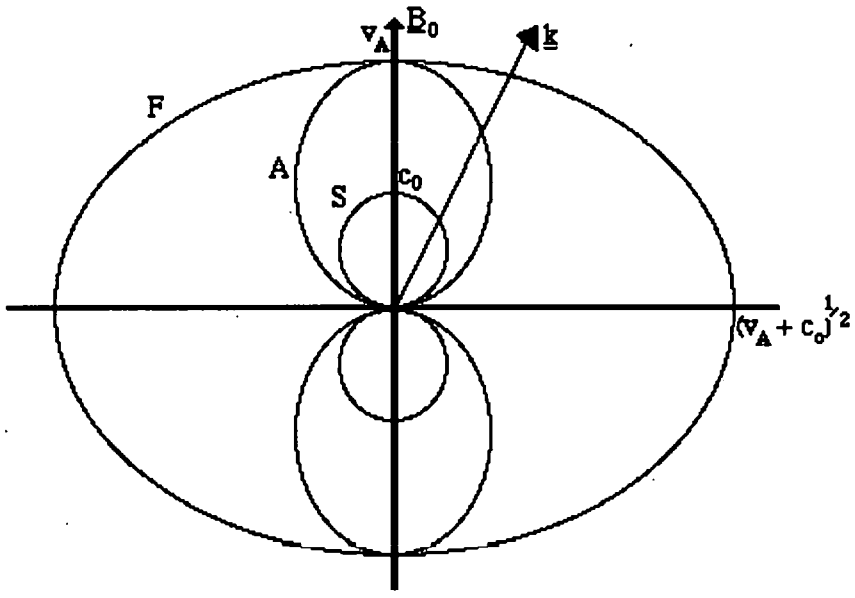

Figure 1.3: Polar diagram for the phase velocities for the fast (F) and slow (S) magnetoacoustic waves and the Alfvén (A) wave propagating at an angle θ to the equilibrium magnetic field, $\mathbf{B}_0$ (after Roberts, 1985).

and for the slow wave gives

$$\omega^2 = \simeq k^2 \cos^2(\theta) c_T^2 = k_z^2 c_T^2, \tag{1.38}$$

where the *magnetoacoustic cusp speed*, c_T, is defined by

$$c_T^2 = \frac{c_0^2 v_A^2}{c_0^2 + v_A^2}. \tag{1.39}$$

Hence, in a low-β plasma, the fast magnetoacoustic wave propagates at the Alfvén speed and is essentially isotropic, but it is emphasized that it is quite distinct from the (incompressible) Alfvén wave. The slow wave propagates one-dimensionally approximately at the sound speed in the direction of the background magnetic field.

In summary, it is seen that the presence of a unidirectional magnetic field in a uniform medium introduces anisotropy into the wave motions. Along with the isotropic sound wave there is the incompressible Alfvén wave which propagates at the speed v_A. Also, there is the slow magnetoacoustic wave, which like the Alfvén wave, is unable to propagate across the magnetic field. Additionally, there is the fast magnetoacoustic wave which is able to propagate in all directions. Both the fast and slow magnetoacoustic waves are driven by tension and pressure forces.

Model	B (G)	N (cm^{-3})	T (K)	a (cm)	ρ_e/ρ_0
A	10	1.0×10^{10}	2.0×10^6	5.0×10^8	0.50
B	10	5.0×10^9	2.0×10^6	1.0×10^8	0.50
C	10	1.5×10^{10}	1.4×10^6	1.0×10^8	0.25
D	10	1.5×10^{10}	1.9×10^6	1.0×10^8	0.25
E	10	1.0×10^{10}	2.0×10^6	1.0×10^8	0.25
F	10	1.0×10^{10}	2.5×10^6	1.0×10^8	0.25
G	100	1.0×10^{11}	3.0×10^6	5.0×10^8	0.50

Table 1.7: Parameters used in this thesis to model hot coronal loops.

T (K)	B (G)	N (cm^{-3})		
		5.0×10^8	5.0×10^9	5.0×10^{10}
1.0×10^6	10	*CH/QR*	*CH/QR*	
	50	*HL*	*HL*	
	100	*HL*	*HL*	
2.0×10^6	10	*CH/QR*	*CH/QR*	
	50	*HL*	*HL*	*HL*
	100	*HL*	*HL*	*HL*
3.0×10^6	50	*HL*	*HL*	*HL*
	100	*HL*	*HL*	*HL*

Table 1.8: Broad classification of typical solar coronal parameter ranges into hot coronal loops (*HL*), quiet region loops (*QR*) and coronal holes (*CH*).

1.7 Wave Propagation in a Structured Atmosphere

We now consider how the density enhancements of coronal loops might modify the effects of mhd waves in an unstructured medium.

To model the loop-like structures observed in the corona (Figure 1.2, Tables 1.1 to 1.4) we consider a coronal loop represented by a dense duct in a homogeneous corona. In other words, the loop is considered as a slab or a cylinder with background magnetic field, $\mathbf{B}_0$, in which the coronal plasma contained inside the duct (with density ρ_0 and of width $2a$) is more dense than the surrounding (external) coronal plasma which has magnetic field $\mathbf{B}_e$ and density ρ_e. Further, we shall assume that the magnetic field is directed along the length of the slab or cylinder. In modelling the loop as a slab (cylinder), we shall ignore any effects due to curvature. Table 1.7 lists the parameters used in this thesis to model hot coronal loops and Table 1.8 indicates the typical parameter ranges for hot coronal loops, quiet region loops and coronal holes.

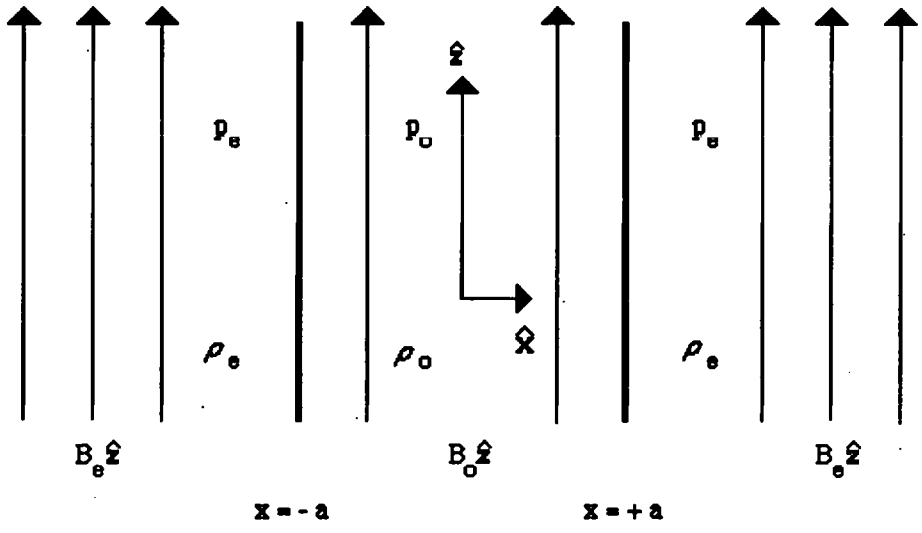

Figure 1.4: Equilibrium configuration of a magnetic slab.

1.7.1 Structuring in a Cartesian Geometry

A slab of uniform magnetic field $B_0\hat{\mathbf{z}}$, confined to a region $|x| < a$, where the gas pressure and density are p_0 and ρ_0 respectively, is now considered. In the region $|x| > a$ the magnetic field, gas pressure and density (all uniform) are $B_e\hat{\mathbf{z}}$, p_e and ρ_e (see Figure 1.4). Thus the equilibrium state may be described by

$$\rho_0(x),\ p_0(x),\ \mathbf{B}_0(x), T_0(x) = \begin{cases} \rho_0,\ p_0,\ \mathbf{B}_0,\ T_0, & |x| < a, \\ \rho_e,\ p_e,\ \mathbf{B}_e,\ T_e, & |x| > a, \end{cases} \tag{1.40}$$

in which the background temperature, $T_0(x)$, is determined from the ideal gas law (1.12).

Consider two-dimensional velocity disturbances, $\mathbf{v}$, of the form

$$\mathbf{v} = (v_x, 0, v_z),\ v_x = \hat{v}_x(x)e^{i(\omega t + kz)},\ v_z = \hat{v}_z(x)e^{i(\omega t + kz)}, \tag{1.41}$$

where k is the wave number in the $\hat{\mathbf{z}}$ direction and ω is the angular frequency. Then, from the linearized momentum equation (1.22), it is seen that the total (gas plus magnetic) pressure, p_T, is uniform:

$$\frac{d}{dx}\left(p_0(x) + \frac{B_0^2(x)}{2\mu}\right) = 0, \tag{1.42}$$

that is

$$p_0 + \frac{B_0^2}{2\mu} = p_e + \frac{B_e^2}{2\mu}. \tag{1.43}$$

Edwin and Roberts (1982) showed that linear perturbations about the equilibrium (1.40) give the following equation for the uniform region $|x| < a$:

$$\frac{d^2\hat{v}_x}{dx^2} - m_0^2\hat{v}_x = 0, \tag{1.44}$$

where

$$m_0^2 = \frac{(k^2c_0^2 - \omega^2)(k^2v_A^2 - \omega^2)}{(c_0^2 + v_A^2)(k^2c_T^2 - \omega^2)}. \tag{1.45}$$

A similar set of equations holds in the uniform region $|x| > a$, namely:

$$\frac{d^2\hat{v}_x^e}{dx^2} - m_e^2\hat{v}_x^e = 0, \tag{1.46}$$

where

$$m_e^2 = \frac{(k^2c_e^2 - \omega^2)(k^2v_{Ae}^2 - \omega^2)}{(c_e^2 + v_{Ae}^2)(k^2c_{Te}^2 - \omega^2)}, \tag{1.47}$$

with

$$c_{Te}^2 = \frac{c_e^2v_{Ae}^2}{c_e^2 + v_{Ae}^2}, \tag{1.48}$$

and the Alfvén and sound speeds in this external region given by

$$v_{Ae} = \frac{B_e}{(\mu\rho_e)^{1/2}}, \tag{1.49}$$

and

$$c_e = \left(\gamma\frac{p_e}{\rho_e}\right)^{1/2}, \tag{1.50}$$

respectively.

Further, using the linearized equations (1.21), (1.22), (1.24) and (1.26), Webb (1980) showed that the perturbed quantities **v**, **b**, ρ and p_T, the total (gas plus magnetic) pressure in the interior, satisfy

$$v_x = \frac{-ikc_0^2}{(\omega^2 - k^2c_0^2)}\frac{d}{dx}\hat{v}_x e^{i(\omega t + kz)}, \tag{1.51}$$

$$b_x = B_0\frac{k}{\omega}v_x, \tag{1.52}$$

$$b_z = -\frac{B_0}{\omega}\frac{(\omega^2 - k^2c_0^2)}{kc_0^2}v_x, \tag{1.53}$$

$$p = -\rho_0\frac{\omega}{k}v_x, \tag{1.54}$$

and

$$p_T = \frac{\rho_0}{\omega kc_0^2}(c_0^2 + v_A^2)(k^2c_T^2 - \omega^2)v_x. \tag{1.55}$$

Similar expressions are obtained for $|x| > a$, namely:

$$v_x^e = \frac{-ikc_e^2}{(\omega^2 - k^2c_e^2)}\frac{d}{dx}\hat{v}_x^e e^{i(\omega t + kz)}, \tag{1.56}$$

$$b_x^e = B_e\frac{k}{\omega}v_x^e; \tag{1.57}$$

$$b_x^e = -\frac{B_e}{\omega}\frac{(\omega^2 - k^2c_e^2)}{kc_e^2}v_x^e; \tag{1.58}$$

$$p^e = -\rho_e\frac{\omega}{k}v_x^e; \tag{1.59}$$

and

$$p_T^e = \frac{\rho_e}{\omega k c_e^2}(c_e^2 + v_{Ae}^2)(k^2c_{Te}^2 - \omega^2)v_x^e. \tag{1.60}$$

In general solving Equations (1.44) and (1.46) results in

$$\hat{v}_x = \begin{cases} \alpha_e e^{m_e(x+a)}, & x < -a, \\ \alpha_0\cosh(m_0x) + \beta_0\sinh(m_0x), & |x| < a, \\ \beta_e e^{-m_e(x-a)}, & x > a, \end{cases} \tag{1.61}$$

where α_0, β_0, α_e and β_e are arbitrary constants and are related by requiring that v_x and p_T are continuous across $x = a$ and $x = -a$. In writing the solutions of Equation (1.61) Edwin and Roberts (1982) assumed that $m_e > 0$ so that $\hat{v}_x^e \to 0$ as $|x| \to \infty$ and the energy of the disturbance is essentially confined to the interior of the slab. Thus we are confining attention to disturbances that are evanescent in the region $|x| > a$ and so the dense coronal loop may be viewed as acting as a waveguide.

By matching the normal component of velocity, Equation (1.61), and the total pressure, Equations (1.55) and (1.60), across $x = \pm a$, Edwin and Roberts (1982) obtained the dispersion relation governing disturbances in a slab of magnetic field $B_0\hat{z}$ embedded in an external field $B_e\hat{z}$ as:

$$\rho_e(k^2v_{Ae}^2 - \omega^2)m_0\left\{\begin{array}{c}\tanh\\ \coth\end{array}\right\}(m_0a) + \rho_0(k^2v_A^2 - \omega^2)m_e = 0, \tag{1.62}$$

where the tanh term corresponds to the sinh (symmetric) and the coth term corresponds to the cosh (asymmetric) solutions in Equation (1.61).

Edwin and Roberts (1982) and Edwin (1984) have discussed, in detail, the rich spectrum of solutions that dispersion relation (1.62) possesses. The solutions of interest to us are those appropriate to a model of the dense coronal loops described in Section 1.1.

The quantity m_0^2 may be positive or negative. Roberts (1981) classifies solutions in Equation (1.61) with $m_0^2 > 0$ as *surface* waves and solutions with $m_0^2(\equiv -n_0^2) < 0$ as *body* waves. The distinction relates only to the waves' spatial structure within the slab. Putting $n_0^2 = -m_0^2$ in Equation (1.62), it is seen that body modes satisfy the dispersion relation

$$\rho_e(k^2v_{Ae}^2 - \omega^2)n_0\left\{\begin{array}{c}-\tan\\ \cot\end{array}\right\}(n_0a) + \rho_0(k^2v_A^2 - \omega^2)m_e = 0. \tag{1.63}$$

So considering the case $v_{Ae}, v_A > c_e, c_0$, and one in which the interior of the slab is denser than its surroundings, it is found that there are no surface ($m_0^2 > 0$) waves but only harmonics

which are confined to two bands $v_A < \omega/k < v_{Ae}$ and $c_T < \omega/k < c_{Te}$ (see Figure 1.5). These bands of body waves ($m_0^2 = -n_0^2 < 0$) correspond to the *fast* and *slow* magnetoacoustic waves of the unstructured atmosphere. The horizontal lines (— — —) in Figure 1.5 represent the cut-offs at $\omega/kv_A = v_{Ae}/v_A$, 1, c_{Te}/v_A and c_T/v_A, respectively.

Additionally, waves are classified as *sausage* modes (- - - in Figure 1.5) or *kink* modes (— in Figure 1.5) depending upon whether $\hat{v}_x$ in Equation (1.61) is an odd or even function of x respectively. In the former case the slab undergoes symmetric oscillations and in the latter the slab oscillates asymmetrically. More specifically, the sausage, or symmetric, mode solutions in Equation (1.61) under coronal conditions may be written as

$$\hat{v}_x = \begin{cases} -\alpha_s \sin(n_0 a) e^{m_e(x+a)}, & x < -a, \\ \alpha_s \sin(n_0 x), & |x| < a, \\ \alpha_s \sin(n_0 a) e^{-m_e(x-a)}, & x > a, \end{cases} \tag{1.64}$$

and the kink, or asymmetric, solutions in Equation (1.61) as

$$\hat{v}_x = \begin{cases} \alpha_k \cos(n_0 a) e^{m_e(x+a)}, & x < -a, \\ \alpha_k \cos(n_0 x), & |x| < a, \\ \alpha_k \cos(n_0 a), e^{-m_e(x-a)} & x > a, \end{cases} \tag{1.65}$$

where α_s and α_k are the (constant) amplitudes of the respective velocity perturbations.

Figure 1.6 shows the two lowest modes of oscillation for asymmetric and symmetric waves of a magnetic slab, in which the modes have been normalised against axial values. It is clear that the axis of symmetry of the slab remains undisturbed for the sausage wave (Roberts, 1985, makes the analogy with a 'pulsating blood vessel') and that in the kink wave case, the slab's axis is moved back and forth during the wave motion.

Defining the root-mean-square-velocity, v_{rms} (an observable quantity) over the interior of the slab by

$$v_{rms} = \left[\frac{1}{2a} \int_{x=-a}^{x=a} \left(\hat{v}_x^2(x) + \hat{v}_z^2(x) \right) dx \right]^{1/2}, \tag{1.66}$$

where $\hat{v}_x(x)$ is given by Equations (1.64) or (1.65) and $\hat{v}_z(x)$ is given by (1.51), with $\hat{v}_z$ related to v_z by Equation (1.41). Then using Equations (1.64) and (1.66) gives

$$\alpha_s^2 = \frac{2m_e a v_{rms}^2}{f_{s1} + k^2 c_0^4 f_{s2}}, \tag{1.67}$$

where

$$f_{s1} = m_e a - \frac{m_e}{2n_0} \sin(2n_0 a), \tag{1.68}$$

and

$$f_{s2} = \frac{n_0^2}{(\omega^2 - k^2 c_0^2)^2} \left(m_e a + \frac{m_e}{2n_0} \sin(2n_0 a) \right). \tag{1.69}$$

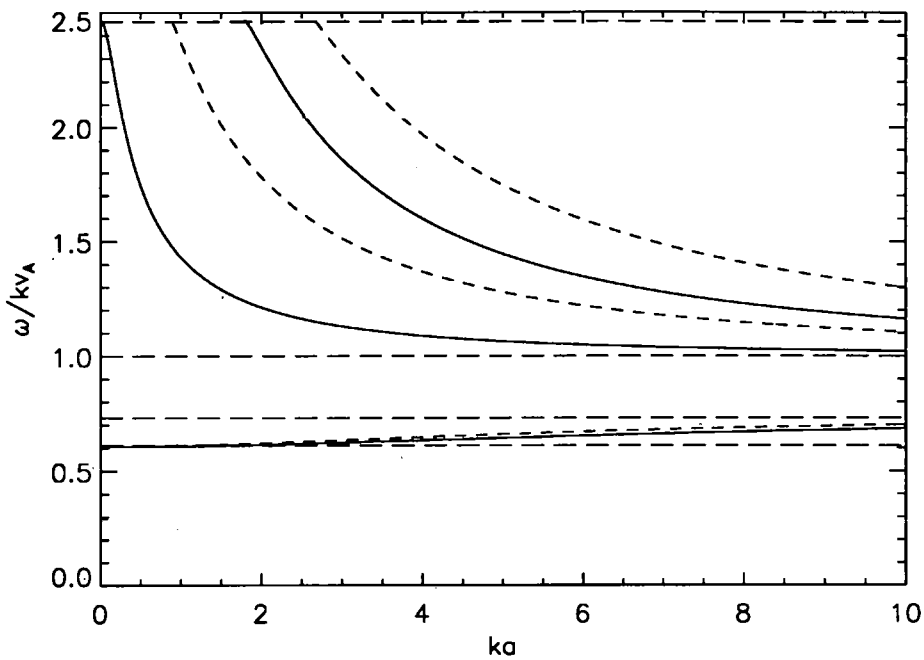

Figure 1.5: The normalized phase-speed ω/kv_A as a function of ka under coronal conditions for a slab model (after Edwin and Roberts, 1982).

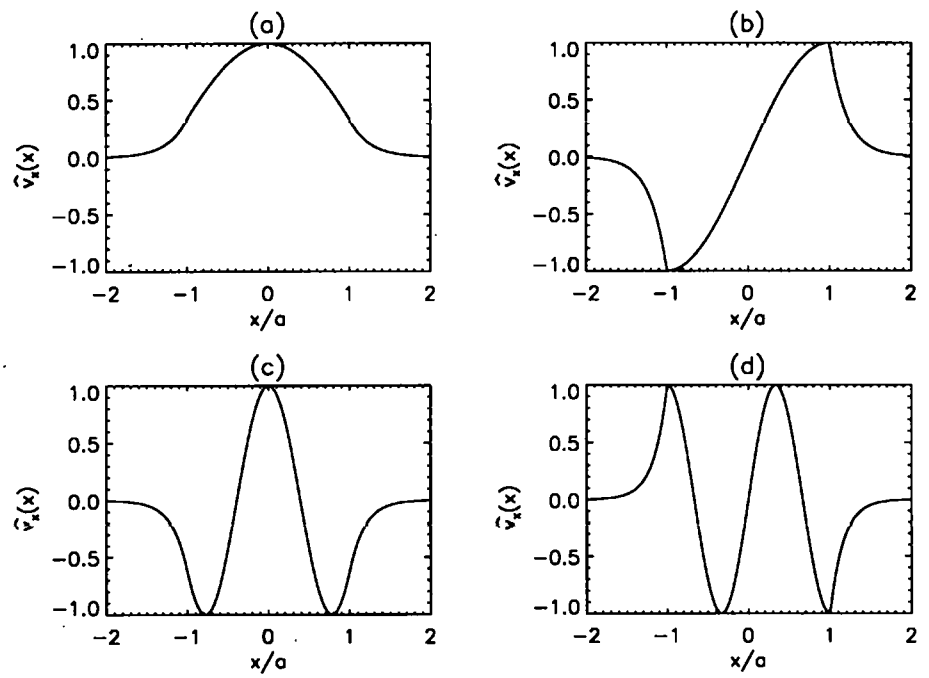

Figure 1.6: Body modes in a slab of width $2a$ (a) lowest-order kink mode (b) lowest-order sausage mode (c) first-order kink mode (d) first-order sausage mode.

for the sausage case.

Similarly, integrating Equation (1.66) for the kink waves gives

$$\alpha_k^2 = \frac{2m_e a v_{rms}^2}{f_{s3} + k^2 c_0^4 f_{s4}}, \tag{1.70}$$

where

$$f_{s3} = m_e a + \frac{m_e}{2n_0}\sin(2n_0 a), \tag{1.71}$$

and

$$f_{s4} = \frac{n_0^2}{(\omega^2 - k^2 c_0^2)^2}\left(m_e a - \frac{m_e}{2n_0}\sin(2n_0 a)\right). \tag{1.72}$$

1.7.2 Structuring in a Cylindrical Geometry

A cylinder of uniform magnetic field $B_0\hat{\mathbf{z}}$, confined to a region $r < a$, where the gas pressure and density are p_0 and ρ_0 respectively, is considered. In the region $r > a$ the magnetic field, gas pressure and density are $B_e\hat{\mathbf{z}}$, p_e and ρ_e (see Figure 1.7). Thus the equilibrium state may be described by

$$\rho_0(r),\ p_0(r),\ \mathbf{B}_0(r),\ T_0(r) = \begin{cases} \rho_0,\ p_0,\ \mathbf{B}_0,\ T_0, & r < a, \\ \rho_e,\ p_e,\ \mathbf{B}_e,\ T_e, & r > a, \end{cases} \tag{1.73}$$

in which the background temperature, $T_0(r)$, is determined from the ideal gas law (1.12).

We shall consider disturbances of the form

$$\nabla \cdot \mathbf{v} = \hat{R}(r)e^{i(\omega t + n\theta + kz)}, \tag{1.74}$$

where $\mathbf{v} = (v_r, v_\theta, v_z)$, ω is the angular frequency, n is the azimuthal wave number and k is the wave number in the $\hat{\mathbf{z}}$ direction. From the linearized momentum equation (1.22), it is seen that the total (gas plus magnetic) pressure, p_T, is uniform:

$$\frac{d}{dr}\left(p_0(r) + \frac{B_0^2(r)}{2\mu}\right) = 0, \tag{1.75}$$

and so Equation (1.43) again applies. Edwin and Roberts (1983) showed that linear perturbations about the equilibrium (1.73) give, in the uniform region inside the cylinder, the following Bessel equation of order n

$$\frac{d^2\hat{R}(r)}{dr^2} + \frac{1}{r}\frac{d\hat{R}(r)}{dr} - \left(m_0^2 + \frac{n^2}{r^2}\right)\hat{R}(r) = 0 \tag{1.76}$$

where m_0^2 is given by Equation (1.45).

A similar set of equations holds in the external region $r > a$, namely:

$$\frac{d^2\hat{R}^e(r)}{dr^2} + \frac{1}{r}\frac{d\hat{R}^e(r)}{dr} - \left(m_e^2 + \frac{n^2}{r^2}\right)\hat{R}^e(r) = 0 \tag{1.77}$$

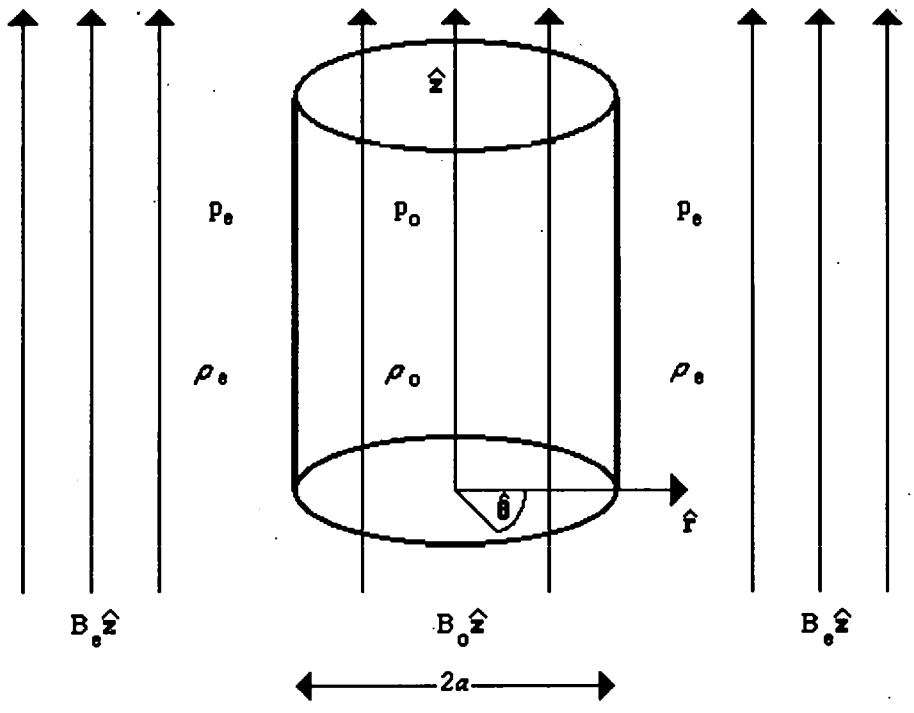

Figure 1.7: Equilibrium configuration of a magnetic cylinder.

where m_e^2 is given by Equation (1.47). In cylindrical (r, θ, z) coordinates, Equation (1.21) becomes

$$\frac{\partial \rho}{\partial t} = -\frac{\rho_0}{r}\frac{\partial (r v_r)}{\partial r} - \frac{\rho_0}{r}\frac{\partial v_\theta}{\partial \theta} - \rho_0 \frac{\partial v_z}{\partial z}. \tag{1.78}$$

The components of Equation (1.22) are

$$\rho_0 \frac{\partial v_r}{\partial t} = -\frac{\partial p}{\partial r} + \frac{B_0}{\mu}\left(\frac{\partial b_r}{\partial z} - \frac{\partial b_z}{\partial r}\right), \tag{1.79}$$

$$\rho_0 \frac{\partial v_\theta}{\partial t} = -\frac{1}{r}\frac{\partial}{\partial \theta}\left(p + \frac{B_0 b_z}{\mu}\right) + \frac{B_0}{\mu}\frac{\partial b_\theta}{\partial z}, \tag{1.80}$$

and

$$\rho_0 \frac{\partial v_z}{\partial t} = -\frac{\partial p}{\partial z}, \tag{1.81}$$

and the components of Equation (1.24) are

$$\frac{\partial b_r}{\partial t} = B_0 \frac{\partial v_r}{\partial z}, \tag{1.82}$$

$$\frac{\partial b_\theta}{\partial t} = B_0 \frac{\partial v_\theta}{\partial z}, \tag{1.83}$$

and

$$\frac{\partial b_z}{\partial t} = -\frac{B_0}{r}\frac{\partial (r v_r)}{\partial r} - \frac{B_0}{r}\frac{\partial v_\theta}{\partial \theta}. \tag{1.84}$$

Further, using Equations (1.79) to (1.84), it may be shown (see e.g. Edwin, 1984) that the perturbed quantities **v**, **b**, ρ and p_T, the total (gas plus magnetic) pressure in the interior, satisfy

$$v_r = -\frac{(c_0^2+v_A^2)(\omega^2-k^2c_T^2)}{\omega^2(\omega^2-k^2v_A^2)}\frac{d}{dr}\hat{R}(r)e^{i(\omega t+n\theta+kz)}, \tag{1.85}$$

$$v_\theta = -\frac{in(c_0^2+v_A^2)(\omega^2-k^2c_T^2)}{\omega^2(\omega^2-k^2v_A^2)}\frac{\hat{R}(r)}{r}e^{i(\omega t+n\theta+kz)}, \tag{1.86}$$

$$v_z = \frac{-ikc_0^2}{\omega^2}\hat{R}(r)e^{i(\omega t+n\theta+kz)}, \tag{1.87}$$

$$b_r = \frac{B_0k}{\omega}v_r, \tag{1.88}$$

$$b_\theta = \frac{B_0k}{\omega}v_\theta, \tag{1.89}$$

$$b_z = -\frac{B_0(\omega^2-k^2c_0^2)}{\omega kc_0^2}v_z, \tag{1.90}$$

$$p = -\frac{\rho_0\omega}{k}v_z, \tag{1.91}$$

and

$$p_T = -\frac{\rho_0(c_0^2+v_A^2)(\omega^2-k^2c_T^2)}{\omega kc_0^2}v_z. \tag{1.92}$$

Similar expressions are obtained for the region $r > a$, namely;

$$v_r^e = -\frac{(c_e^2+v_{Ae}^2)(\omega^2-k^2c_{Te}^2)}{\omega^2(\omega^2-k^2v_{Ae}^2)}\frac{d}{dr}\hat{R}^e(r)e^{i(\omega t+n\theta+kz)}, \tag{1.93}$$

$$v_\theta^e = -\frac{in(c_e^2+v_{Ae}^2)(\omega^2-k^2c_{Te}^2)}{\omega^2(\omega^2-k^2v_{Ae}^2)}\frac{\hat{R}^e(r)}{r}e^{i(\omega t+n\theta+kz)}, \tag{1.94}$$

$$v_z^e = \frac{-ikc_e^2}{\omega^2}\hat{R}^e(r)e^{i(\omega t+n\theta+kz)}, \tag{1.95}$$

$$b_r^e = \frac{B_ek}{\omega}v_r^e, \tag{1.96}$$

$$b_\theta^e = \frac{B_ek}{\omega}v_\theta^e, \tag{1.97}$$

$$b_z^e = -\frac{B_e(\omega^2-k^2c_e^2)}{\omega kc_e^2}v_z^e, \tag{1.98}$$

$$p^e = -\frac{\rho_e\omega}{k}v_z^e, \tag{1.99}$$

and

$$p_T^e = -\frac{\rho_e(c_e^2+v_{Ae}^2)(\omega^2-k^2c_{Te}^2)}{\omega kc_e^2}v_z^e. \tag{1.100}$$

Solutions of Equations (1.76) and (1.77) bounded on the axis of the cylinder, evanescent in its exterior ($m_e > 0$) and such that $n_0^2 = -m_0^2$ are

$$\hat{R}(r) = \begin{cases} A_0 \mathrm{J_n}(n_0 r), & r < a, \\ A_e \mathrm{K_n}(m_e r), & r > a, \end{cases} \tag{1.101}$$

where A_0 and A_e are constants, and $\mathrm{J_n}$ and $\mathrm{K_n}$ are Bessel functions (see Abramowitz and Stegun, 1967) of order n.

Continuity of the radial velocity component, v_r, and the total pressure perturbation, p_T, across the cylinder's boundary, $r = a$, yield the dispersion relationship governing body modes in a cylinder (see also McKenzie, 1970; Meerson, Sasorov and Stepanov, 1978; Edwin and Roberts, 1983)

$$\rho_0(k^2 v_A^2 - \omega^2) m_e \frac{\mathrm{K_n'}(m_e a)}{\mathrm{K_n}(m_e a)} = \rho_e(k^2 v_{A_e}^2 - \omega^2) n_0 \frac{\mathrm{J_n'}(n_0 a)}{\mathrm{J_n}(n_0 a)}. \tag{1.102}$$

The sausage (symmetric) modes are given by $n = 0$ in Equation (1.102) and may be written as

$$\hat{R}(r) = \begin{cases} \alpha_s \mathrm{J_0}(n_0 r), & r < a, \\ \beta_s \mathrm{K_0}(m_e r), & r > a, \end{cases} \tag{1.103}$$

where

$$\alpha_s = f\beta_s \frac{\mathrm{K_0}(m_e a)}{\mathrm{J_0}(n_0 a)};$$

is the (constant, small) amplitude of the Fourier perturbation in Equation (1.74), with

$$f = \frac{\rho_e(c_e^2 + v_{Ae}^2)(\omega^2 - k^2 c_{Te}^2)}{\rho_0(c_0^2 + v_A^2)(\omega^2 - k^2 c_T^2)}. \tag{1.104}$$

The kink solutions in Equation (1.101) may be written as

$$\hat{R}(r) = \begin{cases} \alpha_k \mathrm{J_1}(n_0 r), & r < a, \\ \beta_k \mathrm{K_1}(m_e r), & r > a, \end{cases} \tag{1.105}$$

where

$$\alpha_k = f\beta_k \frac{\mathrm{K_1}(m_e a)}{\mathrm{J_1}(n_0 a)}$$

is the (constant, small) amplitude of the Fourier perturbation. Solutions with $n \geq 2$ are termed *fluting* modes.

Edwin and Roberts (1983) and Edwin (1984) have discussed, in detail, the rich spectrum of solutions that dispersion relation (1.102) possesses. Of interest to us are the solutions typical of circumstances representative of loops found in the corona. Considering the case in which the interior of the cylinder is denser than its surroundings, i.e. $\rho_0/\rho_e < 1$, again it is found that there are no surface waves but only harmonics confined to the two bands $v_A < \omega/k < v_{Ae}$ and $c_T < \omega/k < c_{Te}$ (see Figure 1.8). Again these bands correspond to the fast and slow magnetoacoustic body waves of the unstructured medium. In Figure 1.8 the horizontal lines (— — —) represent the cut-offs

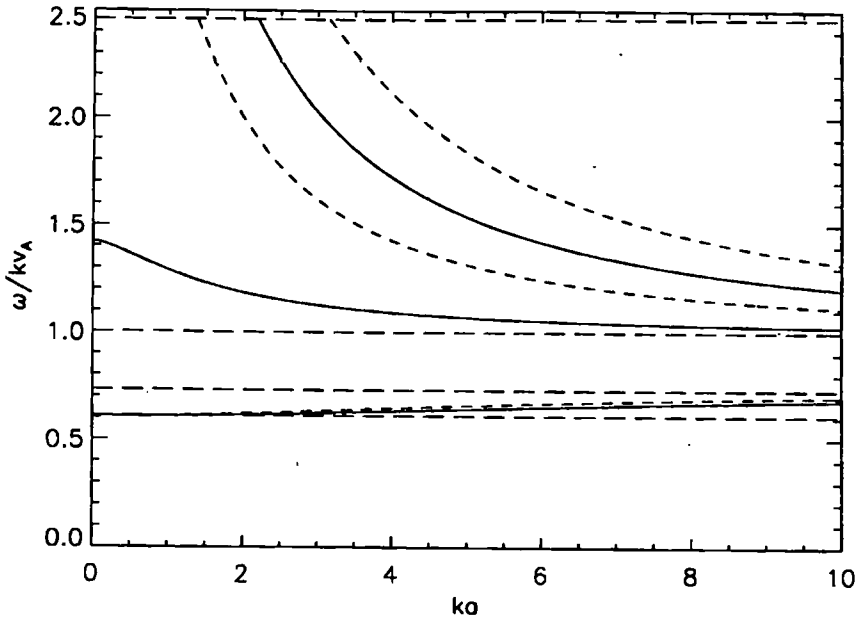

Figure 1.8: The normalized phase-speed ω/kv_A as a function of ka for a cylindrical inhomogeneity of radius a under coronal conditions (after Edwin and Roberts, 1983).

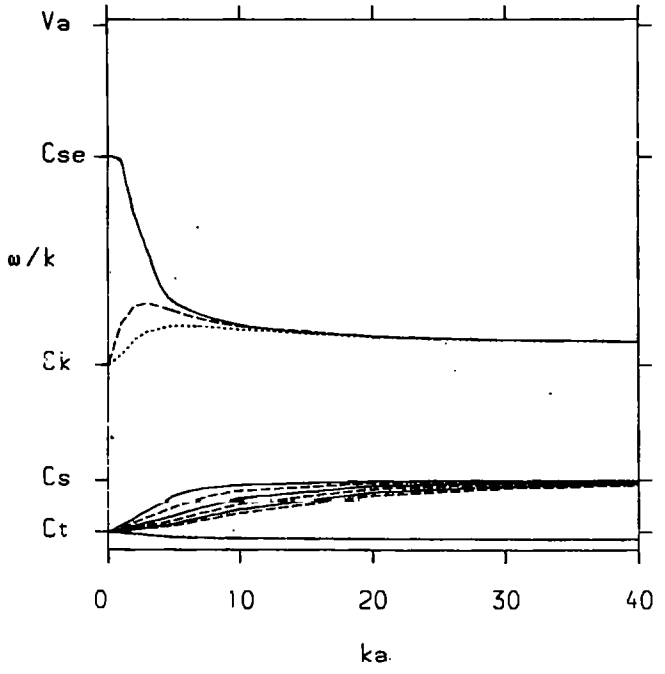

Figure 1.9: The phase-speed ω/k as a function of ka for fast and slow modes in a cylindrical inhomogeneity of radius a (after Evans and Roberts, 1990).

at $\omega/kv_A = v_{Ae}/v_A$, 1, c_{Te}/v_A and c_T/v_A, respectively, and the full (—) and dashed (- - -) lines represent the kink and sausage modes.

Evans and Roberts (1990) later found that the lowest-order kink mode possessed a *hump* as shown in Figure 1.9. Figure 1.9 shows the solutions of dispersion relation (1.102) according to Evans and Roberts (1990). Note that the characteristic speeds used by Evans and Roberts (not shown exactly to scale in Figure 1.9) are $c_T = 5.7$ km s^{-1}, $c_s = 6.4$ km s^{-1}, $c_k = 7.8$ km s^{-1}, $c_{se} = 10.5$ km s^{-1} and $v_A = 12.6$ km s^{-1}. In reproducing the work of Edwin and Roberts (1983) and Edwin (1984) for this thesis the discrepancy in the curves' shape was investigated and no turning point was found in the lowest-order kink mode. The results reproduced here are in agreement with those found by Edwin (1984). The discrepancy in the curves' shapes would appear to be in the accuracy of the calculation of the iterative root-finding scheme used in the numerical codes for solving Equation (1.102). The work of Edwin and Roberts (1983) and Edwin (1984) was reproduced by solving dispersion relation (1.102) numerically by employing Brent's Method (Press *et al.*, 1992) and the method of Bus and Dekker (NAG Ltd., 1988).

Brent's method can be employed to find the root of a one-dimensional function, f, even if one cannot easily compute the function's derivative. The method is guaranteed to converge, so long as the function can be evaluated within the initial interval known to contain a root. The method combines *root bracketing*, *bisection* and *inverse quadratic interpolation* to converge from the neighbourhood of a zero crossing. A root is said to be *bracketed* in the interval (a, b) if $f(a)$ and $f(b)$ have opposite signs. The bisection method is one that cannot fail. The idea is simple. Over some interval the function is known to pass through zero because it changes sign. The function is evaluated at the interval's midpoint and its sign is examined. The midpoint replaces whichever limit of the interval has the same sign. After each iteration the bounds containing the root decrease by a factor of two, i.e. if after n iterations the root is known to lie within an interval size of ϵ_n, then after the next iteration it will be bracketed with an interval size of $\epsilon_{n+1} = \epsilon_n/2$. Inverse quadratic interpolation uses three prior points to fit an inverse quadratic function (x as a quadratic function of y) whose value at $y = 0$ is taken as the next estimate of the root x. Brent's method ensures that the root remains bracketed and the method combines the sureness of bisection with the speed of a higher-order method.

In a similar fashion to our consideration of Equation (1.66) we can define the root-mean-square-velocity, v_{rms}, for a cylindrical volume as

$$v_{rms} = \left[\frac{1}{\pi a^2}\int_{r=0}^{r=a}\left(\hat{v}_r^2(r) + \hat{v}_\theta^2(r) + \hat{v}_z^2(r)\right) r\,dr\,d\theta\right]^{1/2}, \tag{1.106}$$

where $\hat{v}_r$, $\hat{v}_\theta$ and $\hat{v}_z$ are given by Equations (1.85), (1.86) and (1.87), with $v_r = \hat{v}_r(r)e^{(i\omega t + n\theta + kz)}$, etc.. Thus, after integrating Equation (1.106) it is seen that the amplitude of symmetric perturbations can be expressed in terms of v_{rms} by,

$$\beta_e^2 = \frac{\omega^4 n_0^2 v_{rms}^2}{f^2 \mathrm{K}_0^2(m_e a)\left[f_{c1} + k^2 c_0^4 f_{c2}\right]}, \tag{1.107}$$

with

$$f_{c1} = (\omega^2 - k^2 c_0^2)^2 \left[\left(\frac{\mathrm{J}_1(n_0 a)}{\mathrm{J}_0(n_0 a)} \right)^2 + 1 - \frac{2}{n_0 a} \frac{\mathrm{J}_1(n_0 a)}{\mathrm{J}_0(n_0 a)} \right], \tag{1.108}$$

and

$$f_{c2} = n_0^2 \left[\left(\frac{\mathrm{J}_1(n_0 a)}{\mathrm{J}_0(n_0 a)} \right)^2 + 1 \right]. \tag{1.109}$$

Similarly, for asymmetric perturbations we have

$$\beta_k^2 = \frac{\omega^4 n_0^2 v_{rms}^2}{f^2 \mathrm{K}_1^2(m_e a) \left[f_{c3} + k^2 c_0^4 f_{c4} \right]}, \tag{1.110}$$

where

$$f_{c3} = (\omega^2 - k^2 c_0^2)^2 \left[\left(\frac{\mathrm{J}_0(n_0 a)}{\mathrm{J}_1(n_0 a)} \right)^2 + 1 - \frac{2}{n_0^2 a^2} \right], \tag{1.111}$$

and

$$f_{c4} = n_0^2 \left[\left(\frac{\mathrm{J}_0(n_0 a)}{\mathrm{J}_1(n_0 a)} \right)^2 + 1 - \frac{2}{n_0 a} \frac{\mathrm{J}_0(n_0 a)}{\mathrm{J}_1(n_0 a)} \right]. \tag{1.112}$$

1.7.3 Summary of Magnetic Structuring

In a dense coronal loop, the fast and slow magnetoacoustic waves of an infinite medium, Equation (1.36), manifest themselves as two sets of waves:

1. the fast ones with phase speeds lying between v_A and v_{Ae};
2. the slow ones with phase speeds of approximately that of the tube, or cusp, speed, c_T.

The waves may be regarded as sausage or kink modes depending upon whether the duct undergoes symmetric or asymmetric oscillations. Moreover, Equations (1.63) and (1.102) only possess solutions for $m_0^2 (= -n_0^2) < 0$ and so the modes are of oscillatory nature within the duct (see Figure 1.6).

1.8 Outline of Thesis

This thesis is concerned with the dissipation of mhd waves in the solar atmosphere. The outer atmosphere of the Sun, the corona, is known to be structured (Section 1.1). Structuring is taken into account in modelling the wave motion. An attempt will be made at putting forward likely wave candidates that might play some role in contributing towards a hot (10^6 K) corona and those which might exist by surviving the dissipative mechanisms under consideration.

This introductory chapter has presented the general physical features observed in the corona, and the motivation for considering wave motions and dissipation. The basic equations

of mhd have been given Equations (1.3) to (1.13) along with those describing ideal mhd wave propagation in an unstructured (Section 1.6) and a structured atmosphere (Section 1.7).

Chapter 2 presents a discussion of energy and its dissipation in the upper solar atmosphere. The non-ideal equations of mhd are presented and an overview of coronal heating and dissipative effects and mechanisms is given in this second chapter.

Chapter 3 considers a weakly dissipative model for fast and slow, ducted mhd waves, and the lengths over which waves dissipate are calculated.

Chapter 4 considers the nature of wave dissipation in slender structures, and the lengths and damping rates over which slow waves are damped, are calculated.

The final chapter compares the two methods studied in Chapters 3 and 4, along with models considered by other authors. The period ranges over which the waves are dissipated or not, according to the various models, are compared with recorded oscillation phenomena. Finally, suggestions as to which waves might contribute to coronal heating, or as to which waves might survive the dissipation mechanisms and so be observed, are made.

Chapter 2

Energy and its Dissipation in the Upper Solar Atmosphere

2.1 Introduction

In the discussion in the previous chapter concerning mhd waves, the effects of wave dissipation, as introduced by the non-ideal effects such as viscosity, thermal conductivity, resistivity, *etc.*, have been ignored. Confining attention to the case of ideal mhd waves not only makes the mathematical treatment easier but also gives an insight into the physical nature of mhd wave propagation in unstructured and structured atmospheres. However, it is reasonable to assume that the solar plasma is non-ideal and that the introduction of dissipative mechanisms into the description of mhd wave propagation is an important consideration. Solving the mhd equations with consideration given to dissipative mechanisms is non-trivial and given the wealth of literature devoted to the problem, it is quite clear that it is a very complicated topic indeed. The heating of the solar coronal plasma, to temperatures $\sim 10^6$ K compared with 6 600 K in the photosphere, remains an unsolved problem in solar physics; it may therefore be profitable to consider waves being damped due to dissipation and possibly heating up the atmosphere as a result. Although wave theories have long played a role in trying to explain the heating of the solar atmosphere it would be wrong to give the impression that they commanded a monopoly in the coronal-heating literature. A large number of models which do not involve waves have been proposed and their merits will also be discussed in this chapter which discusses non-ideal mhd equations and dissipative mechanisms in connection with the heating of the solar corona.

2.2 Non-Ideal Equations of Magnetohydrodynamics

In general, the non-ideal equation of motion may be written (e.g. see Roberts, 1967; Priest, 1982; as well as Equation (1.4))

$$\bar{\rho}\left(\frac{\partial \bar{\mathbf{v}}}{\partial t}+\bar{\mathbf{v}}\cdot\nabla\bar{\mathbf{v}}\right)=-\nabla\bar{p}+\bar{\mathbf{j}}\times\bar{\mathbf{B}}+\mathbf{F}_v, \tag{2.1}$$

where $\mathbf{F}_v$ represents the effects of viscosity, and all other symbols have their usual meaning (see Chapter 1). Consistent with our assumptions in Chapter 1 (since we are concerned with wave motion in the upper solar atmosphere) we shall again neglect gravitational forces in the term $\mathbf{F}_b$. The energy equation was given as Equation (1.11) and we repeat it here for convenience:

$$\frac{\partial\bar{p}}{\partial t}+\bar{\mathbf{v}}\cdot\nabla\bar{p}-\gamma\frac{\bar{p}}{\bar{\rho}}\left(\frac{\partial\bar{\rho}}{\partial t}+\bar{\mathbf{v}}\cdot\nabla\bar{\rho}\right)=-(\gamma-1)L, \tag{2.2}$$

(L is the energy loss function, which may be written as the rate of energy loss minus the rate of energy gain). Following the discussion in Priest (1982) it may be shown that Equation (2.2), for a perfect gas, may be written in the form(s)

$$\bar{\rho}c_v\left(\frac{\partial\bar{T}}{\partial t}+\bar{\mathbf{v}}\cdot\nabla\bar{T}\right)+\bar{p}\nabla\cdot\bar{\mathbf{v}}=\bar{\rho}c_p\left(\frac{\partial\bar{T}}{\partial t}+\bar{\mathbf{v}}\cdot\nabla\bar{T}\right)-\left(\frac{\partial\bar{p}}{\partial t}+\bar{\mathbf{v}}\cdot\nabla\bar{p}\right)=-L, \tag{2.3}$$

where c_v and c_p are the specific heats at constant volume and pressure respectively.
Now, the internal energy, $\bar{e}$, of an ideal, polytropic gas is given by

$$\bar{e}=\frac{\bar{p}}{(\gamma-1)\bar{\rho}},$$

and on substituting for the gas pressure, $\bar{p}$, in Equation (2.2) we have, on using the equation of continuity, Equation (1.3),

$$\frac{\partial\bar{e}}{\partial t}+\bar{\mathbf{v}}\cdot\nabla\bar{e}+\bar{p}\nabla\cdot\bar{\mathbf{v}}=-L. \tag{2.4}$$

Taking the scalar product of $\bar{\mathbf{v}}$ with the equation of motion (2.1) gives the rate of change of kinetic energy equation

$$\bar{\rho}\left(\frac{\partial}{\partial t}\left(\bar{v}^2/2\right)+\bar{\mathbf{v}}\cdot\nabla(\bar{v}^2/2)\right)=-\bar{\mathbf{v}}\cdot\nabla\bar{p}+\bar{\mathbf{v}}\cdot\bar{\mathbf{j}}\times\bar{\mathbf{B}}+\bar{\mathbf{v}}\cdot\mathbf{F}_b. \tag{2.5}$$

The divergence of the Poynting flux, $\bar{\mathbf{S}}=\bar{\mathbf{E}}\times\bar{\mathbf{B}}/\mu$, may be written as

$$\nabla\cdot\bar{\mathbf{S}}=-\bar{\mathbf{E}}\cdot\bar{\mathbf{j}}-\frac{\partial}{\partial t}(\bar{B}^2/2\mu) \tag{2.6}$$

on using a vector identity and Equations (1.5) and (1.9).

The dot product of $\bar{\mathbf{j}}$ with Ohm's Law (Equation (1.7)) gives, on using a vector identity

$$\bar{\mathbf{E}}\cdot\bar{\mathbf{j}}=\bar{\mathbf{v}}\cdot\bar{\mathbf{j}}\times\bar{\mathbf{B}}+\bar{j}^2/\sigma. \tag{2.7}$$

Combining Equations (2.6) and (2.7) gives the rate of change of magnetic energy

$$\frac{\partial}{\partial t}(\bar{B}^2/2\mu)=-\nabla\cdot\bar{\mathbf{S}}-\bar{\mathbf{v}}\cdot\bar{\mathbf{j}}\times\bar{\mathbf{B}}-\bar{j}^2/\sigma. \tag{2.8}$$

Rewriting Equations (2.4) and (2.5), we may obtain the rate of change of internal energy and the rate of change of kinetic energy in the forms

$$\frac{\partial}{\partial t}(\bar{\rho}\bar{e}) = -\nabla\cdot(\bar{\rho}\bar{e}\bar{\mathbf{v}}) - \bar{p}\nabla\cdot\bar{\mathbf{v}} - L, \tag{2.9}$$

and

$$\frac{\partial}{\partial t}(\bar{\rho}\bar{v}^2/2) = -\nabla\cdot(\bar{\rho}\bar{v}^2\bar{\mathbf{v}}/2) - \bar{\mathbf{v}}\cdot\nabla\bar{p} + \bar{\mathbf{v}}\cdot\bar{\mathbf{j}}\times\bar{\mathbf{B}} + \bar{\mathbf{v}}\cdot\mathbf{F}_b, \tag{2.10}$$

and summing Equations (2.8), (2.9) and (2.10) gives

$$\frac{\partial}{\partial t}(\bar{\rho}\bar{e} + \bar{\rho}\bar{v}^2/2 + \bar{B}^2/2\mu) = -\nabla\cdot\left(\bar{\rho}\bar{e}\bar{\mathbf{v}} + \bar{\rho}\bar{v}^2\bar{\mathbf{v}}/2 + \bar{p}\bar{\mathbf{v}} + \bar{\mathbf{S}}\right) + \bar{\mathbf{v}}\cdot\mathbf{F}_b - (L + \bar{j}^2/\sigma). \tag{2.11}$$

Equation (2.11) states that the rate of change in total (internal plus kinetic plus magnetic) energy is due to the convective energy flux, $\bar{\rho}(\bar{e}+\bar{v}^2/2)\bar{\mathbf{v}}$, the mechanical energy flux $\bar{p}\bar{\mathbf{v}}$, the Poynting flux, $\bar{\mathbf{S}}$, and the dissipation mechanisms contained in the viscous force term $\mathbf{F}_v$, L, and $\bar{j}^2/\sigma$. Similar forms to Equation (2.11) are given, for example, by Roberts (1967), Kuperus, Ionson and Spicer (1981) and Priest (1982).

Considering the equilibrium state given by (1.19) and applying the perturbations (1.20) and neglecting cubed powers of the perturbed quantities in Equation (2.11) gives

$$\frac{\partial U}{\partial t} = -\nabla\cdot\mathbf{F} + \mathbf{v}\cdot\mathbf{F}_b - (L + j^2/\sigma), \tag{2.12}$$

where $U = \rho e + B^2/2\mu$ is the total energy due to internal and magnetic energies (i.e. kinetic energy effects have been neglected), and $\mathbf{F} = \frac{\gamma}{\gamma-1}p\mathbf{v} + \mathbf{S}$ is the total (acoustic plus Poynting) energy flux.

Having considered what forms the non-ideal energy equation may take, we now give attention to what dissipative terms make up $\mathbf{F}_b$ and L.

2.2.1 Viscous Effects

In fluids, the transfer of momentum occurs in part by the transport of fluid volumes having different velocity, which is expressed by the advective $(\mathbf{v}\cdot\nabla)$ term in the equation of motion, Equation (1.4). However, additional transfer is caused by the internal friction due to collisions between particles moving with adjacent layers of the fluid having different velocities. The viscosity of a plasma in the presence of a magnetic field is very complicated because it is given by a tensor quantity. For a strongly magnetized plasma, with the background magnetic field in the z-direction, the effects of viscosity, $\mathbf{F}_v$, may be written as

$$\mathbf{F}_b = -\nabla\cdot\mathbf{\Pi}, \tag{2.13}$$

where $\mathbf{\Pi}$ is the viscosity stress tensor. Braginskii (1965) writes the components of the viscous stress tensor in the form

$$\Pi_{zz} = -\eta_0 W_{zz}, \tag{2.14}$$

$$\Pi_{xx} = -\eta_0(W_{xx} + W_{yy})/2 - \eta_1(W_{xx} - W_{yy})/2 - \eta_3 W_{xy}, \tag{2.15}$$

$$\Pi_{yy} = -\eta_0(W_{xx} + W_{yy})/2 - \eta_1(W_{yy} - W_{xx})/2 + \eta_3 W_{xy}, \tag{2.16}$$

$$\Pi_{xy} = \Pi_{yx} = -\eta_1 W_{xy} + \eta_3(W_{xx} - W_{yy})/2, \tag{2.17}$$

$$\Pi_{xz} = \Pi_{zx} = -\eta_2 W_{xz} - \eta_4 W_{yz}, \tag{2.18}$$

$$\Pi_{yz} = \Pi_{zy} = -\eta_2 W_{yz} - \eta_4 W_{xz}, \tag{2.19}$$

where the rate of strain tensor, $W_{\alpha\beta}$, is given by

$$W_{\alpha\beta} = \frac{\partial v_\alpha}{\partial x_\beta} + \frac{\partial v_\beta}{\partial x_\alpha} - \frac{2}{3}\delta_{\alpha\beta}(\nabla \cdot \mathbf{v}), \tag{2.20}$$

and $\mathbf{v} = (v_x, v_y, v_z)$. The above expressions, Equations (2.14) to (2.19), show that the viscous stress is not a simple function of the velocity derivatives, $\partial v_\alpha/\partial x_\beta$, but depends on combinations of these derivatives given by the rate of strain tensor, $W_{\alpha\beta}$. Braginskii (1965) gives the expressions for the ion viscosity coefficients (normalized against the Boltzmann constant) η_0, η_1, η_2, η_3 and η_4, namely

$$\eta_0 = 0.96 N_{io} T_{io} \tau_{io},$$

$$\eta_1 = \frac{0.3 N_{io} T_{io}}{\omega_{io}^2 \tau_{io}}, \quad \eta_2 = 4\eta_1,$$

$$\eta_3 = \frac{0.5 N_{io} T_{io}}{\omega_{io}}, \quad \eta_4 = 2\eta_3,$$

where N_{io} is the number of ions, T_{io} is the ion temperature (in electron volts),

$$\tau_{io} = \frac{9.6 \times 10^5 T_{io}^{3/2}}{N_{io}} \tag{2.21}$$

is the ion collision time (with a Coulomb logarithm of 22 assumed – see page 18 of Chapter 1), and

$$\omega_{io} = 9.6 \times 10^3 B \tag{2.22}$$

is the ion cyclotron frequency. In Equation (2.22) B is the magnetic field strength (in G). Here we have neglected the electron viscosity coefficients since they are smaller by a factor of $(m_i/m_e)^{1/2}$ (m_i and m_e are the ion and electron masses respectively) and so viscosity is mainly due to the ions. Furthermore, η_1 and η_2 are smaller by factors of $(\omega_{io}\tau_{io})^{-2}$ and η_3 and η_4 are smaller by factors of $(\omega_{io}\tau_{io})^{-1}$. Thus, for a fully-ionized hydrogen plasma, so that $N_{el} = N_{io}$, typical coronal values of $B = 10$ G, $N_{el} = 10^9$ cm^{-3} and $T_{el} = T_{io} = 86$ eV (i.e. 2×10^6 K) say, then $\omega_i \tau_i = 7.4 \times 10^4$, and so clearly η_0 is the largest of the five ion viscosity coefficients. In cgs units η_0 has the value

$$\eta = 1.0 \times 10^{-16} T^{5/2}, \tag{2.23}$$

where we have denoted η_0 by η and have assumed that $T = T_{el} = T_{io}$.

Braginskii (1965, Equation (2.28)) then computes the volumetric heating rate associated with the viscosity coefficient, η_0, namely

$$Q_{vis} = -\Pi_{\alpha\beta}\frac{\partial v_\alpha}{\partial x_\beta},$$

which may be written as

$$Q_{vis} = \frac{\eta}{3}\left(\nabla\cdot\mathbf{v} - 3\frac{\partial v_z}{\partial z}\right)^2. \tag{2.24}$$

Hollweg (1986) states that studies of solar coronal dynamics usually assume scalar pressure and ignore viscosity but viscosity *is* important and its omission may give misleading results.

Hollweg (1985) gives an illuminating discussion on the physical interpretation of viscosity in a magnetized plasma. He stresses that the η_0 terms in the viscous stress tensor are simply a result of the plasma's tendency to develop small anisotropies. The collisions which oppose the production of anisotropy tend to redistribute changes of internal energy which leads to a heating of the plasma.

Hollweg (1985) also gives caution to the apparent importance of the η_0 terms. Although the value of η_0 is numerically larger than the other coefficients for the viscous stresses he warns that it is possible for the divergence of the η_0 part of the viscous stress tensor to vanish and so η_0 plays no part in the equation of motion (e.g. Sonnerup and Priest, 1975). Also, in their treatment of resonant absorption of Alfvén waves, Ofman, Davila and Steinolfson (1994) consider the effects of the full viscous stress tensor with the inclusion of the five dissipation coefficients, η_0 to η_4.

Ruderman (1991) investigates the propagation of surface waves on a magnetic interface in a cold plasma subject to the damping mechanism of ion viscosity. He restricts attention to weakly dissipative waves (i.e. $k_i \ll k_r$ where k_r and k_i are the real and imaginary parts of the wave number $k = k_r + ik_i$) and concludes that the viscous damping of surface waves depends heavily upon the background plasma parameters as well as the direction of wave propagation. Further, he states that the damping is stronger in the case of magnetoacoustic type waves than is the case for Alfvénic behaviour. Building upon these results, Ruderman (1992) considers the propagation of small-amplitude, non-linear, Alfvén waves on a single magnetic interface. Again a cold plasma and anisotropic viscosity are assumed. Ruderman investigates the wave damping numerically and his calculations show that when the wave profile is very steep, viscosity is small which leads to a strong acceleration of wave damping. Further, for small viscosity Ruderman finds that the wave-damping distance predicted by the non-linear approach can be an order of magnitude smaller than the damping distance predicted by the linear theory.

Several authors have considered Equation (2.24) in connection with ion viscous heating of the solar corona (Gordon and Hollweg, 1983; Sahyouni, Kiss'ovski and Zhelyazkov, 1987; Edwin and Zhelyazkov, 1992; Edwin and Laing, 1994; Laing and Edwin, 1994; Porter, Klimchuk and Sturrock, 1994a, b; Laing and Edwin, 1995a, b). The viscous heating rate given by Equation (2.24) is valid for a collisional plasma which requires that the ions undergo many cyclotron orbits between collisions

with

$$\omega_{io}\tau_{io} \gg 1.$$

Here, τ_{io} is given by Equation (2.21). Note that by expressing the ion temperature, T_{io}, in Kelvins, we may reformulate Equation 2.22 in terms of cgs units, namely, $\tau_{io} = 0.75T^{3/2}N_{io}$) and hence we require periods, τ, satisfying

$$\tau > \frac{4.7T^{3/2}}{N_{io}} \tag{2.25}$$

in order for the plasma to be regarded as collisional (and assuming $T = T_{el} = T_{io}$).

Turning our attention to the non-ideal energy equation, Equation (2.12), we now consider what dissipative effects may contribute to L.

2.2.2 Thermal Conduction Effects

It is usually assumed that the corona loses energy via heat conducted along magnetic field lines back down to the chromosphere (Hollweg, 1983). We may pose the question what happens to a particle travelling along a magnetic field line when it arrives at the footpoint of a coronal loop? If there were no collisions, the helical path taken by an electron (or an ion) eventually reverses on itself, that is to say the footpoint acts as a mirror for the particle. Since there is a greater density of other particles at the footponts, collisions become more frequent. Thus, a particle that has travelled largely unimpeded from the top part of the loop may impart much of its kinetic energy to the surrounding particles it collides with near the footpoint. Basically this is a microscopic description of the conduction of heat in a coronal loop - energy in the hot, upper parts of a loop is transported by electrons to the denser, cooler chromospheric layers. The loop, then, cools by loss of energy along magnetic field lines to the chromosphere. However, in contrast, heat conductivity perpindicular to the magnetic field lines is stongly inhibited since electrons are constrained to travel in their helical paths along the field.

The rate of energy loss by thermal conduction is given by (Priest, 1982)

$$L_r = \nabla \cdot \mathbf{q}, \tag{2.26}$$

where $\mathbf{q}$ is the heat flux due to particle conduction which, from Fourier's law, may be written as

$$\mathbf{q} = -\underline{\kappa}\nabla\bar{T}, \tag{2.27}$$

where $\underline{\kappa}$ is the thermal conduction tensor. The divergence of the heat flux may be written as

$$\nabla \cdot \mathbf{q} = \nabla_{\parallel} \cdot (\kappa_{\parallel}\nabla_{\parallel}\bar{T}) + \nabla_{\perp} \cdot (\kappa_{\perp}\nabla_{\perp}\bar{T}), \tag{2.28}$$

where the subscripts $\parallel$ and $\perp$ indicate values parallel and perpendicular to the background magnetic field, $B_0\hat{\mathbf{z}}$. Braginskii (1965) gives the values for the thermal conductivities for electrons and ions as

$$\kappa_{\parallel,el} = \frac{3.16N_{el}T_{el}\tau_{el}}{m_{el}}, \quad \kappa_{\perp,el} = \frac{4.66N_{el}T_{el}}{m_{el}\omega_{el}^2\tau_{el}},$$

$$\kappa_{\parallel,io} = \frac{3.9 N_{io} T_{io} \tau_{io}}{m_{io}}, \quad \kappa_{\perp,io} = \frac{2 N_{io} T_{io}}{m_{io} \omega_{io}^2 \tau_{io}},$$

where τ_{io} and ω_{io} are given by Equations (2.21) and (2.22), and

$$\tau_e = \frac{1.59 \times 10^4 T_{el}^{3/2}}{N_{el}} \tag{2.29}$$

and

$$\omega_e = 1.76 \times 10^7 B,$$

where B is the magnetic field strength (in G). Note that the subscripts *io* and *el* denote ion and electron quantities, respectively, and that T_{el} and T_{io} are electron and ion temperatures in electron volts. In cgs units (erg cm^{-1} s^{-1} K^{-1}) the expressions for the electron and ion thermal conductivities become:

$$\kappa_{\parallel,el} = 8.4 \times 10^{-7} T_{el}^{5/2}, \quad \kappa_{\perp,el} = 2.5 \times 10^{-17} N_{el}^2 / B^2 T_{el}^{1/2}, \tag{2.30}$$

$$\kappa_{\parallel,io} = 3.4 \times 10^{-8} T_{io}^{5/2}, \text{ and } \kappa_{\perp,io} = 3.2 \times 10^{-16} N_{io}^2 / B^2 T_{io}^{1/2},$$

and it is noted that, for coronal values of B, $N_{el} = (N_{io})$ and $T(= T_{el} = T_{io})$, $\kappa_{\parallel,el} \gg \kappa_{\parallel,io}$, $\kappa_{\perp,el} \ll \kappa_{\perp,io}$ and $\kappa_{\parallel,el} \gg \kappa_{\perp,el}$. Hence thermal conduction is carried out mainly by the electrons, along the direction of the background magnetic field. Therefore Equation (2.28) may be approximated, for constant $\kappa_{\parallel,el}$, by

$$\nabla \cdot \mathbf{q} = \kappa_{\parallel,el} \frac{d^2 \bar{T}}{dz^2}. \tag{2.31}$$

Further, if $\kappa_{\parallel,el}$ is assumed both constant and isotropic i.e. $\kappa_{\parallel,el} = \kappa_{\perp,el} = Q$, then Equation (2.28) is approximated by

$$\nabla \cdot \mathbf{q} = Q \nabla^2 \bar{T}. \tag{2.32}$$

Van der Linden and Goossens (1991) argue that although the coefficient, $\kappa_{\perp,el}$, of thermal conductivity perpendicular to the magnetic field is typically some 12 to 15 orders of magnitude smaller than the coefficient $\kappa_{\parallel,el}$, for conduction along field lines, it nevertheless is non-zero and has an important role to play.

Braginskii (1965) considers non-equilibrium, irreversible thermodynamics in which the entropy production (per unit volume) is given by the product of the thermodynamic flux and the force. The irreversible increase of entropy in a non-equilibrium system is called the entropy production which is always greater than zero. Braginskii states that a flux, I_m, (e.g. $\mathbf{q}$) and a force, X_m, (e.g. $\nabla \bar{T}$) are conjugate if the entropy production, Θ, can be expressed in the form

$$\Theta = \sum_m I_m X_m.$$

An important theroem in the thermodynamics of irreversible processes is the principle of symmetry of the knietic coefficients and Braginskii shows that the entropy production per unit volume is given by

$$\Theta_{ther} = \frac{-\mathbf{q}\nabla\bar{T}}{T_0^2} = \frac{Q_{ther}}{T_0},$$

where the plasma heating rate due to heat conduction, Q_{ther}, is given by

$$Q_{\rm ther} = \frac{\kappa_{\parallel,el}}{T_0}(\nabla_\parallel T_{el})^2 + \frac{\kappa_{\perp,el}}{T_0}(\nabla_\perp T_{el})^2 + \frac{\kappa_{\parallel,io}}{T_0}(\nabla_\parallel T_{io})^2 + \frac{\kappa_{\perp,io}}{T_0}(\nabla_\perp T_{io})^2. \tag{2.33}$$

and T_0 represents the background temperature. Equation (2.33) may be approximated by

$$Q_{\rm ther} = \frac{\kappa_{\parallel,el}}{T_0}(\nabla_\parallel T_{el})^2 \tag{2.34}$$

since the heat conduction is due mainly to the electrons and is principally in the direction of the background magnetic field (see also Hollweg, 1983).

Plasma heating rates using Equation (2.34) have been considered by many authors, for example Hollweg (1983), Gordon and Hollweg (1983), Sahyouni, Kiss'ovski and Zhelyazkov (1987), Edwin and Zhelyazkov (1992), Edwin and Laing (1994), Laing and Edwin (1994), Laing and Edwin (1995a, b) and Porter, Klimchuk and Sturrock (1994a). Gordon and Hollweg (1983) (see also Edwin and Zhelyazkov, 1992) give Equation (2.34) as

$$Q_{ther} = \begin{cases} \kappa_{\parallel,el}\left(\frac{k}{\omega}\right)^2 T(\gamma-1)^2(\nabla\cdot\mathbf{v})^2, & \omega < \omega_{cond}, \\ N^2k_B^2Tk^{-2}\kappa_{\parallel,el}^{-1}(\nabla\cdot\mathbf{v})^2, & \omega \geq \omega_{cond}, \end{cases} \tag{2.35}$$

where N represents the background (total) particle density, T represents the background temperature, $\mathbf{v}$ is the velocity and $\omega_{cond} = \kappa_{\parallel,el}k^2(\gamma-1)/Nk_B$, where ω is the angular frequency, k is the wave number, γ is the ratio of specific heats, and k_B is the Bolztmann constant.

Gordon and Hollweg note that the heating due to particle conduction is valid only if the electron mean free path, $l_e(= \tau_e(k_BT_e/m_e)^{1/2})$, is short enough so that

$$kl_e < 1.$$

On using Equation (2.29) for τ_e we see that wave numbers must satisfy

$$k < \frac{N_{el}}{4.9\times10^3T^2}. \tag{2.36}$$

However, there is no need to take Q_{ther} in terms of high and low ω as considered by Gordon and Hollweg. Instead, the following argument may be considered. We shall suppose that the only dissipation term in L in Equation (2.2) is due to thermal conduction so that we are considering the energy equation

$$\frac{\partial\bar{p}}{\partial t} + \bar{\mathbf{v}}\cdot\nabla\bar{p} - \gamma\frac{\bar{p}}{\bar{\rho}}\left(\frac{\partial\bar{\rho}}{\partial t} + \bar{\mathbf{v}}\cdot\nabla\bar{\rho}\right) = -(\gamma-1)\kappa_{\parallel,el}\frac{d^2\bar{T}}{dz^2}. \tag{2.37}$$

Linearizing Equation (2.37) and combining with Equation (1.21) gives

$$\frac{\partial p}{\partial t} + \gamma p_0(\nabla\cdot\mathbf{v}) = (\gamma-1)\kappa_{\parallel,el}\frac{d^2\bar{T}}{dz^2}. \tag{2.38}$$

Using the ideal gas law in the form of Equation (1.13) in Equation (2.38) and Fourier analysing with respect to $e^{i(\omega t+kz)}$ gives for the perturbed temperature, T,

$$T = \frac{-N_0 k_B T_0(\gamma-1)(\nabla\cdot\mathbf{v})}{(\gamma-1)^2\kappa_{\|,el}^2 k^4 + N_0^2 k_B^2\omega^2}\left(\kappa_{\|,el}k^2(\gamma-1) - i\omega N_0 k_B\right), \tag{2.39}$$

where N_0 and T_0 represent the total particle density and temperature at equilibrium (see Equation (1.19)). On substituting Equation (2.39) into Equation (2.34) we obtain

$$Q_{ther} = \frac{N^2 k_B^2\,\kappa_{\|,el}\,k^2\,T\,(\gamma-1)^2\,(\nabla.\mathbf{v})^2}{\kappa_{\|,el}^2\,k^4\,(\gamma-1)^2 + \omega^2\,N^2\,k_B^2}\,. \tag{2.40}$$

Note that in Equation (2.40) we have dropped the subscript '0' and write the background particle density and temperature as N and T, respectively.

So, two different theories are available to estimate the temperature gradient, $\nabla\bar{T}$. Equations (2.31) and (2.32) represent the heat flux considered from a fluid approach and the thermal conduction heating rate given by Equations (2.33) and (2.34) is considered from the kinetic equations of Braginskii (1965).

2.2.3 Radiative Effects

The very fact that we observe coronal holes and coronal loops, particularly in X-rays, means that energy is being radiated away. It is well known that coronal holes and coronal loops lose energy via radiation (Hollweg, 1983). The radiative loss term in the term L of energy equation (2.2) is given by,

$$L_r = N^2 P(T), \tag{2.41}$$

where N represents the total number of particles and $P(T)$ (in ergs cm^{-3} s^{-1}) is the radiative loss function. The fact that radiation loss increases as the square of the particle density for a fully ionized plasma is due to the statistical nature of the collisional exicitations of particle-photon impacts (see for example Foukal, 1990). The function $P(T)$ expresses the temperature dependence of radiative losses from the optically thin (i.e. $T > 2\times10^4$ K) coronal plasma. The calculation of this function requires knowledge of all the spectral lines and continua that contribute to radiation at a given temperature, density and chemical composition. Rosner, Tucker and Vaiana (1978) express $P(T)$ as piecewise continuous functions in the form of power laws, namely,

$$P(T) = \chi T^{\alpha}, \tag{2.42}$$

where the temperature, T, determines the values for χ and α - see Table 2.1. So, for the 1×10^6 – 2×10^6 K coronal temperatures, it is seen that $P(1\times10^6\ \text{K}) = \Lambda$, say, has the value (in ergs cm^3 s^{-1})

$$\Lambda = 1\times10^{-22}. \tag{2.43}$$

Note that the radiative loss function, $P(T)$, has also been given by other authors, for example McWhirter, Thonemann and Wilson (1975) and Raymond and Smith (1977).

Range of T (K)	χ	α
$10^{4.3}$ - $10^{4.6}$	$10^{-21.85}$	0
$10^{4.6}$ - $10^{4.9}$	$10^{-31.0}$	2
$10^{4.9}$ - $10^{5.4}$	$10^{-21.2}$	0
$10^{5.4}$ - $10^{5.75}$	$10^{-10.4}$	-2
$10^{5.75}$ - $10^{6.3}$	$10^{-21.94}$	0
$10^{6.3}$ - $10^{7.0}$	$10^{-17.73}$	-2/3

Table 2.1: The variation with temperature of χ and α according to Rosner, Tucker and Vaiana (1978).

Thus, at coronal temperatures, the volumetric rate at which radiation extracts energy is given by (Gordon and Hollweg, 1983; Sahyouni, Kiss'ovski and Zhelyazkov, 1987; Edwin and Zhelyazkov, 1992; Laing and Edwin, 1995a, b)

$$Q_{rad} = \Lambda N^2,$$

where N, here, represents the *perturbed* total number of particles. However, we have by the equation of continuity,

$$\frac{\partial \bar{N}}{\partial t} + \nabla \cdot (\bar{N}\bar{\mathbf{v}}) = 0.$$

where, following from the notation in Chapter 1, $\bar{N} = N_0 + N$. i.e. a constant background quantity plus a perturbed quantity. Linearizing this last equation yields

$$\frac{\partial N}{\partial t} + N_0(\nabla \cdot \mathbf{v}) = 0.$$

Hence, after Fourier analyzing, we may estimate N by $|N| = N_0|(\nabla \cdot \mathbf{v})|/\omega$. Thus, we may wirte the radiative loss term as

$$Q_{rad} = \Lambda \frac{N^2}{\omega^2}(\nabla \cdot \mathbf{v})^2, \tag{2.44}$$

where we have now dropped the subscript '0' from the term N_0 in Equation (2.44) and now note that in later use of this equation, N refers to the *background* number density in the interior or exterior of a coronal duct.

Wave damping due to optically thin radiation in a gravity-free, structured medium has been considered in detail by Webb and Roberts (1980). They assumed Newton's law of cooling so that the radiative energy loss term in Equation (2.2) is of the form

$$L_r = \rho_0 c_v \frac{T}{\tau_R}, \tag{2.45}$$

where τ_R is the radiative decay time. They considered a cylindrical column (cf. Section 1.7.2) of uniform magnetic field, $B_0\hat{\mathbf{z}}$, in the region $r < a$ embedded in a field-free exterior. By manipulating Equations (1.3), (1.5), (1.6), (1.12), (1.14), (1.16) and (2.2) Webb and Roberts obtain, for $r < a$,

the second-order ordinary differential equation for the amplitude, $\hat{v}_r$, of the radial component of the velocity perturbation (cf. Equation (1.76) with $n = 0$):

$$\frac{d}{dr}\left(\frac{1}{r}\frac{d(r\hat{v}_r)}{dr}\right) - \lambda_0^2\hat{v}_r = 0, \tag{2.46}$$

where

$$\lambda_0^2 = \frac{(k^2v_A^2 - \omega^2)(k^2c_0^2\Omega_0 - \omega^2)}{k^2c_0^2v_A^2\Omega_0 - \omega^2(v_A^2 + c_0^2\Omega_0)}, \tag{2.47}$$

and

$$\Omega_0 = \frac{i\omega + 1/\gamma\tau_R}{i\omega + 1/\gamma\tau_R}.$$

Similar equations to Equations (2.46) and (2.47) hold in the exterior ($r > a$) where $\mathbf{B}_e = \mathbf{0}$ so that λ_e is given by

$$\lambda_e = k^2 - \frac{\omega^2}{c_e^2\Omega_e^2},$$

with Ω_e being the corresponding expression to Ω_0 for the external region. Solutions to Equation (2.46) and its external counterpart and the corresponding solutions for $\mathbf{v}$, $\mathbf{b}$ and p_T are given by Equations (1.85) to (1.100) with λ_0 and λ_e replacing m_0 and m_e respectively. Webb and Roberts investigated the slow modes (essentially those shown in the lower band of Figure 1.8) propagating in a *slender* cylinder, i.e. one for which $ka \ll 1$. Webb and Roberts showed that the damped slow modes in a slender cylinder satisfied a simpler dispersion relation than (1.102), namely,

$$\omega^2(c_0^2\Omega_0 + v_A^2) = k^2c_0^2v_A^2\Omega_0,$$

which, when written out in full, as a cubic in ω is

$$(c_0^2 + v_A^2)\omega^3 - \frac{i}{\tau_R}\left(\frac{c_0^2}{\gamma} + v_A^2\right)\omega^2 - k^2c_0^2v_A^2\omega + \frac{ik^2c_0^2v_A^2}{\gamma\tau_R} = 0. \tag{2.48}$$

In considering a slender cylinder we are restricting attention to circumstances for which $ka \ll 1$. Essentially we reduce the cylinder to a line and consider waves which propagate at approximately the kink speed, c_k, or the tube (or cusp) speed, c_T (see also Figure 1.8). Note that in the adiabatic limit, $\tau_R \to \infty$, Equation (2.48) gives either $\omega = 0$ or the characteristic tube speed $c_T = c_0v_A/(c_0^2 + v_A^2)^{1/2}$ (Equation (1.39)).

For the radiative decay time much greater than the acoustic period ($\tau_S \ll \tau_R$, where $\tau_S = 1/kc_0$ is a typical time scale for acoustic waves), Webb and Roberts give the solutions to Equation (2.48) as

$$\omega_{1,2} \simeq \pm kc_T\left[1 - \left(\frac{\gamma - 1}{8\gamma^2}\right)\left(3 + \frac{c_0^2 + \gamma v_A^2}{c_0^2 + v_A^2}\right)\left(\frac{\tau_S}{\tau_R}\right)^2\right] + \frac{i}{2}\left(\frac{\gamma - 1}{\gamma}\right)\frac{c_T^2}{c_0^2\tau_R} \tag{2.49}$$

and

$$\omega_3 \simeq \frac{i}{\gamma}kc_0\left(\frac{\tau_S}{\tau_R}\right). \tag{2.50}$$

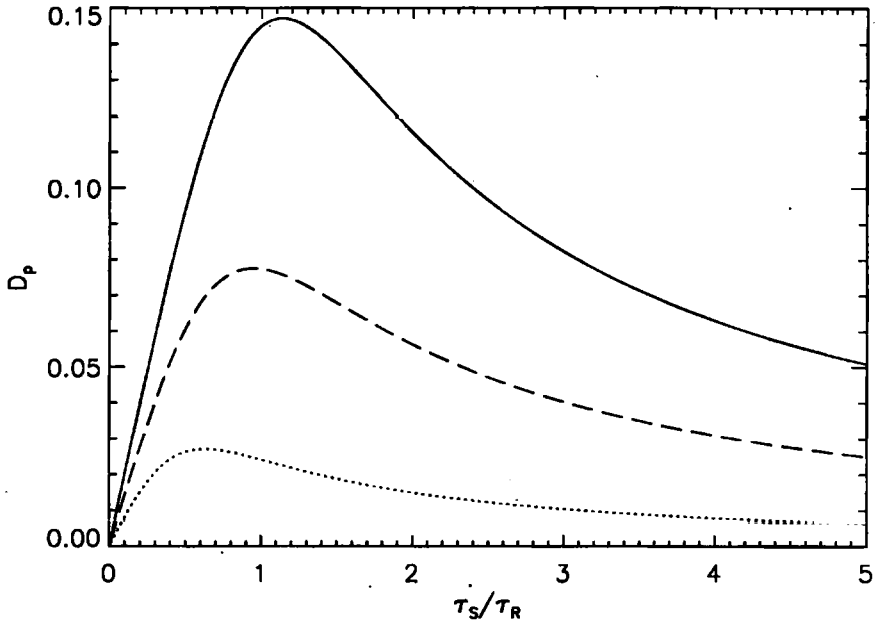

Figure 2.1: The damping per period, D_p, plotted as a function of τ_S/τ_R for $c_0^2/v_A^2 = 0$ (—), $c_0^2/v_A^2 = 1$(– – –) and $c_0^2/v_A^2 = 5$(. . .) (after Webb and Roberts, 1980).

Thus, Webb and Roberts showed that in the $\tau_S \ll \tau_R$ limit, the solution given by Equation (2.49) is simply the tube wave, $\omega = kc_T$, with its propagation speed reduced below that of the adiabatic value. The imaginary term shows that this mode is damped in time. It is noted that the decay rate is greater for a stronger magnetic field. The solution given by Equation (2.50) corresponds to a purely damped mode.

Webb and Roberts define the quantity $D_p = |\mathrm{Re}(i\omega)/\mathrm{Im}(i\omega)|$ as the *damping per period* and it is seen that its behaviour is simply given by

$$D_p \simeq \frac{1}{2}\left(\frac{\gamma-1}{\gamma}\right)\frac{c_T}{c_0}\left(\frac{\tau_S}{\tau_R}\right) \to 0, \text{ as } \frac{\tau_S}{\tau_R} \to 0. \tag{2.51}$$

Solving Equation (2.48) numerically for D_p as a function τ_S/τ_R for three cases of the ratio, c_0^2/v_A^2, results in Figure 2.1. It is seen that the damping is greater for a stronger magnetic field and that there is a maximum in the damping per period.

Note that the opposite limit $\tau_S \gg \tau_R$ corresponds to the isothermal limit.

Alternatively, regarding the frequency, ω, as real then Webb and Roberts recast Equation (2.48) in the form of a quadratic in k, namely

$$k^2 = a + ib, \tag{2.52}$$

where

$$a = \frac{\omega^2}{c_T^2} + \frac{(\gamma-1)\omega^2}{c_0^2(1+(\gamma\omega\tau_R)^2)}, \tag{2.53}$$

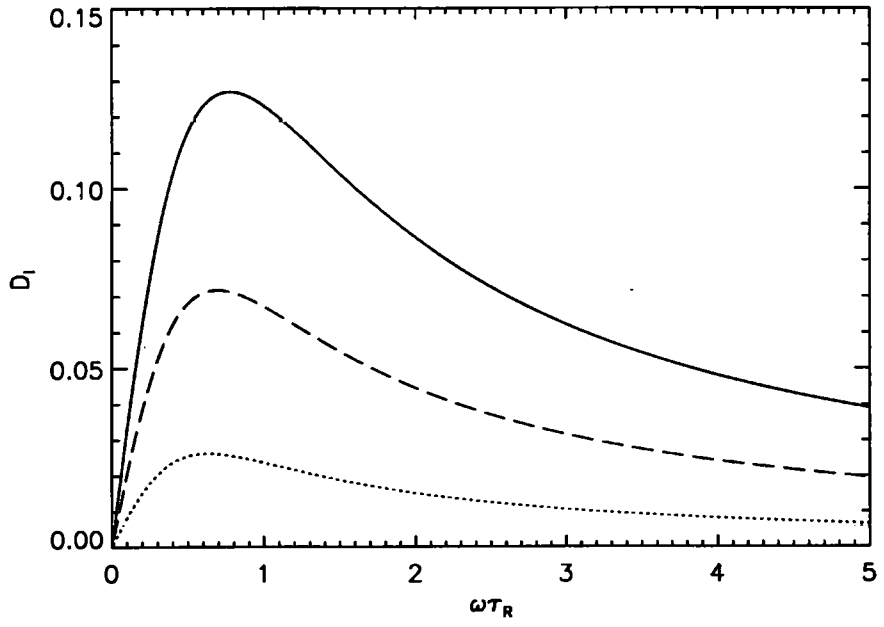

Figure 2.2: The damping per wavelength, D_l, plotted as a function of τ_S/τ_R for $c_0^2/v_A^2 = 0$ (—), $c_0^2/v_A^2 = 1$(− − −) and $c_0^2/v_A^2 = 5$(...) (after Webb and Roberts, 1980).

and

$$b = -\frac{(\gamma-1)\omega^2}{c_0^2(1+(\gamma\omega\tau_R)^2)}(\gamma\omega\tau_R). \tag{2.54}$$

Since k is a complex quantity we may write $k = k_r + ik_i$ and thus from Equation (2.52) we have

$$k_r^2 - k_i^2 = a, \tag{2.55}$$

and

$$2k_rk_i = b. \tag{2.56}$$

However, the sign of k_i is undetermined by Equation (2.52). Thus for a mode with Fourier form $e^{i(\omega t+kz)}$ to describe a wave propagating in the positive z-direction, we require that $\omega k_r < 0$, and so by Equations (2.52), (2.55) and (2.56) we must have $k_i > 0$, so that the waves propagating in the z-direction are damped.

Solving Equation (2.52) for the case when the radiative decay time is very much greater than the period of the waves ($\omega\tau_R \gg 1$) gives

$$k = \pm\frac{\omega}{c_T}\left\{1+\frac{1}{2}(\gamma-1)\frac{c_T^2}{c_0^2}\left(1+\frac{1}{4}(\gamma-1)\frac{c_T^2}{c_0^2}\right)\frac{1}{(\gamma\omega\tau_R)^2} - \frac{i}{2}\left(\frac{\gamma-1}{\gamma}\right)\frac{c_T^2}{c_0^2}\frac{1}{(\gamma\omega\tau_R)}\right\}. \tag{2.57}$$

For this case, it is seen, as was found in the temporally damped case, that the speed of propagation of the tube wave is decreased, the wave decays vertically and that the damping is greater for a stronger magnetic field.

In a similar manner to the definition of damping per period, Webb and Roberts define $D_l = |k_i/k_r|$ as the *damping per wavelength* and its behaviour is seen to be

$$D_l \simeq \frac{1}{2}\left(\frac{\gamma-1}{\gamma}\right)\frac{c_T^2}{c_0^2}(\omega\tau_R)^{-1} \to 0, \text{ as } \omega\tau_R \to \infty. \tag{2.58}$$

Equation (2.52) is solved numerically and is plotted in Figure 2.2 in terms of D_l as a function of $\omega\tau_R$ for three cases of c_0^2/v_A^2. The results of Webb and Roberts, namely Equations (2.49), (2.57), and Figures 2.1 and 2.2, show that the temporal and spatial damping coefficients have similar behaviour, that the damping reaches a maximum value when the acoustic and radiative time scales are comparable and that the damping is stronger for a stronger magnetic field.

Bogdan and Knölker (1988) examine the effects of the propagation of linear, compressive waves in a homogeneous, unstratified, uniformly magnetized radiating fluid. They find that magnetoacoustic waves suffer significantly less radiative damping than a pure acoustic mode of the same frequency and Bogdan and Knölker explain that the magnetic field acts to suppress the temperature fluctuations in the rarefactions and compressions. Schmitz (1990) has considered the damping of one-dimensional plane waves in optically thin regions of stellar atmospheres and finds, in agreement with Webb and Roberts (1980), that radiative damping is very effective if the acoustic wave period is approximately that of the radiation decay time.

2.2.4 Other Dissipative Effects

Having introduced the dissipative mechanisms which will be discussed in the remainder of this thesis, we now discuss other dissipative effects which have been considered by other authors. Further, justification is given for concentrating only on ion viscosity, electron thermal conduction and optically thin radiation.

It must be said that we are ignoring any wave dissipation due to Landau damping because a fluid (i.e. a macroscopic) description of the solar plasma is being employed and we are not dealing with the full kinetic equations (e.g. Sturrock, 1994).

Now, let us for a moment consider the mhd induction equation (Equation (1.10)). By writing the induction equation in a non-dimensionlized form with $\bar{\mathbf{B}} = B\bar{\mathbf{B}}^*$, $\bar{\mathbf{v}} = v\bar{\mathbf{v}}^*$, $t = \tau t^*$ and $\nabla = \nabla^*/l$ where the $*$ denotes non-dimensionlized quantities, it is seen that Equation (1.10) becomes

$$\frac{\partial\bar{\mathbf{B}}^*}{\partial t^*} = \nabla^* \times (\bar{\mathbf{v}}^* \times \bar{\mathbf{B}}^*) + \frac{1}{R_m}\nabla^{*2}\bar{\mathbf{B}}^*,$$

where $R_m = vl/\bar{\eta}(= vl\mu\sigma)$ is the magnetic Reynolds number and v and l represent typical velocity and length scales respectively. Typically in the solar corona $R_m \gg 1$. For example, if we take a coronal loop of length, $l = 10^8$ m, temperature, $T = 2 \times 10^6$ K, and with a typical (Alfvén) speed of 10^6 ms^{-1} then $R_m = 2.4 \times 10^{14}$. This estimate of the Reynolds number suggests that, in the corona, we can essentially ignore the diffusive term ($\bar{\eta}\nabla^2\bar{\mathbf{B}}$) and regard the coronal plasma as perfectly

conducting (i.e. $\bar{\eta} \rightarrow 0, \sigma \rightarrow \infty$). Hence we can use only the convective term ($\nabla \times (\bar{\mathbf{v}} \times \bar{\mathbf{B}})$) in the mhd induction equation. In other words, we may employ the *ideal* form of the induction equation given by Equation (1.16).

However, it must be borne in mind that there can be important exceptions to the above argument. Although it is generally true to state that, in the solar atmosphere, the length scale over which the magnetic field varies is rather large there are situations, for example in current sheets, where the magnetic field changes rapidly. The length scales are then very small and diffusivity may be important. Resistivity can also be important in the phase-mixing of Alfvén waves (Heyvaerts and Priest, 1983). Each magnetic field line in an inhomogeneous plasma oscillates independently with its own natural frequency, $\omega(x) = kv_A(x)$, which results in the build up of strong velocity gradients which eventually lead to very short length scales. So, even if there is a small amount of dissipation, (i.e. viscosity or resistivity) then the energy which has been transferred to the resonant magnetic field lines can be converted to heat.

Two closely related mechanisms by which electric currents can be dissipated are Joule heating (i.e. ohmic dissipation), $\bar{j}^2/\sigma$ (see Equation (2.11)), and magnetic reconnection. In simple Joule heating there are no topological changes in the magnetic flux surfaces of the structure. Magnetic reconnection causes such topological changes which are associated with strong convective flows and Joule heating concentrated in current sheets. Many authors, for example Rosner, Tucker and Vaiana (1978), Hinata (1980, 1981) and those referenced in the remarkable review article by Narain and Ulmschneider (1990) support the idea of Joule heating. These authors claim that Joule heating can provide the necessary coronal heating if magnetic field changes and associated electric currents are concentrated in extremely intense, narrow current sheets.

However, we shall choose to ignore Joule heating since, for typical coronal values, the effect of Joule heating is much smaller than that of viscosity and thermal conduction. Consider the following argument which is based on that of Hollweg (1986). If ΔB represents the change in magnetic field over a distance, l, then by Equation (1.5) $j \sim c\Delta B/4\pi l$ where c denotes the speed of light and all quantities are in cgs units. Hence the Joule heating term is of the order

$$Q_{joule} \sim \frac{(c\Delta B)^2}{(4\pi l)^2 \sigma},$$

where σ is the electrical conductivity (in cgs units). From Equation (2.24) the viscous heating is of the order

$$Q_{vis} \sim \eta \frac{v^2}{l^2},$$

where v is a typical velocity of the plasma. Hence it is seen that

$$\frac{Q_{joule}}{Q_{vis}} = \frac{(c\Delta B)^2}{(4\pi v)^2 \sigma \eta}. \tag{2.59}$$

For an almost adiabatic plasma it can be shown using the ideal gas law, Equation (1.12),

that

$$\frac{\Delta T}{T_0} \simeq (\gamma - 1)\frac{\Delta \rho}{\rho_0},$$

where ΔT and $\Delta \rho$ represent the changes in temperature and density, respectively, over the length, l. From the equation of mass conservation, Equation (1.3), we may estimate $\Delta \rho / \rho_0$ by

$$\frac{|\Delta \rho|}{\rho_0} \simeq \frac{|\nabla \cdot \mathbf{v}|}{\omega}.$$

Hollweg (1986) states that it is usually difficult to estimate the term $(\nabla_{\parallel} T_e)^2$ in Equation (2.34) but by combining the last two equations, Hollweg notes that

$$Q_{ther} \sim \frac{\kappa_{\parallel,el}}{T_0}(\gamma - 1)^2 \frac{v^2}{v_{ph}^2},$$

where v_{ph} is a typical phase velocity and, as before, v represents a typical plasma velocity. Hence it follows that

$$\frac{Q_{joule}}{Q_{ther}} \sim \frac{(c\Delta B v_{ph})^2 T_0}{(4\pi l v(\gamma - 1))^2 \sigma \kappa_{\parallel,el}}. \tag{2.60}$$

Inserting typical coronal values, for example $\Delta B = 10$, $T_0 = 10^6$, $l = 10^8$, $v_{ph} = 10^8$, $v = 3 \times 10^6$, $\kappa_{\parallel,el} = 8.4 \times 10^8$, $\sigma = 5.76 \times 10^{16}$, $\eta = 0.1$ and with $c = 3 \times 10^{10}$, into Equations (2.59) and (2.60) yields

$$\frac{Q_{joule}}{Q_{vis}} \sim 1.09 \times 10^{-8} \text{ and } \frac{Q_{joule}}{Q_{ther}} \sim 0.02.$$

Also we may estimate the relative importance of viscosity and conduction which, for the above parameters, gives

$$\frac{Q_{vis}}{Q_{ther}} \sim \frac{\eta T_0 v_{ph}^2}{((\gamma - 1)l)^2 \kappa_{\parallel,el}} \sim 2.7 \times 10^{-12},$$

and so it would appear that conduction is more important than viscosity.

In modelling coronal loops in the geometries of Section 1.7.1 and 1.7.2 we have assumed a homogeneous background magnetic field, $B_0\hat{\mathbf{z}}$ ($B_e\hat{\mathbf{z}}$ in the external region). The interfaces in the models in Chapter 1 are assumed to be tangential discontinuities separating two media with different physical properties. In reality the spatial inhomogeneities are smooth rather than discontinuous and resonant absorption occurs. The idea of resonant absorption is that, when waves propagate in a medium with a non-uniform Alfvén speed, then the plasma at a resonant (or a singular) point can absorb energy from the external forcing magnetic field. The resonance occurs when the frequency of an incident wave matches the local Alfvén frequency. The mode at the resonant point receives energy from the incident wave and its amplitude grows, but as a result, the incident mode undergoes a loss of energy and decays in amplitude. The point at which resonance occurs is defined as the spatial resonance point and the region about the spatial resonance point is defined as the resonant absorption layer (Ionson, 1978).

Roberts (1981) gives the governing equation for linear waves propagating in a structured medium with magnetic field in the $\hat{z}$-direction and all equilibrium quantities varying with x as:

$$\frac{d}{dx}\left\{\frac{\rho_0(x)(k_z^2v_A^2(x)-\omega^2)}{(m_0^2(x)+k_y^2)}\frac{d\hat{v}_x}{dx}\right\}-\rho_0(x)(k_z^2v_A^2(x)-\omega^2)\hat{v}_x=0, \tag{2.61}$$

where $m_0^2(x)$ is given by

$$m_0^2(x)=\frac{(k^2c_0^2(x)-\omega^2)(k^2v_A^2(x)-\omega^2)}{(c_0^2(x)+v_A^2(x))(k^2c_T^2(x)-\omega^2)}, \tag{2.62}$$

with

$$c_T^2(x)=\frac{c_0^2(x)v_A^2(x)}{c_0^2(x)+v_A^2(x)}, \tag{2.63}$$

and $\hat{v}_x$ is the amplitude of the x-component of velocity,

$$\hat{v}_x=\hat{v}_x(x)e^{i(\omega t+k_yy+k_zz)}.$$

If there exists a distance from the boundary, x^* say, where the local value of one of the natural frequencies (k_zv_A or k_zc_T) (see, for exapmle, Figure 1.5) matches the driving frequency then the coefficient of the second-order term in the differential equation (2.61) vanishes. The equation will be singular at that point and so a singular resonant absorption layer will form. Resonant absorption of Alfvén waves is associated with the singularity $\omega=k_zv_A$ and the point at which the singularity, $\omega=k_zc_T$, occurs is known as the cusp-resonance point. Sedláček (1971) showed that the component, v_y, possesses a singularity and the component, v_x, possesses a logarithmic singularity at which the plasma energy becomes infinite. As the wave energy builds up, the width of the resonant absorption layer decreases until a stationary state emerges in which all the quantities oscillate with the incident frequency and the energy flux can be dissipated viscously or ohmically.

However, resonant absorption will be ignored in the treatment of wave dissipation models contained in Chapters 3 and 4; only true tangential discontinuities of zero thickness will be considered. Of course, if resonant absorption does occur then it will represent an additional dissipative mechanism to the ones studied here.

As the waves propagate upward (i.e. in the z-direction), the oscillations of neighbouring field lines that are in phase at some altitude will become increasingly out of phase due to the non-uniformity of the field. As a result, large magnetic-field and velocity gradients develop and, in the presence of viscosity and resistivity, this mechanism leads to enhanced dissipation and heating.

Dispersion relations (1.63) and (1.102) must be interpreted as meaning that waves are ducted by the loop (i.e. they are evanescent in the loop's exterior) so that $m_e > 0$ (see Equations (1.64), (1.65), (1.103) and (1.105)) and solutions are zero at large distances from the loop. These finite solutions are in contrast to the waves being non-evanescent (sometimes described as *leaky* or *partially guided waves*) in the loop's exterior as considered by, for example, Meerson, Sasorov and Stepanov (1978), Roberts and Webb (1979), Wilson (1980) and Spruit (1982) and all these references contain a detailed discussion on the choice of solutions in the loop's exterior. The wave

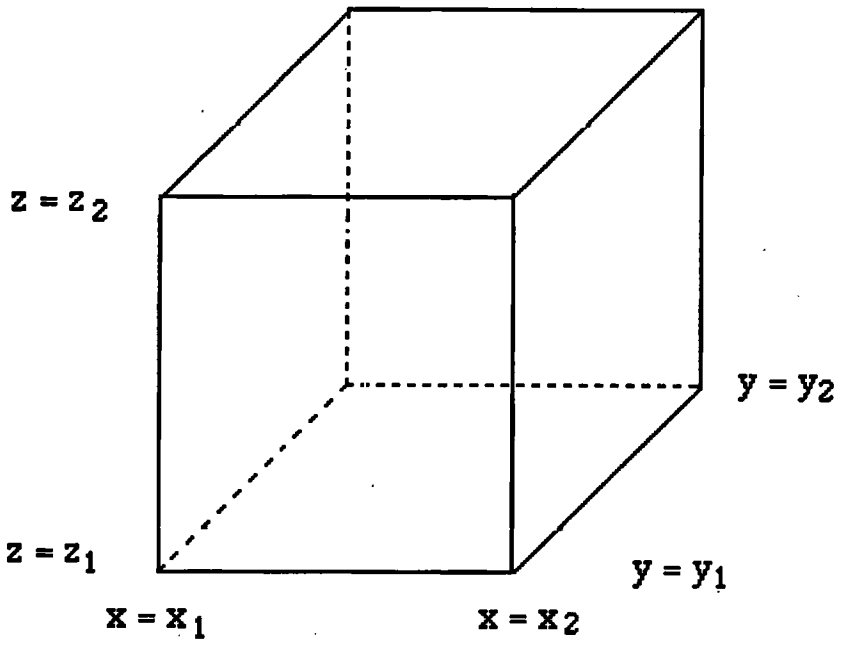

Figure 2.3: A rectangular box with volume $V = (x_2 - x_1)(y_2 - y_1)(z_2 - z_1)$.

propagating in the loop's exterior therefore carries energy *away* from the loop and so the motion of the loop must be damped. However, it must be stressed that there is no *true* dissipation in the models of Meerson, Sasorov and Stepanov, Roberts and Webb, Wilson, or Spruit. The motion of the loop is damped but only because energy is leaking into the external medium. Spruit emphasises that the damping has nothing to do with dissipative processes, it is 'analogous to the acoustic damping of a vibrating membrane in air'.

2.3 Energy Carried by MHD Waves in Structured Media

It is worth restating that the estimate of energy flux density given by Equation (1.1) is for a spatially infinite atmosphere. However, since the corona is known to be structured, one must be wary of rejecting waves based on such an energy-flux-density argument. Consideration is now given as to how much energy the waves in a structured medium possess.

Let us examine first the amount of energy carried by fast and slow magnetoacoustic waves in a slab of inhomogeneity[1] (see Section 1.7.1). The task in hand is to calculate the total energy (acoustic plus Poynting) flux, **F**, *out* of a slab of inhomogeniety. This is done in the following

[1] Similar work to that in this section but which considers the energy of ducted mhd waves in a cylindrical geometry is contained in Laing and Edwin (1995a, b).

way. Consider, first, a rectangular volume, V, with sides $x = x_1, x_2, y = y_1, y_2$, and $z = z_1, z_2$, where x_1, x_2, y_1, y_2, z_1 and z_2 are all constant (see Figure 2.3). Then the total energy (acoustic plus Poynting) flux, $\mathbf{F}$, out of V of the waves is given by

$$\int_{CS} \mathbf{F} \cdot \mathbf{dA},$$

with closed surface, CS, surrounding V, and, as before (see Section 2.2), $\mathbf{F}$ is $\frac{\gamma}{\gamma-1}p\mathbf{v} + \mathbf{S}$ is the total (acoustic plus Poynting) energy flux and $\mathbf{dA}$ is directed out of V. If $\mathbf{dA}_i$ is an element of surface area on face i of the rectangular volume, V, then we may write

$$\begin{aligned}\mathbf{F} \cdot \mathbf{dA} = \; & F_x \mid_{x=x_2} dydz - F_x \mid_{x=x_1} dydz + F_y \mid_{y=y_2} dxdz - F_y \mid_{y=y_1} dxdz \\ & + F_z \mid_{z=z_2} dxdy - F_z \mid_{z=z_1} dxdy. \end{aligned} \tag{2.64}$$

We now suppose that the volume, V, has unit length in the y-direction and that $x_{1,2} \rightarrow \mp\infty$. Further, we impose boundaries at $x = \pm a$ so that the slab model, as described in Section 1.7.1, is recovered (see, for exapmle, Figure 1.4).

Noting that $\mathbf{S} = \mathbf{E} \times \mathbf{B}/\mu$ may be written as $\mathbf{S} = (B^2\mathbf{v} - \mathbf{B}(\mathbf{B} \cdot \mathbf{v}))/\mu$, on using the ideal form of Ohm's Law from Equation (1.7), and a vector identity, then it can be shown that $\mathbf{F}$ has components

$$F_x = -\frac{\gamma}{\gamma-1}\rho_0 \frac{\omega}{k} v_x v_z + \rho_0 v_A^2 \left(v_x - 2\frac{(\omega^2 - k^2c_0^2)}{\omega k c_0^2} v_x v_z - \frac{k}{\omega} v_x v_z \right), \tag{2.65}$$

$$F_y = 0, \tag{2.66}$$

$$F_z = -\rho_0 \left(\frac{\gamma}{\gamma-1}\frac{\omega}{k} v_z^2 + v_A^2 \frac{k}{\omega} v_x^2 \right), \tag{2.67}$$

after using the expressions for b_x, b_z and p given by Equations (1.52), (1.53) and (1.54) in Chapter 1. Substituting $v_x = \hat{v}_x(x)e^{i(\omega t + kz)}$ and Equation (1.51) for v_z, with $\hat{v}_x(x)$ given by Equation (1.64) or (1.65), depending upon whether symmetric or asymmetric disturbances of the slab are being considered, then the components of $\mathbf{F}$ (averaged over time) are given by

$$\begin{aligned}\bar{F}_x \; = \; & i\frac{\gamma}{\gamma-1}\rho_0 \frac{\omega}{k} \hat{v}_x(x) \frac{kc_0^2}{(\omega^2 - k^2c_0^2)} \frac{d\hat{v}_x(x)}{dx} e^{-2k_i z} + \rho_0 v_A^2 \hat{v}_x(x) e^{-2k_i z} \\ + \; & i\rho_0 v_A^2 \hat{v}_x(x) \frac{kc_0^2}{\omega(\omega^2 - k^2c_0^2)} \frac{d\hat{v}_x(x)}{dx} e^{-2k_i z} \left[\frac{2(\omega^2 - k^2c_0^2)}{kc_0^2} + k \right], \end{aligned} \tag{2.68}$$

and

$$\bar{F}_z \; = -\bar{F}(x) e^{-2k_i z}, \tag{2.69}$$

where

$$\bar{F}(x) \; = \frac{\gamma}{\gamma-1}\rho_0 \omega \frac{kc_0^4}{(\omega^2 - k^2c_0^2)^2} \left(\frac{d\hat{v}_x(x)}{dx} \right)^2 + \rho_0 v_A^2 \frac{k}{\omega} \hat{v}_x^2(x). \tag{2.70}$$

Note that in $\bar{F}_x$ and $\bar{F}_z$ above, we have split the wave number, k, into real and imaginary parts so that $k = k_r + ik_i$ where k_r and k_i are both real quantities. The waves which we have considered until

now have been ideal, that is $k = k_r$. We now imagine that the waves contain a *small* non-ideal part to the wave number (i.e. $|k_i/k_r| \ll 1$) brought about by the introduction of dissipative mechanisms (e.g. electron thermal conduction, ion viscosity and radiation) and so the ideal waves are modified slightly.

In considering what happens to the contributions from $\bar{F}_x$, it is noted from Equations (1.64) and (1.65) that $\hat{v}_x(x) \to 0$ as $x \to \pm\infty$ and so the contributions from $\bar{F}_x$ vanish. Thus, the total energy of the waves out of V is given by

$$-\int_{CS} \overline{\mathbf{F}} \cdot \mathbf{dA} = \int \overline{F}_z \mid_{z=z_2} dx - \int \overline{F}_z \mid_{z=z_1} dx. \tag{2.71}$$

After substituting for F_z (Equation (2.69)) it is seen that for $x \to \mp\infty$ Equation (2.71) becomes

$$\int_{CS} \overline{\mathbf{F}} \cdot \mathbf{dA} = I_s \mid_{z_1} e^{-2k_i(z_2-z_1)}, \tag{2.72}$$

where

$$I_s \mid_{z_1} = e^{-2k_i z_1} \int_{-\infty}^{\infty} \bar{F}(x)dx. \tag{2.73}$$

Denoting L_z as the logarithmic decrement of the energy flux, $\mathbf{F}$, then, in a distance,

$$L_z = z_2 - z_1 = 1/2k_i,$$

the energy flux of the waves at a height $z = z_1$, given by $I_s \mid_{z_1}$, has diminished by a factor of $1/e$.

The integral in Equation (2.73) represents the total (acoustic plus magnetic) energy carried by the waves and for a slab of width $2a$, the integral is given by

$$\begin{aligned}
\int_{-\infty}^{\infty} \bar{F}(x)dx &= \int_{-\infty}^{-a} \left\{ \frac{\gamma}{\gamma-1} \frac{\rho_e \omega k c_e^4}{(\omega^2 - k^2 c_e^2)^2} \left(\frac{d}{dx} \hat{v}_x^e(x) \right)^2 + \rho_e v_{Ae}^2 \frac{k}{\omega} (\hat{v}_x^e(x))^2 \right\} dx \\
&+ \int_{-a}^{a} \left\{ \frac{\gamma}{\gamma-1} \frac{\rho_0 \omega k c_0^4}{(\omega^2 - k^2 c_0^2)^2} \left(\frac{d}{dx} \hat{v}_x(x) \right)^2 + \rho_0 v_A^2 \frac{k}{\omega} \hat{v}_x^2(x) \right\} dx \\
&+ \int_{a}^{\infty} \left\{ \frac{\gamma}{\gamma-1} \frac{\rho_e \omega k c_e^4}{(\omega^2 - k^2 c_e^2)^2} \left(\frac{d}{dx} \hat{v}_x^e(x) \right)^2 + \rho_e v_{Ae}^2 \frac{k}{\omega} (\hat{v}_x^e(x))^2 \right\} dx,
\end{aligned} \tag{2.74}$$

where $\hat{v}_x^2$ is given by Equations (1.64) and (1.65) for sausage and kink modes respectively.

In a similar fashion, it may be shown that for the ducted waves of Section 1.7.2 for a cylindrical (r, θ, z) volume, V, for $r \to \infty$, that

$$\int_{CS} \overline{\mathbf{F}} \cdot \mathbf{dA} = I_c \mid_{z_1} e^{-2k_i(z_2-z_1)}, \tag{2.75}$$

where

$$I_c \mid_{z_1} = e^{-2k_i z_1} \int_0^{\infty} \bar{F}(r) r dr, \tag{2.76}$$

with

$$\bar{F}(r) = \rho_0 \frac{\gamma}{\gamma-1} \frac{k c_0^4}{\omega^3} \hat{R}^2(r) + \rho_0 v_A^2 \frac{k}{\omega^5} \frac{(\omega^2 - k^2 c_0^2)^2}{n_0^4} \left[\left(\frac{d}{dr} \hat{R}(r) \right)^2 + \frac{n^2}{r^2} \hat{R}^2(r) \right], \tag{2.77}$$

and $\hat{R}(r)$ is given by Equation (1.103) or (1.105) for sausage or kink modes respectively. The integral in Equation (2.76) represents the total (acoustic plus magnetic) energy carried by the waves and for a cylinder of radius a, the integral is given by

$$\begin{aligned}\int_0^\infty \bar{F}(r)rdr &= \frac{k}{\omega^3}\int_0^a \left\{\frac{\gamma}{\gamma-1}\rho_0 c_0^4 \hat{R}^2(r)\right\} rdr \\ &+ \frac{k}{\omega^3}\int_0^a \left\{\rho_0 v_A^2 \frac{(\omega^2-k^2c_0^2)^2}{\omega^2 n_0^4}\left[\left(\frac{d}{dr}\hat{R}(r)\right)^2 + \frac{n^2}{r^2}\hat{R}^2(r)\right]\right\} rdr \\ &+ \frac{k}{\omega^3}\int_a^\infty \left\{\frac{\gamma}{\gamma-1}\rho_e c_e^4 (\hat{R}^e(r))^2\right\} rdr \\ &+ \frac{k}{\omega^3}\int_a^\infty \left\{\rho_e v_{Ae}^2 \frac{(\omega^2-k^2c_e^2)^2}{\omega^2 n_0^4}\left[\left(\frac{d}{dr}\hat{R}^e(r)\right)^2 + \frac{n^2}{r^2}(\hat{R}^e(r))^2\right]\right\} rdr, \end{aligned} \tag{2.78}$$

where $\hat{R}(r)$ is again given by Equation (1.103) or (1.105) for sausage or kink modes respectively. Note that the first term in each of the braces in Equation (2.74) represents the acoustic flux and the second term represents the Poynting (electromagnetic) flux.

The energy flux density for waves propagating along a slab representing a coronal loop may be readily calculated by evaluating

$$E_{\rm fd} = \frac{1}{2a}\int_{-a}^{a} \bar{F}(x)dx, \tag{2.79}$$

where $\bar{F}(x)$ is given by Equation (2.70). For the sausage waves of dispersion relation (1.63) with $\hat{v}_x(x) = \alpha_s \sin(n_0 x)$, the integration of Equation (2.79) gives

$$E_{\rm fd} = \rho_0 v_{rms}^2 v_{\rm sgs}, \tag{2.80}$$

where

$$v_{\rm sgs} = \frac{k\{v_A^2 f_{s1} + c_0^4\gamma\omega^2 f_{s2}/(\gamma-1)\}}{\omega\{f_{s1} + k^2 c_0^4 f_{s2}\}}, \tag{2.81}$$

with f_{s1} and f_{s2} given by Equations (1.68) and (1.69) respectively. Similarly, integrating Equation (2.79) for the kink modes with $\hat{v}_x(x) = \alpha_k \cos(n_0 x)$ yields

$$E_{\rm fd} = \rho_0 v_{rms}^2 v_{\rm sgk}, \tag{2.82}$$

where

$$v_{\rm sgk} = \frac{k\{v_A^2 f_{s3} + c_0^4\gamma\omega^2 f_{s4}/(\gamma-1)\}}{\omega\{f_{s3} + k^2 c_0^4 f_{s4}\}}, \tag{2.83}$$

with f_{s3} and f_{s4} given by Equations (1.71) and (1.72) respectively.

In a similar fashion, the energy flux density for waves propagating along a cylinder of radius a representing a coronal loop may be calculated by evaluating

$$E_{\rm fd} = \frac{1}{\pi a^2}\int_0^a \bar{F}(r)rdr, \tag{2.84}$$

where $\bar{F}(r)$ is given by Equation (2.77).

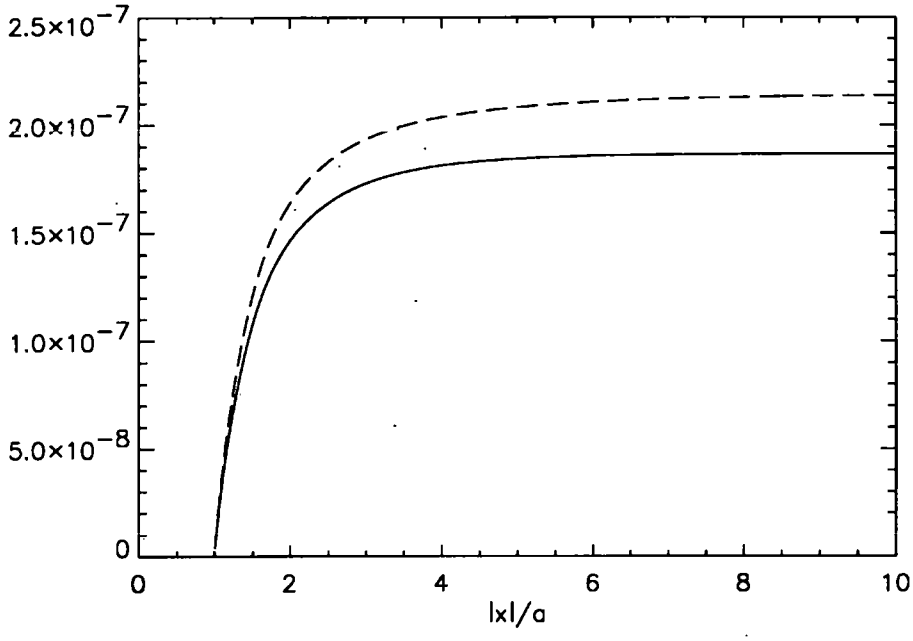

Figure 2.4: The ratio of the external to internal energy terms as a function of x (as given by terms on the right-hand-side of Equation (2.74) integrated between 0 and x) for slow (—) and fast (- - -) kink waves for the parameters of Model A of Table 1.7.

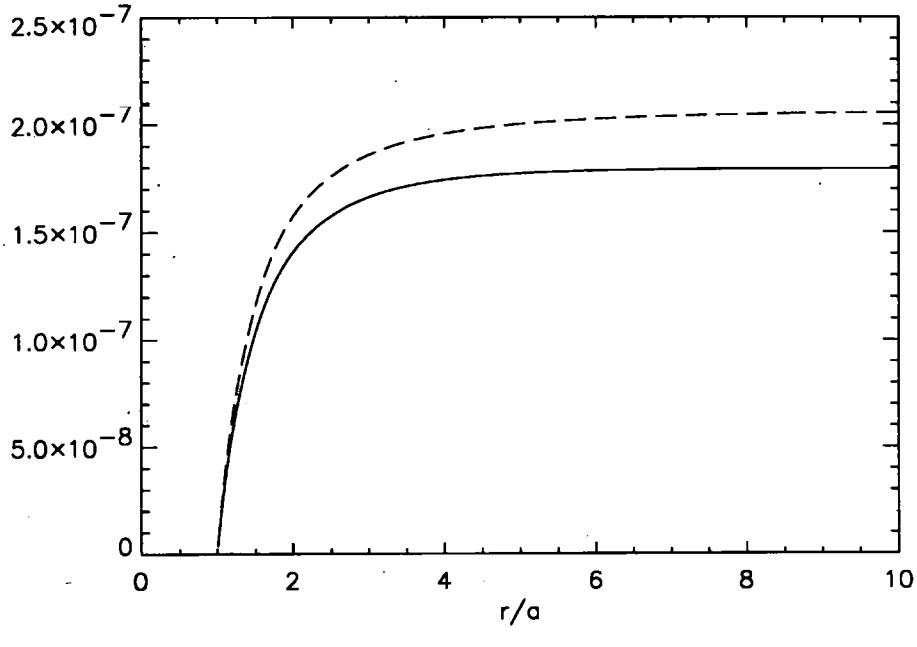

Figure 2.5: The ratio of the external to internal energy terms as a function of r (as given by terms on the right-hand-side of Equation (2.78) integrated between 0 and r) for slow (—) and fast (- - -) kink waves for the parameters of Model A of Table 1.7 (after Laing and Edwin, 1995b).

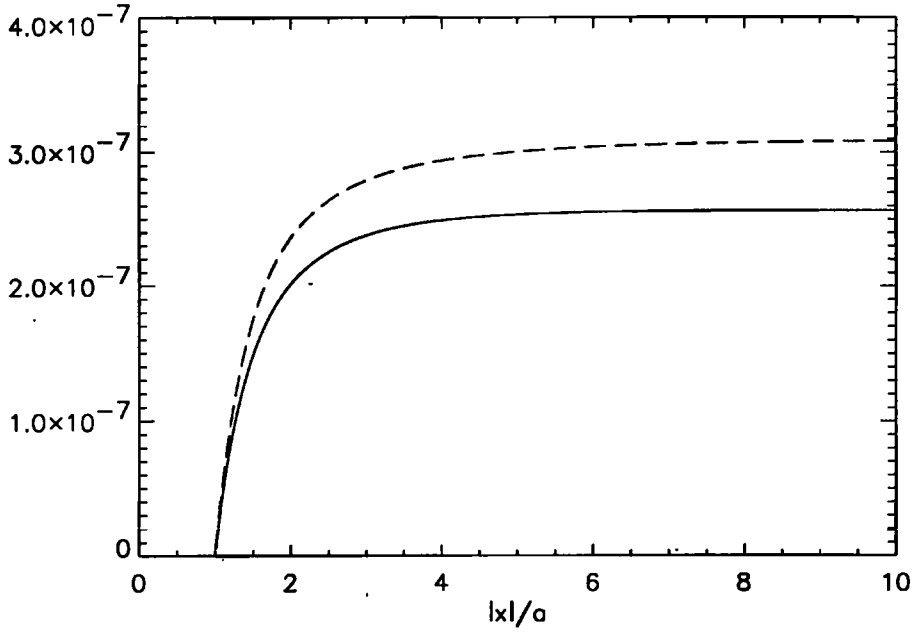

Figure 2.6: The ratio of the external to internal energy terms as a function of x (as given by terms on the right-hand-side of Equation (2.74) integrated between 0 and x) for slow (—) and fast (---) sausage waves for the parameters of Model A of Table 1.7.

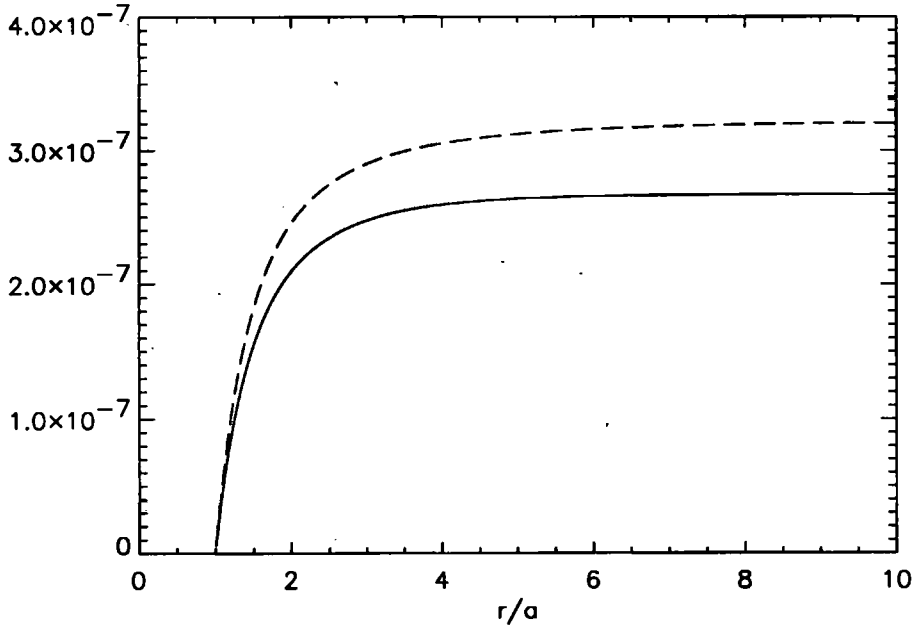

Figure 2.7: The ratio of the external to internal energy terms as a function of r (as given by terms on the right-hand-side of Equation (2.78) integrated between 0 and r) for slow (—) and fast (---) sausage waves for the parameters of Model A of Table 1.7.

For the sausage waves of dispersion relation (1.102), Laing and Edwin (1995b) have shown that the integration of Equation (2.84) with $\hat{R}(r)$ given by Equation (1.103) yields

$$E_{\rm fd} = \rho_0 v_{rms}^2 v_{\rm cgs}, \tag{2.85}$$

where

$$v_{\rm cgs} = \frac{k\{v_A^2 f_{c1} + c_0^4 \gamma \omega^2 f_{c2}/(\gamma - 1)\}}{\omega\{f_{c1} + k^2 c_0^4 f_{c2}\}}, \tag{2.86}$$

with f_{c1} and f_{c2} given by Equation (1.108) and (1.109) respectively. By integrating Equation (2.84) in a similar manner, Laing and Edwin (1995b) show the energy flux density for the kink modes is

$$E_{\rm fd} = \rho_0 v_{rms}^2 v_{\rm cgk} \tag{2.87}$$

where

$$v_{\rm cgk} = \frac{k\{v_A^2 f_{c3} + c_0^4 \gamma \omega^2 f_{c4}/(\gamma - 1)\}}{\omega\{f_{c3} + k^2 c_0^4 f_{c4}\}}, \tag{2.88}$$

with f_{c3} and f_{c4} given by Equation (1.111) and (1.112) respectively.

It is noted that Equations (2.85) and (2.87) are similar in form to their counterparts in a slab geometry (Equations (2.80) and (2.82)). In a 'cold' plasma, one in which $c_0 = c_e = 0$ (and therefore one in which the slow waves do not exist) Equations (2.80), (2.82), (2.85) and (2.87) all reduce to

$$E_{\rm fd} = \rho_0 v_{rms}^2 k v_A^2/\omega. \tag{2.89}$$

So, for an approximately uniform medium in which $\omega/k \approx v_A \approx v_{Ae}$ (see Figures 1.5 and 1.8), we recover Equation (1.1) for the energy flux density of fast waves travelling with Alfvén-type speeds in an infinite medium.

The factors $v_{\rm sgs}$ and $v_{\rm sgk}$ for the Cartesian case, and $v_{\rm cgs}$ and $v_{\rm cgk}$ for the cylindrical case, are functions of ω and k and other parameters such as B, N, T etc. where ω and k are linked by the dispersion relations given in Section 1.7, Equations (1.63) and (1.102) respectively. So, any effect of the structuring should be apparent from the variations of $v_{\rm sgs}$ and $v_{\rm sgk}$ ($v_{\rm cgs}$ and $v_{\rm cgk}$). Figures 1.5 and 1.8 show that whereas the fast waves are obviously dispersive, the slow waves are not, being confined to the narrow band between c_T and c_{Te}. Thus we expect very little difference to emerge from considering the slow waves propagating in a structured medium compared with those propagating in an infinite atmosphere.

The mhd waves that we are considering are ducted by the slab (or cylinder); they are evanescent in the duct's exterior. We now give consideration to the total energy carried by the waves. That is to say we shall examine how much energy the waves possess in the exterior of the duct. The ratio of the energy in the external region of the slab, as given by the integration of the first and third terms of Equation (2.74) over the region $|a|$ to $|x|$, to the energy in the interior, as given by the integration of the second term in Equation (2.74), is shown in Figures 2.4 and 2.6 for

the slow and fast, kink and sausage waves, respectively. (Figures 2.5 and 2.7 are the corresponding diagrams for a cylindrical geometry with the ratio of the energy in the external region, given by the integration of the third and fourth terms in Equation (2.78) over the region a to r, to the first and second integrals in Equation (2.78) which represent the energy in the cylinder).

Figures 2.4 and 2.5 show that, for the slow and fast kink waves, the proportion of the total energy in the external region (from $|a|$ to $|x|$) is very small ($\sim 10^{-7}$). Most of the energy is confined to the duct but there is a small proportion of the total energy in the external region. Similarly, most of the energy is confined to the duct for slow and fast sausage waves (Figures 2.6 and 2.7). Therefore the energy of the sausage and kink waves of the slab and cylindrical models is confined mainly to the duct. Hence the slab and cylindrical models (of density enhancements in the solar corona) are acting as 'waveguides' which channel the energy of the waves in the direction of the background magnetic field.

Furthermore, a comparison between the acoustic and electromagnetic (Poynting) contributions to the total flux in Equations (2.74) and (2.78) shows that, for slow ducted waves, most of the energy is acoustic energy (Figure 2.8). Figure 2.9 shows that most of the energy, for the fast ducted wave, comes from the electromagnetic terms of Equations (2.74) and (2.78). Of course, these results are not unexpected given that (Chapter 1) the slow, ducted waves (with phase velocity $\simeq c_T$) are acoustic-type waves and the fast, ducted waves are Alfvénic in nature.

Having considered the total energy flux of the waves, we now return to the energy flux density equations. In order to compare the energy carried by the waves in a structured situation (Equations (2.80), (2.82), (2.85) and (2.87)) with those in an unstructured medium we use the parameters of Table 1.7, and insert the details into these equations. The resulting energy flux densities for a structured medium are also compared with the requirements given in Table 1.6.

The energy flux density for fast kink waves propagating along a slab with $v_{rms} = 50$ km s^{-1} and the parameters of Model D of Table 1.7 is shown by the solid line (—) in Figure 2.10. Clearly, calculating the energy flux density for waves associated with a smaller value of v_{rms} results in a smaller value for E_{fd} (decreasing v_{rms} by a factor of 10 results in E_{fd} decreasing by a factor of 100). The unstructured energy flux density calculation using Equation (1.1) gives $\epsilon_f = 7.89 \times 10^6$ erg cm^{-2} s^{-1} (shown by the dotted line (...) in Figure 2.10) and $\epsilon_f = 7.89 \times 10^4$ erg cm^{-2} s^{-1} for large and small values of v_{rms} respectively.

Figure 2.11 shows the energy flux density, calculated by Equation (2.82), plotted against period for slow and fast waves propagating along a slab. The slow and fast waves are represented by the solid (—) and dashed (- - -) lines respectively in Figure 2.11. The parameters used in the calculation are those of Model E in Table 1.7 with a *small* (5 km s^{-1}) value for the root-mean-square velocity, v_{rms}. The figure shows that the energy flux density is not constant but varies slightly with the variation greater for the fast waves. This variation is present because a structured situation is being considered. The waves are ducted and hence are subjected to dispersion. For comparison with an unstructured medium the values for the slow and fast wave energy flux densities, ϵ_s and ϵ_f

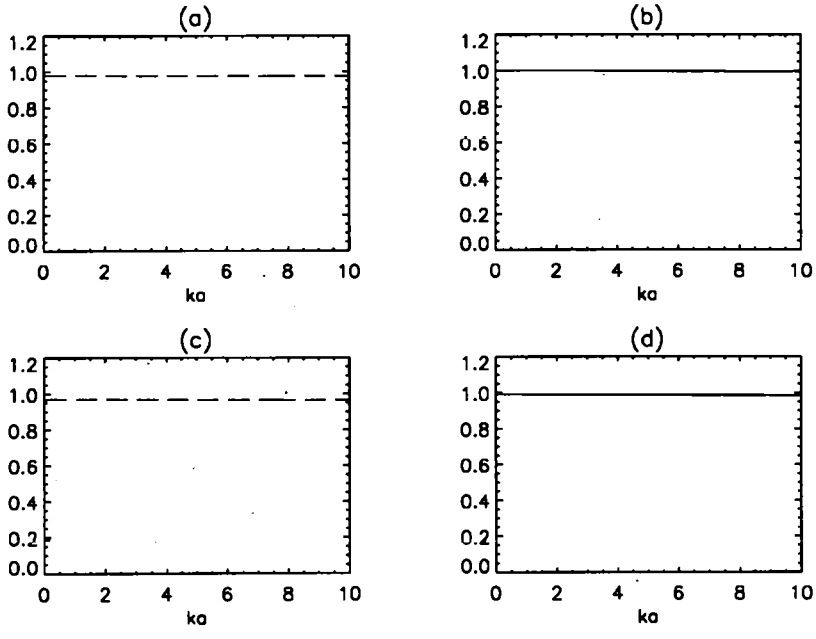

Figure 2.8: The acoustic to total energy flux ratio versus ka for slow sausage (—), and slow kink (- - -) waves propagating in a slab ((a) and (c)) and in a cylinder ((b) and (d)) for the parameters of Model A of Table 1.7.

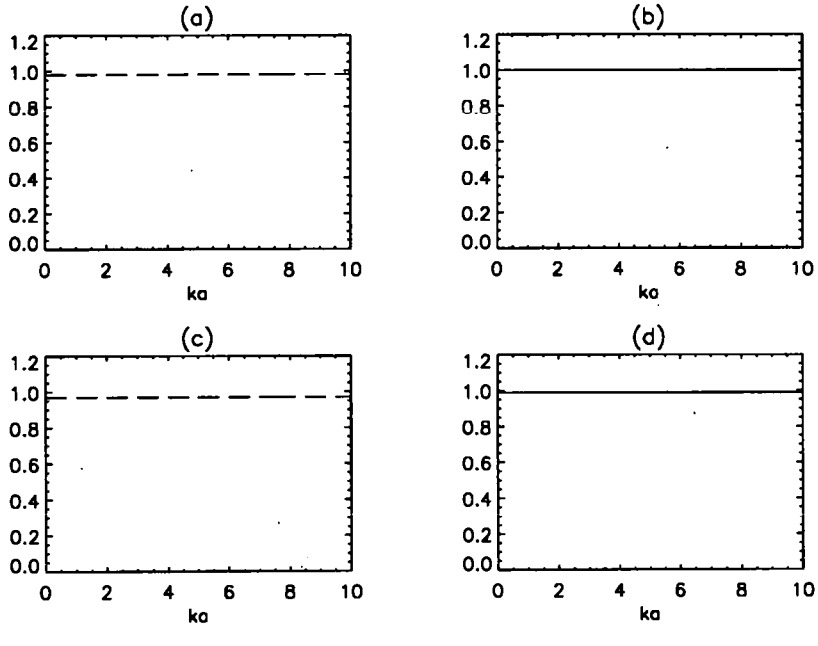

Figure 2.9: The Poynting to total energy flux ratio versus ka for fast sausage (—), and fast kink (- - -) waves propagating in a slab ((a) and (c)) and in a cylinder ((b) and (d)) for the parameters of Model A of Table 1.7.

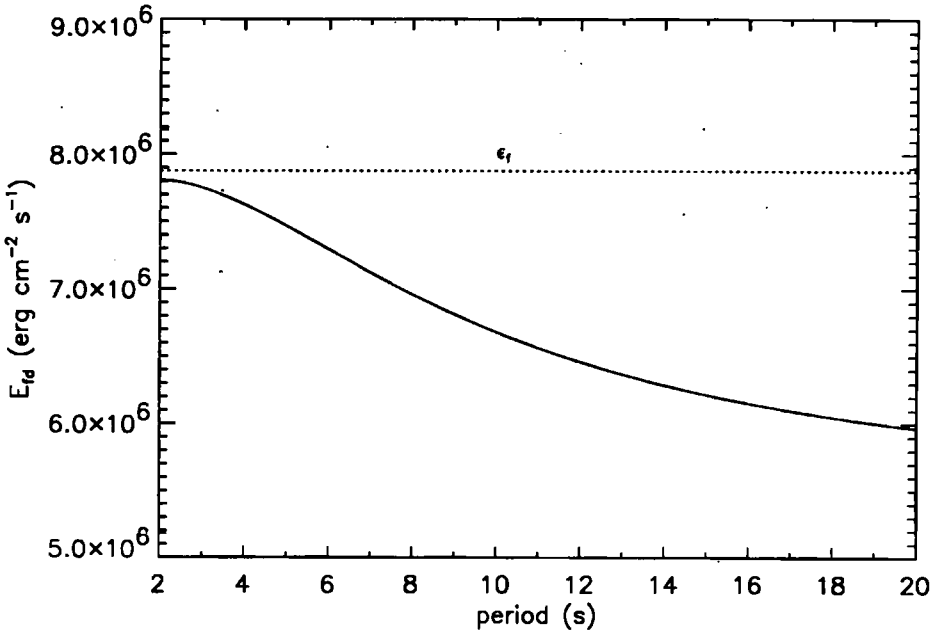

Figure 2.10: The energy flux density versus period for fast kink waves ducted by a slab (—) and for fast waves propagating in an unstructured medium (...). The parameters are for Model D of Table 1.7 with a *large* root-mean-square velocity amplitude v_{rms} (50 km s^{-1}).

respectively, as given by Equation (1.1), are shown in the figure. In the unstructured situation for the parameters of Model E, $\epsilon_s = 3.90 \times 10^4$ erg cm^{-2} s^{-1} and $\epsilon_f = 6.47 \times 10^4$ erg cm^{-2} s^{-1}.

Figure 2.12 displays the energy flux density for slow kink waves propagating along a slab with the parameters of Model G and with $v_{rms} = 50$ km s^{-1}. The calculation for an unstructured medium gives $\epsilon_s = 5.76 \times 10^7$ erg cm^{-2} s^{-1}.

In carrying out the energy flux density calculations for the sausage mode waves it was found that Equation (2.80) produced very similar results to those given in Figures 2.10 to 2.12 and so the results are not presented. The corresponding energy flux calculations for kink waves propagating along a magnetic cylinder are also similar and were presented in Laing and Edwin (1995b).

From Figures 2.10 to 2.12 it is clearly seen that the energy flux density for a spatially infinite medium, given by Equation (1.1), is a very good estimate for the energy flux density of a structured situation. Thus, estimates of the required amounts of energy given by the simple arguments of Athay and White (1979) and Hollweg (1990) (listed in Table 1.6) are appropriate to the structured situation described here.

Thus we see that if the parameters of Model E were representative of the quiet corona, then both the fast and slow ducted waves could supply enough energy (see Figure 2.11) to meet the necessary requirements of a few times 10^6 erg cm^{-2} s^{-1}. Clearly, if the parameters of Model E are applied to a hot coronal loop, then the waves need to be associated with a root-mean-square

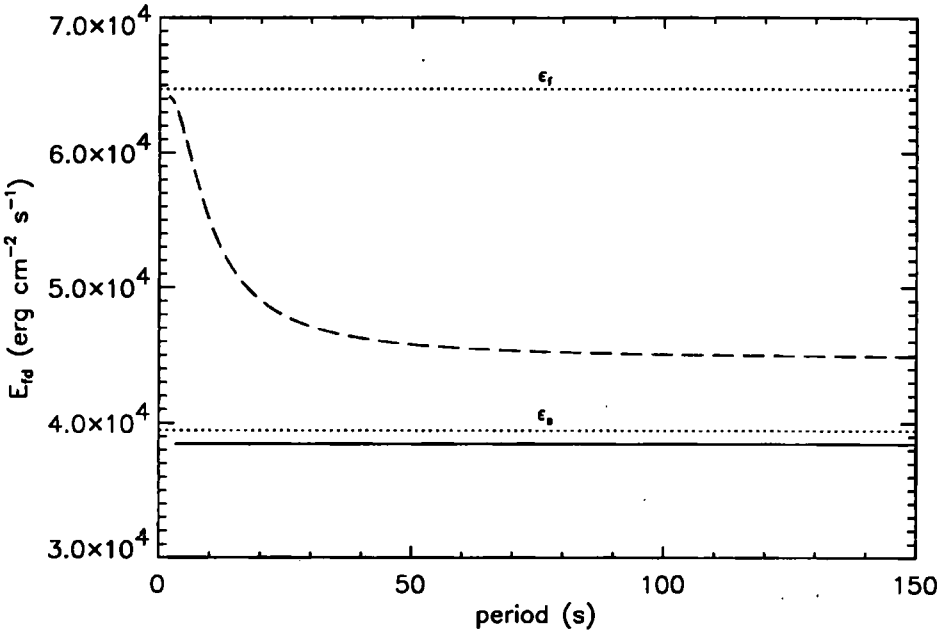

Figure 2.11: The energy flux density versus period for slow (—) and fast (- - -) kink waves ducted by a slab. The upper and lower dotted lines (labelled ϵ_f and *epsilon*$_s$) represent the energy flux density versus period for fast and slow waves propagating in an unstructured medium. The parameters are for Model E of Table 1.7 with a *small* root-mean-square velocity amplitude v_{rms} (5 km s^{-1}).

velocity amplitude in excess of 50 km s^{-1} in order for the energy flux density requirements of 10^7 erg cm^{-2} s^{-1} to be satisfied. Figures 2.10 and 2.12 show that, given a large enough v_{rms}, there is enough energy available to the waves to heat the hot loops of Models D and G.

So, from the energy flux density calculations undertaken in this section, we conclude that provided the fast and slow ducted waves can be associated with large enough root-mean-square velocity amplitudes then the ducted waves can supply enough energy to heat the corona.

Having established that the ducted waves can possess sufficient energy to meet the coronal heating requirements given in Table 1.6, two models are investigated in the following two chapters in order to see how the ducted waves may best surrender their energies to the upper solar atmosphere. Before pursuing such models it is important to say *how* dissipation is measured in this thesis.

2.4 A Measure of Dissipation Lengths

The question of what is meant by dissipating waves is now asked, i.e. what measure is going to be used in order to determine whether waves dissipate or do not dissipate? Is it the length over which they dissipate that is appropriate or the length measured in wavelengths? If dissipation lengths are measured in wavelengths then how many wavelengths are required? One may pose the

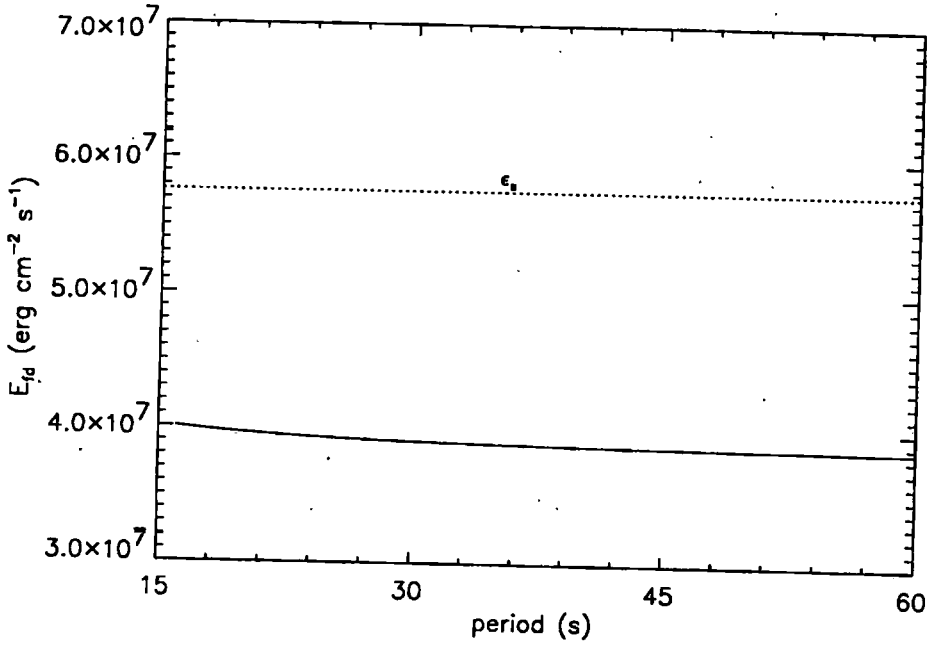

Figure 2.12: The energy flux density versus period for slow kink waves ducted by a slab (—) and for slow waves propagating in an unstructured medium (...). The parameters are for Model G of Table 1.7 with a *large* root-mean-square velocity amplitude v_{rms} (50 km s^{-1}).

question: Are 'a few wavelengths' of propagation enough? Rosner, in the discussion following the paper by Hollweg (1991), points out that dissipation in a few wavelengths is a rather general property of wave-scattering in random media.

Part of the problem is providing an appropriate length scale (other than the wavelength) against which the dissipation lengths of the waves may be measured. Gordon and Hollweg (1983) chose to express results in fractions of the solar radius (7×10^{10} cm) as their criterion. The pressure scale height in the corona (10^{10}cm) is another measure; waves travelling at least this distance could be regarded as dissipationless. Similon and Sudan (1989) do calculations with respect to radii of curvature of loops, data on which, from Table 1.3, would seem to range from 5 000 km to 50 000 km for hot loops. On the other hand, the model of a coronal loop as a relatively long, thin structure with correspondingly anisotropic variables assumes its length (and thus dissipation length for waves travelling along the loop) to be greater than its radius. From Table 1.3 it would appear that radii of 1 000 km to 15 000 km are appropriate sizes to bear in mind and lengths of the order of 10 times these values are possible damping lengths. Given that there is variation in the criteria for measuring dissipation, we shall assume that mhd waves are dissipated efficiently if the dissipation lengths are less than 4×10^9 cm.

2.5 Summary

This chapter has reviewed some of the ideas regarding dissipative mechanisms in mhd wave theories for coronal heating. The non-ideal equations of mhd have been presented and a 'measure of dissipation' for waves in the upper solar atmosphere has been given. Energy-flux-density calculations for ducted waves have shown that the waves can carry sufficient energy to meet coronal heating requirements but only if the waves are associated with large root-mean-square velocity amplitudes. It has been argued why the dissipative mechanisms for ion viscosity, electron heat conduction and radiation are important in the upper solar atmosphere and why they have been included in the models to be studied in the remainder of this thesis. In the following chapter the merits of a 'weakly dissipative' environment are considered.

Chapter 3

MHD Waves in a Weakly Dissipative Environment

3.1 Introduction

This chapter concentrates on ducted magnetohydrodynamic waves in a weakly dissipative environment subject to ion viscosity, electron thermal conduction and optically thin radiation. The discussion in Chapter 2 saw the problem of dissipation linked to a set of non-ideal equations. In general, it is a non-trivial task to solve the non-ideal equations. The scheme presented now tackles dissipative effects but in a way that the non-ideal effects can be neglected from the equations under consideration, i.e. a weakly dissipative model scheme is to be considered. A definition of what is meant by 'weak dissipation' will be made in due course in this chapter.

The scheme adopted, although not a new one, is simple yet ingenious. The underlying principle is to simply calculate the energy of the ideal waves (discussed in Chapter 1), i.e. the energy being carried by the waves described by the dispersion relations (1.63) and (1.102) in the absence of dissipation, and then, quite separately, to imagine that this energy is used up, converted by the various dissipative mechanisms. The method then yields the length over which the waves surrender a factor of $1/e$ of their energy to dissipation. Such a simple scheme allows dissipation to be investigated, but avoids a dispersion relation with dissipative terms.

3.2 A Weakly Dissipative Approach

In Section 2.2, which discussed the non-ideal mhd equations, it was shown that the non-ideal equations of motion (Equation (2.1)) and energy (Equation (2.2)) together with the Poynting flux, $\mathbf{S}$, may be combined to yield Equation (2.12). Neglecting dissipative effects, i.e. ignoring the dissipative mechanisms, viscous and ohmic dissipation, which make up L, yields the adiabatic form

of Equation (2.12), namely

$$\frac{\partial U}{\partial t} = -\nabla \cdot \mathbf{F}, \tag{3.1}$$

where, as before, $U = \rho e + B^2/2\mu$ is the total (internal plus magnetic) energy (kinetic energy effects have been neglected) and $\mathbf{F} = \frac{\gamma}{\gamma-1} p\mathbf{v} + \mathbf{S}$ is the total energy (acoustic plus Poynting) flux.

Consider now that any energy passing into a fixed volume, V, is dissipated, i.e. U is converted to heat due to the dissipative mechanisms of ion viscosity, electron thermal conduction, and radiation in an optically thin atmosphere and can be equated to the sum of their volumetric energy loss rates. That is,

$$\frac{\partial U}{\partial t} = Q_{total}, \tag{3.2}$$

where $Q_{total} = Q_{vis} + Q_{ther} + Q_{rad}$, and Q_{vis}, Q_{ther}, and Q_{rad} are given by Equations (2.24), (2.40) and (2.44) respectively. So combining Equations (3.1), (3.2) and applying Gauss' Theorem we have

$$\int_V Q_{total} dV = -\int_{CS} \mathbf{F} \cdot \mathbf{dA}, \tag{3.3}$$

for a fixed volume, V, with closed surface, CS. Then, averaging over time and by using Equations (2.71) and (2.72) we may write Equation (3.3) as

$$\int_{z_1}^{z_2}\int_{-\infty}^{\infty} \bar{Q}_{total} dx dz = e^{-2k_i z_1} e^{-2k_i(z_2 - z_1)} \int_{-\infty}^{\infty} \bar{F}(x) dx, \tag{3.4}$$

for some z_1 and z_2. The left-hand-side of Equation (3.4) is the energy (averaged over time) dissipated in the volume, V, with the assumption that $x_1, x_2 \to \mp\infty$ (see Figure 2.3). The right-hand-side of Equation (3.4) is the (time averaged) energy flux passing into V.

As remarked in Chapter 2, the energy flux of the waves, at a height $z = z_1$, diminishes by a factor of $1/e$ over a distance, $L_z = z_2 - z_1 = 1/2k_i$. Thus, we determine the height of volume, V, by writing $z_2 - z_1 = L_z$ and so the logarithmic decay, or dissipation length, for the waves in a Cartesian geometry is given by

$$L_z = \frac{\int_{-\infty}^{\infty} \bar{F}(x) dx}{\int_{-\infty}^{\infty} \bar{Q}_{total} dx}, \tag{3.5}$$

where $\bar{F}(x)$ is given by Equation (2.70) so that the numerator can be written as

$$\begin{aligned}
\int_{-\infty}^{\infty} \bar{F}(x) dx &= \frac{\gamma}{\gamma-1} \rho_e \omega \frac{k c_e^4}{(\omega^2 - k^2 c_e^2)^2} \left\{ \int_{-\infty}^{-a} \left(\frac{d\hat{v}_x(x)}{dx} \right)^2 dx + \int_a^{\infty} \left(\frac{d\hat{v}_x(x)}{dx} \right)^2 dx \right\} \\
&+ \rho_e v_{Ae}^2 \frac{k}{\omega} \left\{ \int_{-\infty}^{-a} \hat{v}_x^2(x) dx + \int_a^{\infty} \hat{v}_x^2(x) dx \right\} \\
&+ \frac{\gamma}{\gamma-1} \rho_0 \omega \frac{k c_0^4}{(\omega^2 - k^2 c_0^2)^2} \left\{ \int_{-a}^{a} \left(\frac{d\hat{v}_x(x)}{dx} \right)^2 dx \right\} \\
&+ \rho_0 v_A^2 \frac{k}{\omega} \left\{ \int_{-a}^{a} \hat{v}_x^2(x) dx \right\}.
\end{aligned} \tag{3.6}$$

The denominator may be expressed as

$$\begin{aligned}\int_{-\infty}^{\infty} \overline{Q}_{total} dx &= \frac{1}{(\omega^2 - k^2 c_e^2)^2} \int_{-\infty}^{-a} D_{ext} \left(\frac{d}{dx}\hat{v}_x(x)\right)^2 dx \\ &+ \frac{1}{(\omega^2 - k^2 c_0^2)^2} \int_{-a}^{a} D_{int} \left(\frac{d}{dx}\hat{v}_x(x)\right)^2 dx \\ &+ \frac{1}{(\omega^2 - k^2 c_e^2)^2} \int_{a}^{\infty} D_{ext} \left(\frac{d}{dx}\hat{v}_x(x)\right)^2 dx, \end{aligned} \tag{3.7}$$

where

$$D_{int} = \omega^4 d_0 + \frac{\eta}{3}(\omega^2 - 3k^2 c_0^2)^2, \tag{3.8}$$

$$D_{ext} = \omega^4 d_e + \frac{\eta}{3}(\omega^2 - 3k^2 c_e^2)^2, \tag{3.9}$$

η is given by Equation (2.23) and the terms d_0 and d_e are given by

$$d = \frac{\Lambda N^2}{\omega^2} + \frac{N^2 k_B^2 \kappa_{\parallel,el} k^2 T(\gamma - 1)^2}{\kappa_{\parallel,el}^2 k^4 (\gamma - 1)^2 + \omega^2 N^2 k_B^2}, \tag{3.10}$$

for values of N inside ($N = N_0$ for $|x| < a$) and outside ($N = N_e$ for $|x| > a$) the slab respectively.

The investigation of ducted wave energy in Section 2.4 indicated that, for both the fast and slow and symmetric and asymmetric modes, most of the wave energy was confined to the duct (see Figures 2.4 and 2.6). Nevertheless, for completeness, we include both internal and external contributions to the energy in all our subsequent calculations regarding the amount of energy available to be dissipated by the waves.

We note also, that for a cylindrical volume, V, Equation (3.5) becomes

$$L_z = \frac{\int_0^{\infty} \bar{F}(r) r dr}{\int_0^{\infty} \overline{Q}_{total} r dr}, \tag{3.11}$$

where $\bar{F}(r)$ is given by Equation (2.77) so that the numerator becomes

$$\begin{aligned}\int_0^{\infty} \bar{F}(r) r dr &= \rho_0 \frac{\gamma}{\gamma - 1} \frac{k c_0^4}{\omega^3} \int_0^a \hat{R}^2(r) r dr + \rho_e \frac{\gamma}{\gamma - 1} \frac{k c_e^4}{\omega^3} \int_a^{\infty} \hat{R}^2(r) r dr \\ &+ \rho_0 v_A^2 \frac{k}{\omega^5} \frac{(\omega^2 - k^2 c_0^2)^2}{n_0^4} \int_0^a \left\{ \left(\frac{d}{dr}\hat{R}(r)\right)^2 + \frac{n^2}{r^2}\hat{R}^2(r) \right\} r dr \\ &+ \rho_e v_{Ae}^2 \frac{k}{\omega^5} \frac{(\omega^2 - k^2 c_e^2)^2}{m_e^4} \int_a^{\infty} \left\{ \left(\frac{d}{dr}\hat{R}(r)\right)^2 + \frac{n^2}{r^2}\hat{R}^2(r) \right\} r dr. \end{aligned} \tag{3.12}$$

The denominator of Equation (3.11) becomes

$$\int_0^{\infty} \overline{Q}_{total} r dr = \frac{1}{\omega^4} \int_0^a D_{int} \hat{R}^2(r) r dr + \frac{1}{\omega^4} \int_a^{\infty} D_{ext} \hat{R}^2(r) r dr, \tag{3.13}$$

where D_{int} and D_{ext} are given by Equations (3.8) and (3.9) respectively.

Since we have effectively neglected any dissipative effects in arriving at the dissipation-length equations (3.5) and (3.11) we must impose that the waves are *weakly* dissipative (see Chapter 2) in the sense that

$$\frac{k_i}{k} \ll 1, \tag{3.14}$$

where k_i is the imaginary part of the wave number and k is the real part of the wave number component along the background magnetic field (i.e. in the $\hat{\mathbf{z}}$ direction). In other words, the number of wavelengths of the ideal waves, n_λ, travelled by the waves before being dissipated in the distance L_z must satisfy $n_\lambda \gg 1/4\pi$.

3.3 Calculations of Dissipation Lengths

If the energy being carried by the waves is to contribute to the heating of the solar corona then it must be dissipated as heat. Here, the dissipative mechanisms of ion viscosity, electron thermal conduction and radiation in an optically thin atmosphere as described by Equations (2.24), (2.40) and (2.44) are considered. Performing the integrations for Equation (3.5) yields the dissipation length, L_s, for the fast and slow magnetoacoustic sausage modes, propagating along a slab of half-width a:

$$L_s = \frac{k\left\{\rho_0\left[v_A^2 f_{s1} + \frac{\gamma}{\gamma-1}c_0^4\omega^2 f_{s2}\right] + \rho_e\left[v_{Ae}^2 f_{s5} + \frac{\gamma}{\gamma-1}c_e^4\omega^2 f_{s6}\right]\right\}}{\omega\left\{f_{s2}D_{int} + f_{s6}D_{ext}\right\}}, \tag{3.15}$$

where f_{s1} and f_{s2} are given by Equations (1.68) and (1.69) respectively, and

$$f_{s5} = \sin^2(n_0 a), \tag{3.16}$$

and

$$f_{s6} = \frac{m_e^2}{(\omega^2 - k^2 c_e^2)^2}\sin^2(n_0 a). \tag{3.17}$$

A similar expression for L_k, the length over which the energy flux of the fast and slow kink waves falls to $1/e$ of its original value, is given by

$$L_k = \frac{k\left\{\rho_0\left[v_A^2 f_{s3} + \frac{\gamma}{\gamma-1}c_0^4\omega^2 f_{s4}\right] + \rho_e\left[v_{Ae}^2 f_{s7} + \frac{\gamma}{\gamma-1}c_e^4\omega^2 f_{s8}\right]\right\}}{\omega\left\{f_{s4}D_{int} + f_{s8}D_{ext}\right\}}, \tag{3.18}$$

where f_{s3} and f_{s4} are given by Equations (1.71) and (1.72) respectively, and

$$f_{s7} = \cos^2(n_0 a), \tag{3.19}$$

and

$$f_{s8} = \frac{m_e^2}{(\omega^2 - k^2 c_e^2)^2}\cos^2(n_0 a). \tag{3.20}$$

Integration of Equation (3.11) (Laing and Edwin, 1995a, b) shows that the dissipation length, L_s, for the fast and slow magnetoacoustic sausage modes propagating along a cylinder of radius a, is given by

$$L_s = \frac{k\left\{\rho_0 m_e^2 f^2\left[v_A^2 f_{c1} + \frac{\gamma}{\gamma-1}c_0^4\omega^2 f_{c2}\right] + \rho_e n_0^2\left[v_{Ae}^2 f_{c5} + \frac{\gamma}{\gamma-1}c_e^4\omega^2 f_{c6}\right]\right\}}{\omega\left\{m_e^2 f^2 f_{c2}D_{int} + n_0^2 f_{c6}D_{ext}\right\}}, \tag{3.21}$$

where f, f_{c1} and f_{c2} are given by Equations (1.104), (1.108) and (1.109) and

$$f_{c5} = (\omega^2 - k^2 c_e^2)^2 \left[\frac{2}{m_e a} \frac{\mathrm{K}_1(m_e a)}{\mathrm{K}_0(m_e a)} + 1 - \left(\frac{\mathrm{K}_1(m_e a)}{\mathrm{K}_0(m_e a)} \right)^2 \right], \tag{3.22}$$

and

$$f_{c6} = m_e^2 \left[\left(\frac{\mathrm{K}_1(m_e a)}{\mathrm{K}_0(m_e a)} \right)^2 - 1 \right]. \tag{3.23}$$

Laing and Edwin (1995a, b) also give the corresponding expression for L_k, the length over which the energy flux of the fast and slow kink modes falls to $1/e$ of its original value:

$$L_k = \frac{k \left\{ \rho_0 m_e^2 f^2 \left[v_A^2 f_{c3} + \frac{\gamma}{\gamma - 1} c_0^4 \omega^2 f_{c4} \right] + \rho_e n_0^2 \left[v_{Ae}^2 f_{c7} + \frac{\gamma}{\gamma - 1} c_e^4 \omega^2 f_{c8} \right] \right\}}{\omega \left\{ m_e^2 f^2 f_{c4} D_{int} + n_0^2 f_{c8} D_{ext} \right\}}, \tag{3.24}$$

where f, f_{c3} and f_{s4} are given by Equations (1.104), (1.111) and (1.112) respectively, and with

$$f_{c7} = (\omega^2 - k^2 c_e^2)^2 \left[\frac{2}{m_e^2 a^2} + 1 - \left(\frac{\mathrm{K}_0(m_e a)}{\mathrm{K}_1(m_e a)} \right)^2 \right], \tag{3.25}$$

$$f_{c8} = m_e^2 \left[\left(\frac{\mathrm{K}_0(m_e a)}{\mathrm{K}_1(m_e a)} \right)^2 + \frac{2}{m_e a} \frac{\mathrm{K}_0(m_e a)}{\mathrm{K}_1(m_e a)} - 1 \right], \tag{3.26}$$

and D_{int} and D_{ext} given by Equations (3.8) and (3.9) respectively.

Equations (3.15), (3.18), (3.21) and (3.24) are of the form

$$L_{s,k} = L_{s,k}(\omega, k, \rho_0, \rho_e, a, B_0, B_e, N_0, N_e, T), \tag{3.27}$$

where ω and k are linked by the dispersion relations; Equation (1.63) for the slab case, and Equation (1.102) for the cylindrical case. Here, N_0 and N_e denote the (total) particle density inside and outside the duct, respectively. It is seen from Equations (1.11) and (1.16) that the plasma beta, β, links B, N and T. The assumption of a fully-ionized hydrogen plasma links ρ and N (e.g. $\rho_0 = N_0 m_p/2$). Further, since dense coronal loops are being modelled we recall from Chapter 1 that the density ratio, ρ_e/ρ_0, must satisfy $0 < \rho_e/\rho_0 < 1$.

At this point it is important to point out the constraints inherent in this weakly dissipative model. The method of estimating the dissipation lengths, L_s and L_k, in the previous section, the limitations of the model for the coronal structure and the criteria for efficient dissipation, as discussed in Section 2.5, mean that several constraints have to be satisfied.

1. The model is only valid for weakly dissipative situations in the sense that n_λ, the number of wavelengths (of the ideal waves) travelled by the waves before being dissipated must satisfy $n_\lambda \gg 1/(4\pi)$. Thus to ensure this criterion is fulfilled only dissipation lengths of at least one wavelength are allowed.

2. On the other hand, if the dissipation lengths are too long the waves will escape from the corona before their energy can be converted into heat. We require that the dissipation lengths are less than 4×10^9 cm for efficient dissipation (see Section 2.5).

3. The model relies on its being valid for a collisional plasma and so the criteria given by Braginskii (1965), i.e. Equations (3.25) and (3.36) must be satisfied, namely wave periods, τ, must satisfy $\tau > 4.7T^{3/2}/N_{io}$ and wave numbers, k satisfy $k < N_{el}/(4.9 \times 10^3 T^2)$. It turns out that this is not a restriction for the slow waves.

4. We wish to confine our attention to the coronal situation of Figures 1.5 and 1.8 in which the fast and slow waves (of a spatially infinite medium) are manifest as two bands of waves. Thus, as stated in Chapter 1, this will be ensured if we consider the range $0 < \beta \lesssim 1$, or stated alternatively, $8\pi N k_B T/B^2 < 1$.

These constraints mean that it is not always possible to use the model to investigate all variations of the parameters pertinent to hot loops, quiet coronal loops and coronal holes which were discussed in Chapter 1. It was found that the collisional criteria given in 3 above, fail easily for low density (10^9 cm^{-3}), high temperature (3×10^6 K) situations for the fast waves.

Computer programs in the C language (Kernighan and Ritchie, 1988) were written to compute the dissipation lengths of Equations (3.15), (3.18), (3.21) and (3.24). Firstly, the ideal dispersion relations (1.63) and (1.102) were solved numerically by employing Brent's Method (Press *et al.*, 1992) in order to relate ω to k for the various modes of Figures 1.5 and 1.8. Then the dissipation lengths of the various modes were computed by inserting the solved values of ω and k into Equations (3.15), (3.18), (3.21) and (3.24).

The task is to examine the variation of $L_{s,k}$ as the parameters of Equation (3.27) vary. However, it is important to remember that Equations (3.15), (3.18), (3.21) and (3.24) are subject to constraints.

These constraints mean that it is not always possible to use the model to investigate all variations of the parameters pertinent to hot loops, quiet coronal loops and coronal holes which were discussed in Chapter 1. It was found that the collisional criteria given in 3 above, fail easily for low density (10^9 cm^{-3}), high temperature (3×10^6 K) situations for the fast waves.

3.4 Dissipation of Ducted Fast Magnetoacoustic Waves

The ideal dispersion relations (1.63) and (1.102) were solved numerically for the fast waves, i.e. for the modes lying in the band $v_A < \omega/k < v_{Ae}$ of Figures 1.5 and 1.8. The resulting values of ω and k were substituted into Equations (3.15), (3.18), (3.21) and (3.24) and the lengths over which the ducted fast magnetoacoustic waves dissipated were calculated[1].

The results of the lowest-order kink, L_{k0}, and lowest-order sausage, L_{s0}, fast magnetoacoustic modes with the parameters of Model B from Table 1.7 are shown in Figures 3.1 to 3.4. In general it was found that the dissipation length, when measured in wavelengths, appeared to possess a minimum (see Figures 3.3 and 3.1). The existence of a minimum in the dissipation length when

[1]The work in this section forms the basis for Laing and Edwin (1995a).

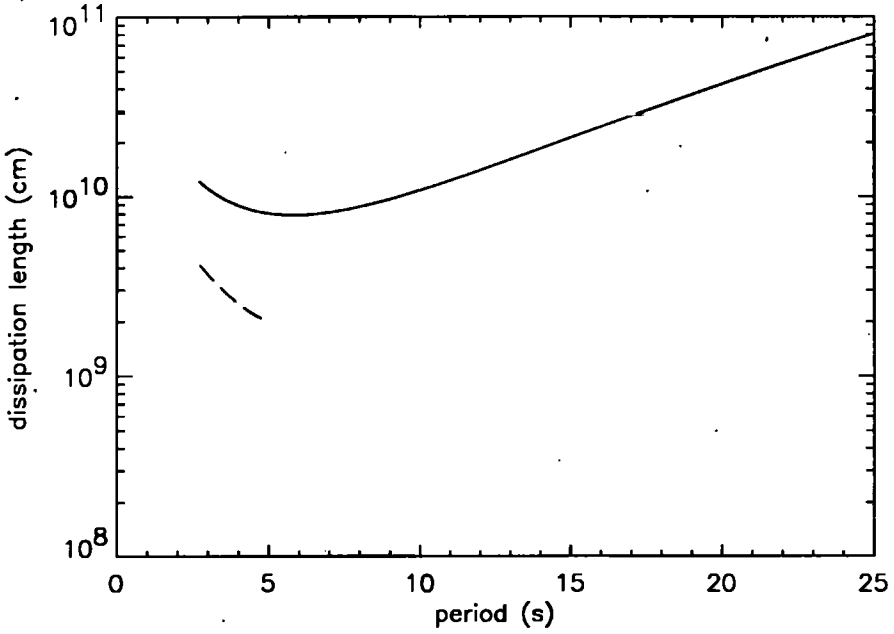

Figure 3.1: The dissipation length versus period for the fast modes L_{k0} (—) and L_{s0} (---) propagating in a slab with the parameters of Model B of Table 1.7.

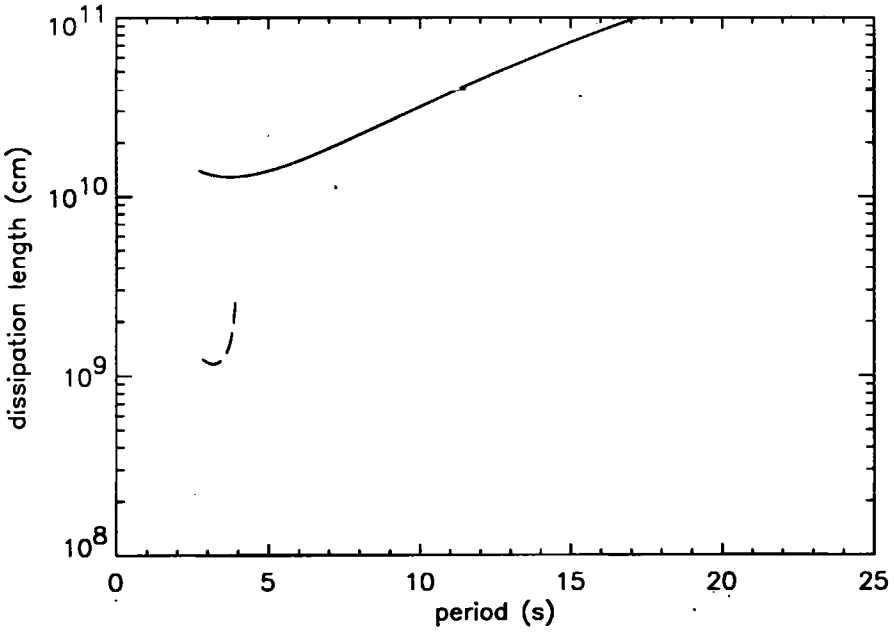

Figure 3.2: The dissipation length versus period for the fast modes L_{k0} (—) and L_{s0} (---) propagating in a cylinder with the parameters of Model B of Table 1.7.

measured in wavelengths is due to the fact that the wavelength of the waves has a dependancy proportional to $1/k$. Moreover, what is more apparent from the figures is that the minimum for the lowest-order kink mode occurs at about 20 wavelengths for waves with periods of about 10 s in the slab case, and in the cylindrical case this minimum occurs at about 7 s when the dissipation length is approximately 55 wavelengths. An analytical investigation into this problem is rather unwieldy especially when one considers, for example, the intricate way in which ω and k of Equations (3.15) and (3.18) are interlinked by the dispersion relation (1.63). On the whole there seems to be a significant difference in dissipation lengths between coronal loops modelled as ducted slabs and cylinders. However, as is seen from Figures 3.1 and 3.2, the dissipation lengths of the ducted fast, kink, magnetoacoustic waves, in terms of a true distance and not on wavelength (which has $1/k$ spatial dependence), are seen to be of the same order of magnitude (10^{10} cm) for the slab and cylindrical geometries. The dissipation lengths of the fast, sausage, magnetoacoustic waves are also seen to be of the same order (10^9 cm) for the two geometries. Since it was remarked in Section 2.5 that measurement of dissipation lengths in terms of wavelengths was one way of giving a 'measure of dissipation', it will prove convenient to quote the dissipation lengths of fast magnetoacoustic waves in terms of wavelengths. Thus, the conditions, e.g. magnetic field strength, density, etc., which give rise to the shortest dissipation lengths may be easily found.

Figures 3.1 and 3.2 demonstrate that the lowest order fast magnetoacoustic wave has a dissipation length of about one order of magnitude greater than the lowest-order sausage mode. The left-hand cut-offs of the figures mark where the collisional criteria of Equations (2.25) and (2.36) fail, that is to say only periods of more than 2 s are valid for this weakly dissipative model. The right-hand cut-offs of the sausage modes represent the ω/kv_{Ae} cut-offs of the dispersion curves (e.g. see Figures 1.5 and 1.8).

The relative importance of the three dissipation mechanisms of ion viscosity, electron thermal conduction, and radiation, given by Equations (2.24), (2.40) and (2.44), for a coronal loop treated as a magnetic slab and cylinder are shown in Figures 3.5 and 3.6 respectively. It is seen that for ka values of less than about 0.1 (i.e. wave periods > 10 s), electron thermal conduction is the most important of the three dissipative terms considered here. The ratio of the volumetric radiation loss to the total energy loss is too small to be seen in Figures 3.5 and 3.6.

The dissipation lengths for fast magnetoacoustic waves propagating along a magnetic slab and cylinder representing a coronal loop were investigated for the parameter ranges of Table 1.8. The results, in terms of the minima (expressed both in wavelengths and as a true distance), for the lowest-order, L_{k0}, and first-order, L_{k1}, kink and lowest-order, L_{s0}, sausage modes are shown in Tables 3.1 and 3.3 for two values of the magnetic field strength of 10 and 50 G for the slab case. Here $a = 5 \times 10^8$ cm and $\rho_0/\rho_e = 0.5$. The corresponding tables for the cylindrical case are Tables 3.2 and 3.4. The gaps in the tables indicate regions where no reasonable combinations of temperature and pressure density could be found so that the plasma could be considered collisional. Also, in order to ensure that the plasma is representative of the corona ($\beta < 1$), some entries in Tables 3.1 and 3.2

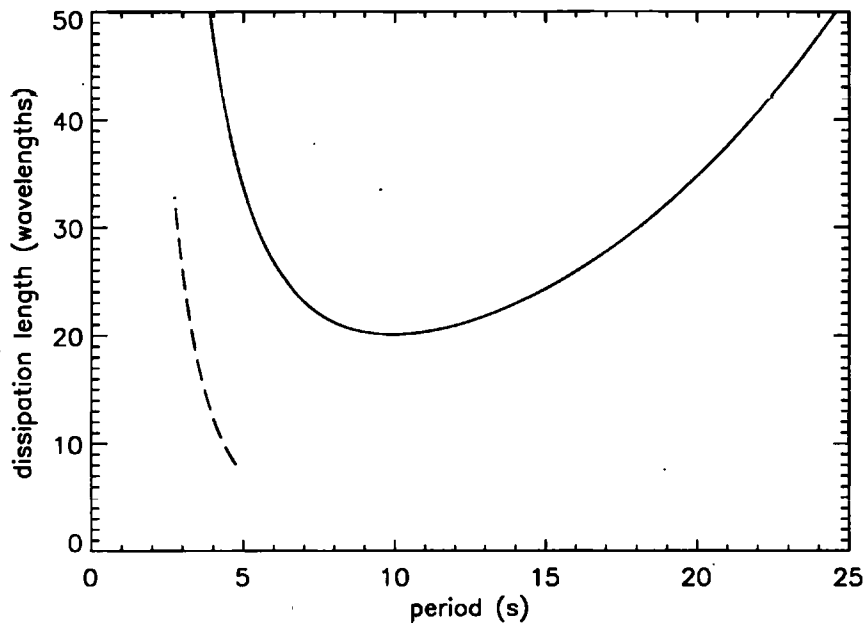

Figure 3.3: The dissipation length (in wavelengths) versus period for the fast modes L_{k0} (—) and L_{s0} (---) propagating in a slab with the parameters of Model B of Table 1.7.

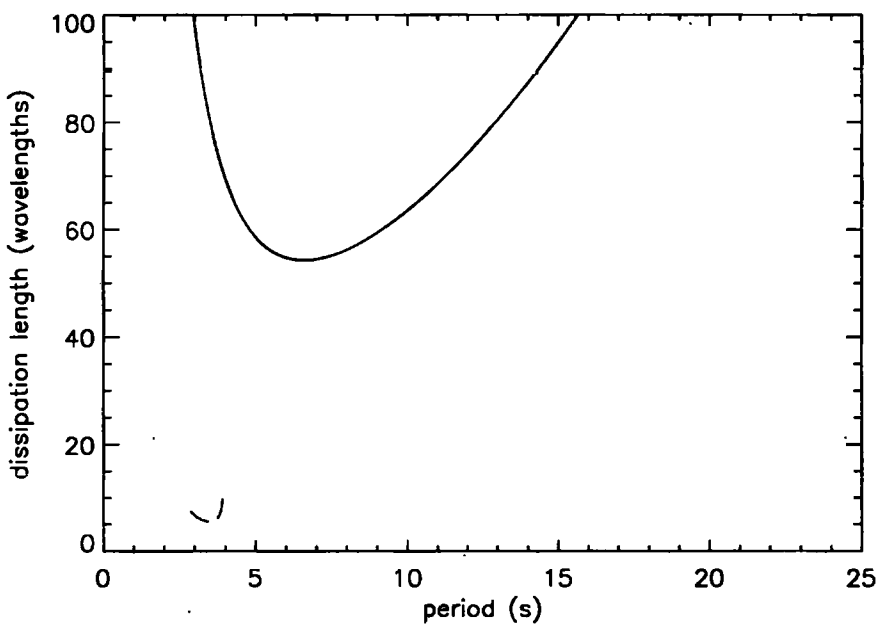

Figure 3.4: The dissipation length (in wavelengths) versus period for the fast modesL_{k0} (—) and L_{s0} (---) propagating in a cylinder with the parameters of Model B of Table 1.7.

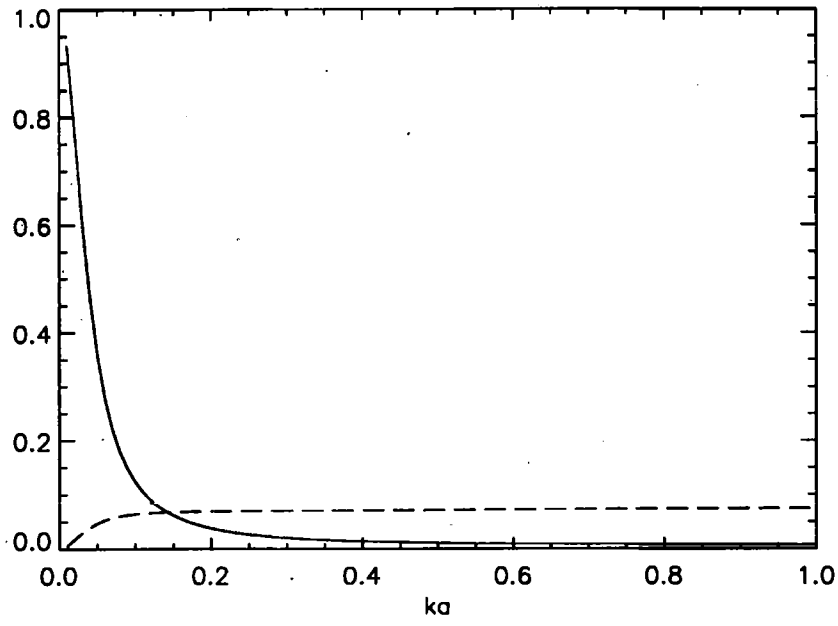

Figure 3.5: Relative importance of the dissipative terms: Q_{ther}/Q_{total} (—) and Q_{vis}/Q_{total} (- - -) for fast waves propagating in a slab with the parameters of Model B of Table 1.7.

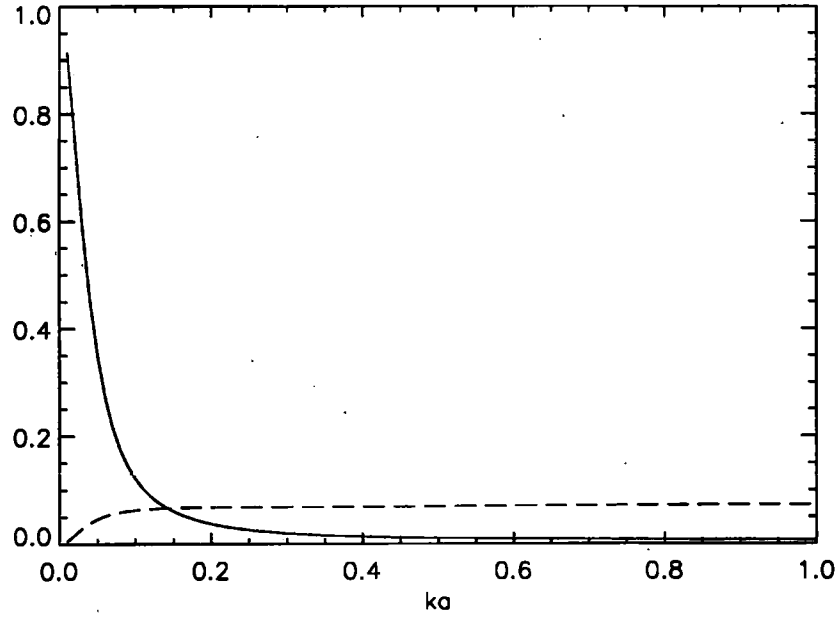

Figure 3.6: Relative importance of the dissipative terms: Q_{ther}/Q_{total} (—) and Q_{vis}/Q_{total} (- - -) for fast waves propagating in a cylinder with the parameters of Model B of Table 1.7.

T (K)	mode	N (cm^{-3})		
		5.0×10^8	5.0×10^9	5.0×10^{10}
1.0×10^6	L_{k0}	4.5×10^{11} (360.0)	2.5×10^{11} (200.0)	(B = 15 G) 1.0×10^{10} (5.5)
	L_{s0}	1.2×10^{11} (98.0)	5.8×10^{10} (63.0)	4.9×10^9 (3.7)
	L_{k1}		2.0×10^{10} (35.0)	4.2×10^9 (5.4)
2.0×10^6	L_{k0}		3.4×10^{10} (25.0)	(N = 1.0×10^{10}) 8.7×10^9 (3.7)
	L_{s0}		1.0×10^{10} (8.6)	2.5×10^9 (2.2)
	L_{k1}		3.8×10^9 (5.4)	1.4×10^9 (1.9)
3.0×10^6	L_{k0}		2.2×10^{10} (11.0)	(N = 1.0×10^{10}) 4.0×10^9 (3.7)
	L_{s0}		5.8×10^9 (4.3)	2.5×10^9 (2.2)
	L_{k1}		2.9×10^9 (3.6)	1.4×10^9 (1.9)

Table 3.1: Minimum dissipation lengths (in cm) of the modes L_{k0}, L_{s0}, and L_{k1} for fast waves propagating in a 10 G magnetic slab. The lengths, as measured in wavelengths, are shown in parentheses.

have to be changed to those values of magnetic field strength and density given in parentheses.

It was found that when B is increased the dissipation length increases so that the damping lengths become unrealistically large if B is a few tens of gauss. It was also found that the dissipation length decreases with mode order. This is encouraging from the point of view of effective dissipation, i.e. very short dissipation lengths, but as is seen from the tables there are very few instances in which the weakly dissipative theory holds for these higher-order modes and for which the plasma may be regarded as collisional. Further, it is unlikely that, in the upper solar atmosphere, the higher-order modes will be excited as readily as the lower- order ones. From these calculations, however, it is clear that the sausage waves have much shorter dissipation lengths than have the lowest-order kink waves - in fact the next higher-order kink waves have dissipation lengths comparable with the lowest order symmetric ones.

It is difficult to make general statements about the variation of effective dissipation with temperature and density. However if the plasma beta is increased then the damping increases in the main. Since β is proportional to both density and temperature this usually means that the

T (K)	mode	N (cm^{-3})		
		5.0×10^8	5.0×10^9	5.0×10^{10}
				(B = 15 G)
1.0×10^6	L_{k0}	3.2×10^{11} (470.0)	1.6×10^{11} (250.0)	2.0×10^{10} (13.0)
	L_{s0}	5.3×10^{10} (61.0)	3.3×10^{10} (46.0)	4.2×10^9 (4.7)
	L_{k1}		1.6×10^{10} (30.0)	3.8×10^9 (5.5)
				($N = 1.0 \times 10^{10}$)
2.0×10^6	L_{k0}		3.6×10^{10} (39.0)	8.5×10^9 (12.0)
	L_{s0}		5.5×10^9 (6.4)	2.3×10^9 (3.6)
	L_{k1}		3.1×10^9 (4.7)	1.5×10^9 (2.8)
				($N = 1.0 \times 10^{10}$)
3.0×10^6	L_{k0}		3.0×10^{10} (23.0)	3.9×10^9 (5.3)
	L_{s0}		3.5×10^9 (3.9)	1.7×10^9 (1.7)
	L_{k1}		2.4×10^9 (3.3)	1.2×10^9 (1.8)

Table 3.2: Minimum dissipation lengths (in cm) of the modes L_{k0}, L_{s0}, and L_{k1} for fast waves propagating in a 10 G magnetic cylinder. The lengths, as measured in wavelengths, are shown in parentheses (from Laing and Edwin, 1995a).

T (K)	mode	N (cm^{-3})		
		5.0×10^8	5.0×10^9	5.0×10^{10}
1.0×10^6	L_{k0}		8.0×10^{12} (6500)	1.1×10^{12} (260)
	L_{s0}		2.1×10^{12} (1700)	2.1×10^{11} (160)
	L_{k1}			1.5×10^{11} (180)
2.0×10^6	L_{k0}		1.2×10^{12} (1000)	7.8×10^{11} (230)
	L_{s0}		3.2×10^{11} (280)	1.3×10^{11} (100)
	L_{k1}			6.0×10^{10} (83)
3.0×10^6	L_{k0}			2.4×10^{11} (140)
	L_{s0}			5.7×10^{10} (47)
	L_{k1}			1.7×10^{10} (28)

Table 3.3: Dissipation lengths in a slab as for Table 3.1 but for a magnetic field strength of 50 G.

T (K)	mode	N (cm^{-3})		
		5.0×10^8	5.0×10^9	5.0×10^{10}
1.0×10^6	L_{k0}		4.8×10^{12} (8100)	1.9×10^{12} (910)
	L_{s0}		9.5×10^{11} (1100)	1.6×10^{11} (180)
	L_{k1}			1.3×10^{11} (170)
2.0×10^6	L_{k0}		7.6×10^{11} (1300)	6.6×10^{11} (580)
	L_{s0}		1.5×10^{11} (170)	8.4×10^{10} (94)
	L_{k1}			4.7×10^{10} (74)
3.0×10^6	L_{k0}			1.3×10^{11} (200)
	L_{s0}			2.8×10^{10} (37)
	L_{k1}			1.3×10^{10} (24)

Table 3.4: Dissipation lengths in a cylinder as for Table 3.2 but for a magnetic field strength of 50 G (from Laing and Edwin, 1995a).

T (K)	N (cm^{-3})	β	mode	Dissipation length (cm)	ka	period (s)
1.4×10^6	1.5×10^{10}	0.73	L_{k0}	1.5×10^9 (7.2)	3.0	7.4
			L_{s0}	8.7×10^8 (3.5)	2.5	7.5
			L_{k1}	3.6×10^8 (2.0)	3.6	4.1
		0.00	$L_{k0}(cold)$	5.4×10^9 (11.9)	1.4	21.3
1.9×10^6	1.5×10^{10}	0.99	L_{k0}	1.4×10^9 (3.8)	2.0	9.8
			L_{s0}	5.1×10^8 (1.5)	1.9	13.3
			L_{k1}	2.9×10^8 (1.0)	2.7	4.4
		0.00	$L_{k0}(cold)$	4.0×10^9 (7.3)	1.2	24.7
2.0×10^6	1.0×10^{10}	0.69	L_{k0}	2.7×10^9 (7.0)	1.7	9.7
			L_{s0}	1.0×10^9 (2.3)	1.5	8.1
			L_{k1}	3.4×10^8 (1.3)	2.4	4.0
		0.00	$L_{k0}(cold)$	6.0×10^9 (10.0)	1.0	21.8
2.5×10^6	1.0×10^{10}	0.87	L_{k0}	2.8×10^9 (6.1)	1.4	11.1
			L_{s0}	8.0×10^8 (1.1)	1.5	7.7
			L_{k1}	3.1×10^8 (1.5)	2.2	4.0
		0.00	$L_{k0}(cold)$	6.3×10^9 (8.4)	0.8	26.0

Table 3.5: Four sets of coronal parameters for which dissipation of fast waves would be possible in a 10 G magnetic slab of half-width 10^8 cm and density ratio 0.25.

T (K)	N (cm^{-3})	β	mode	Dissipation length (cm)	ka	period (s)
1.4×10^6	1.5×10^{10}	0.73	L_{k0}	1.6×10^9 (9.5)	3.8	5.9
			L_{s0}	4.6×10^8 (2.4)	3.3	4.8
			L_{k1}	1.3×10^8 (1.8)	5.0	2.3
		0.0	$L_{k0}(cold)$	5.3×10^9 (21)	2.5	13
1.9×10^6	1.5×10^{10}	0.99	L_{k0}	9.7×10^8 (5.9)	3.8	5.8
			L_{s0}	3.9×10^8 (1.5)	2.4	5.4
			L_{k1}	1.1×10^8 (0.8)	4.5	2.3
		0.0	$L_{k0}(cold)$	5.4×10^9 (17)	1.9	16
2.0×10^6	1.0×10^{10}	0.69	L_{k0}	3.3×10^9 (13)	2.4	7.3
			L_{s0}	4.9×10^8 (1.5)	1.9	5.2
			L_{k1}	2.7×10^8 (1.1)	2.6	3.5
		0.0	$L_{k0}(cold)$	8.8×10^9 (25)	1.8	14
2.5×10^6	1.0×10^{10}	0.87	L_{k0}	3.7×10^9 (14)	2.4	7.0
			L_{s0}	4.6×10^8 (1.2)	1.7	5.1
			L_{k1}	2.5×10^8 (1.0)	2.5	3.3
		0.0	$L_{k0}(cold)$	9.3×10^9 (25)	1.7	15

Table 3.6: Four sets of coronal parameters for which dissipation of fast waves would be possible in a 10 G magnetic cylinder of radius 10^8 cm and density ratio 0.25 (from Laing and Edwin, 1995a).

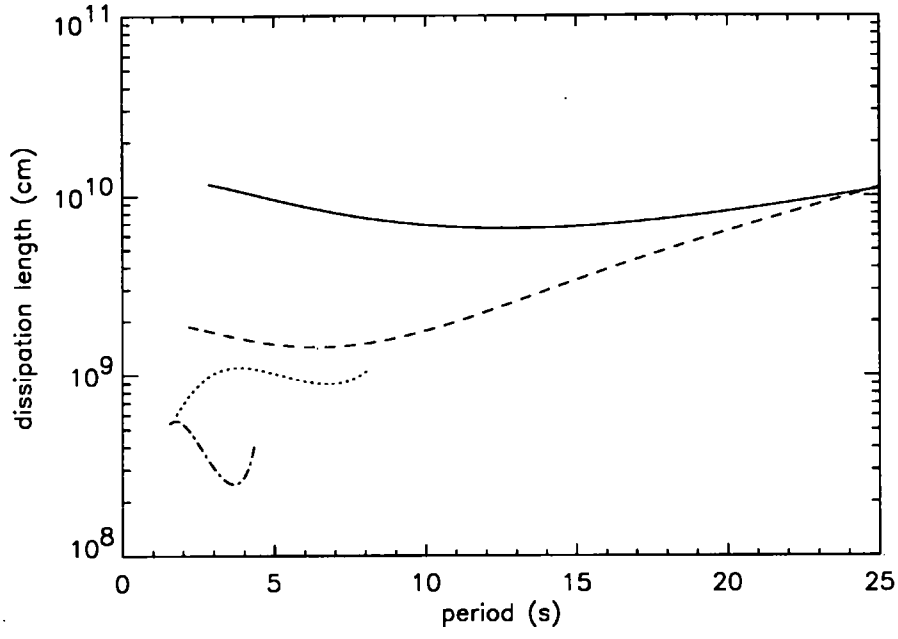

Figure 3.7: The dissipation length (in cm) versus period for the fast modes L_{k0} (---), L_{k1}(.-.-), L_{s0} (....) and $L_{k0}(cold)$ (—) for a magnetic slab. The parameters are for the third case of Table 3.5.

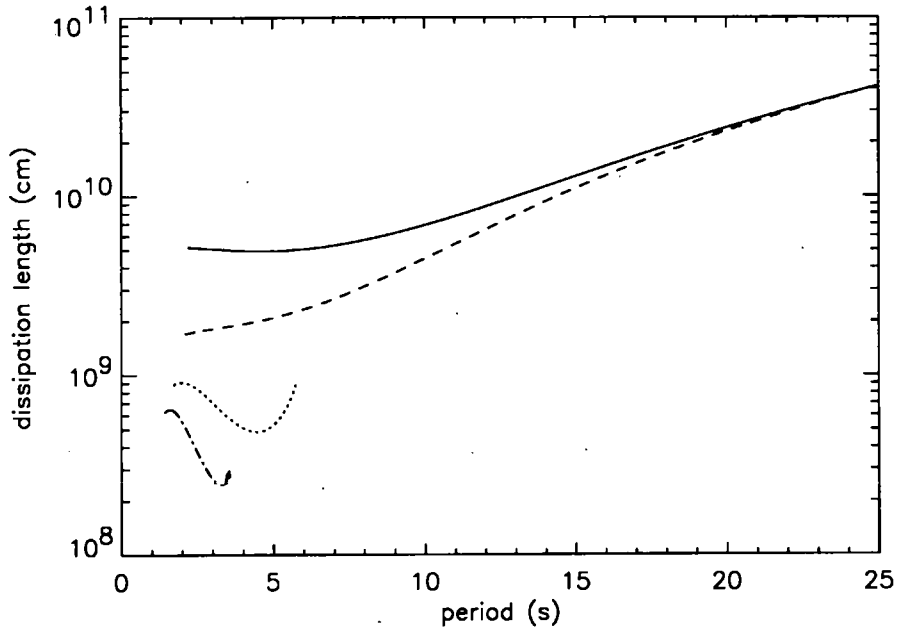

Figure 3.8: The dissipation length (in cm) versus period for the fast modes L_{k0} (---), L_{k1}(.-.-), L_{s0} (....) and $L_{k0}(cold)$ (—) for a magnetic cylinder. The parameters are for the third case of Table 3.6.

higher the temperature and density the shorter is the dissipation length. When the loop radius a was increased, it was found, for example, that the curves of Figures 3.1 and 3.2 were shifted to the right and so it is only the waves with longer periods that experience more effective dissipation.

A systematic variation of parameters led to a set of 'best case' scenarios (see Tables 3.5 and 3.6) for which the parameters (satisfying the criteria of Braginskii) provided the most efficient (in the sense of shortest) dissipation lengths. The corresponding minimum dissipation lengths for the lowest-order sausage and the first-order kink modes are shown in Tables 3.5 and 3.6. The dissipation length, both in wavelengths and as a true distance, for the lowest-order kink modes in 'cold' plasma (in which $c_0 = c_e = 0$) are also shown in Tables 3.5 and 3.6. Figures 3.7 to 3.14 show the dissipation lengths both in terms of true distances and in wavelengths, for the two lowest-order kink modes and the lowest-order sausage mode, for a set of parameters for which dissipation appears possible (the third case of Tables 3.5 and 3.6) plotted as functions of period, and of wave number k. Figures 3.7 to 3.14 also show the corresponding curves for a 'cold' plasma, i.e. one with $\beta = 0$. From the 'best case' scenarios it can be seen that the only possible candidates for dissipation are waves with periods of about 2 to 10 s in fields of less than 15 G. In this period range the dissipation is more effective in the warm plasma situation (see, for example, Figures 3.7 - 3.10).

3.5 Dissipation of Ducted Slow Magnetoacoustic Waves

Having considered the lengths over which fast ducted waves dissipate, attention is now given to the dissipation lengths of slow ducted waves[2]. The ideal dispersion relations (1.63) and (1.102) are now solved numerically for the slow waves, i.e. the modes lying in the narrow band $c_T < \omega/k < c_{Te}$ of Figures 1.5 and 1.8. The resulting values of ω and k are, in turn, substituted into Equations (3.15), (3.18), (3.21) and (3.24), and the lengths over which the ducted slow magnetoacoustic waves dissipate are calculated.

Since the ducted slow waves are confined to such a narrow band between c_T and c_{Te}, we shall consider only the lowest-order kink and sausage modes because the higher-order modes show very little variation as compared with these principal modes. Intuitively, the higher-order slow modes should possess very similar dissipation lengths to the lowest-order slow modes, and this was indeed found to be the case. Moreover, the investigation into the dissipation lengths of the ducted slow magnetoacoustic waves found

1. very little variation between the dissipation lengths of the first-order kink and sausage modes (this again is to be expected given the narrow bands of Figures 1.5 and 1.8 in which the slow modes exist);

[2]The work in this section forms the basis for Laing and Edwin (1995b).

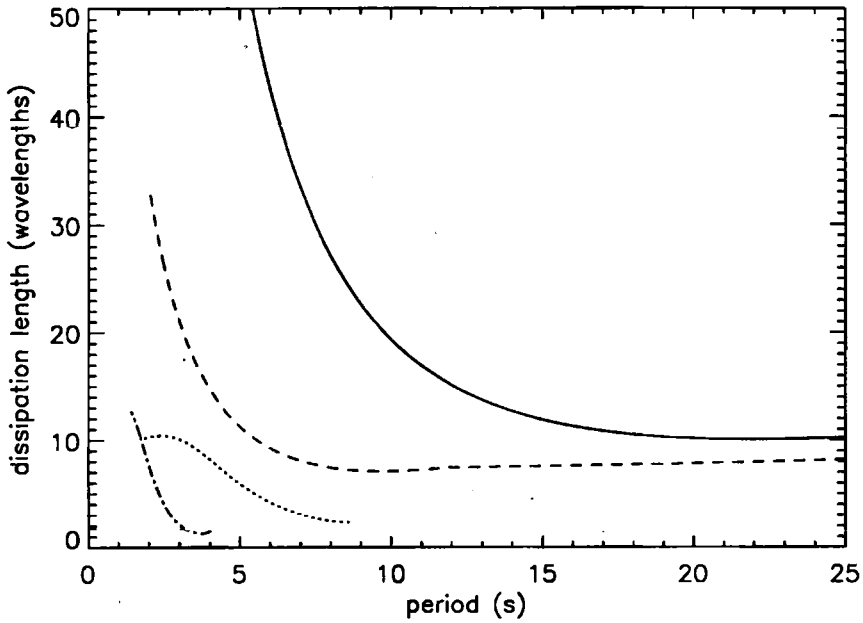

Figure 3.9: The dissipation length (in wavelengths) versus period for the fast modes L_{k0} (---), L_{k1} (.-.-), L_{s0} (....) and $L_{k0}(cold)$ (—) for a magnetic slab. The parameters are for the third case of Table 3.5.

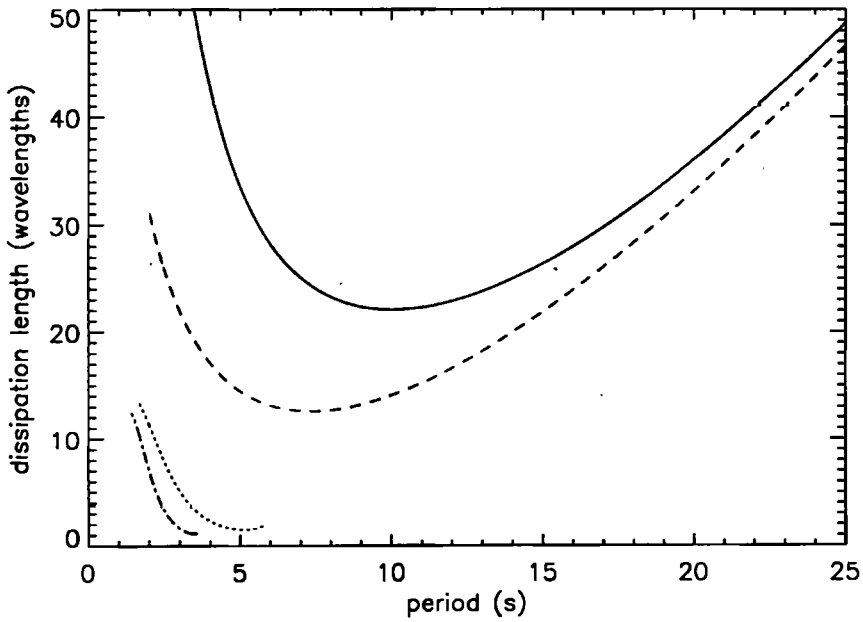

Figure 3.10: The dissipation length (in wavelengths) versus period for the fast modes L_{k0} (---), L_{k1} (.-.-), L_{s0} (....) and $L_{k0}(cold)$ (—) for a magnetic cylinder. The parameters are for the third case of Table 3.6 (after Laing and Edwin, 1995a).

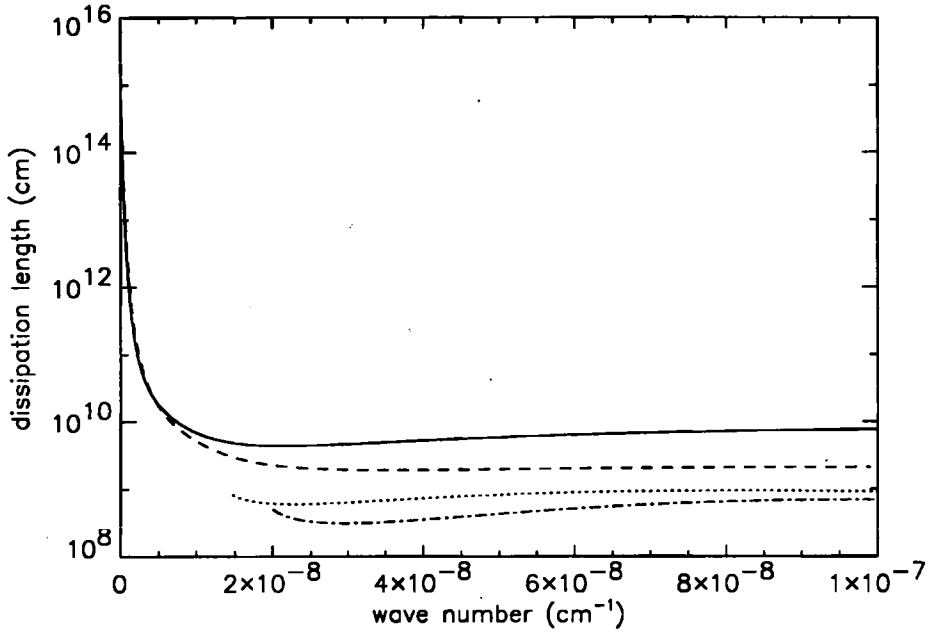

Figure 3.11: The dissipation length (in cm) versus wave number for the fast modes L_{k0} (---), L_{k1} (.-.-), L_{s0} (....) and $L_{k0}(cold)$ (—) for a magnetic slab. The parameters are for the third case of Table 3.5.

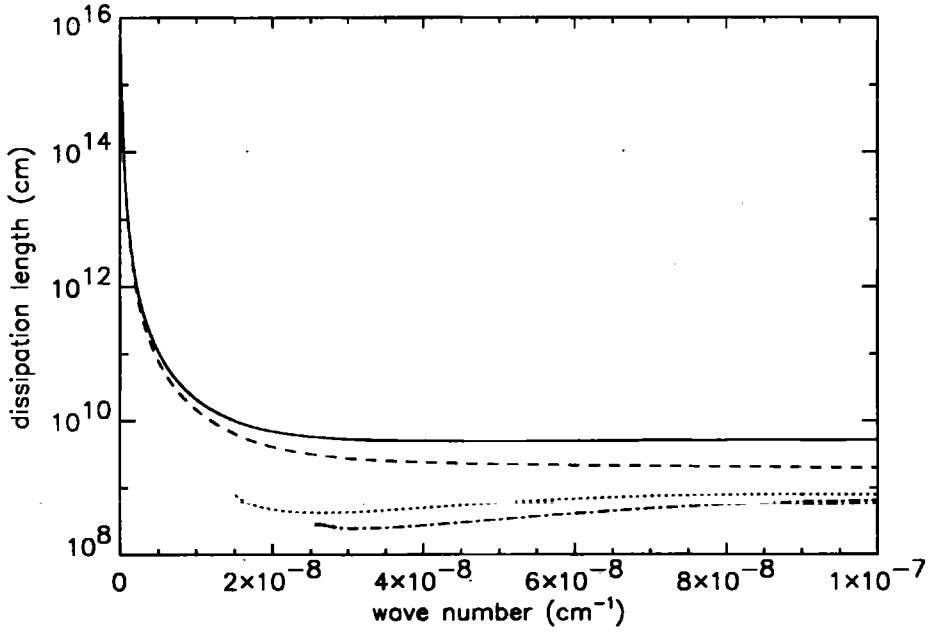

Figure 3.12: The dissipation length (in cm) versus wave number for the fast modes L_{k0} (---), L_{k1} (.-.-), L_{s0} (....) and $L_{k0}(cold)$ (—) for a magnetic cylinder. The parameters are for the third case of Table 3.6.

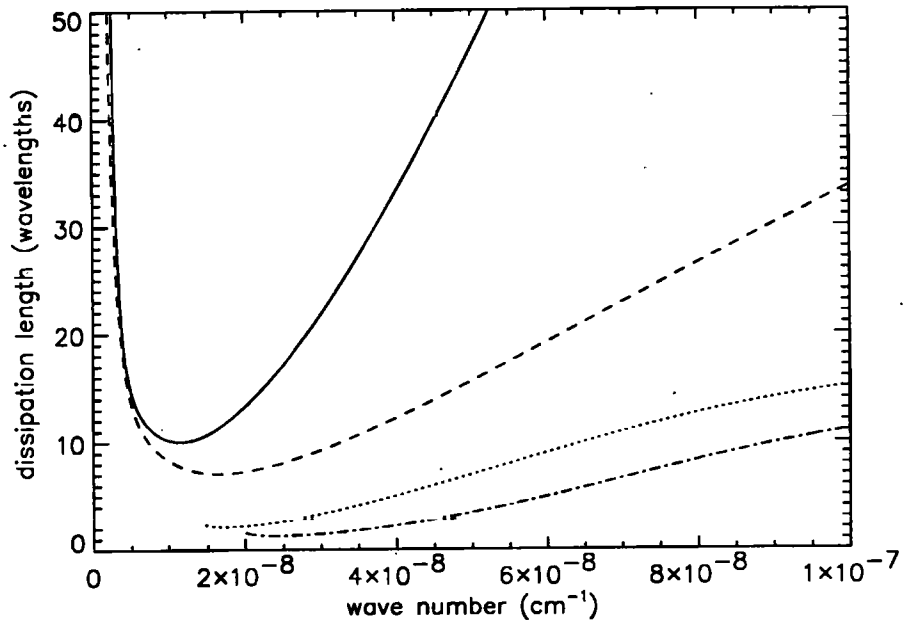

Figure 3.13: The dissipation length (in wavelengths) versus wave number for the fast modes L_{k0} (---), L_{k1} (.-.-), L_{s0} (....) and $L_{k0}(cold)$ (—) for a magnetic slab. The parameters are for the third case of Table 3.5.

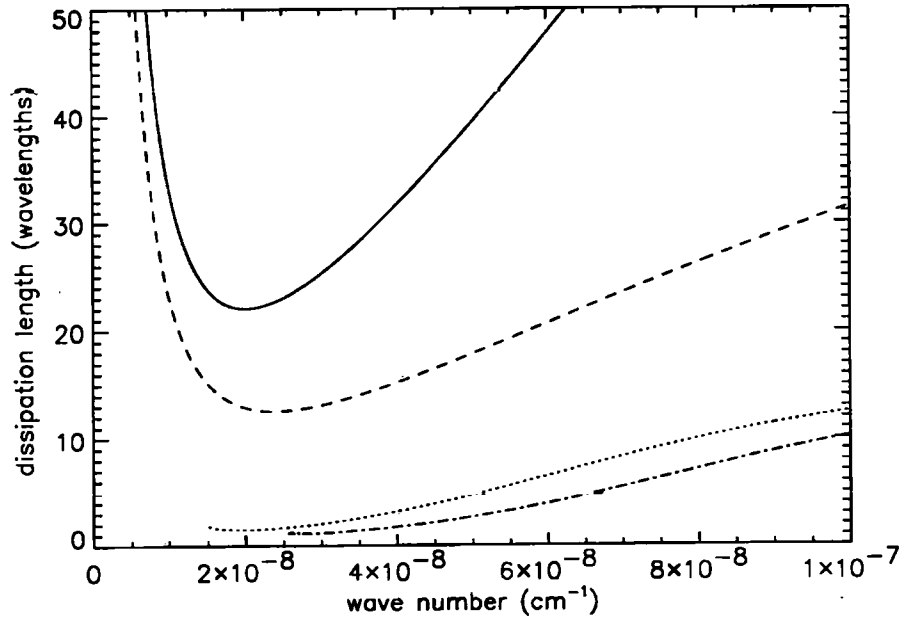

Figure 3.14: The dissipation length (in wavelengths) versus wave number for the fast modes L_{k0} (---) and L_{k1} (.-.-), L_{s0} (....) and $L_{k0}(cold)$ (—) for a magnetic cylinder. The parameters are for the third case of Table 3.6 (after Laing and Edwin, 1995a).

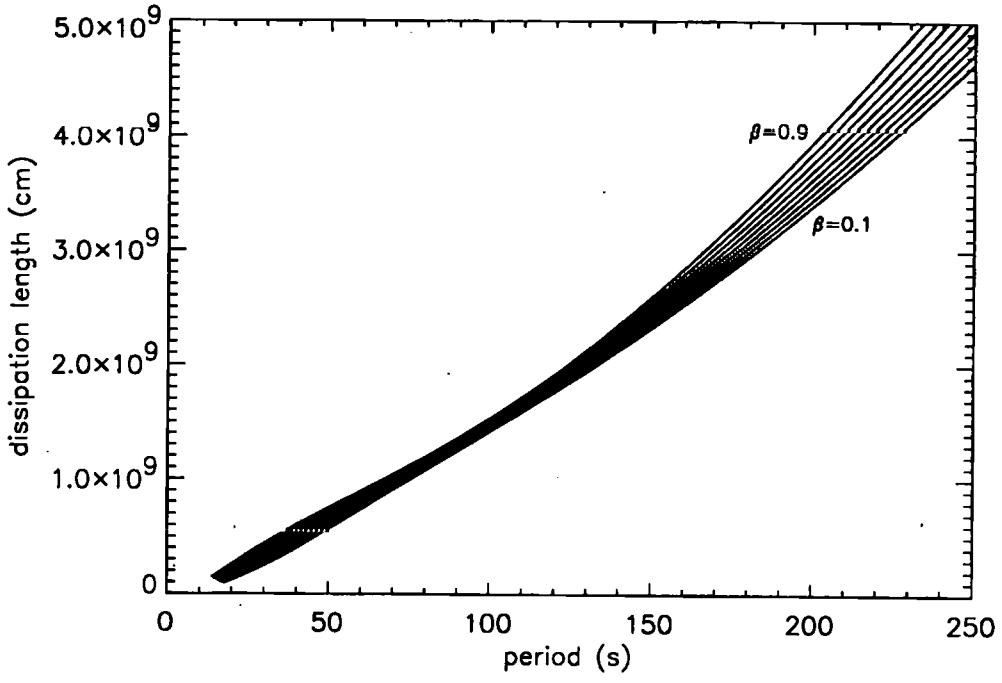

Figure 3.15: Graphs showing the variation of dissipation length with period for various values of β, the plasma beta, for slow waves propagating in a cylindrical duct of radius 5 $\times$ 10^8 cm and external to internal density ratio of 0.5. The dissipation lengths are in cm, periods are in s and $\beta = 0.1, 0.2, \ldots, 0.9$ (after Laing and Edwin, 1995b).

2. very little difference between the dissipation lengths of slow ducted waves in loops modelled by Cartesian or cylindrical geometries (again a not-unexpected result given that the slow modes are confined the narrow bands of Figures 1.5 and 1.8).

Hence, only the results for the slow kink wave propagating along a cylindrical duct will be presented in the remainder of this section.

Firstly, the values of the plasma beta were varied between 0 and 1. From Figure 3.15 it is seen that, for dissipation to take place (according to the criteria given in Section 3.3), waves are limited to having periods lying in the range of a few seconds to 225 s. For the slow-wave investigation the dissipation length increases with increase in β which is the opposite behaviour to that shown for the fast waves for small β. Perhaps this result is not so surprising when we consider that β represents the ratio of the gas to magnetic pressure and this behaviour will be oppositely orientated for slow and fast waves since the gas and magnetic pressures are in (out of) phase for the fast (slow) magnetoacoustic waves (see Section 1.6).

The dissipation length, both as a true distance and in wavelengths, for the lowest-order slow kink mode is shown in Figures 3.16 and 3.17 for the parameters of Model B in Table 1.7 (see Figures 3.2 and 3.4 for the corresponding results for the fast waves). In contrast to the fast waves

possessing a minimum when the dissipation length is plotted in terms of wavelengths, the slow waves have a maximum. However, it must be borne in mind that when the dissipation length is plotted in such a way (as shown Figure 3.17) then a $1/k$ spatial dependence is introduced into the dissipation length. It is noted from Figure 3.17 that the slow waves possess dissipation lengths of a few wavelengths, and so it seems that efficient dissipation is possible.

The relative importance of the three dissipative mechanisms is shown in Figures 3.18 and 3.19 and again it is seen that electron thermal conduction is the most dominant term. Figure 3.18 shows the relative importance of the dissipative terms plotted as a function of dimensionless wave number, ka, over the range $0 < ka < 1$. The parameters of model B of Table 1.7 have been used to compute Figure 3.18. Figure 3.19 also shows the relative importance of the dissipative terms but plotted as a function of period. Note that a low value of ka corresponds to a large value for the period (i.e. $ka = 0.1$ corresponds to a wave period of 300.0 s and a $ka = 10.0$ corresponds to a wave period of 3.0 s) and so Figure 3.19 represents the relative importance of the dissipative terms plotted over the range $10 > ka > 0$. For $ka \ll 1$ it is noted that electron thermal conduction and radiation are the important dissipation mechanisms.

When the external to internal density ratio (ρ_e/ρ_0) is varied between the values 0 and 1, it is found that there is no noticeable variation in dissipation length. Hence the ratios of 0.25 or 0.5 are used in the subsequent examination.

Investigating the variation of dissipation length with loop radius, a, it is found that, in general, the length increases with increase in radius implying that, in an unstructured medium, when the radius of the cylinder is infinitely large, there is no dissipation taking place. However, the infinite-medium situation is actually represented by a scaled value of the radius that takes into account the allowable wavelengths, i.e. $ka \gg 1$. A comparison between the results of the dissipation lengths for slow waves in an unstructured medium and in the $ka \gg 1$ limit of the structured case is left until Chapter 5.

It was found that the dissipation decreased (weakly) with increase in magnetic field strength (see Figure 3.20), a result that is not anticipated given the effect of variation in β. The pattern is however, consistent with that of the fast waves, that is, the stronger is the field the less likely are the waves to lose their energy.

As shown in Figure 3.21 an increase in the density resulted in the dissipation length being increased. This behaviour is consistent with the variation of dissipation length with β, since β is directly proportional to density.

For wave periods $\lesssim$ 80 s, it was found that the dissipation length decreased with increase in temperature (see Figure 3.22), which is not as expected from the β variation. Also, the dissipation length was not monotonic with increase in temperature for waves with periods $\gtrsim$ 80 s. For periods $\gtrsim$ 225 s, the dissipation length increases with increase in temperature.

In Table 3.7 we give the values of the parameters B, N and T for which, according to our model, and the four criteria given in Section 3.3, the slow waves are dissipated. The loop is modelled

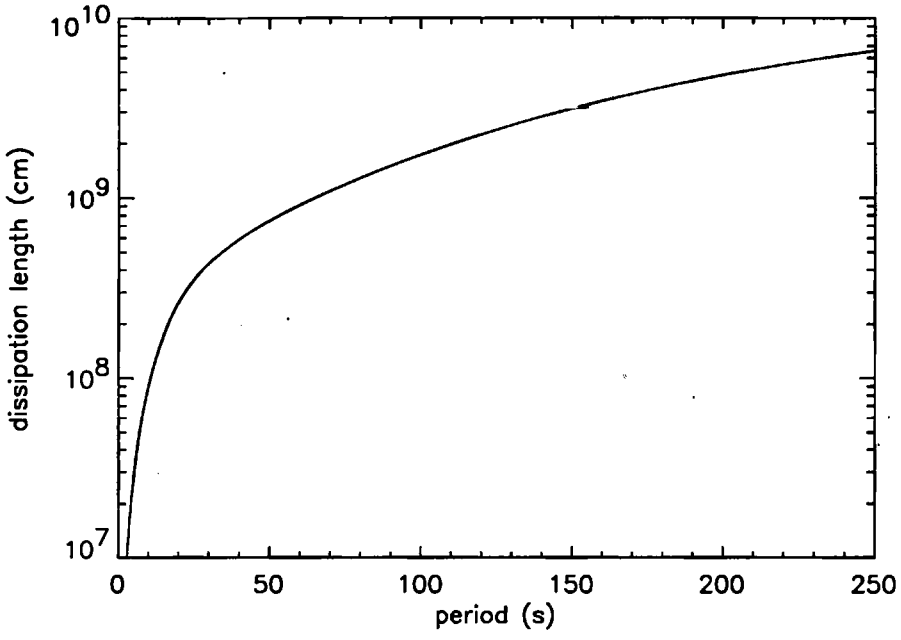

Figure 3.16: The dissipation length versus period for the lowest-order slow kink mode propagating in a cylinder with the parameters of Model B of Table 1.7.

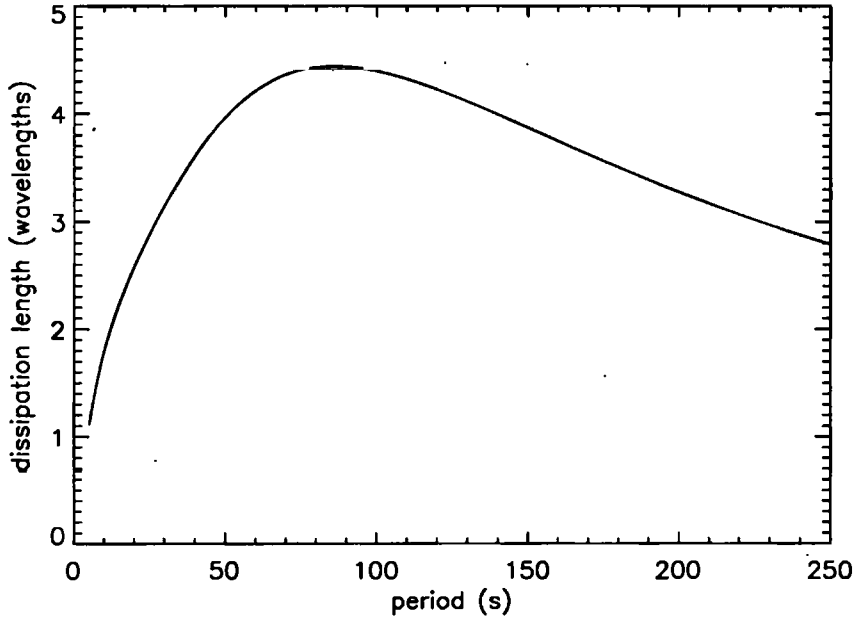

Figure 3.17: The dissipation length (in wavelengths) versus period for the lowest-order slow kink mode propagating in a cylinder with the parameters of Model B of Table 1.7.

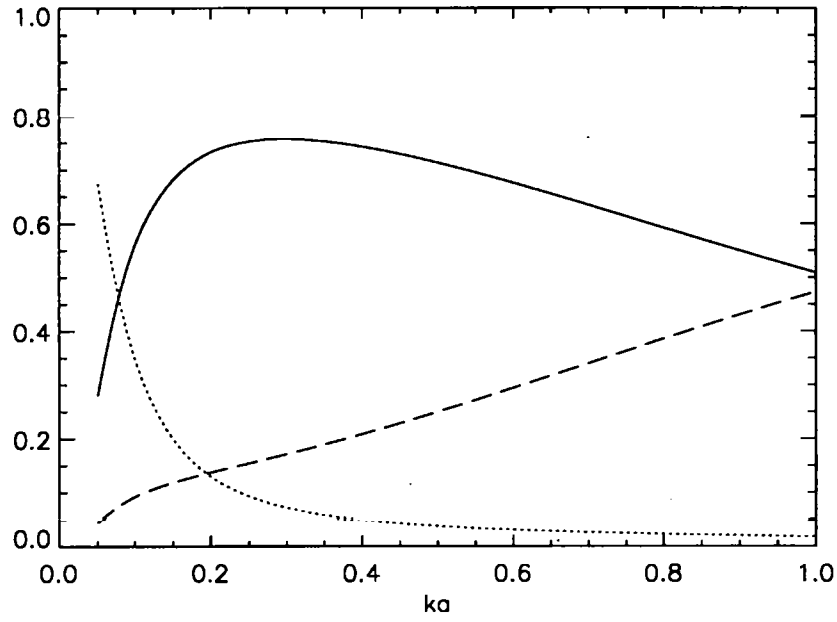

Figure 3.18: Relative importance of the dissipative terms plotted as a function of dimensionless wave number: Q_{ther}/Q_{total} (—), Q_{vis}/Q_{total} (- - -), and Q_{rad}/Q_{total} (...) for slow waves propagating in a cylinder with the parameters of Model B of Table 1.7.

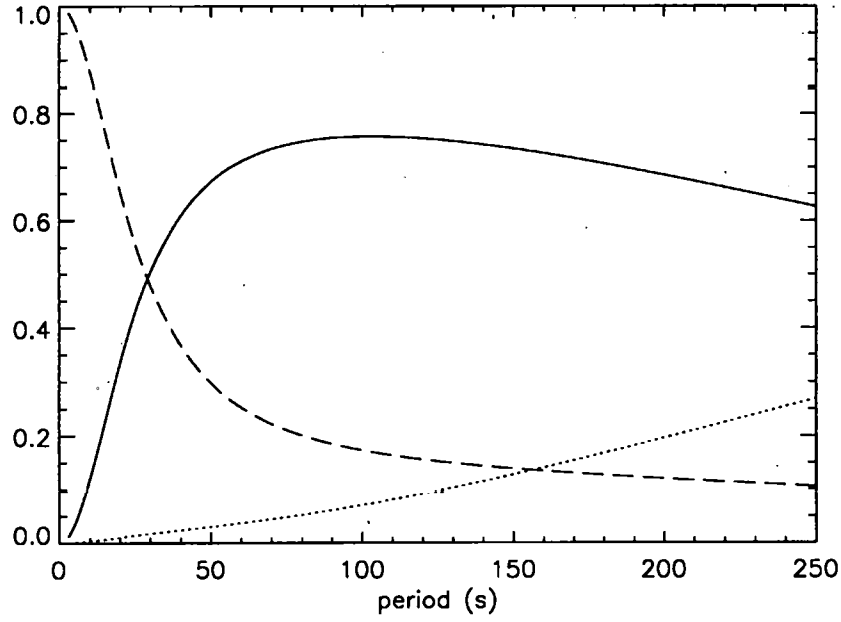

Figure 3.19: Relative importance of the dissipative terms plotted as a function of period (s): Q_{ther}/Q_{total}(—), Q_{vis}/Q_{total} (- - -), and Q_{rad}/Q_{total} (...) for slow waves propagating in a cylinder with the parameters of Model B of Table 1.7.

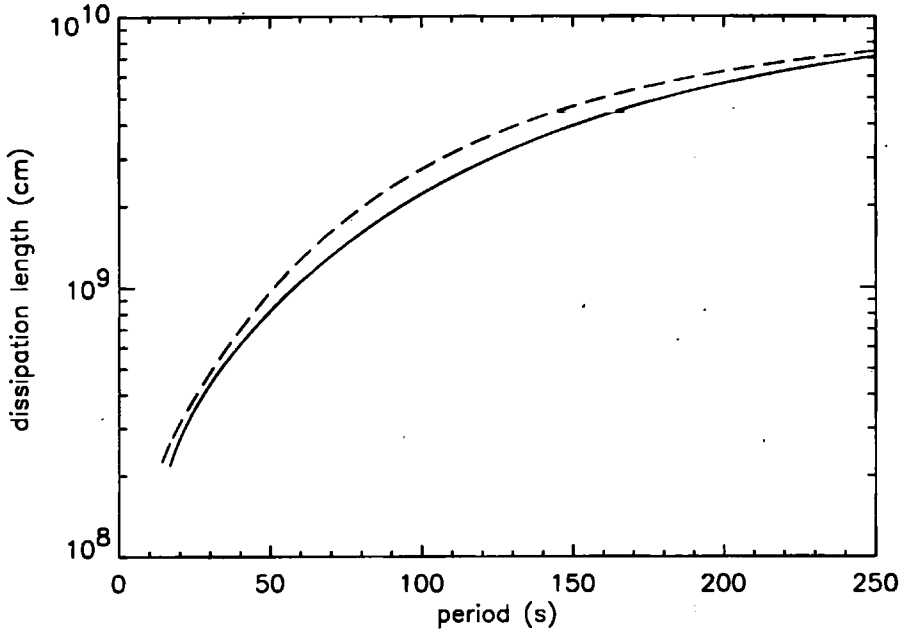

Figure 3.20: Dissipation length versus period for the slow waves with the parameters of Model A of Table 1.7 with $B = 10$ G (—) and 100 G (- - -).

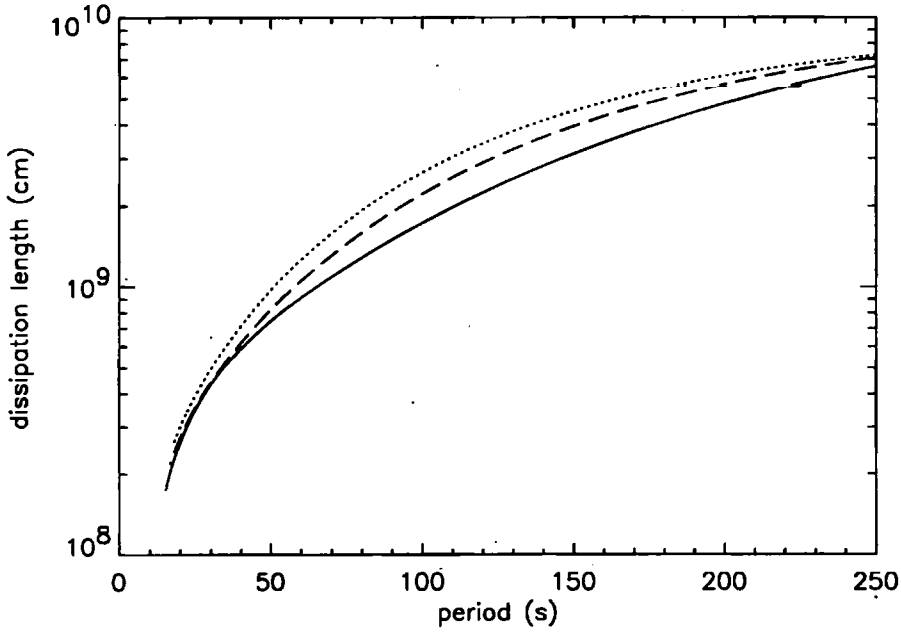

Figure 3.21: Dissipation length versus period for the slow waves with the parameters of Model A of Table 1.7 with $N = 10^9$ cm^{-3} (—), 10^{10} cm^{-3} (- - -) and 10^{11} cm^{-3} (...).

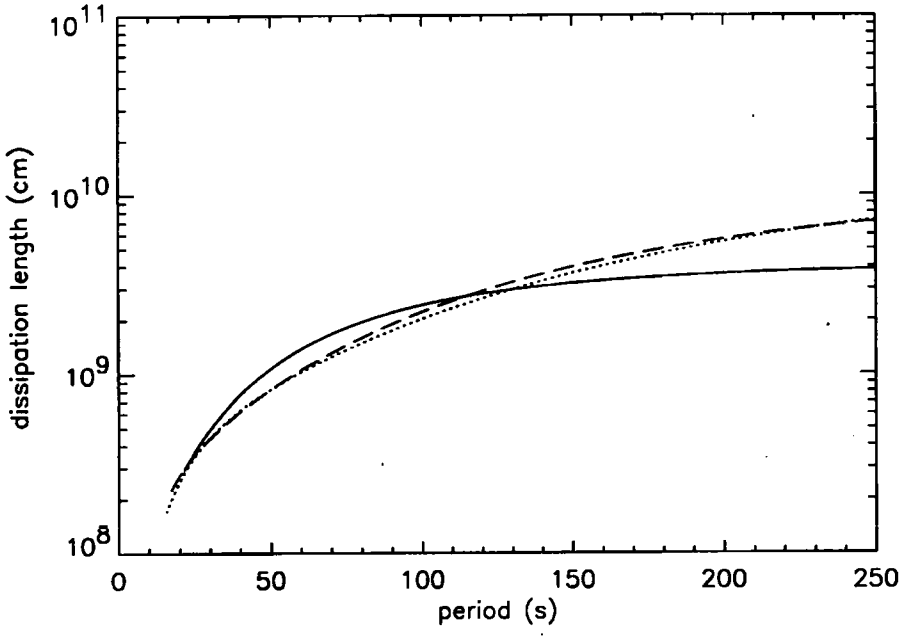

Figure 3.22: Dissipation length versus period for the slow waves with the parameters of Model A of Table 1.7 with $T = 1 \times 10^6$ K (—), 2×10^6 K (- - -) and 3×10^6 K (...).

as a cylinder of radius 5×10^8 cm and the density inside the cylinder is twice that in its exterior. The gaps in the table appear where not all the four criteria are satisfied. In general, and in keeping with the patterns of B, N and T variation given above, the most effective dissipation is for lower N and lower T but smaller B.

3.6 Dissipation of Waves in a Cold Plasma

The dissipation of fast magnetoacoustic waves in a cold plasma[3] using the model presented in this chapter has been previously studied by Gordon and Hollweg (1983), Sahyouni, Kiss'ovski and Zhelyazkov (1987) and Edwin and Zhelyazkov (1992). For a cold plasma in which $c_0 = c_e = 0$ (and therefore one in which the slow waves do not exist) the dissipation lengths for the fast sausage and kink magnetoacoustic modes, as given by Equations (3.15) and (3.18) for the Cartesian case, reduce to

$$L_s = \frac{k\rho_0 v_A^2 a^2 \{\sin^2(n_0 a) + m_e a - \frac{m_e}{2n_0}\sin(2n_0 a)\}}{\omega\{(n_0 a)^2(d_0 + \eta/3)(m_e a + \frac{m_e}{2n_0}\sin(2n_0 a)) + (m_e a)^2(d_e + \eta/3)\sin^2(n_0 a)\}}, \tag{3.28}$$

and

$$L_k = \frac{k\rho_0 v_A^2 a^2 \{\cos^2(n_0 a) + m_e a + \frac{m_e}{2n_0}\sin(2n_0 a)\}}{\omega\{(n_0 a)^2(d_0 + \eta/3)(m_e a - \frac{m_e}{2n_0}\sin(2n_0 a)) + (m_e a)^2(d_e + \eta/3)\cos^2(n_0 a)\}}, \tag{3.29}$$

[3]The work in this section forms the basis for Edwin and Laing (1994) and Laing and Edwin (1994).

T (K)	N (cm^{-3})		
	1.0×10^9	1.0×10^{10}	1.0×10^{11}
1.0×10^6		10 G : 25 - 225 s 25 G : 26 - 210 s 50 G : 26 - 200 s 75 G : 27 - 200 s 100 G : 27 - 180 s	25 G : 15 - 30 s 50 G : 15 - 23 s 75 G : 15 - 21 s 100 G : 15 - 21 s
2.0×10^6		10 G : 70 - 150 s 25 G : 80 - 140 s 50 G : 80 - 140 s 75 G : 80 - 140 s 100 G : 80 - 140 s	50 G : 15 - 50 s 75 G : 15 - 40 s 100 G : 15 - 40 s
3.0×10^6			50 G : 15 - 75 s 75 G : 15 - 60 s 100 G : 15 - 60 s

Table 3.7: Period ranges over which slow waves propagating in a coronal loop are dissipated (from Laing and Edwin, 1995b).

on noting that $\rho_e/\rho_0 = v_A^2/v_{Ae}^2$ for a cold plasma (see Equations 1.28 and 1.49). Similarly Equations (3.21) and (3.24) reduce to the dissipation lengths for fast sausage and kink magnetoacoustic modes in a cold plasma, namely:

$$L_s = \frac{k v_A^2 \rho_0 a^2}{\omega} \frac{C_n}{C_d}, \tag{3.30}$$

where

$$\begin{aligned} C_n &= \frac{1}{(n_0 a)^2}\left[\left(\frac{\mathrm{J}_1(n_0 a)}{\mathrm{J}_0(n_0 a)}\right)^2 + 1 - \frac{2}{n_0 a}\frac{\mathrm{J}_1(n_0 a)}{\mathrm{J}_0(n_0 a)}\right] \\ &+ \frac{1}{(m_e a)^2}\left[\frac{2}{m_e a}\frac{\mathrm{K}_1(m_e a)}{\mathrm{K}_0(m_e a)} + 1 - \left(\frac{\mathrm{K}_1(m_e a)}{\mathrm{K}_0(m_e a)}\right)^2\right], \end{aligned} \tag{3.31}$$

and

$$C_d = (d_0 + \eta/3)\left[\left(\frac{\mathrm{J}_1(n_0 a)}{\mathrm{J}_0(n_0 a)}\right)^2 + 1\right] + (d_e + \eta/3)\left[\left(\frac{\mathrm{K}_1(m_e a)}{\mathrm{K}_0(m_e a)}\right)^2 - 1\right], \tag{3.32}$$

for the sausage modes, and

$$L_k = \frac{k v_A^2 \rho_0 a^2}{\omega} \frac{C_n}{C_d}, \tag{3.33}$$

where

$$C_n = \frac{1}{(n_0 a)^2}\left[\left(\frac{\mathrm{J}_0(n_0 a)}{\mathrm{J}_1(n_0 a)}\right)^2 + 1 - \frac{2}{n_0^2 a^2}\right] + \frac{1}{(m_e a)^2}\left[\frac{2}{m_e^2 a^2} + 1 - \left(\frac{\mathrm{K}_0(m_e a)}{\mathrm{K}_1(m_e a)}\right)^2\right], \tag{3.34}$$

and

$$C_d = (d_0+\eta/3)\left[\left(\frac{\mathrm{J}_0(n_0a)}{\mathrm{J}_1(n_0a)}\right)^2+1-\frac{2}{n_0a}\frac{\mathrm{J}_0(n_0a)}{\mathrm{J}_1(n_0a)}\right] + (d_e+\eta/3)\left[\left(\frac{\mathrm{K}_0(m_ea)}{\mathrm{K}_1(m_ea)}\right)^2+\frac{2}{m_ea}\frac{\mathrm{K}_0(m_ea)}{\mathrm{K}_1(m_ea)}-1\right], \quad (3.35)$$

for the kink modes, respectively.

Equations (3.28) and (3.29) are simply the equations given by Gordon and Hollweg (1983) for their consideration of the weakly dissipative model in a slab of cold plasma (see also Edwin and Zhelyazkov, 1992). Equation (3.33) has previously been given by Edwin and Zhelyazkov (1992) correcting the expression given by Sahyouni, Kiss'ovski and Zhelyazkov (1987) for a cylinder of cold plasma. Equation (3.30) has not been discussed previously.

The model used by Gordon and Hollweg for dissipating the waves by electron thermal conduction could only be implemented satisfactorily in the extremes of high and low frequency of the waves. As a result of describing Q_{ther} by Equation (2.35), the term d in Equations (3.28) and (3.29) is no longer given by Equation (3.10). Instead Gordon and Hollweg give it as

$$d = \Lambda\frac{N^2}{\omega^2}+\begin{cases}\kappa_{\parallel,el}\left(\frac{k}{\omega}\right)^2T(\gamma-1)^2, & \omega<\omega_{cond},\\ N^2k_B^2Tk^{-2}\kappa_{\parallel,e}^{-1}, & \omega\geq\omega_{cond},\end{cases} \quad (3.36)$$

where $\omega_{cond}=\kappa_{\parallel,el}k^2(\gamma-1)/Nk_B$ (see also Edwin and Zhelyazkov, 1992).

Gordon and Hollweg concluded that efficient dissipation occurred if the wave periods were less than a few tens of seconds and if the background magnetic field were less than about 10 G. In particular, Case IV of their paper considers the propagation of kink waves in a duct formed by a slab of cold plasma.

Sahyouni, Kiss'ovski and Zhelyazkov used this same method to evaluate the damping of kink waves ducted in a cylinder of plasma and found, surprisingly, despite only a change in geometry, that efficient dissipation occurred if the wave periods were longer than 200 s and the background magnetic field were smaller than 5 G.

Edwin and Zhelyazkov investigated the reasons behind these two differing conclusions and resolved the matter in favour of Gordon and Hollweg observing that the paper by Sahyouni, Kiss'ovski and Zhelyazkov had erred in several ways:

1. only a low-frequency model for Q_{ther} was assumed, i.e. only dissipation lengths of waves with frequencies $\omega<\omega_{cond}$ in Equation (2.35) were used;

2. the waves were not regarded as dispersionless and no account was taken of the variation of Q_{ther} with frequency;

3. the factor d in Equation (3.36) was taken to be the same inside and outside the duct even though the density ratio ρ_e/ρ_0 was not unity.

Further, the expression given by Sahyouni, Kiss'ovski and Zhelyazkov for the dissipation lengths of the fast waves has been calculated incorrectly. Edwin and Zhelyazkov thus concluded that the dissipation length of the waves increases with magnetic field strength and decreases with increase in density, and is a few wavelengths for waves with periods of several seconds in the active corona.

Although Equations (3.28), (3.29) and (3.33) have been previously obtained by Gordon and Hollweg (1983), Sahyouni, Kiss'ovski and Zhelyazkov (1987) and Edwin and Zhelyazkov (1992), there have been flaws in *all* of their work (Laing and Edwin, 1994; Edwin and Laing, 1994). The flaw is a consequence of Gordon and Hollweg describing the electron thermal conduction term in terms of low and high frequency. Whilst this in itself gave an adequate description in the extremes of high and low frequency of the waves, it did not describe the dissipation mechanism correctly for all frequencies. Gordon and Hollweg considered the limits of a quantity, i.e. frequency, which is a function of wave number. Consider Equation (2.40) written in the non-dimensionlized form:

$$Q_{ther} = \frac{C_1(\nabla.\mathbf{v})^2}{C_2^2K^2 + W^2}, \tag{3.37}$$

where $W = \omega/kv_A$ and $K = ka$ are dimensionless variables, and $C_1 = \kappa_{\|,el}T(\gamma-1)^2/v_A^2$ and $C_2 = \kappa_{\|,el}(\gamma-1)/Nk_Bv_Aa$ are constants for a given set of coronal parameters. Equation (3.37) then replaces Equations (42b) and (43b) of Gordon and Hollweg (1983) in the low ($K \to 0$) and high ($K \to \infty$) wavenumber limits, respectively. Similarly it replaces Equation (5) of Edwin and Zhelyazkov (1992) in these limits. It is noted that since the waves are dispersive and that $1 < W < v_{Ae}/v_A$, for the bands of fast waves in Figures 1.5 and 1.8, then, from these figures, $W \to v_{Ae}/v_A$ as $K \to 0$, whilst $W \to 1$ as $K \to \infty$. These limits are not the low- and high-frequency limits referred to in Gordon and Hollweg (Equation (2.35)). Further, Gordon and Hollweg were self-contradictory in their description of the Q_{ther} term as the figures in their paper were not computed using the low- and high-frequency descriptions in the text of that paper (see Figures 3.23 and 3.24).

The results for the lowest order, fast, kink wave propagating in a cold plasma slab for the parameters of Model B of Table 1.7 are shown in Figures 3.23 and 3.24. Curves A and A' show the dissipation length in terms of distance and wavelength respectively, using Equation (2.40) as the expression for Q_{ther}. They show that the dissipation length, L_k, is at least of the order of the coronal scale height and that in terms of wavelengths the minimum dissipation length is about 20.

Curve B' is essentially the uppermost curve of Figure 2 (d) of Gordon and Hollweg (1983) (i.e. the curve represented by Curve B in Figure 3.23) but here expressed in terms of wavelengths and not on a logarithmic scale. However it must be noted that Gordon and Hollweg were self-contradictory and that this curve was not drawn using the low- and high-frequency descriptions of Equation (2.35). The curve correctly represents the low- and high-wavenumber limits of Equation (3.37). Indeed Curves C and C' are the ones that would result were the low- and high-frequency descriptions of Gordon and Hollweg (Equation (2.35)) to be implemented. Thus Curves C and C', together with the figures in Edwin and Zhelyazkov (1992), are erroneous ones.

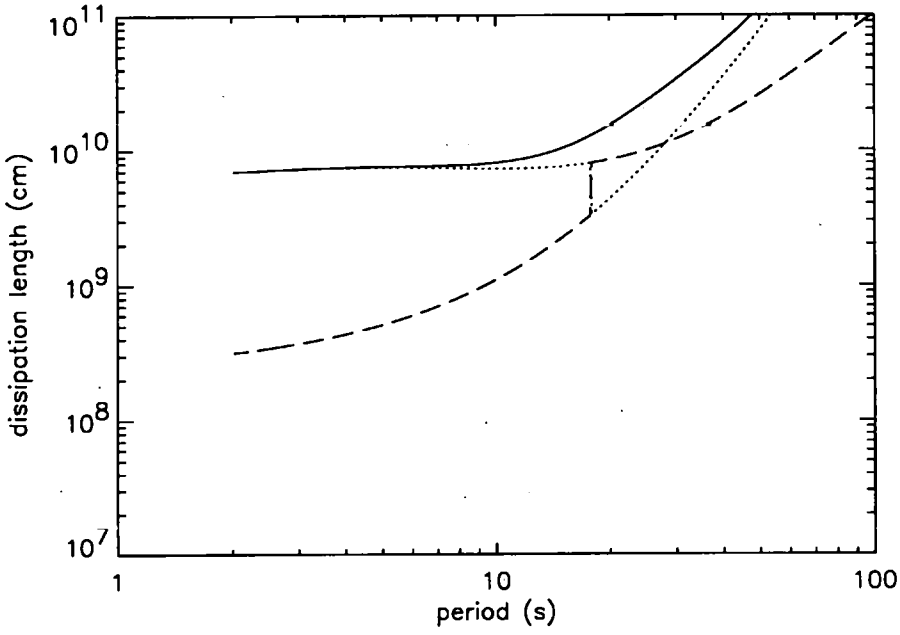

Figure 3.23: Dissipation lengths versus period for the fast magnetoacoustic kink mode ducted by a slab of cold plasma are shown for three different models of the thermal conduction rate: that given by Equation (2.40) (—, Curve A); limiting form of (3.37) (..., Curve B) and (2.35)(- - -, Curve C).

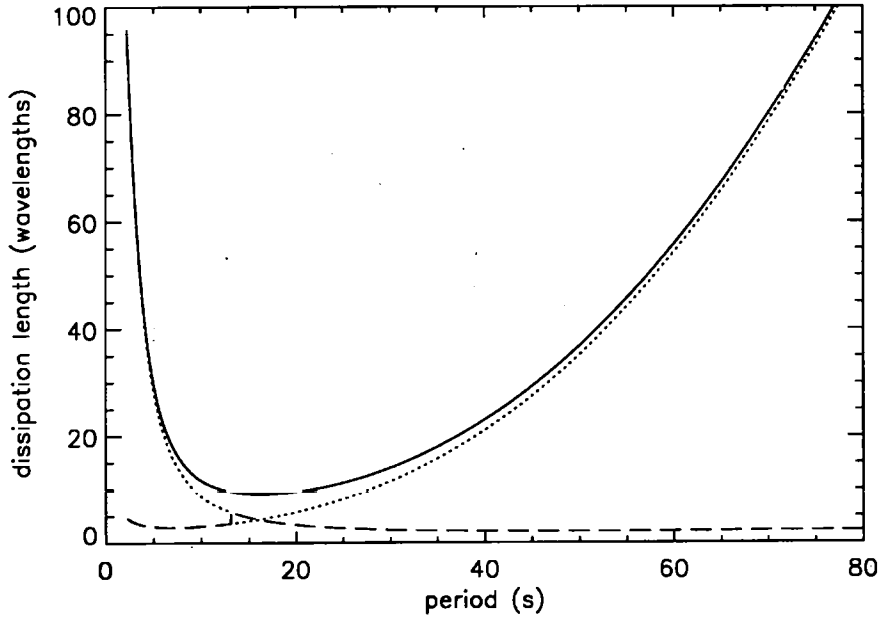

Figure 3.24: Dissipation lengths (in wavelengths) for the fast magnetoacoustic kink mode ducted by a slab of cold plasma are shown for three different models of the thermal conduction rate: that given by Equation (2.40) (—, Curve A'); limiting form of (3.37) (..., Curve B') and (2.35)(- - -, Curve C').

Comparison of Curves A and B, and A' and B' thus shows that taking the limiting forms for Q_{ther} does not reveal the dissipative behaviour at intermediate frequencies. The dissipation lengths, which are of the order of the coronal scale height when using these limiting forms, are shown to be unacceptably long (i.e. more than a few wavelengths) if Equation (2.40) is used as a more accurate description of Q_{ther}.

So by expressing the electron thermal conduction by Equation (2.40) all frequencies can be accurately described. Further, Gordon and Hollweg's inconsistency in describing the electron thermal conduction term was not appreciated by Sahyouni, Kiss'ovski and Zhelyazkov (1987) and Edwin and Zhelyazkov (1992). Both of these papers computed the dissipation lengths using the low- and high-frequency expressions given by Gordon and Hollweg. Therefore the previously known results for a cold plasma cylinder are in error.

As a final comment on the cold-plasma results we note that whilst it is generally accepted that the magnetic pressure dominates over the gas pressure in the corona, then the assumption of a cold plasma is a reasonable one but it does lead to anomalies when one is considering the temperature-dependent, dissipative mechanisms. On the one hand the plasma is considered to be of zero degrees Kelvin, on the other it has a temperature of a million degrees Kelvin! By considering a warm plasma, one is able to avoid these difficulties. Given that there have been flaws in all of these papers on the dissipation of magnetoacoustic waves in a cold plasma, using a weakly dissipative method, the results contained in Section 3.5 for a warm plasma supersede those given by Gordon and Hollweg (1983), Sahyouni, Kiss'ovski and Zhelyazkov (1987), and Edwin and Zhelyazkov (1992).

3.7 Summary

The model presented in this chapter for the dissipation of mhd waves in a weakly dissipative environment propagating along a coronal loop, regarded as a slab and as a cylinder, is a simple one. The corona was regarded as a warm, collisional plasma and the mhd waves were considered to be in a non-ideal environnment that was subjected to dissipation by ion viscosity, electron thermal conduction and optically thin radiation. The investigation found that electron thermal conduction was the most important of the three dissipative terms.

Dissipation lengths for fast and slow, sausage and kink modes have been calculated. The expressions for the dissipation lengths of waves in a cold plasma previously studied by other authors could be recovered. Moreover, it has been shown that these previous studies were all flawed and that wave dissipation is more effective in a warm plasma.

It was found that as the mode-order of the ducted waves increased, then the dissipation length was reduced. For fast waves it was found that dissipation was favoured in regions of low magnetic field ($\lesssim$15 G) which have high temperatures (3.0×10^6 K) and high densities (5.0×10^{10} cm^{-3}). For slow waves, dissipation was favoured in regions of low densities (10^9 cm^{-3}), low temperatures (1.0×10^6 K), with smaller magnetic field strengths (10 G).

It was found that there was very little difference between the dissipation lengths of slow ducted waves in coronal loops modelled by Cartesian or cylindrical geometries. It was found that the dissipation lengths of fast ducted waves in loops modelled by Cartesian and cylindrical geometries were of the same order of magntitude but, on the whole, loops modelled as a slab produced longer dissipation lengths than loops modelled as a cylinder.

Fast waves which are likely to dissipate efficiently have periods of 2 to 10 seconds duration and slow waves that are likely to dissipate have periods that range from tens to hundreds of seconds (15 - 225 s).

Chapter 4

Dissipative Effects In Slender Structures

4.1 Introduction

The investigation in the previous chapter centred on ducted waves in a weakly dissipative environment. Although the method in that chapter was straight-forward, it was seen that not all coronal conditions could be sensibly described by the model. However, as well as yielding dissipation lengths and giving period ranges for which fast and slow waves would/would not dissipate, the investigation found that electron thermal conduction was the most important of the dissipative mechanisms considered. Moreover, in the situations for which $ka \lesssim 0.15$ and $ka \lesssim 0.2$ (see Figures 3.5 and 3.18), that is to say for slender structures, it was found that conduction was important for the fast waves and that for the slow waves, both thermal conduction and radiation were important dissipative mechanisms.

The task undertaken in this chapter is to build upon the results of Chapter 3 by including the dissipative effects of thermal conduction and optically thin radiation in the mhd equations from the outset. Thus a fully dissipative dispersion relation may be obtained and damping rates and dissipation lengths may be evaluated. In turn, suggestions as to the sorts of waves and wave-periods which may be relevant to coronal heating, or indeed may be associated with recorded oscillatory phenomena, can be made. As in the previous chapters, we shall model a coronal loop by using Cartesian and cylindrical geometries.

4.2 Dissipative Modes

In Chapter 2 we have shown that the energy equation may take the form (see Equation (2.3)):

$$\bar{\rho}c_p\left(\frac{\partial}{\partial t}+(\bar{\mathbf{v}}\cdot\nabla)\right)\bar{T}-\left(\frac{\partial}{\partial t}+(\bar{\mathbf{v}}\cdot\nabla)\right)\bar{p}=-L, \tag{4.1}$$

where $\bar{p},\bar{\rho},\bar{T}$ and $\bar{\mathbf{v}}$ have their usual meanings and L is the energy loss function which may be written as the rate of energy loss minus the rate of energy gain. If we now specify L by

$$L=-Q\nabla^2\bar{T}-\bar{\rho}\mathcal{L}(\bar{\rho},\bar{T}), \tag{4.2}$$

where Q is a (uniform) heat transport coefficient which takes into account the effect of thermal conduction (i.e. we are no longer considering anisotropic thermal conduction as described by Equations (2.26) and (2.27)) and $\mathcal{L}(\bar{\rho},\bar{T})$ represents the heat loss exclusive of thermal conduction (Field, 1965), then by describing radiative effects by Equation (2.41), we can attempt to pursue a non-ideal dispersion relation. In particular, we describe the energy equation in the form:

$$\bar{\rho}c_p\left(\frac{\partial}{\partial t}+(\bar{\mathbf{v}}\cdot\nabla)\right)\bar{T}-\left(\frac{\partial}{\partial t}+(\bar{\mathbf{v}}\cdot\nabla)\right)\bar{p}=Q\nabla^2\bar{T}-\bar{\rho}^2\bar{\chi}\bar{T}^{\alpha}+\bar{\rho}a_0, \tag{4.3}$$

where we have assumed isotropic thermal conduction and that the term $\bar{\rho}^2\bar{\chi}\bar{T}^{\alpha}$ models the heat loss through radiation in an optically thin atmosphere. The coefficients, $\bar{\chi}$ ($\bar{\chi}$ denotes χ modified by a factor of $1/\bar{\mu}^2m_p^2$) and α, are temperature-dependent and are given as piecewise-continuous functions (see Table 2.1). To maintain an energy balance at equilibrium $p=p_0,\rho=\rho_0,\mathbf{v}=\mathbf{0}$ and $T=T_0$ (where p_0, ρ_0 and T_0 are all constants), a heating term, a_0, is included.

We shall again use the Cartesian (cylindrical) representation given in Section 1.7.1 (1.7.2) to model a coronal loop. From Equation (4.3) we see that for there to be equilibrium,

$$a_0(x)=\begin{cases}\rho_0\bar{\chi}T_0^{\alpha}, & |x|<a,\\ \rho_e\bar{\chi}T_0^{\alpha}, & |x|>a,\end{cases} \tag{4.4}$$

i.e. the heating term takes a different value in the two regions. So for coronal (10^6 K) temperatures $\chi=1.0\times10^{-22}$ ($\bar{\chi}=1.6\times10^{26}$ and $\alpha=0$).

Perturbing the equilibrium state by writing $\bar{p}=p_0+p$, $\bar{\rho}=\rho_0+\rho$, $\bar{\mathbf{B}}=B_0\hat{\mathbf{z}}+\mathbf{b}$ and $\bar{T}=T_0+T$, and expanding the term $\bar{\rho}\mathcal{L}(\bar{\rho},\bar{T})$ (i.e. $\bar{\rho}^2\bar{\chi}\bar{T}^{\alpha}$) in a Taylor series and linearizing, yields Equation (4.3), for $|x|<a$:

$$\rho_0c_p\frac{\partial T}{\partial t}-\frac{\partial p}{\partial t}=Q\nabla^2T-\rho_0^2\bar{\chi}T_0^{\alpha}-\rho_0^2\bar{\chi}\alpha T_0^{\alpha-1}T-2\rho_0\rho\bar{\chi}T_0^{\alpha}+\rho_0a_0+\rho a_0. \tag{4.5}$$

Now noting that $a_0=\rho_0\bar{\chi}T_0^{\alpha}$, we may rewrite Equation (4.5) as

$$\rho_0c_p\frac{\partial T}{\partial t}-\frac{\partial p}{\partial t}=Q\nabla^2T-a_0\rho_0\alpha\frac{T}{T_0}-\rho a_0. \tag{4.6}$$

The equations of continuity (1.3), solenoidal constraint (1.6), momentum (1.14) and induction (1.16) and ideal gas law (1.12), for $|x| < a$, may be written as

$$\frac{\partial \rho}{\partial t} + \rho_0 \nabla \cdot \mathbf{v} = 0, \tag{4.7}$$

$$\nabla \cdot \mathbf{b} = 0, \tag{4.8}$$

$$\rho_0 \frac{\partial \mathbf{v}}{\partial t} = -\nabla \left(p + \frac{\mathbf{B}_0 \cdot \mathbf{b}}{\mu} \right) + \frac{1}{\mu} (\mathbf{B}_0 \cdot \nabla) \mathbf{b}, \tag{4.9}$$

$$\frac{\partial \mathbf{b}}{\partial t} = (\mathbf{B}_0 \cdot \nabla) \mathbf{v} - (\nabla \cdot \mathbf{v}) \mathbf{B}_0, \tag{4.10}$$

and

$$\frac{p}{p_0} = \frac{\rho}{\rho_0} + \frac{T}{T_0}, \tag{4.11}$$

respectively.

Here, as in Section 1.7.1, we are considering a Cartesian geometry with the perturbed quantities $p(x), \rho(x)$, etc.. having the Fourier form $e^{i(\omega t + kz)}$. We may Fourier analyze Equations (4.6) to (4.10) to yield the following relationships between the perturbed quantities (for $|x| < a$):

$$\kappa \frac{d^2}{dx^2} \frac{T(x)}{T_0} - \left\{ i\omega + \kappa k^2 + (\alpha - 1)(\gamma - 1) \frac{a_0}{c_0^2} \right\} \frac{T(x)}{T_0} = -\frac{(\gamma - 1)}{\gamma} \left(i\omega - \frac{\gamma a_0}{c_0^2} \right) \frac{p(x)}{p_0}, \tag{4.12}$$

where $\kappa = Q/\rho_0 c_p$ is the (constant) thermal diffusivity,

$$i\omega \rho + \rho_0 \frac{dv_x}{dx} + i\rho_0 k v_z = 0, \tag{4.13}$$

$$\frac{db_x}{dx} + ikb_z = 0, \tag{4.14}$$

$$i\omega \rho_0 v_x = -\frac{d}{dx} \left(p + \frac{B_0 b_z}{\mu} \right) + \frac{ikB_0 b_x}{\mu}, \tag{4.15}$$

$$\omega \rho_0 v_z = -kp, \tag{4.16}$$

$$\omega b_x = kB_0 v_x, \tag{4.17}$$

and

$$i\omega b_z = -B_0 \frac{dv_x}{dx}. \tag{4.18}$$

It can then be shown, after some algebra, that combining Equations (4.13) to (4.18) with Equation (4.11) results in

$$\left\{ \frac{d^2}{dx^2} - m_{0d}^2 \right\} \frac{p(x)}{p_0} = \alpha_1 \left\{ \frac{d^2}{dx^2} - \frac{(k^2 v_A^2 - \omega^2)}{v_A^2} \right\} \frac{T(x)}{T_0}, \tag{4.19}$$

where

$$m_{0d}^2 = \frac{(k^2 v_A^2 - \omega^2)(k^2 c_0^2/\gamma - \omega^2)}{(c_0^2/\gamma + v_A^2)(k^2 c_R^2 - \omega^2)},$$

$$c_R^2 = \frac{c_0^2 v_A^2/\gamma}{c_0^2/\gamma + v_A^2},$$

and

$$\alpha_1 = \frac{v_A^2\omega^2}{(c_0^2/\gamma + v_A^2)(\omega^2 - k^2 c_R^2)}.$$

Eliminating $p(x)$ between Equations (4.12) and (4.19) gives a fourth-order differential equation in $T(x)$ (*cf.* Edwin 1984), namely

$$\begin{aligned}
&\kappa D^4 \frac{T(x)}{T_0} \\
&- \left\{ i\omega + \kappa k^2 + \kappa m_{0d}^2 + (\alpha - 1)(\gamma - 1)\frac{a_0}{c_0^2} - \frac{\alpha_1(\gamma - 1)}{\gamma}(i\omega - \frac{\gamma a_0}{c_0^2}) \right\} D^2 \frac{T(x)}{T_0} \\
&+ \left\{ i\omega m_{0d}^2 + \kappa k^2 m_{0d}^2 + m_{0d}^2(\alpha - 1)(\gamma - 1)\frac{a_0}{c_0^2} - \frac{(\gamma - 1)}{\gamma}\frac{(k^2 v_A^2 - \omega^2)}{v_A^2}(i\omega - \frac{\gamma a_0}{c_0^2})\alpha_1 \right\} \frac{T(x)}{T_0} \\
&= 0, \qquad (4.20)
\end{aligned}$$

where

$$D^2 \equiv \frac{d^2}{dx^2},$$

and the four boundary conditions, continuity of v_x, p_T, T and $\kappa\frac{dT}{dx}$, require to be satisfied across the boundary at $x = \pm a$.

In theory, one can solve for $T(x)$ in Equation (4.20). Then it can be shown from Equation (4.12) that $p(x)$ is given by

$$p(x) = \frac{-\gamma p_0}{(\gamma - 1)(i\omega - \gamma a_0/c_0^2)} \left[\kappa \frac{d^2}{dx^2}\frac{T(x)}{T_0} - \left\{ i\omega + \kappa k^2 + (\alpha - 1)(\gamma - 1)\frac{a_0}{c_0^2} \right\} \frac{T(x)}{T_0} \right]. \qquad (4.21)$$

From Equations (4.11), (4.13), (4.16) and (4.18) we see that

$$b_x = B_0 \left(1 - \frac{k^2 c_0^2}{\gamma\omega^2} \right) \frac{p(x)}{p_0} - B_0 \frac{T(x)}{T_0}, \qquad (4.22)$$

and from Equations (4.17) and (4.15) we have

$$v_x = \frac{-i\omega}{\rho_0(k^2 v_A^2 - \omega^2)} \frac{d}{dx} \left(p(x) + B_0 b_x(x)/\mu \right). \qquad (4.23)$$

Note that Equation (4.20) is the Cartesian counterpart to Equation (5.17) of Edwin (1984) which was derived for an axisymmetric cylindrical geometry (i.e. no θ component). However, the two equations differ in the respect that Edwin (1984) considered a Newton's Law of Cooling (see Equation (2.45)) for the form of the radiative loss term whereas Equation (4.20) models radiative effects through the piecewise-continuous function given by Rosner, Tucker and Vaiana (1978).

Using Equation (4.3) and the cylindrical counterparts to Equations (4.12) through to (4.19) it may be shown that the fourth-order differential equation in $T(r)$ for an axisymmetric cylindrical geometry is given by Equation (4.20) with D^2 given by $d^2/dr^2 + r^{-1}d/dr$.

To investigate the solutions of Equation (4.20) we can consider the two simpler, separate cases of radiative, non-conducting modes and conducting, non-radiative modes.

4.3 Radiative, Non-Conducting Modes

When thermal conduction is neglected ($\kappa = 0$) but radiative effects are considered, explicit mention of temperature can be removed from Equations (4.12) and (4.19) so that the velocity perturbation satisfies:

$$-\left\{i\omega + (\alpha-1)(\gamma-1)\frac{a_0}{c_0^2} - \frac{(\gamma-1)}{\gamma}(i\omega - \frac{\gamma a_0}{c_0^2})\alpha_1\right\} D^2 v_x(x)$$
$$+\left\{i\omega m_{0d}^2 + m_{0d}^2(\alpha-1)(\gamma-1)\frac{a_0}{c_0^2} - \frac{(\gamma-1)}{\gamma}\frac{(k^2v_A^2-\omega^2)}{v_A^2}(i\omega - \frac{\gamma a_0}{c_0^2})\alpha_1\right\} v_x(x)$$
$$= 0, \tag{4.24}$$

where $D^2 \equiv d^2/dx^2$ in a Cartesian geometry and $D^2 \equiv d^2/dr^2 + r^{-1}d/dr$ in a cylindrical geometry. Note that in removing explicit mention of temperature from the problem we need only concern ourselves with the boundary conditions of continuity of v_x and p_T. Note further that the pressure perturbation, also satisfies Equation (4.24) so that $p(x)$ and, in turn $v(x)$, satisfies:

$$\left(D^2 - \lambda_0^2\right) v_x = 0, \tag{4.25}$$

where

$$\lambda_0^2 = \frac{(k^2v_A^2-\omega^2)(k^2c_0^2\nu_0-\omega^2)}{k^2c_0^2v_A^2\nu_0 - \omega^2(v_A^2+c_0^2\nu_0)},$$

$$\nu_0 = \frac{i\omega+\omega_0}{i\omega+\Omega_0},$$

$$\omega_0 = \frac{(\gamma-1)a_0}{c_0^2},$$

$$\Omega_0 = \alpha\gamma(\gamma-1)\frac{a_0}{c_0^2},$$

and the other field variables ρ, b etc. may be related to v_x by Equations (1.51) to (1.55). Note that in the adiabatic limit, $\nu_0 = 1$, we recover the *ideal* equations in Sections 1.7.1 and 1.7.2 for the Cartesian and cylindrical geometries respectively.

An equation similar to Equation (4.25) holds in the exterior of the duct, namely

$$\left(D^2 - \lambda_e^2\right) v_x^e = 0, \tag{4.26}$$

where

$$\lambda_e^2 = \frac{(k^2v_{Ae}^2-\omega^2)(k^2c_e^2\nu_e-\omega^2)}{k^2c_e^2v_{Ae}^2\nu_e - \omega^2(v_{Ae}^2+c_e^2\nu_e)},$$

$$\nu_e = \frac{i\omega+\omega_e}{i\omega},$$

and

$$\omega_e = \frac{(\gamma-1)a_e}{c_e^2},$$

where $a_e = \rho_e \bar{\chi} T_e^\alpha$ If we now write $\varphi_0^2 = -\lambda_0^2$ and assume that $\mathcal{R}e(\varphi_0) > 0$ then Equation (4.25) has the solution

$$v_x = C_1 \sin(\varphi_0 x) + C_2 \cos(\varphi_0 x), \tag{4.27}$$

where C_1 and C_2 are constants.

Confining attention to disturbances that are evanescent in the exterior, $|x| > a$, Equation (4.26) has the solutions

$$v_x^e = \begin{cases} C_3 e^{\lambda_e(x+a)}, & x < -a, \\ C_3 e^{-\lambda_e(x-a)}, & x > a, \end{cases} \tag{4.28}$$

where C_3 is a constant and we have assumed that $\mathcal{R}e(\lambda_e) > 0$.

Matching the normal component of velocity and the total pressure across the boundaries at $x = \pm a$ gives the dispersion relation for symmetric waves (i.e. we suppose that $C_2 = 0$ in Equation (4.27)) travelling in a radiative slab, namely

$$-\rho_e \left(k^2 v_{Ae}^2 - \omega^2\right) \varphi_0 \tan(\varphi_0 a) + \rho_0 \left(k^2 v_A^2 - \omega^2\right) \lambda_e = 0. \tag{4.29}$$

For the axisymmetric (i.e. no θ component) cylindrical case, it may easily be shown that $\hat{R}(r)$ satisfies an equation such as Equation (4.25), namely

$$\left(\frac{d^2}{dr^2} + \frac{1}{r}\frac{d}{dr} - \lambda_0^2\right) \hat{R}(r) = 0, \tag{4.30}$$

where λ_0^2 is as before and the other field variables ρ, b etc. may be related to $\hat{R}(r)$ by Equations (1.85) to (1.92). An equation similar to Equation (4.30) holds in the exterior,

$$\left(\frac{d^2}{dr^2} + \frac{1}{r}\frac{d}{dr} - \lambda_e^2\right) \hat{R}^e(r) = 0. \tag{4.31}$$

For the axisymmetric solution bounded on the axis ($r = 0$) of the cylinder, we take for $r < a$,

$$\hat{R}(r) = A_0 \mathrm{J}_0(\varphi_0 r), \tag{4.32}$$

where A_0 is a constant. In the external region, attention is confined to disturbances that are evanescent so that for $r > a$,

$$\hat{R}^e(r) = A_1 \mathrm{K}_0(\lambda_e r), \tag{4.33}$$

where A_1 is a constant and again we have assumed that $\mathcal{R}e(\lambda_e) > 0$.

Matching the radial component of velocity and the total pressure across the cylinder boundary yields the dispersion relation for a 'radiative cylinder', namely

$$\rho_0(k^2 v_A^2 - \omega^2)\lambda_e \frac{\mathrm{K}_1(\lambda_e a)}{\mathrm{K}_0(\lambda_e a)} = \rho_e(k^2 v_{Ae}^2 - \omega^2)\varphi_0 \frac{\mathrm{J}_1(\varphi_0 a)}{\mathrm{J}_0(\varphi_0 a)}. \tag{4.34}$$

Equations (4.29) and (4.34) are the Cartesian and cylindrical counterparts of the dispersion relation obtained by Webb and Roberts (1980) for a cylindrically structured medium subject to

radiative loss by Newton's law of cooling (see Equation (2.45)). Note that the radiative loss term in the model considered here is that of Rosner, Tucker and Vaiana (1978), shown in Table 2.1, with $\chi = 1.0 \times 10^{-22}$ and $\alpha = 0$ ($\bar{\chi} = 1.6 \times 10^{26}$) for coronal ($10^6$ K) temperatures.

4.3.1 Consideration of Slender Structures

In order to investigate further the complicated dispersion relations (4.29) and (4.34) we shall suppose that the slab and cylinder are slender and so attention is confined to circumstances for which ka is small. If it is assumed that $\mathcal{R}e(\varphi_0 a) \to 0$ and $\mathcal{R}e(\lambda_e a) \to 0$ as $ka \to 0$ then for $ka \ll 1$ it may be shown, in a similar fashion to the work of Roberts and Webb (1979), Webb and Roberts (1980) and Edwin (1984), that for body waves Equation (4.34) reduces to

$$(c_0^2\nu_0 + v_A^2)\omega^2 - k^2 c_0^2 \nu_0 v_A^2 = 0, \tag{4.35}$$

which, when written out in full with ν_0 given as before, is a cubic equation in ω:

$$(c_0^2 + v_A^2)\omega^3 - i(v_A^2\Omega_0 + c_0^2\omega_0)\omega^2 - k^2 c_0^2 v_A^2 \omega + ik^2 c_0^2 v_A^2 \omega_0 = 0. \tag{4.36}$$

Inserting the expression for ω_0 yields the cubic:

$$\begin{aligned}(c_0^2 + v_A^2)\omega^3 - i\left(\frac{\alpha\gamma(\gamma-1)a_0 v_A^2}{c_0^2} + a_0(\alpha-1)(\gamma-1)\right)\omega^2 \\ -k^2 c_0^2 v_A^2 \omega + ik^2 v_A^2(\gamma-1)(\alpha-1)a_0 \\ = \ 0.\end{aligned} \tag{4.37}$$

Identifying τ_h, the non-dimensionlized radiative heating decay time, with $c_0^2/\gamma(\gamma-1)a_0$, then Equation (4.37) may be written as:

$$(c_0^2 + v_A^2)\omega^3 - \frac{i}{\tau_h}(\alpha v_A^2 + (\alpha-1)\frac{c_0^2}{\gamma})\omega^2 - k^2 c_0^2 v_A^2 \omega + \frac{ik^2 c_0^2 v_A^2(\alpha-1)}{\gamma\tau_h} = 0, \tag{4.38}$$

and in the adiabatic limit ($\tau_h \to \infty$) Equation (4.38) gives $\omega = 0$ or $\omega = k^2 c_T^2$, where c_T is the characteristic tube speed of the cylinder (see Chapter 2).

The dispersion relation (4.38) may be analyzed from two points of view. As suggested by Webb and Roberts (1980) we may specify the wave number, k, as a given real quantity and solve for complex frequency, ω. Alternatively, and of interest here so that we may investigate spatial damping, we solve Equation (4.38) for k given ω.

4.3.2 Investigation of Spatial Damping

Following from the discussions in Chapter 2 (Sections 2.4 and 2.5), the dissipation length of the waves is taken as the e-folding distance $1/2k_i$ and only assumed to be a dissipation length if $\lesssim 4 \times 10^9$ cm.

The parameters of magnetic field strength, B, density, N and temperature, T, were varied over the coronal ranges given in Table 1.8. It was found that increasing the magnetic field strength

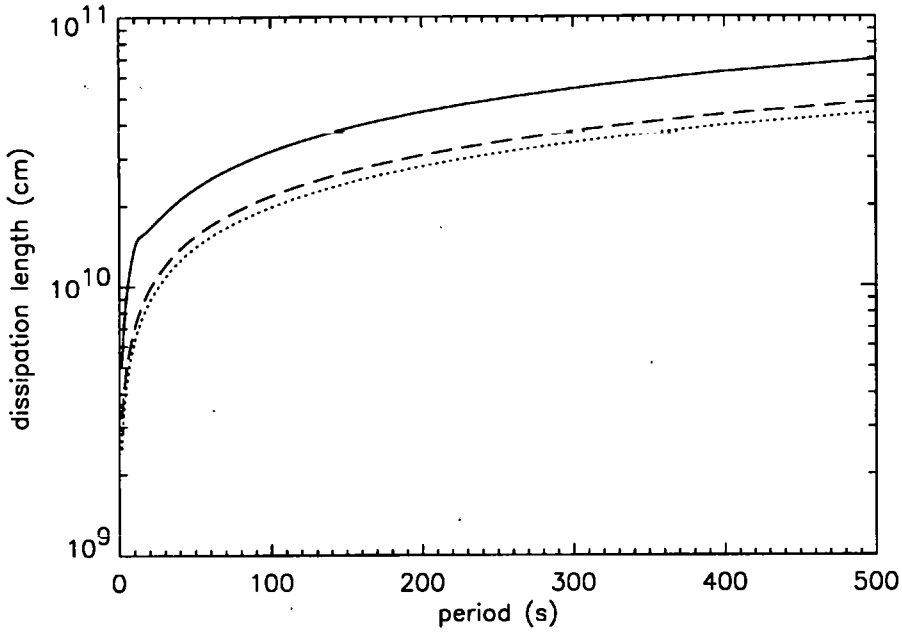

Figure 4.1: The dissipation length versus period for waves in a slender structure with magnetic field strength of 10 G (—), 50 G (---) and 100 G (....) subject to radiative damping. The parameters other than the magnetic field strength are those of Model B of Table 1.7.

resulted in a decrease of the dissipation length (see Figure 4.1). Moreover, in keeping with the fact that ducted slow magnetoacoustic waves are under investigation here, there is only a weak dependence on the magnetic field. As is shown in Figure 4.2 increasing the density produced a decrease in the dissipation length and increasing the background temperature of the plasma results in an increase in the dissipation length (Figure 4.3).

These results, of varying the magnetic field strength, density and temperature, suggest that slow, ducted magnetoacoustic waves radiate their energy more easily in regions of high magnetic field strength (100 G), high density (10^{11} cm^{-3}) and low temperatures 1×10^6 K. Further, the investigation found that the waves only underwent efficient dissipation when they had

1. periods of less than 100 s in a region of low magnetic field strength (10 G), high density (10^{11} cm^{-3}) and low temperature (1×10^6 K).

2. periods of less than 130 s in a region of high magnetic field strength (50 G), high density (10^{11} cm^{-3}) and low temperature (1×10^6 K).

3. periods of less than 120 s in a region of high magnetic field strength (50 G), high density (10^{11} cm^{-3}) and a temperature of (2×10^6 K).

Thus, this model demonstrates that the waves in a slender structure are reluctant to surrender their energy to radiation alone; there are relatively few circumstances under which the waves

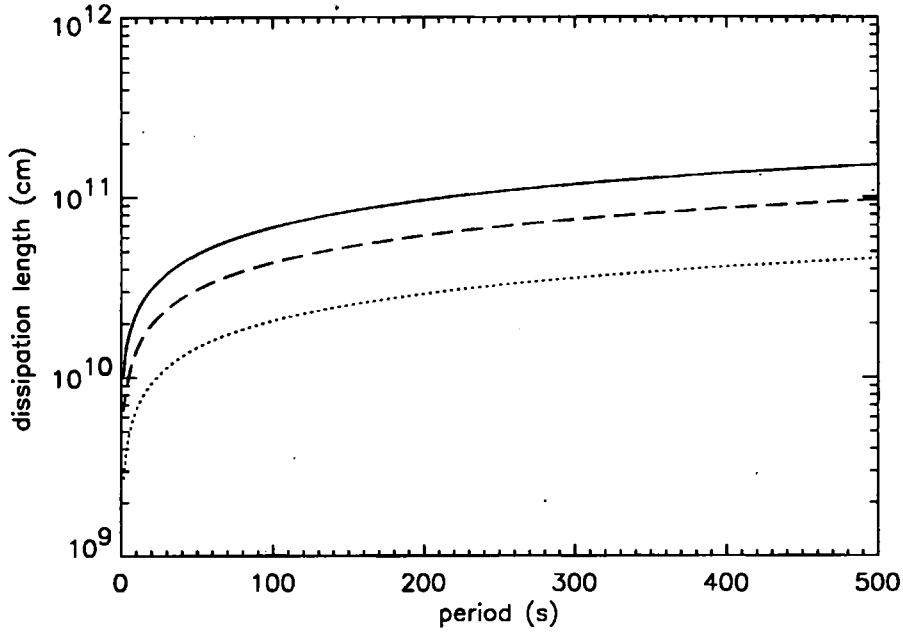

Figure 4.2: The dissipation length versus period for waves in a slender structure with density strength of 10^9 cm^{-3} (—), 10^{10} cm^{-3} (---) and 10^{11} cm^{-3} (....) subject to radiative damping. The parameters other than those of density are those of Model B of Table 1.7.

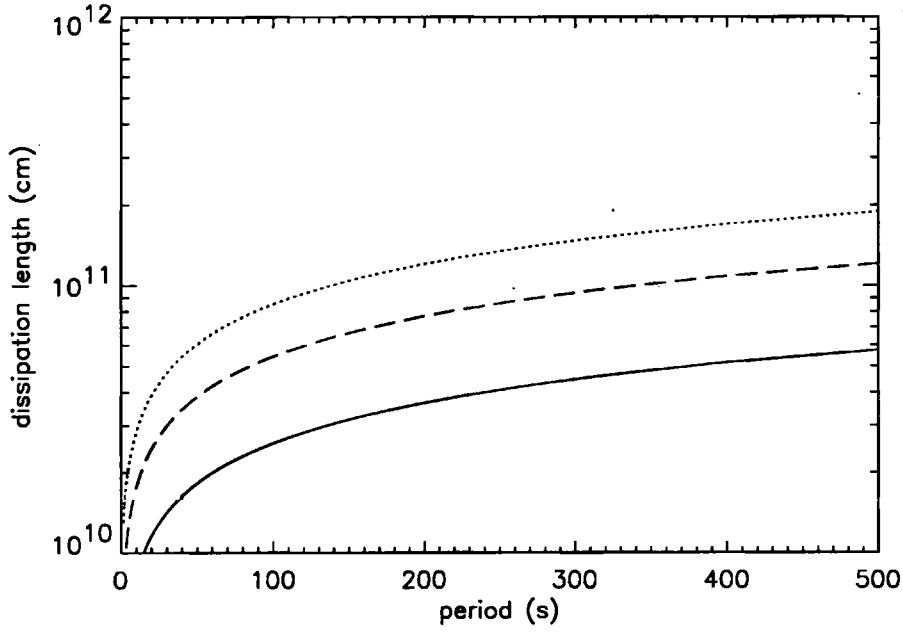

Figure 4.3: The dissipation length versus period for waves in a slender structure with background temperature 1×10^6 K (—), 2×10^6 K (---) and 3×10^6 K (....) subject to radiative damping. The parameters other than those of temperature are those of Model B of Table 1.7.

dissipate in distances of less than 4×10^9 cm (i.e. those listed in 1, 2 and 3 above). Clearly then, it is very difficult for the waves to dissipate their energy efficiently and the results suggest that, in the limited number of situations described, only waves with periods of less than about 100 s are able to overcome the threshold of radiative energy loss.

Having considered the radiative effects upon waves in a slender structure we now turn to the conducting, non-radiating solutions of Equation 4.20.

4.4 Conducting, Non-Radiating Modes

In Chapter 3, thermal conduction was shown to be more important in damping the waves than was radiation, so we must be wary of relying upon the results of the previous section for giving us information about conditions under which waves would or would not dissipate in the corona.

Neglecting terms involving radiative losses, Equation (4.20) becomes

$$Kc_T aD^4\frac{T(x)}{T_0} - \left\{i\omega + Kc_T ak^2 + Kc_T am_{0d}^2 - \frac{i\omega\alpha_1(\gamma-1)}{\gamma}\right\} D^2\frac{T(x)}{T_0}$$
$$+\left\{i\omega m_{0d}^2 + Kc_T ak^2 m_{0d}^2 - \frac{i\omega\alpha_1(\gamma-1)(k^2v_A^2-\omega^2)}{\gamma v_A^2}\right\}\frac{T(x)}{T_0} = 0, \tag{4.39}$$

where we have written $K = \kappa/c_T a$ as the non-dimensionalized thermal conductivity. Note that $D^2 \equiv d^2/dx^2$ in a Cartesian geometry and $D^2 \equiv d^2/dr^2 + r^{-1}d/dr$ in a cylindrical geometry (Edwin 1984). Since the coefficients in the differential equation are all constant, $T(x) = \exp(i\lambda x)$ is a solution with λ satisfying:

$$Kc_T a\lambda^4 + \lambda^2\left\{i\omega + Kc_T ak^2 + Kc_T am_{0d}^2 - \frac{i\omega\alpha_1(\gamma-1)}{\gamma}\right\} + Kc_T ak^2m_{0d}^2 + i\omega m_{0d}^2$$
$$- \frac{i\omega\alpha_1(\gamma-1)(k^2v_A^2-\omega^2)}{\gamma v_A^2} = 0. \tag{4.40}$$

4.4.1 Dispersion Relation For Waves Travelling in a Dense Loop

In general, the solution to Equation (4.39) is

$$T = A_1e^{i\lambda_1 x} + A_2e^{-i\lambda_1 x} + A_3e^{i\lambda_2 x} + A_4e^{-i\lambda_2 x}, \tag{4.41}$$

where $\lambda_1 \neq \lambda_2$ and A_1, A_2, A_3 and A_4 are constants. We consider disturbances of the slab with solutions of the form

$$T = A_1(e^{i\lambda_1 x} + e^{-i\lambda_1 x}) + A_3(e^{i\lambda_2 x} + e^{-i\lambda_2 x}), \tag{4.42}$$

so that we may examine symmetric disturbances of the slab. Using Equations (4.42), (4.21), (4.22) and (4.23) results in expressions for the heat flux, the total pressure and the normal component of velocity, namely:

$$\kappa\frac{dT}{dx} = i\kappa(\lambda_1A_1(e^{\lambda_1 x} - e^{-\lambda_1 x}) + \lambda_2A_2(e^{\lambda_2 x} - e^{-\lambda_2 x})), \tag{4.43}$$

$$p_T = A_1 F_1(e^{\lambda_1 x} + e^{-\lambda_1 x}) + A_2 F_2(e^{\lambda_2 x} + e^{-\lambda_2 x}), \tag{4.44}$$

and

$$v_x = \frac{\omega}{\rho_0(k^2 v_A^2 - \omega^2)} \left(\lambda_1 A_1 F_1(e^{\lambda_1 x} - e^{-\lambda_1 x}) + \lambda_2 A_2 F_2(e^{\lambda_2 x} - e^{-\lambda_2 x})\right), \tag{4.45}$$

where

$$F_j = \frac{ip_0\gamma^2(-\kappa\lambda_j^2 - \kappa k^2 - i\omega)(c_0^2/\gamma + v_A^2)(\omega^2 - k^2 c_R^2)}{(\gamma-1)T_0\omega^3 c_0^2} - \frac{B_0^2}{\mu T_0}, \tag{4.46}$$

and

$$c_R^2 = \frac{c_0^2 v_A^2}{(c_0^2 + \gamma v_A^2)},$$

for $j = 1, 2$. (Note that it is actually Equation (4.45) that determines the form of solution taken, i.e. the velocity perturbations are fixed on the axis.)

In the exterior of the slab, an equation similar to Equation (4.39) holds and we seek solutions of the form of Equation (4.41) i.e. $T^e = A_{e1}e^{\lambda_{e1}x} + A_{e2}e^{-\lambda_{e1}x} + A_{e3}e^{\lambda_{e2}x} + A_{e4}e^{-\lambda_{e2}x}$ but in which the disturbances decay as $x \to \pm\infty$ and for which $\lambda_{e1} \neq \lambda_{e2}$ with $\mathcal{R}e(\lambda_{e1}) > 0$ and $\mathcal{R}e(\lambda_{e2}) > 0$.

By matching Equations (4.42) to (4.45) for the temperature, heat flux, total pressure and normal component of velocity in $|x| < a$ to a similar set in the region $|x| > a$ gives the dispersion relation in the determinant form:

$$\begin{vmatrix} 1 & 1 & -1 & -1 \\ \kappa\lambda_1\Phi_1 & \kappa\lambda_2\Phi_2 & \kappa_e\lambda_{e1} & \kappa_e\lambda_{e2} \\ F_1 & F_2 & -d_1 & -d_2 \\ \frac{\lambda_1 F_1 \Phi_1}{V_A} & \frac{\lambda_2 F_2 \Phi_2}{V_A} & \frac{\lambda_{e1} d_1}{\rho_r V_e} & \frac{\lambda_{e2} d_2}{\rho_r V_e} \end{vmatrix} = 0, \tag{4.47}$$

where

$$d_j = \frac{ip_e\gamma^2(\kappa_e\lambda_{ej}^2 - \kappa_e k^2 - i\omega)(c_e^2/\gamma + v_{Ae}^2)(\omega^2 - k^2 c_{Re}^2)}{(\gamma-1)T_0\omega^3 c_e^2} - \frac{B_e^2}{\mu T_0}, c_{Re}^2 = \frac{c_e^2 v_{Ae}^2}{(c_e^2 + \gamma v_{Ae}^2)},$$

$\Phi_j = \tan(\lambda_j a)$, $V_A = (k^2 v_A^2 - \omega^2)$, $V_e = (k^2 v_{Ae}^2 - \omega^2)$ and $\rho_r = \rho_e/\rho_0$,

for $j = 1, 2$.

Edwin (1984) has already considered the cylindrical case of Equation (4.39) and showed that, for symmetric disturbances, the dispersion relation may be cast in the form of a determinant, namely

$$\begin{vmatrix} 1 & 1 & -1 & -1 \\ \kappa\lambda_1\Phi_1 & \kappa\lambda_2\Phi_2 & \kappa_e\lambda_{e1}\Psi_1 & \kappa\lambda_{e2}\Psi_2 \\ F_1 & F_2 & -d_1 & -d_2 \\ \frac{\lambda_1 F_1 \Phi_1}{V_A} & \frac{\lambda_2 F_2 \Phi_2}{V_A} & \frac{-\lambda_{e1} d_1 \Psi_1}{\rho_r V_e} & \frac{-\lambda_{e2} d_2 \Psi_2}{\rho_r V_e} \end{vmatrix} = 0, \tag{4.48}$$

where $\lambda_1, \lambda_2, \lambda_{e1}, \lambda_{e2}, F_1, F_2, d_1, d_2, V_A, V_e$ and ρ_r are as before but now

$$\Phi_j = \frac{\mathrm{J}_1(\lambda_j a)}{\mathrm{J}_0(\lambda_j a)} \text{ and } \Psi_j = \frac{\mathrm{K}_1(\lambda_{ej} a)}{\mathrm{K}_0(\lambda_{ej} a)}.$$

In considering the dominant terms of Equation (4.40) with $K \ll 1$ results in the characteristic equation (4.40) having the solutions (Edwin, 1984)

$$\lambda_1 = \pm m_0 \left[1 - \frac{(m_0^2 - k^2)(m_0^2 - m_{0d}^2)(k^2 c_0^2/\gamma - \omega^2)\gamma K c_T a}{2i\omega m_{0d}^2 (k^2 c_0^2 - \omega^2)}\right] \tag{4.49}$$

and

$$\lambda_2 = \frac{\pm i^{1/2}\omega^{1/2}(k^2 c_0^2 - \omega^2)^{1/2} m_{0d}}{\gamma^{1/2}(k^2 c_0^2/\gamma - \omega^2)^{1/2} m_0 K^{1/2} c_T^{1/2} a^{1/2}}. \tag{4.50}$$

Before examining Equations (4.47) and (4.48), we may recover two special cases, namely

1. When K and $K_e (= \kappa_e/c_T a)$ both $\to 0$ then

   (a) Equation (4.47) has either the degenerate roots $\omega^2 = k^2 c_T^2$ and $\omega^2 = k^2 c_{Te}^2$ or

   $$-\rho_e(k^2 v_{Ae}^2 - \omega^2) n_0 \tan(n_0 a) + \rho_0 (k^2 v_A^2 - \omega^2) m_e = 0, \tag{4.51}$$

   and hence the symmetric dispersion relation for waves propagating in a Cartesian slab (Section 1.7.1) is recovered.

   (b) Equation (4.48) has either the degenerate roots $\omega^2 = k^2 c_T^2$ and $\omega^2 = k^2 c_{Te}^2$ or

   $$m_e \frac{\mathrm{K}_1(m_e a)}{\mathrm{K}_0(m_e a)}(k^2 v_A^2 - \omega^2) = \frac{\rho_e}{\rho_0} n_0 \frac{\mathrm{J}_1(n_0 a)}{\mathrm{J}_0(n_0 a)}(k^2 v_{Ae}^2 - \omega^2), \tag{4.52}$$

   and hence the symmetric dispersion relation for waves propagating in a cylinder (Section 1.7.2) is recovered.

2. In the limit of $K \gg 1$ and $K_e \gg 1$, then

   (a) Equation (4.47) reduces to one in which either $\omega^2 = 0$ or the isothermal equivalent of Equation (4.51) is recovered, namely

   $$-\rho_e(k^2 v_{Ae}^2 - \omega^2) n_{0d} \tan(n_{0d} a) + \rho_0 (k^2 v_A^2 - \omega^2) m_{ed} = 0, \tag{4.53}$$

   where $n_{0d}^2 = -m_{0d}^2$ and

   $$m_{ed}^2 = \frac{(k^2 v_{Ae}^2 - \omega^2)(k^2 c_e^2/\gamma - \omega^2)}{(c_e^2/\gamma + v_{Ae}^2)(k^2 c_{Re}^2 - \omega^2)},$$

   $$c_{Re}^2 = \frac{c_e^2 v_{Ae}^2/\gamma}{c_e^2/\gamma + v_{Ae}^2}.$$

   (b) Equation (4.48) yields either $\omega^2 = 0$ or the isothermal equivalent of Equation (4.52), namely

   $$m_e \frac{\mathrm{K}_1(m_e a)}{\mathrm{K}_0(m_{ed} a)}(k^2 v_A^2 - \omega^2) = \frac{\rho_e}{\rho_0} n_{0d} \frac{\mathrm{J}_1(n_{0d} a)}{\mathrm{J}_0(n_{0d} a)}(k^2 v_{Ae}^2 - \omega^2). \tag{4.54}$$

Following the discussion in Edwin (1984), if it is assumed that the environment of the loop is isothermal so that $|\lambda_{e1}|a \to 0, |\lambda_{e2}|a \to 0$ as $|k|a \to 0$ (and so the perturbations of velocity and temperature in the environment are small), then taking the $|k|a \ll 1$ limit of Equation (4.47) results in

$$\frac{\kappa_e \cos(\lambda_1 a)\cos(\lambda_2 a)(F_1 - F_2)(d_1 - d_2)}{\rho_r V_e a^2} = 0. \tag{4.55}$$

In the case when $F_1 = F_2$ we have from Equation (4.46) either equal roots $\lambda_1 = \lambda_2$ or the spurious solution $\omega^2 = k^2 c_R^2$. We can also similarly rule out the case when $d_1 = d_2$. Further, it may be shown that only the case $\cos(\lambda_2 a) = 0$ produces roots. On using Equation (4.50) for the case when $K \ll 1$, we obtain

$$(c_0^2 + v_A^2)\omega^3 - \frac{i\kappa(2n+1)^2\pi^2(c_0^2/\gamma + v_A^2)\omega^2}{4a^2} - k^2 c_0^2 v_A^2 \omega + \frac{i\kappa(2n+1)^2\pi^2 k^2 c_0^2 v_A^2}{4a^2} = 0, \tag{4.56}$$

where $n = 0, 1, 2, \ldots$.

Edwin (1984) showed that if the environment is isothermal so that $|\lambda_{e1}|a \to 0, |\lambda_{e2}|a \to 0$ as $|k|a \to 0$ (and so the perturbations of velocity, total pressure and temperature in the environment are small), then taking the $|k|a \ll 1$ limit of Equation (4.48) results in

$$(c_0^2 + v_A^2)\omega^3 - \frac{i\kappa j_n(0)^2\gamma}{a^2}\left(\frac{c_0^2}{\gamma} + v_A^2\right)\omega^2 - k^2 c_0^2 v_A^2 \omega + \frac{i j_n(0)^2}{a^2}\kappa k^2 c_0^2 v_A^2 = 0, \tag{4.57}$$

where $j_n(0)$ are the zeros of the Bessel function J_0 ($j_1(0) = 2.40$, $j_2(0) = 5.52$, etc..)

Dispersion relations (4.56) and (4.57) have the same form, i.e. they are cubic equations in ω, and are similar to the equation considered for the radiative case of the previous section (Equation (4.37)), and the cubic equation (2.48) investigated by Webb and Roberts (1980).

In arriving at Equations (4.56) and (4.57), it is important to take note of the assumptions which have been made in deriving them from the general dispersion relations given by Equations (4.47) and (4.48). The assumptions lead to a restriction upon the range of periods to which the model is applicable.

1. Firstly we have assumed that $ka \ll 1$. Given that we are describing slow modes, and so $\omega \approx kc_T$, then it follows that $\omega \ll c_T/a$; in other words we have a lower bound on the period.

2. Secondly we have assumed that $K \ll 1$.

3. The environment of the duct has been considered to be isothermal and so the velocity, total pressure and temperature fluctuations in the environment have been neglected.

In pursing the investigation further, we only consider dispersion relation (4.57) and note that the corresponding solutions in the Cartesian case will be similar in nature. Further, we are primarily interested in spatial damping of Equation (4.57) and so we shall assume that ω is a known real quantity and we shall solve for k.

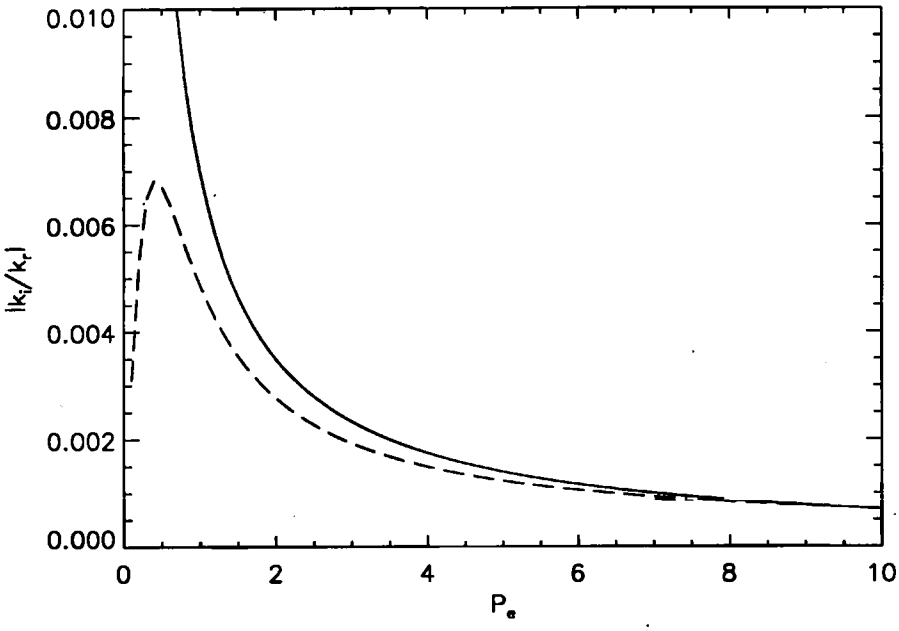

Figure 4.4: Damping per wavelength, $|k_i/k_r|$, versus P_e for solutions given by the exact solution of dispersion relation (4.57) (---) and by the approximate expression (4.58) (—).

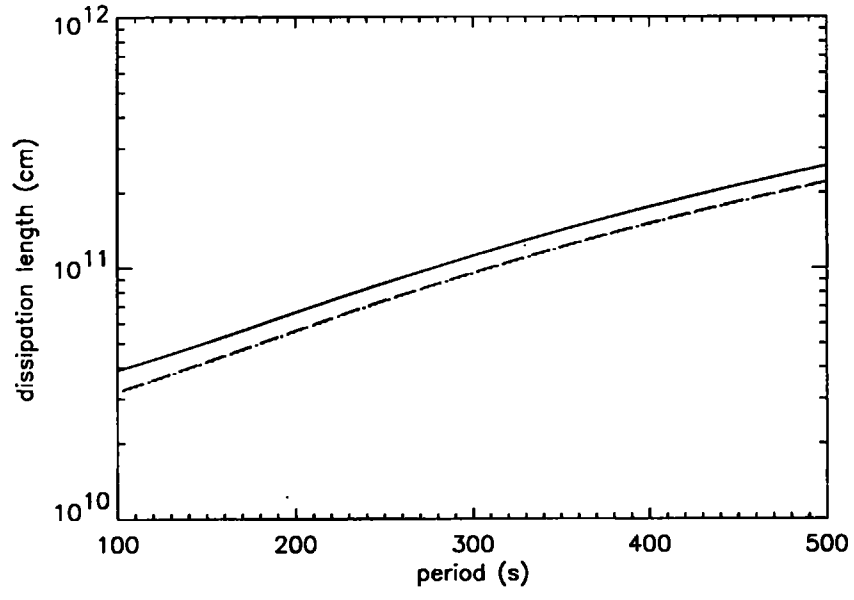

Figure 4.5: The dissipation length versus period for waves in a slender structure with magnetic field strength of 10 G (—), 50 G (---) and 100 G (....) according to Equation (4.57). The parameters other than the magnetic field strength are those of Model B of Table 1.7 but with ρ_e/ρ_0 undefined.

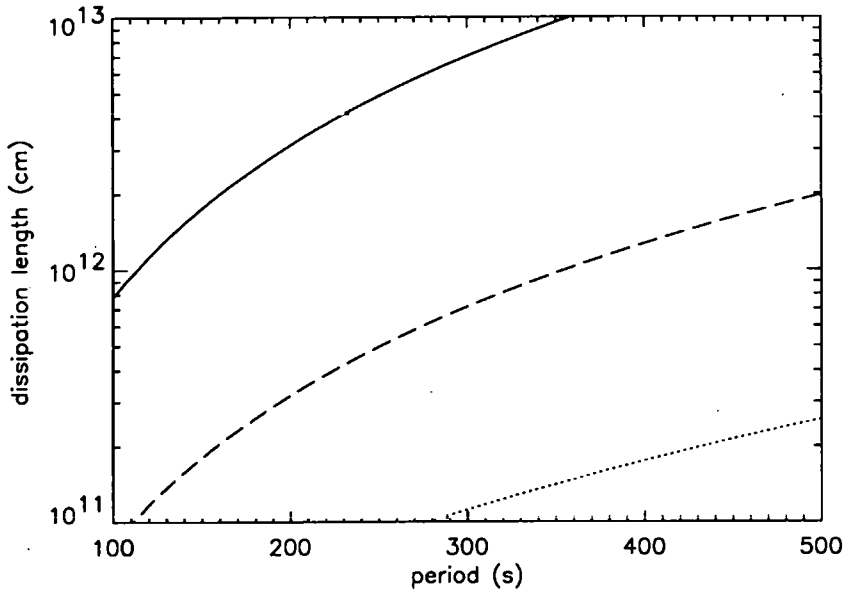

Figure 4.6: The dissipation length versus period for waves in a slender structure with density strength of 10^9 cm^{-3} (—), 10^{10} cm^{-3} (- - -) and 10^{11} cm^{-3} (....) according to Equation (4.57). The parameters other than those of density are those of Model B of Table 1.7 but with ρ_e/ρ_0 undefined.

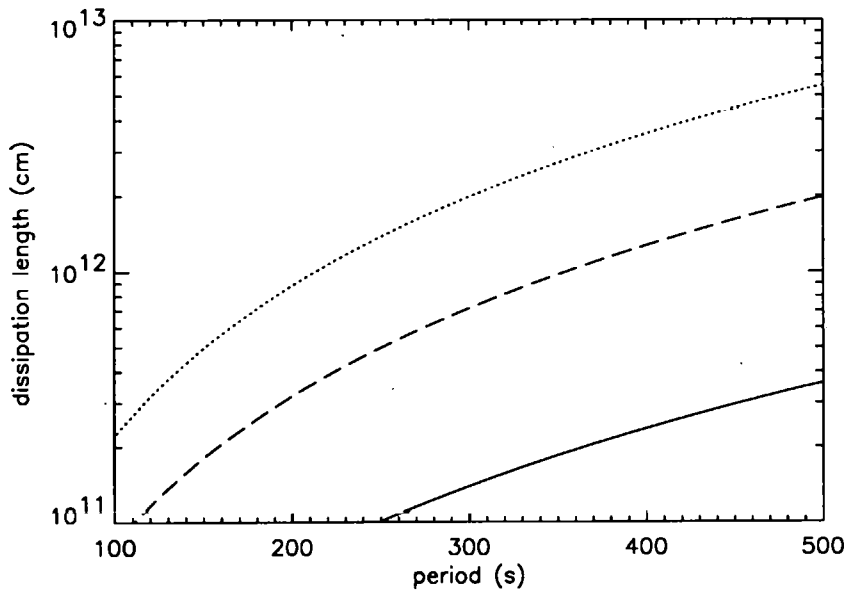

Figure 4.7: The dissipation length versus period for waves in a slender structure with background temperature 1×10^6 K (—), 2×10^6 K (- - -) and 3×10^6 K (....) according to Equation (4.57). The parameters other than those of temperature are those of Model B of Table 1.7 but with ρ_e/ρ_0 undefined.

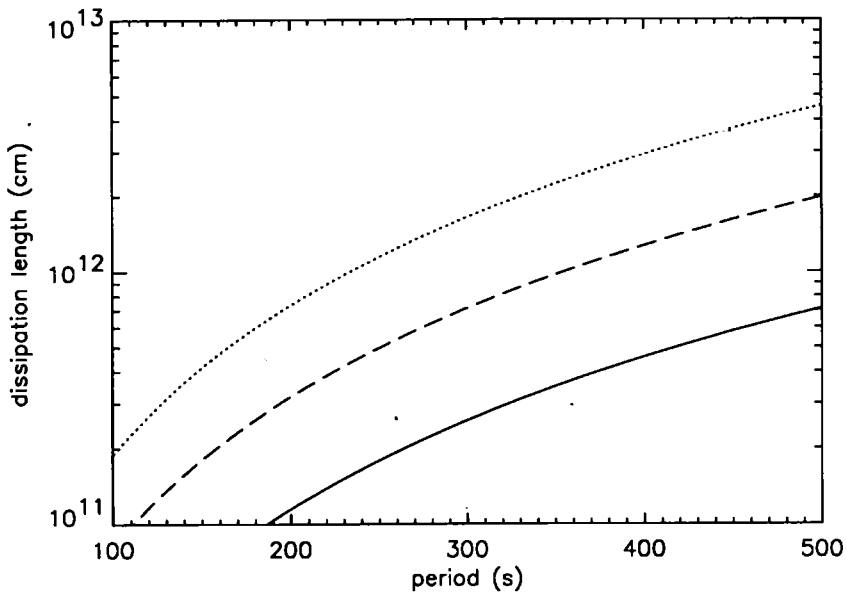

Figure 4.8: The dissipation length versus period for waves in a slender structure with radius of loop 10^7 cm (—), 5×10^8 cm (---) and 1×10^9 cm (....) according to Equation (4.57). The parameters are those of model B of Table 1.7 but with ρ_e/ρ_0 undefined.

Identifying $1/\gamma\tau_R$ of Equation (2.48) with $j_n(0)^2\kappa/a^2$ of Equation (4.57) and following the analysis of Webb and Roberts (1980) (see Chapter 2), the analytical solution of Equation (4.57) for $\omega\tau_R \gg 1$, i.e. $a^2\omega/\gamma j_n(0)^2\kappa \gg 1$, i.e. $\mathrm{P_e} \gg 1$ where $\mathrm{P_e} = \mathrm{a}^2\omega/\kappa$ is the Péclet number, is given by

$$k_{1,2} \approx \pm\frac{\omega}{c_T}\left\{1 + O(1/\mathrm{P_e})^2 - \frac{i}{2}\frac{(\gamma-1)}{\gamma}\frac{c_T^2}{c_0^2}\frac{j_n(0)^2\kappa}{a^2\omega}\right\}. \tag{4.58}$$

Equation (4.57) is investigated for large $\mathrm{P_e}$ ($\mathrm{P_e} \gg 1$). Figure 4.4 shows the variation of the damping per wavelength (defined as $|k_i/k_r|$ by Webb and Roberts, 1980, where k_r is the real part of the wave number and k_i is the imaginary part of the wave number) with $\mathrm{P_e}$. From this figure it is evident that the solution given by Equation (4.58) represents a very good approximation to the exact solution of Equation (4.57). However, for the results which now follow, we solve Equation (4.57) exactly.

The constant thermal diffusivity, κ, has the value

$$\kappa = 8.4 \times 10^{-7}\frac{T_0^{5/2}}{\rho_0 c_p}\ \mathrm{cm^2 s^{-1}},$$

where T_0 is given by the temperatures of Table 4.1. So, from the parameters of Table 1.8, it is seen that, typically, κ ranges from 2.43×10^{13} to 3.80×10^{16} $\mathrm{cm^2\ s^{-1}}$ in the solar corona.

The lengths over which the slow waves would dissipate were investigated for the parameters of Table 1.8. Varying the magnetic field strength (Figure 4.5) results in the dissipation length decreasing with an increase in magnetic field strength. It is noted that there is a weak dependence

T (K)	N (cm^{-3})		
	1.0×10^9	1.0×10^{10}	1.0×10^{11}
1.0×10^6	10 G : 3.4 - 7.6 s 50 G : 3.8 - 7.7 s 100 G : 3.8 - 7.7 s	10 G : 4.3 - 23 s 50 G : 3.8 - 24 s 100 G : 3.8 - 24 s	10 G : 7.5 - 63 s 50 G : 4.0 - 78 s 100 G : 3.8 - 80 s
2.0×10^6	10 G : 2.8 - 3.2 s 50 G : 2.7 - 3.2 s 100 G : 2.7 - 3.2 s	10 G : 3.4 - 9.4 s 50 G : 2.7 - 10 s 100 G : 2.7 - 10 s	10 G : 7.0 - 22 s 50 G : 3.0 - 31 s 100 G : 2.8 - 33 s
3.0×10^6		10 G : 3.0 - 5.5 s 50 G : 2.2 - 6.0 s 100 G : 2.2 - 6.1 s	10 G : 6.8 - 12 s 50 G : 2.5 - 18 s 100 G : 2.3 - 20 s

Table 4.1: Period ranges over which slow waves propagating in a coronal loop are dissipated according to Equation (4.57).

on the magnetic field and this is consistent with the fact that we are investigating slow waves. (Note that this result is easily seen from the approximate solution (4.58).) Figure 4.6 shows that when the density was increased then the dissipation length decreased and that an increase in temperature saw the dissipation length increasing (Figure 4.7). It was found that increasing the width of the duct caused an increase in the dissipation length (see Figure 4.8) (a result which is easily seen from the approximate solution (4.58)).

Thus, from the investigation of the variation of the magnetic field strength, B, density, N, temperature, T and loop radius, a, it is apparent that the conditions most favourable to the dissipation of slow waves are regions of high (100 G) magnetic field strength, high (10^{11} cm^{-3}) density and low temperatures (1×10^6 K) in a loop of small (10^7 cm) radius.

Table 4.1 gives the period ranges for which the waves would damp in a distance of less than 4×10^9 cm for a coronal loop with $a = 10^7$ cm. The lower bound of the period in each cell represents the restriction that $\omega \ll c_T/a$ and the upper bound gives the periods for which the dissipation length is 4×10^9 cm. From Table 4.1 it is seen that slow waves with periods of less than 80 s can damp in a distance of less than 4×10^9 cm, and so may contribute to coronal heating.

4.4.2 Equations Describing a Slender Loop

By considering the slender-flux-tube equations of Webb and Roberts (1978) we can adopt a different approach to the problem in hand, one employed by Edwin (1984) in her investigation of waves in conducting, magnetic flux tubes. By introducing the variable $\xi = x/a$ Equations (1.3), (1.14), (1.16) and (4.3) become, after linearizing and Fourier analyzing:

$$i\omega\rho + \frac{\rho_0}{a}\frac{\partial v_x}{\partial \xi} + i\rho_0 k v_z = 0, \tag{4.59}$$

$$i\omega\rho_0 v_x = -\frac{1}{a}\frac{\partial}{\partial \xi}\left(p + \frac{B_0 b_z}{\mu}\right) + \frac{ikB_0 b_x}{\mu}, \tag{4.60}$$

$$\omega\rho_0 v_x = -kp, \tag{4.61}$$

$$\omega b_x = kB_0 v_x, \tag{4.62}$$

$$i\omega b_z = -\frac{B_0}{a}\frac{\partial v_r}{\partial \xi}, \tag{4.63}$$

and

$$i\omega\frac{T(\xi)}{T_0} = \frac{\kappa}{a^2}\left(\frac{\partial^2}{\partial\xi^2} - k^2a^2\right)\frac{T(\xi)}{T_0} + \frac{i\omega(\gamma-1)p(\xi)}{\gamma p_0}, \tag{4.64}$$

where we have considered only the effects of thermal conduction in Equation (4.3) and as defined previously, $\kappa = Q/\rho_0 c_p$ is the constant thermal diffusivity. Further, we have on linearizing the ideal gas law (1.12)

$$p = \frac{\tilde{R}}{\tilde{\mu}}\rho_0 T + \frac{\tilde{R}}{\tilde{\mu}}\rho T_0. \tag{4.65}$$

It may be shown, for a slender slab with zero total pressure perturbation in its environment that Equation (4.60) becomes

$$\frac{\partial}{\partial\xi}\left(p + \frac{B_0 b_z}{\mu_0}\right) = 0. \tag{4.66}$$

Combining Equations (4.59) to (4.65) yields

$$\frac{1}{\mathrm{P_e}}\frac{\partial^2}{\partial\xi^2}T(x) = \left(i + \frac{\kappa k^2}{\omega} - \frac{i(\gamma-1)}{\gamma\left[1 + \frac{\tilde{R}T_0}{\tilde{\mu}v_A^2} - \frac{\tilde{R}T_0k^2}{\tilde{\mu}\omega^2}\right]}\right)T(x), \tag{4.67}$$

where $\mathrm{P_e} = \mathrm{a}^2\omega/\kappa$ is the Péclet number.

At this point it is convenient to summarize the assumptions which have been made in order to arrive at Equation (4.67).

1. First of all, we are considering a slender slab, i.e. $|k|a \ll 1$ such that the total pressure perturbation across the slab is zero.

2. Attention is confined to only the slow modes, i.e. $\omega/k \sim c_T$ and so $\omega \ll c_T/a$.

In order to solve Equation (4.67) we assume that $\mathrm{P_e} \gg 1$ and so the temperature does not vary across across the structure. In terms of 1 and 2 above this implies that $\kappa/ac_T \ll 1$ must hold. Neglecting the left-hand side of Equation (4.67) gives

$$(c_0^2 + v_A^2)\omega^3 - ik^2\kappa\gamma(c_0^2/\gamma + v_A^2)\omega^2 - k^2c_0^2v_A^2\omega + ik^4\kappa c_0^2v_A^2 = 0. \tag{4.68}$$

Once more, a dispersion relation in the form of a cubic in ω has been obtained. As before, we are primarily concerned with the spatial damping and so we may specify ω in Equation (4.68) as a given real quantity and solve for k which will then be inherently complex due to the presence of the dissipative terms.

Rewriting Equation (4.68) as

$$(c_0^2+v_A^2)\omega^3 - ik^2Kc_Ta\gamma(c_0^2/\gamma+v_A^2)\omega^2 - k^2c_0^2v_A^2\omega + ik^4Kc_Tac_0^2v_A^2 = 0, \tag{4.69}$$

where $K = \kappa/c_Ta$, it can be shown in the adiabatic limit ($K \ll 1$) that Equation (4.69) has the approximate solution

$$k \simeq \pm\frac{\omega}{c_T}\left\{1+O(K^2)-\frac{i}{2}\frac{(\gamma-1)}{c_0^2}\omega\kappa\right\}. \tag{4.70}$$

Equation (4.69) is investigated for small K ($K \ll 1$). Figure 4.9 shows the variation of the damping per wavelength (k_i/k_r) with K. Figure 4.9 indicates that the solution given by Equation (4.70) represents a very good approximation to the exact solution of Equation (4.69). For the following results, we solve Equation (4.69) exactly.

Again, the lengths over which the slow waves would dissipate was investigated for the parameters of Table 1.8 (with the thermal diffusivity given by $\kappa = 8.4\times10^{-7}T_0^{5/2}/\rho_0c_p$). Figure 4.10 shows that varying the magnetic field strength results in the dissipation length decreasing with an increase in magnetic field strength. An increase in density results in a decrease in the dissipation length (Figure 4.11) and increasing the background temperature causes an increase in the dissipation length (Figure 4.12). It was found that increasing the width of the duct caused an increase in the dissipation length (see Figure 4.13).

It is then apparent that conditions most favoured for dissipation are loops of small (10^7 cm) radii with a high (100 G) magnetic field strength, high (10^{11} cm^{-3}) density and low (1×10^6 K) temperature.

Table 4.2 gives the period ranges for which the waves would damp in a distance of less than 4×10^9 cm for a coronal loop with $a = 10^7$ cm. Note that the lower bound of the period in each cell represents the restriction that $\omega \ll c_T/a$ and the upper bound gives the periods for which the dissipation length is 4×10^9 cm. From Table 4.2 it is seen that slow waves with periods of less than 38 s can damp in a distance of less than 4×10^9 cm, and so may contribute to coronal heating.

We note at this stage that *qualitatively* the results of varying the magnetic field strength, etc. for the two models described in Sections 4.4.1 and 4.4.2 are similar. However, we leave the comparison of Table 4.1 with Table 4.2 (and with Table 3.7) until Chapter 5.

4.5 Summary

This chapter has investigated the dissipative effects of optically thin radiation and isotropic conduction on a slender structure. By including the effects of radiation and conduction in the equation of energy it was shown that dispersion relations (e.g. Equations (4.34) and (4.47) which contains dissipative terms could be obtained. To further simplify matters the investigation was restricted to slender ($ka \ll 1$) structures. In effect the duct is to reduced to a line and since slow waves were being investigated, essentially one considers the tube wave, $\omega \simeq kc_T$ (see Equation (1.38).

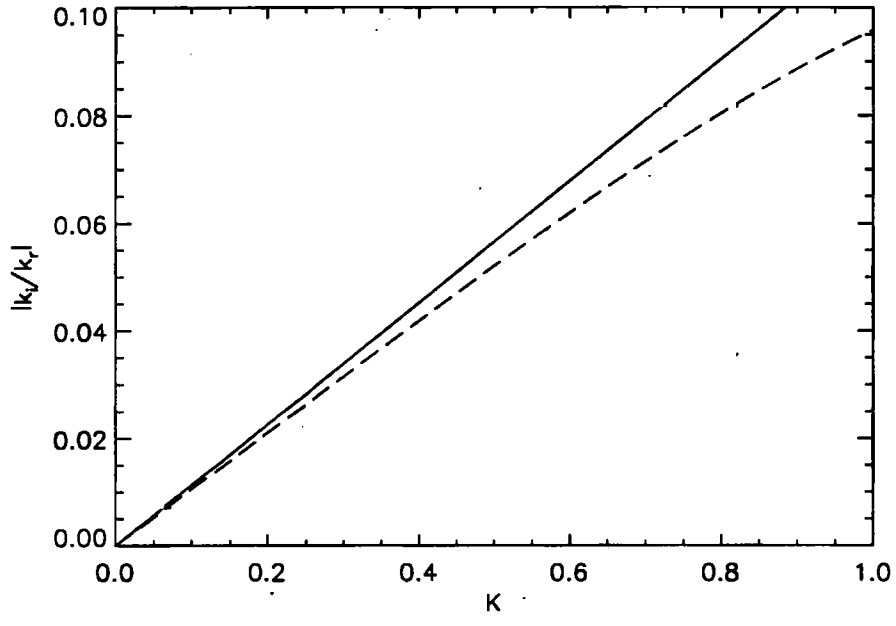

Figure 4.9: Damping per wavelength, $|k_i/k_r|$, versus K for solutions given by the exact solution of dispersion relation (4.69) (---) and by the approximate expression (4.70) (—).

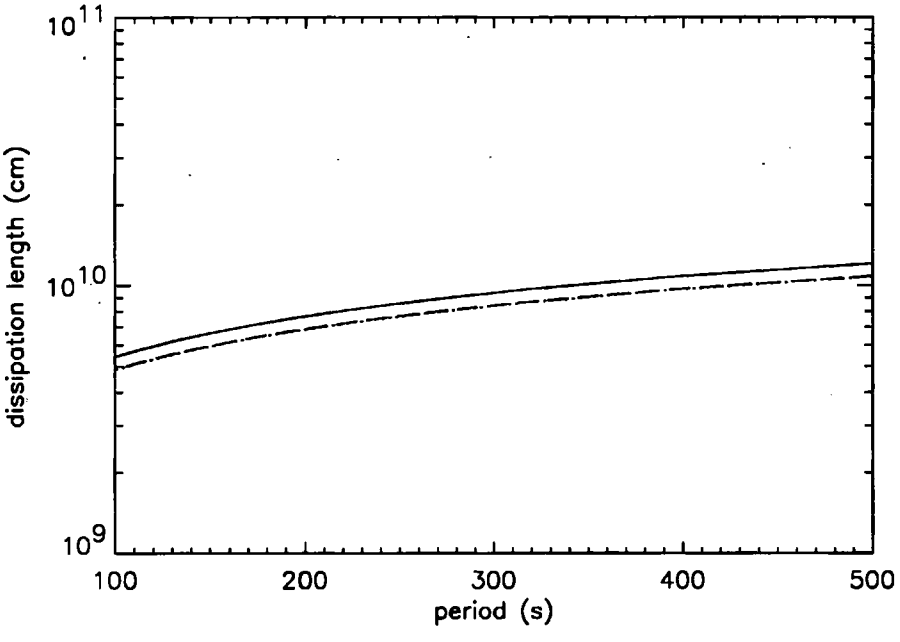

Figure 4.10: The dissipation length versus period for waves in a slender structure with magnetic field strength of 10 G (—), 50 G (---) and 100 G (....) for $P_e > 1$. The parameters other than the magnetic field strength are those of Model B of Table 1.7 but with ρ_e/ρ_0 undefined.

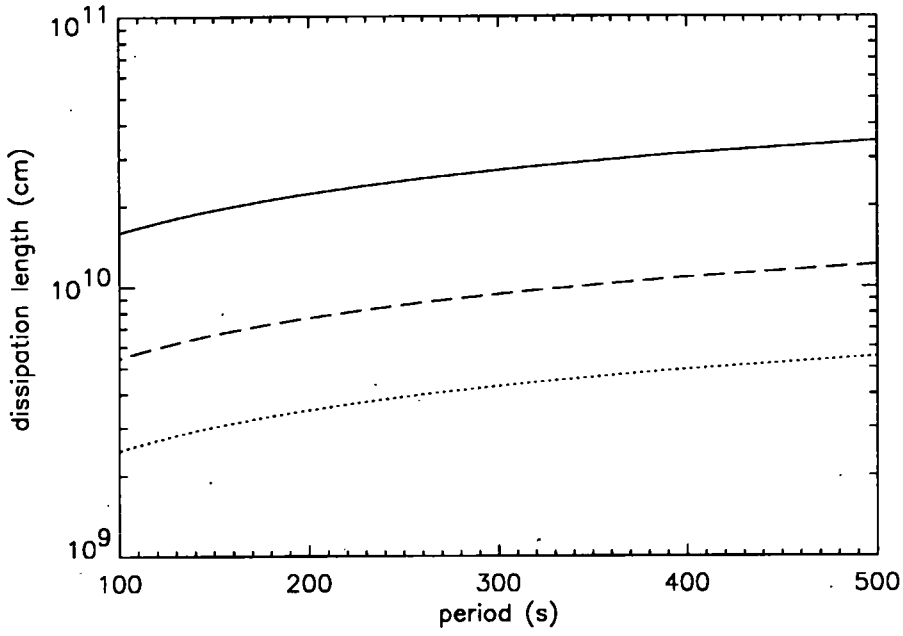

Figure 4.11: The dissipation length versus period for waves in a slender structure with density strength of 10^9 cm^{-3} (—), 10^{10} cm^{-3} (---) and 10^{11} cm^{-3} (....) for $P_e > 1$. The parameters other than those of density are those of Model B of Table 1.7 but with ρ_e/ρ_0 undefined.

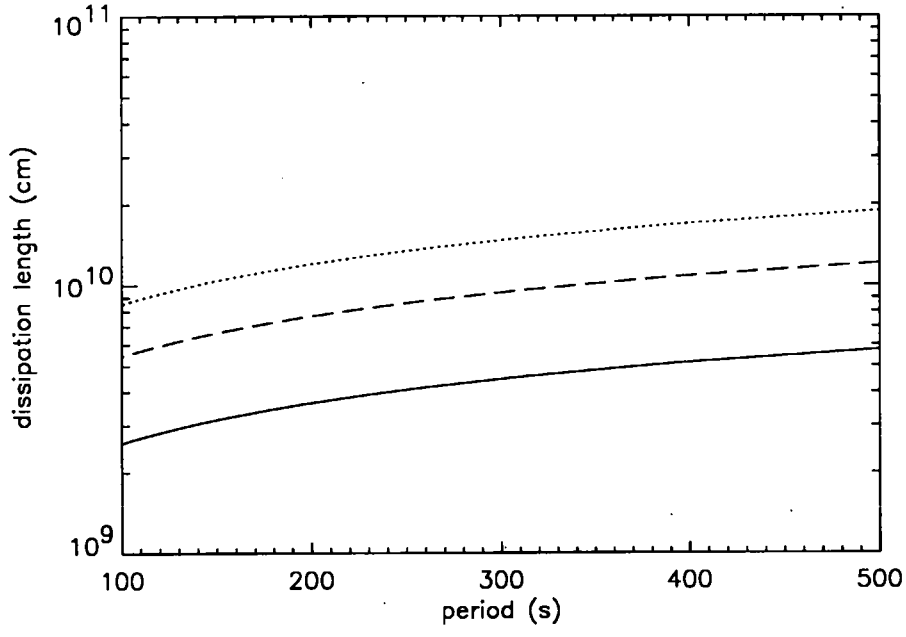

Figure 4.12: The dissipation length versus period for waves in a slender structure with background temperature 1×10^6 K (—), 2×10^6 K (---) and 3×10^6 K (....) for $P_e > 1$. The parameters other than those of temperature are those of Model B of Table 1.7 but with ρ_e/ρ_0 undefined.

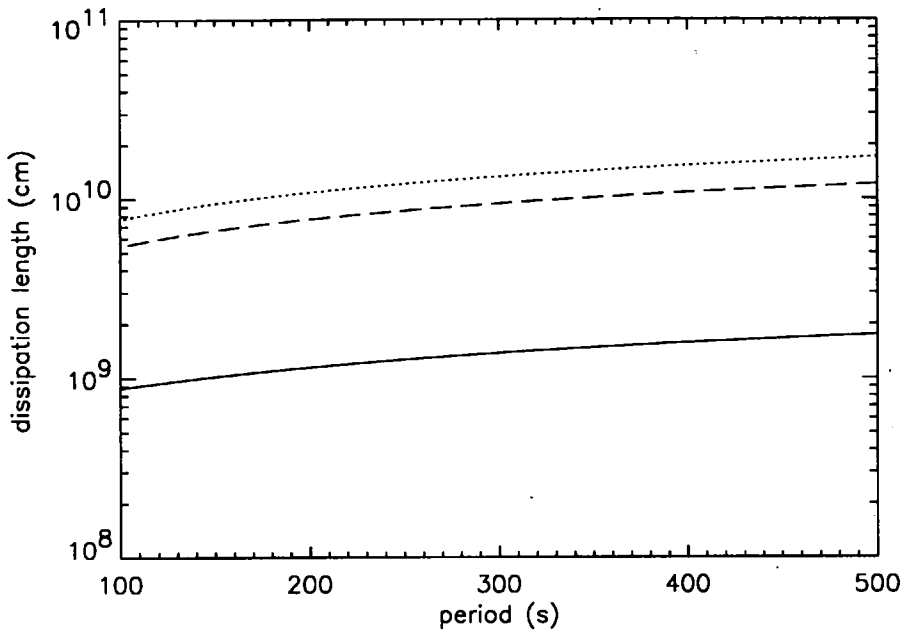

Figure 4.13: The dissipation length versus period for waves in a slender structure with radius of loop 10^7 cm (—), 5×10^8 cm (---) and 1×10^9 cm (....) for $P_e > 1$. The parameters are those of Model B of Table 1.7.

T (K)	N (cm^{-3})		
	1.0×10^9	1.0×10^{10}	1.0×10^{11}
1.0×10^6	10 G : 3.8 - 38 s 50 G : 3.8 - 36 s 100 G : 3.8 - 36 s	10 G : 4.3 - 29 s 50 G : 3.8 - 27 s 100 G : 3.8 - 27 s	10 G : 7.5 - 21 s 50 G : 4.0 - 17 s 100 G : 3.8 - 15 s
2.0×10^6	10 G : 2.8 - 28 s 50 G : 2.7 - 27 s 100 G : 2.7 - 27 s	10 G : 3.4 - 18 s 50 G : 2.7 - 16 s 100 G : 2.7 - 16 s	10 G : 7.0 - 14 s 50 G : 3.0 - 11 s 100 G : 2.8 - 9.7 s
3.0×10^6	10 G : 2.3 - 23 s 50 G : 2.2 - 22 s 10 G : 2.2 - 21 s	10 G : 3.0 - 13 s 50 G : 2.2 - 12 s 100 G : 2.2 - 21 s	10 G : 6.8 - 11 s 50 G : 2.5 - 8.6 s 100 G : 2.3 - 7.9 s

Table 4.2: Period ranges over which slow waves propagating in a coronal loop of radius 10^7 cm are dissipated for $P_e > 1$.

In effect we are considering left-most-part of the dispersion diagrams 1.5 and 1.8. Equations (4.58) and (4.70) shows that the tube wave is modified slightly by thermal conduction effects. The effects of radiation and conduction were treated separately. It was found that the waves subject to radiation would dissipate more easily in regions of high (100 G) magnetic field strength, high (10^{11} cm^{-3}) density and low (1×10^6 K) temperatures. However, it was found that there were very few cases in which the waves would dissipate in distances of less than 4×10^9 cm (our criterion for efficient dissipation). Two approaches to the investigation of the dissipation of slow waves in a slender ($ka \ll 1$) structure, subject to isotropic conduction, were considered. Both approaches concluded that the conditions most favourable for dissipation were loops of small (10^7 cm) radii with high (100 G) magnetic field strength, high (10^{11} cm^{-3}) density and low (1×10^6 K) temperatures. One approach (Section 4.4.1) considered the environment of the loop to be isothermal and so neglected velocity, temperature and total pressure perturbations in the environment. It was found that wave periods in the range 2 - 80 s were likely to dissipate effectively. The other approach (Section 4.4.2) considered the slender-flux-tube equations with zero total pressure perturbation in the environment and large Péclet number. This second method found that waves in the period range 2 - 38 s were likely to dissipate.

Chapter 5

Observed or Dissipated Waves?

5.1 Thesis Summary

This thesis has examined several dissipation mechanisms in the context of the dissipation of magnetohydrodynamic waves in the upper solar atmosphere. The work contained in the thesis is of importance because it attempts to correlate coronal waves that are observed with those that are not dissipated. This correlation permits suggestions as to which waves might dissipate and so heat the corona and which waves which might survive the dissipation mechanisms and so be observed. This final summary is made in Section 5.4.

A review of coronal features has been made in the introductory chapter together with the observational evidence for oscillatory phenomena. The basic equations of mhd were presented and since the upper solar atmosphere is known to be highly structured, a review of mhd wave propagation in structured media has been presented. Table 1.8 gives the broad classification of how coronal features fit with the parameter ranges used in this thesis. Comment is now made upon what the parameter models (see Table 1.7) considered in this thesis mean in terms of observed coronal features. Model G, with its large values for magnetic field strength, density and temperature, is fairly typical of a hot coronal loop. Models A - F are also fairly representative of hot coronal loops *but* with a weak (10 G) magnetic field. However, if one insists that hot coronal loops possess large ($\gtrsim$100 G) magnetic field strengths as Table 1.4 suggests, then the 10 G models, A to F, need to be associated with other coronal features. Perhaps then, Models A to F should be catagorized in the following way.

- Model A - quiet region loop.
- Model B - quiet region loop.
- Model C - no feature with these parameters.
- Model D - quiet region loop.

- Model E - quiet region loop.
- Model F - no feature with these parameters.

Models A and G were chosen to represent quiet region loops and active region loops, respectively. The investigation of dissipation lengths for the weakly dissipative model in Chapter 3 found that the parameters of Models B to F produced the shortest dissipation lengths, i.e. these were the parameters for which coronal heating was likely to occur. Thus, Models B to F are a *consequence* of the investigation carried out in Chapter 3. On comparing the parameters of these models to typical coronal features, one finds that Models C and F are *not* representative of any coronal situations.

Chapter 2 was concerned with energy and its dissipation in the upper solar atmosphere. The non-ideal equations of mhd were presented and coronal heating theories together with dissipation mechanisms were discussed. Detailed calculations of the energy carried by waves propagating in structured media were given and it was shown that the energy flux density for a spatially infinite medium is a very good estimate to the structured situation. Moreover, the energy calculations in this chapter show that reliable measurements of velocity amplitudes will be invaluable in deciding whether the dissipating waves (satisfying dissipation lengths of less than 4×10^9 cm) of Chapters 3 and 4 can contribute to heating the corona.

Chapter 3 considered the dissipation of mhd waves in a weakly dissipative environment. A coronal loop was modelled both as a slab and as a cylinder. The ducted waves were subject to dissipation by ion viscosity, electron thermal conduction and optically thin radiation. The investigation found that, on the whole, electron thermal conduction was the most important of the three dissipation terms. The scheme described in this chapter, as described by Gordon and Hollweg (1983), is an ingenious one because, although it is dissipation that is under investigation, consideration of a fully dissipative dispersion relation can be avoided. The basic principle involved was simply to calculate the energy of the ideal mhd waves (presented in Chapter 1) and then quite separately to imagine that this energy is used up, converted by the dissipative mechanisms. The lengths over which the fast and slow, symmetric and asymmetric waves dissipate, are calculated. Chapter 3 pointed out errors in the previous known studies which used this weakly dissipative scheme regarding the dissipation of waves in a cold plasma. It was shown that wave dissipation is more effective in the warm plasma situation. The investigation found that fast waves are likely to dissipate in regions of low ($\lesssim$ 15 G) magnetic field strength with periods of 2 to 10 s. Slow waves which are likely to dissipate have periods that range from about 15 - 225 s duration. Although the method adopted in Chapter 3 is a simple one, requiring only the energy and the dissipated fluxes to be calculated, it is limited in only being applicable to describing a collisional plasma. Since dissipative terms have not been included in the mhd equations used to derive the dispersion relation, the method is further restricted in only being able to describe weak dissipation. Such restrictions were shown to limit the number of coronal situations which could be described.

The investigation in Chapter 3 showed that electron thermal conduction (and radiation) were important at small values of ka, i.e. $ka \ll 1$, where k is the wave number and a represents the radius of the loop. By considering a slender structure, the analysis carried out in Chapter 4 allowed the dissipation mechanisms of radiation and conduction to be included in the mhd equations (i.e. the non-ideal equations) and so a dispersion relation which included dissipation could be obtained. In order to simplify matters, the mechanisms of optically thin radiation and isotropic conduction were considered separately. It was found that on the whole, the effect of radiation acting alone was insufficient to damp the slow symmetric waves under investigation in a distance of less than our criterion value of 4×10^9 cm. Two situations for the dissipation of slow waves in a slender structure subject to isotropic thermal conduction were investigated. In one method, the loop was considered to have isothermal boundaries, and so by assuming that the temperature, total pressure and velocity fluctuations in the exterior of the loop were negligible, a dispersion relation (containing dissipative effects) in the form of a quadratic in the wave number, k, could be obtained. A subsequent investigation of the spatial damping of this quadratic found that wave periods in the range 2 - 80 s could be dissipated efficiently. The second method, in which the slender-flux-tube equations were used, assumed a large Péclet number ($P_e = \omega a^2/\kappa \gg 1$) which allowed the temperature to be decoupled from the other equations and resulted in a quartic equation for the wave number. This method found that, in general, waves with periods 2 - 38 s were likely to dissipate.

5.2 Comparison of Dissipative Models

So far, nothing has been said about how the results of the wave dissipation models of Chapter 3 and 4 compare with each other and with other models in the literature. Therefore it is the task in this section to compare the models with each other and with similar work considered by other authors.

In comparing the results for the fast waves of Chapter 3 with the dissipation of fast waves in a cold plasma, as considered by Gordon and Hollweg (1983), one must bear in mind that Gordon and Hollweg only estimated the electron thermal conduction term, Q_{ther}, for intermediate frequencies, i.e. for frequencies, $\omega \approx \kappa_{\parallel,el} k^2(\gamma - 1)/N k_B$. However, the results obtained by Gordon and Hollweg are in line with those found for the dissipation of fast waves in a warm plasma given in Chapter 3, namely:

1. When the magnetic field strength is increased the dissipation length increases so that damping lengths become unrealistically large if B is more than a few tens of gauss, i.e. waves dissipate much less efficiently in regions of strong magnetic field.

2. It is difficult to make general statements about the variation of dissipation length with density and temperature since increasing the density (or temperature) did not always result in a decrease in the dissipation length.

3. As a is increased it is only the waves with longer periods that experience more effective dissipation.

It is clear from both investigations of the weakly dissipative model of Chapter 3 applied to both warm and cold plasmas that dissipation is efficient if the periods of the ducted waves are shorter than a few tens of seconds (i.e. 2 - 10 s) and only if the background magnetic field is less than about 15 G.

Porter, Klimchuk and Sturrock (1994a) found in their model of waves propagating in an unstructured atmosphere, subject to electron thermal conduction, ion viscosity and radiation, that increasing the magnetic field strength caused a decrease in the damping rate of the fast magnetoacoustic waves. This result is in agreement with 1 above. Further, Porter, Klimchuk and Sturrock were unable to make a general statement of how the damping rate was effected by changing the density but they did find a clear variation of the damping rate with temperature, namely increasing the temperature resulted in the damping rate increasing. Porter, Klimchuk and Sturrock found that, typically, fast waves with periods less than 75 s propagating in an unstructured medium representative of quiet regions would dissipate, which is in agreement with 1 and 3 above. For active regions they find that only fast waves with periods of less than 1 s would dissipate. As a consequence of using the volumetric loss rate due to viscosity, as given by Equation (2.24) (from Braginskii, 1965), the plasma has been assumed collisional and, as has been shown, the scheme in Chapter 3 is limited to describing wave dissipation for fast waves which have periods in excess of 2 s. Therefore one cannot use the model to predict whether fast waves with periods of less than 1 s are dissipated or not. Porter, Klimchuk and Sturrock also use the Braginskii form for ion viscosity but for small periods they only calculate the fast mode damping rate due to electron thermal conduction and hence are not restricted to describing wave periods greater than 2 seconds. Considering fast ducted waves, subject only to ion viscosity and radiation, Porter, Klimchuk and Sturrock (1994b) find that only waves with periods of less than 1 s are damped efficiently. In examining Table 3.7 for a weakly dissipative environment, we see that slow waves with periods 15 - 140 s can dissipate efficiently in hot loops and that in quiet regions the waves which experience efficient dissipation have periods in the range 15 - 225 s. These ranges are approximately those given by Porter, Klimchuk and Sturrock (1994a), namely wave periods less than 100 s and 300 s are dissipated efficiently in active regions and quiet regions respectively.

The weakly dissipative model of Chapter 3 and the work by Porter, Klimchuk and Sturrock (1994a, b) are different in the respect that

1. the two approaches used to investigate dissipative effects are different - Porter, Klimchuk and Sturrock (1994a, b) manipulate the linearized equations of mhd to obtain a dispersion relation which contains dissipative terms. The method in Chapter 3 calculates quantities of *ideal* waves and determines a dissipation length in the form of a logarithmic decrement by supposing that the energy of the (ideal) waves is converted to heat through volumetric energy loss rates;

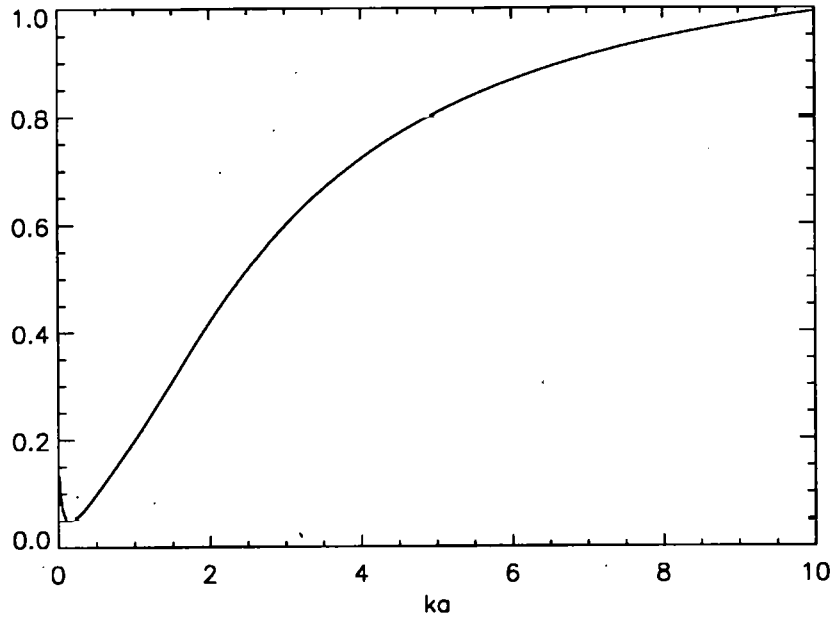

Figure 5.1: The ratio of slab to cylinder dissipation lengths versus ka using Equations (3.18) and (3.24) using the parameters of Model B of Table 1.7.

2. the model in Chapter 3 was applied to a structured medium; Porter, Klimchuk and Sturrock (1994a) investigate dissipation in an unstructured medium;

3. the criteria for effective dissipation are different; wave dissipation in the model of Chapter 3 is regarded as being efficient if the waves dissipate in distances of less than 4×10^9 cm whereas Porter, Klimchuk and Sturrock (1994a, b) derive a required minimum damping rate by equating the volumetric wave heating rate with the optically thin radiative cooling rate. (Indeed Porter, Klimchuk and Sturrock give their results mainly in the form of damping rate as a function of wave period whereas this thesis has presented the results mainly in the form of dissipation length versus wave period.)

One would expect close agreement between the results of Chapter 3 for the Cartesian and cylindrical cases in the large, $ka \gg 1$, limit, since the waves are unable to *sense* that they are ducted and essentially the waves are propagating in an unstructured medium. Further, one would expect that these should be similar to the corresponding results of dissipation in an unstructured medium. Figure 5.1 shows the ratio of the slab-to-cylinder dissipation lengths for the lowest-order kink mode plotted against ka. It is seen that for large ka (> 5) the dissipation lengths are approximately the same. Figure 5.2 can be compared to Figure 5b of Porter, Klimchuk and Sturrock (the one case in which they do give a plot of *damping length* versus period for fast waves in an unstructured medium). As is shown in Figure 5.2, large ka values ($ka \gg 1$) for the Cartesian and cylindrical ducts

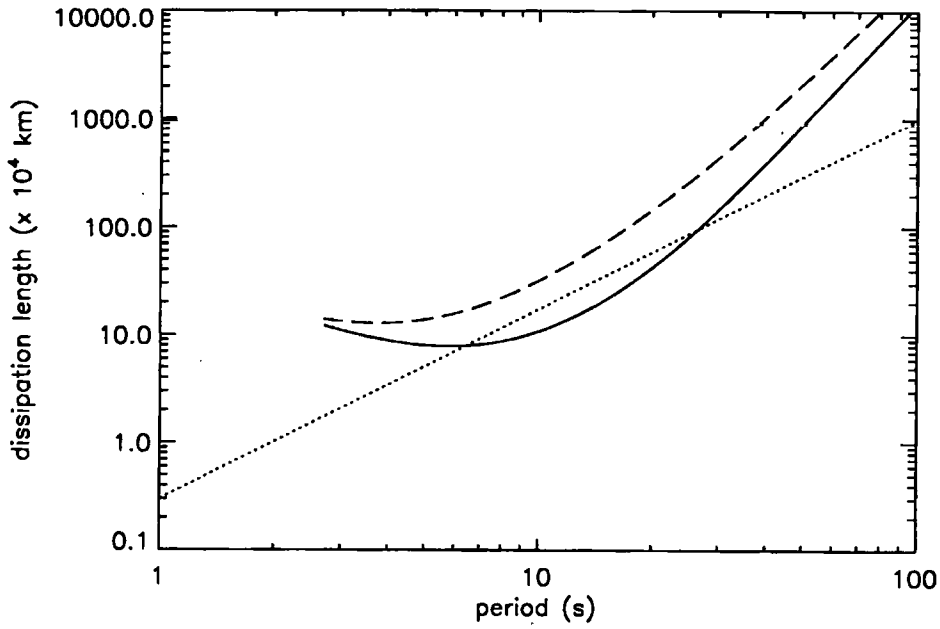

Figure 5.2: The dissipation length versus period for the lowest-order fast mode propagating in a slab (—) and cylinder (---) with the parameters of Model B of Table 1.7. The dissipation length given by Porter, Klimchuk and Sturrock (1994a) is approximated by (....).

produce similar dissipation lengths to the unstructured situation considered by Porter, Klimchuk and Sturrock (1994a). Further, in considering large ka ($ka \gg 1$) values Figures 3.19 shows that ion viscosity is the more dominant dissipation term at high frequencies. This is consistent with the statements of Gordon and Hollweg (1983) and Porter, Klimchuk and Sturrock (1994a, b).

Moreover, it can be shown that in a cold plasma, for $ka \gg 1$, the dissipation lengths of the asymmetric waves as given by Equations (3.29) and (3.33) reduce to

$$L_k = \frac{3v_A\rho_0 a^2}{\eta(ka)^2(\omega^2/k^2v_A^2 - 1)}. \tag{5.1}$$

By considering the dissipation lengths for large values of ka (see Figure 5.3) we can recover approximately the dissipation lengths given by Porter, Klimchuk and Sturrock (1994a) for the slow waves of Chapter 3. It is of no surprise that we can recover the 'unstructured' situation given that in Chapter 1 we saw that the ducted slow waves are essentially propagating at the tube speed, c_T, and are effectively dispersionless. It is noted that the variation of dissipation length with magnetic field strength and density for the slow waves of Chapter 3 are consistent with the findings of Porter, Klimchuk and Sturrock (1994a). Porter, Klimchuk and Sturrock (1994a) found that the damping was more effective with increase in temperature. This is again consistent with results in Chapter 3 but only for waves with periods less than 80 s.

The investigation of dissipation of slow, symmetric waves subject to isotropic thermal

conduction in the two models of Sections 4.4.1 and 4.4.2 found that, qualitatively, the models had similar behaviour for the dependence of magnetic field strength, density, temperature and loop radius. It was found that the dissipation length increased when either the magnetic field strength was increased, the density was decreased, the temperature was increased or the loop radius was decreased. It is noted that the behaviour of the dissipation length with density and temperature for the models in Chapter 4 is similar to that found for the weakly dissipative scheme used in Chapter 3 and the models also find that there is a weak dependence on dissipation with magnetic field strength.

Tables 4.1 and 4.2 give the period ranges over which slow, symmetric waves are dissipated according to the models in Sections 4.4.1 and 4.4.2 for the coronal parameters of Table 1.8. In of both the tables of Chapter 4, the lower bound of the period in each cell represents the restriction $\omega \ll c_T/a$ (see page 109). Since the values of magnetic field strength, density, temperature and loop radius are the same for the corresponding cells of Tables 4.1 and 4.2, then the lower bound of the period for corresponding cells is the same. The upper bound of the period in each cell gives the periods for which the dissipation length is 4×10^9 cm. The dissipation length, $1/2k_i$, is found by solving the quadratic (in k) equation (4.57) of Section 4.4.1 and the quartic (in k) equation (4.68) of Section 4.4.2 and so the upper bounds on the periods are different.

Three different models for the dissipation of slow waves propagating along a coronal loop have been presented. Table 3.7 gives the period ranges over which slow waves propagating along a loop of radius 5×10^8 cm are dissipated for the weakly dissipative scheme of Chapter 3. Tables 4.1 and 4.2 give the period ranges for which slow waves are dissipated in slender structures and have been calculated for a small loop size (10^7 cm). The difference in period ranges over which dissipation occurs in Tables 3.7 and Tables 4.1 and 4.2 is a result of considering slender (i..e. $ka \ll 1$) structures for the models in Chapter 4.

5.3 Suggestions for Further Work

Clearly, the model presented in Chapter 3 for calculating the dissipation lengths of ducted waves is a simple one. Unfortunately the model is unable to describe satisfactorily all coronal conditions due to the constraints outlined in Chapter 3. However, the model did give an insight into the kinds of waves which were favourable for coronal heating and these waves were explored further in Chapter 4.

The area for further work concerning the model in Chapter 3 centres on, not the calculation of the volumetric energy loss rates, but on how the dispersion relation (i.e. the relationship between the angular frequency, ω, and the wave number, k) influences the dissipation lengths of the waves. The equations for computing the dissipation lengths are given by Equations (3.15), (3.18), (3.21) and (3.24) and are of the form

$$L_{s,k} = L_{s,k}(\omega, k, \rho_0, \rho_e, a, B_0, B_e, N_0, N_e, T),$$

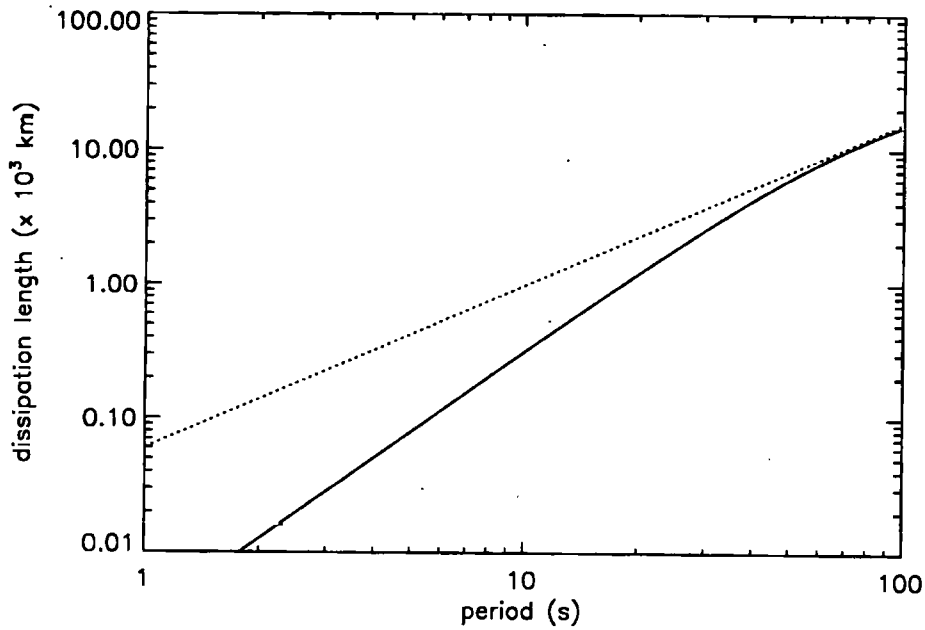

Figure 5.3: The dissipation length versus period for the slow, symmetric waves of Chapter 3 propagating in a cylinder (—) with the parameters of Model B of Table 1.7. The dissipation length given by Porter, Klimchuk and Sturrock (1994a) is approximated by (....).

The investigation in Chapter 3 revealed the variation of the dissipation length when the magnetic field, density etc. was varied. Of course, varying these parameters modifies the dispersion diagram for the ducted waves in the sense that the size of the bands of fast and slow waves are either enlarged or are reduced, i.e. the regions $v_A < \omega/k < v_{Ae}$ and $c_T < \omega/k < c_{Te}$ of Figure 1.5. However, one may consider a different ducted situation and thus solve its associated dispersion relation for ω and k. In principle one could feed these values of ω and k into $L_{s,k}$ and compute a dissipation length. One could then ask how are the results for Chapter 3 changed when one

1. uses a smooth density profile to model the duct;
2. takes into account the observed curvature of coronal loops;
3. takes into account the observed twisting magnetic field lines in some coronal loops.

Thus the simple model in Chapter 3 could be used to gain some insight to the dissipation of waves in a *more* realistic coronal loop situation.

The results of Chapter 3 were given terms of a dissipation length. There is no need to restrict attention to only finding lengths over which the waves surrender their energy. One may equally recast the problem in terms of temporal damping and thus provide dissipation rates of the various ducted wave modes.

In Chapter 4, only the dissipation of slow waves propagating in slender structures was considered because the model in Chapter 3 indicated that the dissipation of fast was unfavourable, except in regions of low magnetic field strength. However, there is no need to restrict attention to only slow waves because the investigation could be pursued in a similar for fast waves, i..e. waves propagating at approximately v_A for $ka \ll 1$.

In principle it could be possible to solve Equations (4.47) and (4.48) numerically. Of course, this would be a non-trivial task given the complicated way in which ω and k are linked by the variables d_j etc. and that, when written out fully, the left-hand-side of Equations (4.47) and (4.48) contains 24 terms. However, such an investigation would simply require a root-solving procedure (e.g. Brent's method) and would be worth while pursuing in order to provide information regarding the nature of the dissipation of the slow waves at *all* values of ka.

5.4 Waves in the Upper Solar Atmosphere

The results in Chapters 3 and 4 have mainly been illustrated in the form of dissipation length varying with periodicity; wave period is a quantity which may be measured as a result of observations. A comparison is now made between the results of the investigations pursued in this thesis and the results from work carried out by other authors and with the observed oscillations listed in Chapter 1. Further, suggestions as to which waves are likely to be observable, and which dissipated, and so perhaps contribute to coronal heating are made.

Figure 5.4 gives a comparison of the period ranges of dissipating and non-dissipating waves of the models of Chapters 3 and 4, and the work of Porter, Klimchuk and Sturrock (1994a) with observed periods of oscillation in the upper solar atmosphere. The figure clearly indicates that waves with periods in excess of 300 s are likely to escape dissipation and so do not contribute to coronal heating. Thus, the many-minute period oscillations detected by Harrison (1987) and Švestka (1994) are not candidates for coronal heating. One may argue that the reason why waves with these periods are detected is that the waves easily survive the dissipation mechanisms (i.e. the waves are not dissipated efficiently). Of course, if this is the case, then many more coronal oscillations in the period range 300 - 1000 s should be detected. As Figure 5.4 indicates, there have not been, as yet, any reported coronal oscillations of 300 - 1000 s. For very short wave periods, i.e. waves with periods of less than one second, one may argue similarly that the many reports of fast coronal oscillations suggest that waves with very short periods are not subject to efficient dissipation. The model in Chapter 3 is unable to describe fast waves with periods of less than 2 s but Porter, Klimchuk and Sturrock (1994a) indicate that fast waves with short periods can be associated with coronal heating. According to Figure 5.4 periods in the range 40 - 300 s can be associated with both dissipating and non-dissipating waves. Given that fast waves have a larger energy flux density than slow waves, and so have more energy available to be dissipated (Chapter 2), it is then proposed that waves with periods of 2 to 10 s are likely to contribute to coronal heating and that waves with periods of a few

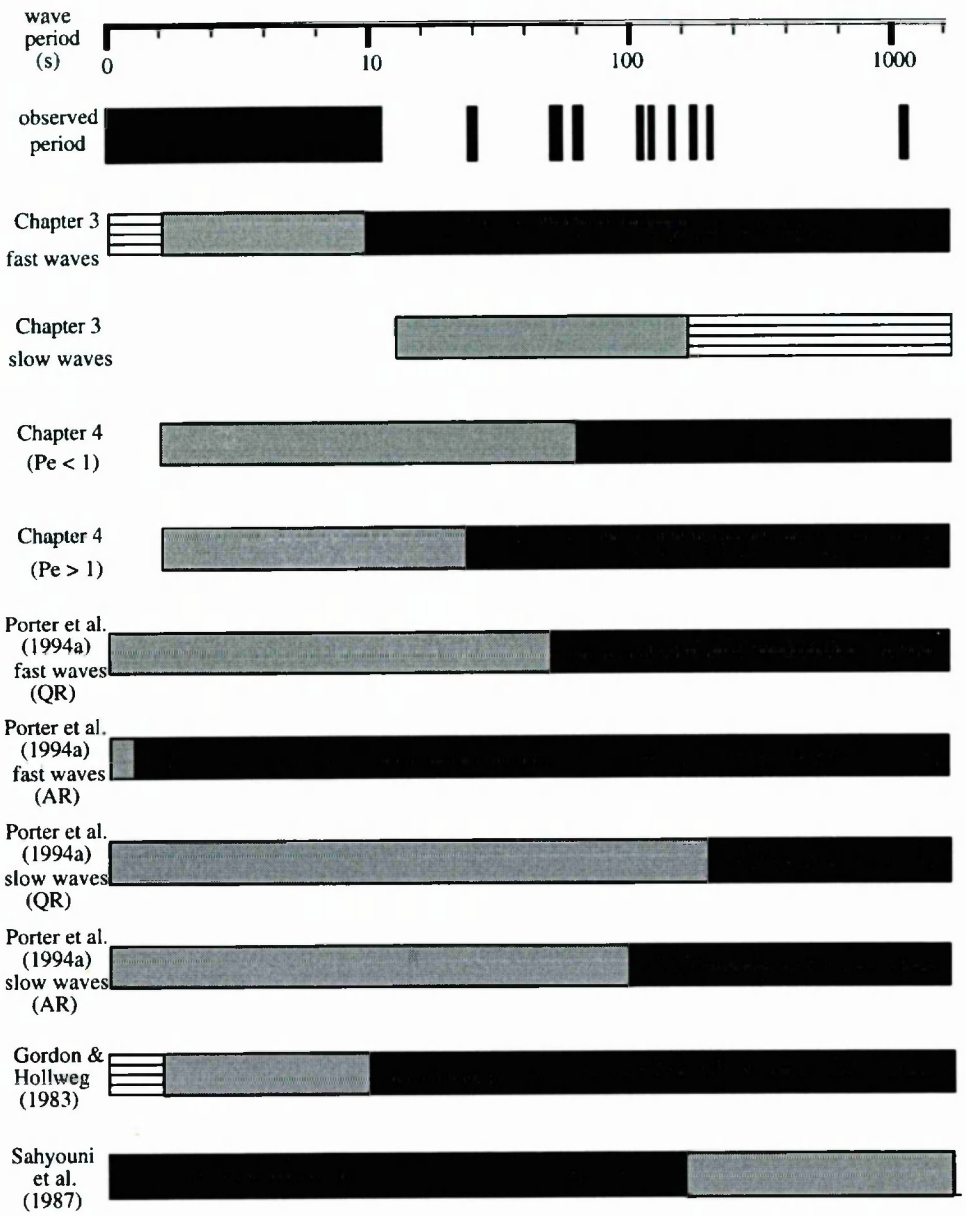

Figure 5.4: Comparison of dissipating (light shading) and non-dissipating (dark shading) waves with observed coronal oscillations. The horizontal stripes indicate the period ranges for which the models are not valid. QR and AR are quiet and active coronal regions respectively.

and many tens of seconds are likely to survive dissipation.

From the results in this thesis 'windows' of period ranges have been identified in which waves may contribute to coronal heating or in which the waves are likely to be observable. Moreover from Figure 5.4 it is evident that the observations are not consistent with the principle that dissipating waves are unlikely to be observed. The very fact that there has been a great wealth of fast (1 - 2 s) pulsations reported in the literature seems to be more suggestive that fast mhd waves do not contribute to coronal heating! For slow waves to contribute they certainly need to be associated with large velocity amplitudes. As remarked in Chapter 2 it is clear that until there are improved diagnostics for observations of waves, the coronal heating problem will remain unanswered. However, it is hoped that more convincing arguments will be given when the results of the CDS and SUMER instruments, currently undergoing calibration, on board the orbiting SOHO spacecraft, are known. Indeed until we have more detailed measurements it is difficult to progress very much further from the statements of Wentzel (1977): 'It seems difficult for heating by hydromagnetic waves to meet simultaneously the requirements of a large enough heating rate, an approximate dissipation length comparable to the loop length, a field-aligned heating characterised by smaller widths than lengths, and finally a velocity amplitude that agrees with observations.'

References

Abramowitz, M. and Stegun, I.A.: 1967, *Handbook of Mathematical Functions*, Dover, New York.

Acton, L.W., Culhane, J.L., Gabriel, A.H., Wolfson, C.J., Rapley, C.G., Phillips, K.J.H., Antonucci, E., Bentley, R.D., Hayes, R.W., Joki, E.G., Jordan, C., Kayat, M.A., Kent, B., Leibacher, J.W., Nobles, R.A., Parmer, A.N., Strong, K.T. and Veck, N.J.: 1981, *Astrophys. J.* **244**, L137.

Acton, L.W., Tsuneta, S., Ogawara, S., Bentley, R.D., Bruner, M.E., Canfield, R.C., Culhane, J.L., Doscheck, G.A., Hiei, E., Hirayama, T., Hudson, H.S., Kosugi, T., Lang, J., Lemen, J.R., Nishimura, J., Makishima, K., Uchida, Y. and Watanabe, T.: 1992, *Science* **258**, 618.

Anderson, L.S. and Athay, R.G.: 1989, *Astrophys. J.* **336**, 1089.

Antonucci, E., Gabriel, A.H. and Patchett, B.E.: 1984, *Solar Phys.* **93**, 85.

Aschwanden, M.J.: 1987, *Solar Phys.* **111**, 113.

Aschwanden, M.J., Benz, A.O., Dennis, B.R. and Gaizauskas, V.: 1993, *Astrophys. J.* **416**, 857.

Aschwanden, M.J., Benz, A.O., Dennis, B.R. and Kundu, M.R.: 1994, *Astrophys. J. Supp.* **90**, 631.

Aschwanden, M.J., Benz, A.O. and Montello, M.L.: 1994, *Astrophys. J.* **431**, 432.

Athay, R.G. and White, O.R.: 1978, *Astrophys. J.* **226**, 1135.

Athay, R.G. and White, O.R.: 1979, *Astrophys. J.* **229**, 1147.

Basri, G.S. and Linsky, J.L.: 1979, *Astrophys. J.* **234**, 1023.

Beckers, J.M.: 1972, *Ann. Rev. Astron. Astrophys.* **10**, 73.

Beckers, J.M. and Tallant, P.: 1969, *Solar Phys.* **7**, 351.

Biermann, L.: 1946, *Naturwissenschaften* **33**, 118.

Bogdan, T.J. and Knölker, M.: 1989, *Astrophys. J.* **339**, 579.

Braginskii, S.I.: 1965, *Rev. Plasma Phys.* **1**, 205.

Bray, R.J., Cram, L.E., Durrant, C.J. and Loughhead, R.E.: 1991, *Plasma Loops in the Solar Corona*, Cambridge University Press, Cambridge.

Browning, P.K.: 1991, *Plasma Physics and Controlled Fusion* **33**, 539.

Browning, P.K. and Priest, E.R.: 1984, *Astron. Astrophys.* **131**, 283.

Bruner, E.C.: 1978, *Astrophys. J.* **226**, 1140.

Cargill, P.: 1995, in J.R. Kuhn and M.J. Penn (eds.), *Infrared Tools For Solar Astrophysics: What's Next?*, World Scientific, Singapore.

Cheng, C.-C.: 1980, *Astrophys. J.* **238**, 743.

Cheng, C.-C., Doschek, G. A. and Feldman, U.: 1979, *Astrophys. J.* **227**, 1037.

Cowling, T.G.: 1976, *Magnetohydrodynamics*, Adam Hilger, Bristol.

Cram, L.E. and Damé, L.: 1983, *Astrophys. J.* **272**, 355.

Davila, J.M.: 1987, *Astrophys. J.* **317**, 514.

Deubner, F.-L. and Fleck, B.: 1990, *Astron. Astrophys.* **228**, 506.

Doschek, G.A. and Feldman, U.: 1977, *Astrophys. J.* **212**, L143.

Doschek, G.A., Feldman, U. and Bohlin, J.D.: 1976, *Astrophys. J.* **205**, L177.

Edwin, P.M.: 1984, Ph.D. Thesis, St Andrews University.

Edwin, P.M. and Laing, G.B.: 1994, in V. Rušin, P. Heinzel and J.-C. Vial (eds.), *Solar Coronal Structures*, VEDA, Slovakia.

Edwin, P.M. and Roberts, B.: 1982, *Solar Phys.* **76**, 239.

Edwin, P.M. and Roberts, B.: 1983, *Solar Phys.* **88**, 179.

Edwin, P.M. and Zhelyazkov, I.: 1992, *Solar Phys.* **139**, 7.

Endler, F. and Deubner, F.-L.: 1983, *Astron. Astrophys.* **121**, 291.

Evans, D.J. and Roberts, B.: 1990, *Astrophys. J.* **348**, 346.

Feldman, U. and Behring, W.E.: 1974, *Astrophys. J.* **189**, L45.

Feldman, U. and Doschek, U.: 1977, *Astrophys. J.* **212**, L147.

Ferraro, V.C.A. and Plumpton, C.: 1961, *An Introduction to Magnetofluid Mechanics*, Oxford University Press, Oxford.

Field, G.B.: 1965, *Astrophys. J.* **142**, 531.

Flå, T., Habbal, S.R., Holzer, T.E. and Leer, E.: 1984, *Astrophys. J.* **280**, 382.

Foukal, P.V.: 1975, *Solar Phys.* **43**, 327.

Foukal, P.V.: 1990, *Solar Astrophysics*, Wiley-Interscience, New York.

Fu, Q.-J., Gong, Y.-F. Jin, S.-Z. and Zhao, R.-Y.: 1990, *Solar Phys.* **130**, 161.

Gilman, P.A.: 1986, in P.A. Sturrock (ed.), *Physics of the Sun* **1**, 95.

Giovanelli, R.G.: 1972, *Solar Phys.* **27**, 71.

Goossens, M.: 1994, *Space Sci. Rev.* **68**, 51.

Goossens, M., Ruderman, M.S. and Hollweg, J.V.: 1995, *Solar Phys.* **157**, 75.

Gordon, B.E. and Hollweg, J.V.: 1983, *Astrophys. J.* **266**, 373.

Grossmann, W. and Smith, R.A.: 1988, *Astrophys. J.* **332**, 476.

Habbal, S.R., Leer, E. and Holzer, T.E.: 1979, *Solar Phys.* **64**, 287.

Haisch, B.M. and Schmitt, J.H.M.M.: 1996, *Publ. Astron. Soc. Pacific* **108**, 113.

Harrison, R.A.: 1987, *Astron. Astrophys.* **182**, 337.

Hassler, D.M., Rottman, G.J., Shoub, E.C. and Holzer, T.E.: 1990, *Astrophys. J.* **348**, L77.

Heyvaerts, J. and Priest, E.R.: 1983, *Astron. Astrophys.* **117**, 220.

Hiei, E.: 1994, in V. Rušin, P. Heinzel and J.-C. Vial (eds.), *Solar Coronal Structures*, VEDA, Slovakia.

Hinata, S.: 1980, *Astrophys. J.* **235**, 258.

Hinata, S.: 1981, *Astrophys. J.* **246**, 532.

Hollweg, J.V.: 1978, *Geophys. Res. Lett.* **5**, 731.

Hollweg, J.V.: 1983, in M.Neugebauer (ed.) *Solar Wind Five*, Washington : NASA-CP-2280, 5.

Hollweg, J.V.: 1985, *J. Geophys. Res.* **90**, 7620.

Hollweg, J.V.: 1986, *Astrophys. J.* **306**, 730.

Hollweg, J.V.: 1987, *Astrophys. J.* **312**, 880.

Hollweg, J.V.: 1990, *Comp. Phys. Rep.* **12**, 205.

Hollweg, J.V.: 1991, in P. Ulmschneider, E.R. Priest and R. Rosner (eds.), *Mechanisms of Chromospheric and Coronal Heating*, Springer-Verlag, New York.

Ionson, J.A.: 1978, *Astrophys. J.* **226**, 650.

Kernighan, B.W. and Ritchie, D.M.: 1988, *The C Programming Language*, Prentice-Hall International, London.

Kjeldseth Moe, O. and Nicolas, K.R.: 1977, *Astrophys. J.* **211**, 579.

Kneer, F. and von Uexküll, M.: 1985, *Astron. Astrophys.* **144**, 443.

Koutchmy, S., Žugžda, Y.D. and Locăns, V.: 1983, *Astron. Astrophys.* **120**, 185.

Krieger, A.S., Timothy, A.F. and Roelof, E.C.: 1973, *Solar Phys.* **29**, 505.

Kuperus, M., Ionson, J.A. and Spicer, D.S.: 1981, *Ann. Rev. Astron. Astrophys.* **19**, 7.

Laing, G.B. and Edwin, P.M.: 1994, *Solar Phys.* **151**, 191.

Laing, G.B. and Edwin, P.M.: 1995a, *Solar Phys.* **157**, 103.

Laing, G.B. and Edwin, P.M.: 1995b, *Solar Phys.* **161**, 269.

Leblanc, Y.: 1970, *Astron. Astrophys.* **4**, 315.

Lee, M.A.: 1980, *Astrophys. J.* **240**, 693.

Lee, M.A. and Roberts, B.: 1986, *Astrophys. J.* **301**, 430.

Leibenberg, D.H., Bessey, R.J. and Watson, R.: 1975, *Solar Phys.* **44**, 345.

Leibenberg, D.H. and Hoffman, M.M.: 1974, in G. Newkirk (ed.), *Coronal Disturbances*, IAU Symp. **57**, 485.

Li, H.-W., Messerotti, M., and Zlobec, P.: 1987, *Solar Phys.* **111**, 137.

Lighthill, M.J.: 1960, *Phil. Trans. Roy. Soc.* **A252**, 397.

Lites, B.W.: 1988, *Astrophys. J.* **334**, 1054.

McKenzie, J.F.: 1970, *J. Geophys. Res.* **75**, 5331.

McWhirter, R.W.P., Thonemann, P.C. and Wilson, R.: 1975, *Astron Astrophys.* **40**, 63.

Mangeney, A. and Pick, M.: 1989, *Astron. Astrophys.* **224**, 242.

Meerson, B.I., Sasorov, P.V. and Stepanov, A.V.: 1978, *Solar Phys.* **58**, 165.

NAG Ltd.: 1988, *The NAG Fortran Library Manual-Mark 13*, Numerical Algorithms Group, Oxford.

Narain, U. and Ulmschneider, P.: 1990, *Space Sci. Rev.* **54**, 377.

Narain, U. and Ulmschneider, P.: 1995, *Space Sci Rev.* **75**, 453.

Nocera, L., Leroy, B. and Priest, E.R.: 1984, *Astron. Astrophys.* **133**, 387.

Ofman, L., Davila, J.M. and Steinolfson, R.S.: 1994, *Astrophys. J.* **421**, 360.

Osterbrock, D.E.: 1961, *Astrophys. J.* **134**, 347.

Parker, E.N.: 1979, *Cosmical Magnetic Fields*, Oxford University Press, New York.

Parker, E.N.: 1987, *Physics Today* **40**, 36.

Parker, E.N.: 1990, *Geophys. Astrophys. Fluid Dyn.* **53**, 40.

Parker, E.N.: 1991, *Astrophys J.* **372**, 719.

Parker, E.N.: 1992, *J. Geophys. Res.* **97**, 4311.

Pasachoff, J.M.: 1991, in P. Ulmschneider, E.R. Priest and R. Rosner (eds.), *Mechanisms of Chromospheric and Coronal Heating*, Springer Verlag, New York.

Pasachoff, J.M. and Ladd, E.F.: 1987, *Solar Phys.* **109**, 365.

Phillips, K.J.H.: 1992, *Guide to the Sun*, Cambridge University Press, Cambridge.

Pick, M., Trottet, G. and MacQueen, R.M.: 1979, *Solar Phys.* **63**, 369.

Poedts, S., Goossens, M. and Kerner, W.: 1990, *Astrophys. J.* **360**, 279.

Porter, L.J., Klimchuk, J.A. and Sturrock, P.A.: 1994a, *Astrophys. J.* **435**, 482.

Porter, L.J., Klimchuk, J.A. and Sturrock, P.A.: 1994b, *Astrophys. J.* **435**, 502.

Press, W.H., Teukolsky, S.A., Vetterling, W.T. and Flannery, B.P.: 1992, *Numerical Recipes in C*, Cambridge University Press, Cambridge.

Priest, E.R.: 1981, *Solar Flare Magnetohydrodynamics*, Gordon and Breach Science Publishers Ltd., London.

Priest, E.R.: 1982, *Solar Magnetohydrodynamics*, Reidel, Dordrecht, Holland.

Priest, E.R.: 1992, in M. Dubois, D. Gressilon and P. Hennequin (eds.), *Cargese 92 Workshop on Magnetic Turbulence and Transport*, Cambridge University Press, Cambridge.

Rae, I.C. and Roberts, B.: 1981, *Geophys. Astrophys. Fluid Dyn.* **18**, 197.

Raymond, J.C. and Smith, B.W.: 1977, *Astrophys. J. Supp. Series* **35**, 419.

Roberts, B.: 1981, *Solar Phys.* **69**, 39.

Roberts, B.: 1985, in E.R. Priest (ed.) *Solar System Magnetic Fields*, Reidel, Dordrecht.

Roberts, B.: 1988, in B. Buti (ed.) *Planetary and Solar Plasma Physics*, World Scientific, Singapore.

Roberts, B. and Webb, A.R.: 1979, *Solar Phys.* **64**, 77.

Roberts, P.H.: 1967, *An Introduction to Magnetohydrodynamics*, Longmans, London.

Rosner, R., Tucker, W.H. and Vaiana, G.S.: 1978, *Astrophys. J.* **220**, 643.

Ruderman, M.S.: 1991, *Solar Phys.* **131**, 11.

Ruderman, M.S.: 1992, *Astrophys. J.* **339**, 724.

Rušin, P., Heinzel, V. and Vial, J.-C. (eds.): 1994, *Solar Coronal Structures*, VEDA, Slovakia.

Saba, J.L.R. and Strong, K.T.: 1991, *Astrophys. J.* **375**, 789.

Sahyouni, W., Kiss'ovski, Zh. and Zhelyazkov, I.: 1987, *Z. Naturforsch.* **42a**, 1443.

Sakurai, T., Goossens, M. and Hollweg, J.V.: 1991, *Solar Phys.* **133**, 227.

Schmitz, F.: 1990, *Astron. Astrophys.* **229**, 177.

Schrijver, C.J.: 1992, *Astron. Astrophys.* **258**, 507.

Schwartz S.J. and Leroy, B.: 1982, *Astron. Astrophys.* **112**, 93.

Schwarzschild, M.: 1948, *Astrophys. J.* **107**, 1.

Sedláček, Z.: 1971, *J. Plasma Phys.* **5**, 239.

Shklovskii, I.S.: 1965, *Physics of the Solar Corona*, Pergamon Press, London.

Similon, P.L. and Sudan, R.N.: 1989, *Astrophys. J.* **336**, 442.

Sonnerup, B.U.Ö. and Priest, E.R.: 1975, *J. Plasma Physics* **14**, 283.

Spruit, H.C.: 1982, *Solar Phys.* **75**, 3.

Steinolfson, R.S., Priest, E.R., Poedts, S., Nocera, L. and Goossens, M.: 1986, *Astrophys. J.* **304**, 526.

Steinolfson, R.S. and Davila, J.M.: 1993, *Astrophys. J.* **415**, 354.

Stenflo, J.O.: 1989, *Ann. Rev. Astron. Astrophys.* **1**, 3.

Stewart, R.T.: 1976, *Solar Phys.* **50**, 437.

Sturrock, P.A.: 1994, *Plasma Physics*, Cambridge University Press, Cambridge.

Švestka, Z.: 1994, *Solar Phys.* **152**, 505.

Takakura, T., Kaufmann, P., Costa, J.E.R., Degaonkar, S.S., Ohki, K. and Nitta, N.: 1983, *Nature* **302**, 317.

Tsubaki, T.: 1977, *Solar Phys.* **51**, 121.

Tsubaki, T.: 1988, in C. Altrock (ed.) *Solar and Stellar Coronal Structures and Dynamics*, Sunspot, NM:NSO.

Ulmschneider, P. and Bohn, U.H.: 1981, *Astron. Astrophys.* **99**, 173.

Vaiana, G.S., Krieger, A.S. and Timothy, A.F.: 1973, *Solar Phys.* **32**, 81.

Vaiana, G.S., Cassinelli, J.P., Fabbiano, G., Giacconi, R., Golub, L., Gorenstein, B., Haisch, B.M., Harnden Jr., F.R., Johnson, H.M., Linsky, J.L., Maxson, C.W., Mewe, R., Rosner, R., Seward, F., Topka, K. and Zwaan, C.: 1981, *Astrophys. J.* **244**, 163.

Van der Linden, R.A.M. and Goossens, M.: 1991, *Solar Phys.* **131**, 79.

Webb, A.R.: 1980, Ph.D. Thesis, St Andrews University.

Webb, A.R. and Roberts, B.: 1980, *Solar Phys.* **68**, 71.

Wentzel, D.G.: 1977, *Solar Phys.* **52**, 163.

White, O.R. and Athay, R.G.: 1979, *Astrophys. J. Suppl.* **39**, 317.

White, S.M., Kundu, M.R. and Gopalswamy, N.: 1992, *Astrophys. J. Supp.* **78**, 599.

Wilson, P.R.: 1980, *Astron. Astrophys.* **87**, 121.

Wright, C.S. and Nelson, G.J.: 1987, *Solar Phys.* **111**, 385.

Yoshida, T., Tsuneta, S., Golub, L., Strong, K. and Ogawara, Y.: 1995, *Publ. Astron. Soc. Japan* **47**, L15.

Zhao, R.-Y., Mangeney, A. and Pick, M.: 1991, *Astron. Astrophys.* **241**, 183.

Zirin, H. and Stein, A.: 1972, *Astrophys. J.* **178**, L85.

Zirker, J.B.: 1993, *Solar Phys.* **148**, 43.

Zlobec, P., Messerotti, M., Dulk, G.A. and Kucera, T.: 1992, *Solar Phys.* **141**, 165.

Zweibel, E.: 1980, *Solar Phys.* **66**, 305.